Indirect Selective Laser Sintering of an Apatite-Mullite Glass-ceramic

by

Ruth Davina Goodridge

Submitted in accordance with the requirements for the degree of
Doctor of Philosophy

University of Leeds
School of Mechanical Engineering

April, 2004

The candidate confirms that the work submitted is her own and that appropriate credit has been given where reference has been made to the work of others.

This thesis is dedicated to the memory of Sue Westwood,
who made the early days of my PhD so much fun.

ACKNOWLEDGEMENTS

I would like to thank the following people who have proved invaluable in helping me through this work:

- My supervisors Kenny Dalgarno and Dave Wood for their guidance and support throughout my PhD.
- Nigel Bubb for his technical assistance and for always being readily available to answer my endless questions and provide helpful advice.
- Jon Lorrison, without whom my PhD would have been considerably more dull and certainly less satisfying. His cheerful efforts to introduce me to the joys of the misery machine were particularly appreciated.
- Jonathan Knowles from the Eastman Dental Institute for running numerous X-ray diffraction analyses.
- Richard Lomas, John Keaney, and Mark Eagle at Yorkshire Tissue Bank for performing the *in vitro* cytotoxicty tests.
- Professor Ohtsuki at Nara Institute for Science and Technology, Japan, for hosting me on the JSPS Summer Programme, which allowed me to carry out *in vitro* and *in vivo* bioactivity tests on my samples. All the staff and students that helped me with this work, but in particular to Akari Takeuchi, Takahiro Kawai, and Francisco Balas.
- The organisations that provided funding for the work – the Engineering and Physical Sciences Research Council and School of Mechanical Engineering, University of Leeds for funding my PhD. Also to the Japan Society for the Promotion of Science and British Council for funding my work in Japan.
- Various friends, colleagues, and housemates who helped to make this possible just by providing a distraction from all those hours of sintering and months of writing. Particularly to Jon, whose kept me going the last few months and made the more challenging times a little less stressful.
- My sister Helen, for random phonecalls about cells and things.
- My parents, for their support, both financial and personal, and for their continual encouragement and belief in me in everything I do.

ABSTRACT

The main objective of this work was to determine the feasibility of using indirect selective laser sintering (SLS) to produce parts for bone replacement applications from glass-ceramic materials. A castable glass based on the system $SiO_2 \cdot Al_2O_3 \cdot P_2O_5 \cdot CaO \cdot CaF_2$ that crystallises to a glass-ceramic with apatite and mullite phases was produced, ground to a powder and blended with an acrylic binder at various ratios by mass. An experimental sinterstation with a 250W CO_2 laser was used to determine the viability of indirectly sintering the glass ceramic across a range of processing parameters. Green parts with good structural integrity were produced using a wide range of processing conditions, allowing both monolayer and multilayer components to be constructed. The effect of powder properties, such as glass particle size and binder content, on the surface qualities and structural integrity of the parts was also examined.

Following SLS the parts were post-processed to remove the binder which may otherwise have rendered them unsuitable for biological use, and fully crystallise the material, evolving the apatite and mullite phases to improve both biological and mechanical properties. The parts were heated to 1200°C using a number of different time-temperature profiles, following which the processed material was analysed by DTA, XRD, SEM, μCT, and tested for its flexural strength. An increase in strength was achieved by infiltrating the brown parts with PMMA and a resorbable phosphate glass, although the latter altered the crystal phases present in the material.

In vitro cytotoxicity and bioactivity tests were carried out to assess the biological properties of the produced parts. The laser sintered material was found to be non-toxic by both contact and extract methods. There was no evidence of an apatite layer forming on the surface of the material when soaked in a simulated body fluid suggesting that the material was unlikely to exhibit bioactive behaviour *in vivo*. However, following implantation in rabbit tibiae for 4 weeks, bone was seen to have grown into the porous structure of the laser sintered parts, and appeared to form a close bond with the material surface.

CONTENTS

References

LIST OF FIGURES

LIST OF TABLES

NOMENCLATURE AND ABBREVIATIONS

μCT	Micro-Computed Tomography
3DP	Three-Dimensional Printing
ANOVA	Analysis of Variance
ASTM	American Society for Testing and Materials
A-M	Apatite-Mullite glass-ceramic
A-W	Apatite-Wollastonite glass-ceramic
CAD	Computer Aided Design
CAE	Computer Aided Engineering
CT	Computed Tomography
DMEM	Dulbecco's Modified Eagles Medium
DTA	Differential Thermal Analysis
EDX	Electron Dispersive X-ray Microanalysis
FDM	Fused Deposition Modelling
HA	Hydroxyapatite
HCA	Hydroxycarbonate Apatite
HDF	Human Dermal Fibroblasts
I	Rate of nuclei formation
I_B	Index of Bioactivity
ICDD	International Centre for Diffraction Data
ICP (-AES)	Inductively Coupled Plasma Atomic Emission Spectroscopy
LDIG X	(University of) Leeds Dental Institute Glass X
LG X	(University of) Limerick Glass X
LOM	Laminated Object Manufacturing
LPS	Liquid phase sintering
MG-63	An immortalised human osteoblastic cell line
MRI	Magnetic Resonance Imaging
MTT	3-(4,5-dimethylthiazol-2-yl)-2,5-diphenyltetrazolium bromide
ONT	Optimum Nucleation Temperature
PCL	Poly(ε-caprolactone)
PGA	Poly(glycolic acid)
PLLA	Poly(L-lactic acid)

PMMA	Polymethylmethacrylate
PP X	Post-processing route X
SEM	Scanning Electron Microscopy
SBF	Simulated body fluid
SFF	Solid Freeform Fabrication
SLA	Stereolithography
SLS	Selective Laser Sintering
SSS	Solid state sintering
STL	Standard Template Library
T_g	Glass transition temperature
Tp_n	Temperature at which the nth crystallisation event occurs
TF-XRD	Thin film X-ray Diffraction
U	Rate of crystal growth
UHMWPE	Ultra High Molecular Weight Polethylene
UV	Ultraviolet
VCS	Viscous Composite Sintering
VGS	Viscous Glass Sintering
XRD	X-ray Diffraction

FORMULAE

Fluoroapatite	$Ca_5(PO_4)_3(F)$
Mullite	$Al_6Si_2O_{13}$
Anorthite	$CaAl_2Si_2O_8$
Whitlockite	$Ca_3(PO_4)_2$

LDIG105 (A-M)	$4.5SiO_2 \cdot 3Al_2O_3 \cdot 1.6P_2O_5 \cdot 3CaO \cdot 2CaF_2$
Phosphate glass	$50\%P_2O_5 \cdot 40\%CaO \cdot 10\%Na_2O$
Bioglass®-type glass	$46.1SiO_2 \cdot 24.4Na_2O \cdot 26.9CaO \cdot 2.6P_2O_5$
Commercial glass	$72.6SiO_2 \cdot 1.8Al_2O_3 \cdot 3.8MgO \cdot 7.9CaO \cdot 12.1Na_2O \cdot 0.1Fe$

Chapter 1 Introduction

There is a clinical need for anatomically shaped biomaterials to replace or reinforce skeletal defects resulting from tumours, trauma, disease, wear and congenital defects. Despite the ability of bone to naturally regenerate itself, it can only repair voids up to a certain size and if the defect is too large then a replacement material is required to fill the void and bridge the defect, thus regaining continuity between bone tissues. The current clinical gold standard for bone reconstruction is the autogenous trabecular graft where osseous tissue is taken from another location of the patient's body and transplanted to the defect site. The advantages of these grafts include good and rapid osseous integration, explaining why they are still the method used in more than half of bone grafting procedures [Millennium RG, 2001]. However there are a number of important limitations with these materials including limited availability, donor site morbidity, tendency towards resorption before osteogenesis is complete, and occasionally a compromise in mechanical properties [Jones and Hench, 2001]. Therefore attention is increasingly turning towards the use of synthetic materials as bone substitutes which offer greater availability, reproducibility, and reliability. However creating a synthetic bone replacement material that can accurately mimic the complex, porous structure of human bone tissue is a considerable challenge and has been the subject of much research over recent years.

The rationale for the use of ceramics as bone replacement materials is based on their structural similarity to the mineral phase of natural bone. They are generally well tolerated by tissues, with negligible foreign body reactions and demonstrate good resistance to the corrosive nature of body fluids [Jarcho, 1981]. In addition some compositions of ceramics and glasses have been found to be "bioactive", which means that when implanted into a bony defect they elicit a specific biological response at the bone:implant interface which results in the formation of a direct physicochemical bond with the natural bone. Traditionally synthetic implants have been constructed from biologically nearly inert materials, which are usually encapsulated by a fibrous tissue when implanted into the body. Whilst these materials may have good biocompatibility, the fibrous layer prevents them from bonding directly with bone, and thus problems often arise with loosening of the implants as a secure attachment between the implant and surrounding bone tissue has not been achieved. By using a bioactive material the chances of achieving secure fixation of the implant are increased.

The current problems associated with loosening of implants would be further improved by the production of custom-made and porous implants which would ensure better fits and increase the interfacial area between the implant and bone, thereby reducing the movement of the device in the tissue. At present standard sized implants are selected from a finite range provided by manufacturers and chosen to be the best fit from preoperative radiographs. However with significant variations in skeletal morphology between patients, not every individual will fit into this standard range, with many being between sizes. Furthermore, defects resulting from disease or genetics often demand special requirements. To achieve close fits healthy bone stock is often removed to accommodate the implant, which can lead to problems especially in young patients with device stability and should revision surgery be necessary there may be a shortage of bone to work with. There is therefore a need in both reconstructive and orthopaedic surgery for a method of producing custom made implants at a reasonable cost, thus manufacturing an implant to fit an existing bone, rather than adjusting the bones to fit a standard implant. By creating a custom made implant of appropriate geometry, the time taken to perform the implantation procedure would be reduced and consequently so too would the risks to the patient. In addition they would produce a securer fit, particularly when the device is uncemented, and thus increase the longevity of the device.

In the last twenty years, a series of layer manufacturing techniques have been developed that allow objects of virtually any shape to be built directly from a computer aided design (CAD) representation of the part without the need for specialised moulds, dies, or tooling. This technology is unique in that it uses additive rather than subtractive techniques to build parts on a layer-by-layer basis. Having been mainly developed for consumer products and the automotive industry, these techniques are increasingly being considered and applied in the medical field. At present the main medical application of this technology is in the construction of physical models of patient's bones. There are already a number of established methods of scanning bodies and creating computer images of the human skeletal structure, and the images produced can be converted into three-dimensional computer models. Since these scanning measurement technologies, such as computed tomography (CT) and magnetic resonance imaging (MRI) are also layer based methodologies, the transfer of the imaging data to input data for the layer manufacturing system is relatively straightforward. The produced models can be used for preoperative planning and surgical simulation, allowing surgeons to practice complex procedures before they operate, thus saving time during the actual procedure and reducing the risk to the patient. Communication between the physician, surgeons and patient is improved as the damage to the bone can be seen clearly and thus appropriate treatment can be agreed.

By applying this technology to bioactive materials, there is the potential to produce structures with controlled shape and internal architecture that could be used as bone replacement materials. This would allow a closer fit and reduce the amount of bone tissue to be removed during surgery to accommodate the implant. Complex geometries could be achieved that are not possible by conventional moulding or other fabrication processes, and bones could be designed or CT data modified (as would be useful, for example, in reconstructive surgery). A further advantage of these techniques is the ability to control the internal structure of porous channels producing a highly regular and reproducible interconnected network. Interconnected pores provide a framework for bone to grow into the matrix of the material, increasing the interfacial area between the implant and the tissue, thereby reducing the movement of the implant in the tissue. They also allow a blood supply to reach the connective ingrown tissue thus preventing necrosis of the penetrating cells.

This work has therefore considered the potential for using one of these layer manufacturing techniques, known as selective laser sintering, to produce bioactive implants for use in bone replacement applications. This technique allows complex three-dimensional objects to be built by selectively fusing successive thin layers of the powdered material. An apatite-mullite (A-M) glass-ceramic was chosen as the bioactive material due to its reported bioactivity, good fracture toughness, and mechanical strength [Clifford and Hill, 1996]. Previous work has attempted to directly laser sinter this material with limited success [Lorrison, 2003]. This was attributed to high surface tensions experienced upon melting, a large viscosity change at the glass transition temperature and intra-process crystallisation. However it is thought that by adopting an indirect method where the relatively high melting temperature glass is blended with a low melting binder, polymer-bound "green" parts with superior structural integrity may be produced when laser sintered. These parts can subsequently be post-processed to thermally remove the binder and sinter the higher melting temperature glass.

1.1 Outline of Thesis

The main part of this thesis begins with Chapter 2, where the reader is introduced to the area of research from which this project arose. It aims to provide reference material and review current literature to facilitate understanding of the rationale behind the work, the methods used to meet objectives, and discussion in subsequent chapters of the results achieved. The chapter brings together information of the two main technologies, layer manufacturing and bioceramics, combined in this project to construct bone replacement material of potentially complex geometry. At the end of this chapter the overall aims and objectives of the project are outlined.

Chapter 3 provides a rationalisation of the choice of materials for this work and details the methods used to produce them. It is intended as a reference for the experiments involving these materials that are described in subsequent chapters.

Chapter 4 details the experimental methods used in the production and characterisation of green parts by selective laser sintering. It looks at the effect of powder properties and fabrication parameters on the production of these parts and their resulting mechanical properties and surface qualities.

Following production of green parts by selective laser sintering, post-processing was carried out in order to thermally remove the binder and fully crystallise the material. This is described in Chapter 5, along with details of attempts to infiltrate the parts with a second material in order to increase their strength.

Chapter 6 describes the assessment of the biocompatibility of the glass-ceramic parts produced by indirect selective laser sintering using extract and contact cytotoxicity assays. The ability of the material to form a direct bond with bone tissue is evaluated by both *in vitro* and *in vivo* studies.

The findings from this work are brought together in Chapter 7 where conclusions are drawn and further work suggested.

Chapter 2 Literature Review

The intention of this chapter is to introduce the reader to the area of research from which this project arose. It aims to provide reference material and review current literature to facilitate understanding of the rationale behind the work, the methods used to meet objectives, and discussion in subsequent chapters of the results achieved.

When developing engineered materials for medical applications, it is important to have an understanding of the natural material that the synthetic one is designed to replace. It is therefore deemed appropriate to begin this chapter by considering the roles that natural bone is expected to fulfil, and looking at the way that nature has devised a complex composite structure to provide suitable mechanical and biological properties to meet these demands. It is also important to have an understanding of the formation and growth of bone and the way that it responds to injury and repair.

The next section considers the situations when a bone replacement material may be required and the ideal properties that the material should possess. A brief explanation of how the body responds to the implantation of a foreign material into a bony defect and the interactions that occur between the natural and synthetic materials is presented. The techniques used to secure the implants into bony defects and the consequences of inadequate fixation are considered. It is at this point that the concept of bioactive materials is introduced. This should facilitate understanding of the subsequent discussion of the advantages and short-comings of the materials currently used to repair bone defects, and those being developed. Particular attention is given to developments being made in the area of bioactive glass-ceramics, the material chosen for use in this study.

Section 2.3 introduces the group of manufacturing technologies known as 'layer manufacturing' and the potential advantages of using one of these techniques for the production of custom-made implants is explored. Particular attention is given to selective laser sintering, the layer manufacturing process used in this study. For readers unfamiliar with any of the techniques used to characterise parts produced by selective laser sintering, a brief explanation of the principles of these techniques is given towards the end of this chapter. Finally, the aims and objectives of the work presented in this thesis are outlined.

2.1 Natural bone

Bone is a specialised form of dense connective tissue that serves as the primary structural material for a vast range of vertebrates. As the precise structure and properties of bone has been adapted to suit each particular species, this literature review will focus primarily on human bone.

2.1.1 Functions of Human bone

Human bone has 4 main functions [Martini, 1995]:

- To provide structural support for the body against external forces, e.g. gravity. Bone is also required, either individually or as a group, to provide a framework for the attachment of soft tissues and organs.
- To act as a lever system to transfer the magnitude and directions of the forces generated by skeletal muscles and ligaments.
- To provide protection for vital internal organs and delicate tissues. For example, the heart and lungs are protected by the ribs, brain by the skull, spinal cord by the vertebrae etc.
- To act as a mineral reserve – 97% of the body's calcium is stored in bone. In addition, energy reserves in the form of lipids are stored in areas of yellow marrow.

2.1.2 Composition and Structure of Human Bone

Bone is a composite material containing both organic (35%) and inorganic (65%) components [Martin *et al.*, 1998]. The organic components include cells (osteoblasts, osteocytes and osteoclasts) and 'osteoid', which consists of a collagenous framework set within a glycosaminoglycan gel. This gel contains specific glycoproteins (e.g. osteocalcin) which strongly bind calcium. The collagen molecules are secreted by osteoblasts and self-assemble into bundles of interlacing fine parallel fibrils. There are fifteen different types of collagen in mature bone, each determined by the particular sequence of amino acids in its molecules, although those of Type I are by far the most abundant [Boyd *et al.*, 1956]. The specialised support cells reside either on the surface of bone or within small cavities (lacunae) within the bone.

The inorganic mineral component of bone tissue is predominantly calcium phosphate, $Ca_3(PO_4)_2$, which interacts with calcium hydroxide, $Ca(OH)_2$ to form crystals of hydroxyapatite, $Ca_{10}(PO_4)_6(OH)_2$. These crystals are hexagonal and are arranged in parallel layers that traverse the collagen fibrils. [Weiner and Traub, 1986]. As the crystal particles are significantly larger than the diameter of a single collagen fibril, the crystal layers span several adjacent collagen fibrils [Weiner, 1999]. The hydroxyapatite crystals bond to the collagen fibres via interactions of the polar groups on the protein molecules with the calcium phosphate crystal structure [Lees and Davidson, 1977].

The collagen fibrils are organised into fibres which are typically laid down parallel to one another to produce mature (lamellar) bone. It has been suggested that the fibre orientations alternate from layer to layer [Martin and Burr, 1989], or progressively rotate by about 30° in one direction [Weiner et al, 1999] although the evidence for this is still under debate. Occasionally, if bone is rapidly formed (such as in the foetus or certain pathological conditions for example fracture callus or hyperparathyroidism), the fibres are randomly arranged in an irregular, loosely inter-twined pattern and this is called woven, immature or primitive bone. In foetal bones and in the repair of a fracture, this mechanically weak, disorganised bone is gradually replaced through remodelling and the deposition of more resilient lamellar bone (see section 2.1.5).

Bone is a porous material, and whilst the porosity of mature bone varies continuously between approximately 5-95%, the majority of bone can be considered as being either "compact" (of low porosity) or "spongy" (of high porosity). Compact bone (also called cortical or dense bone) consists of a large number of closely packed, irregularly spaced cylinders of bone, termed osteons or haversian systems, which can be seen in Figure

2.1.2A. These structures are made up of a central osteonic (haversian) canal approximately 200μm in diameter which contains blood vessels and some nerves, surrounded by concentric rings (lamellae) of bony tissue, with the collagen fibres of successive lamellae running at approximately right angles to those in the previous one.

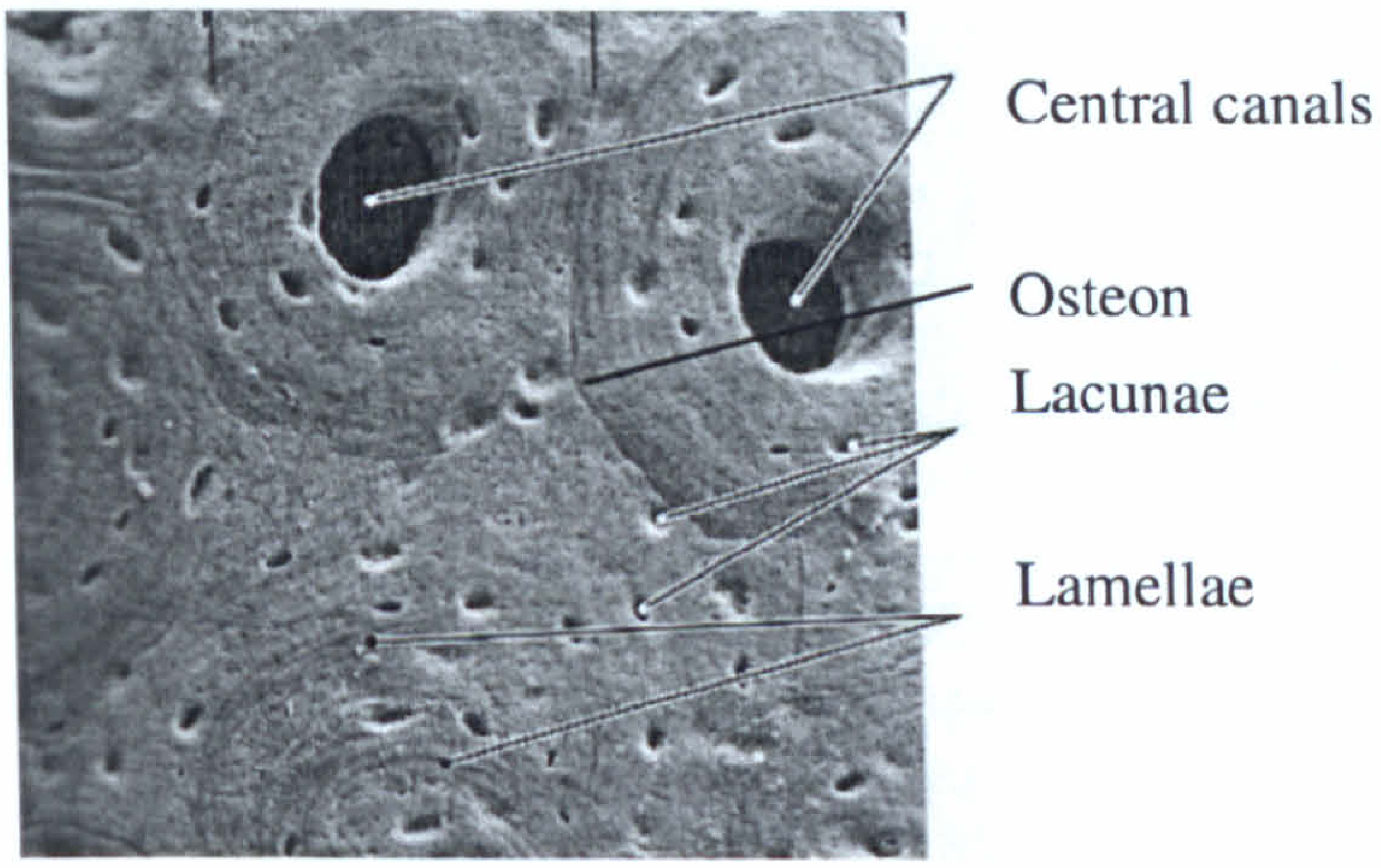

Figure 2.1.2 A: Scanning Electron Micrograph of compact bone [Martini, 1995]

Spongy bone (also called cancellous or trabecular bone) consists of a 3-dimensional pattern of branching plates or struts (trabeculae) approximately 100μm thick [ref.26 in Martin, 1999]. There are no Haversian canals in these structures as they are too thin to contain any osteons. Instead the spaces between the trabeculae are occupied by connective tissue or bone marrow.

Long bones, e.g. the femur, are composed of a rigid outer shell of cortical bone with a porous, cancellous interior, as shown in Figure 2.1.2B. Flat bones, e.g. the calvaria, have a sandwich structure of dense cortical outer layers with a thin, reinforcing cancellous structure within [Rho *et al,* 1998]. Apart from at joints where it is covered with articular cartilage, bone is enclosed in a fibrous outer membrane called the periosteum.

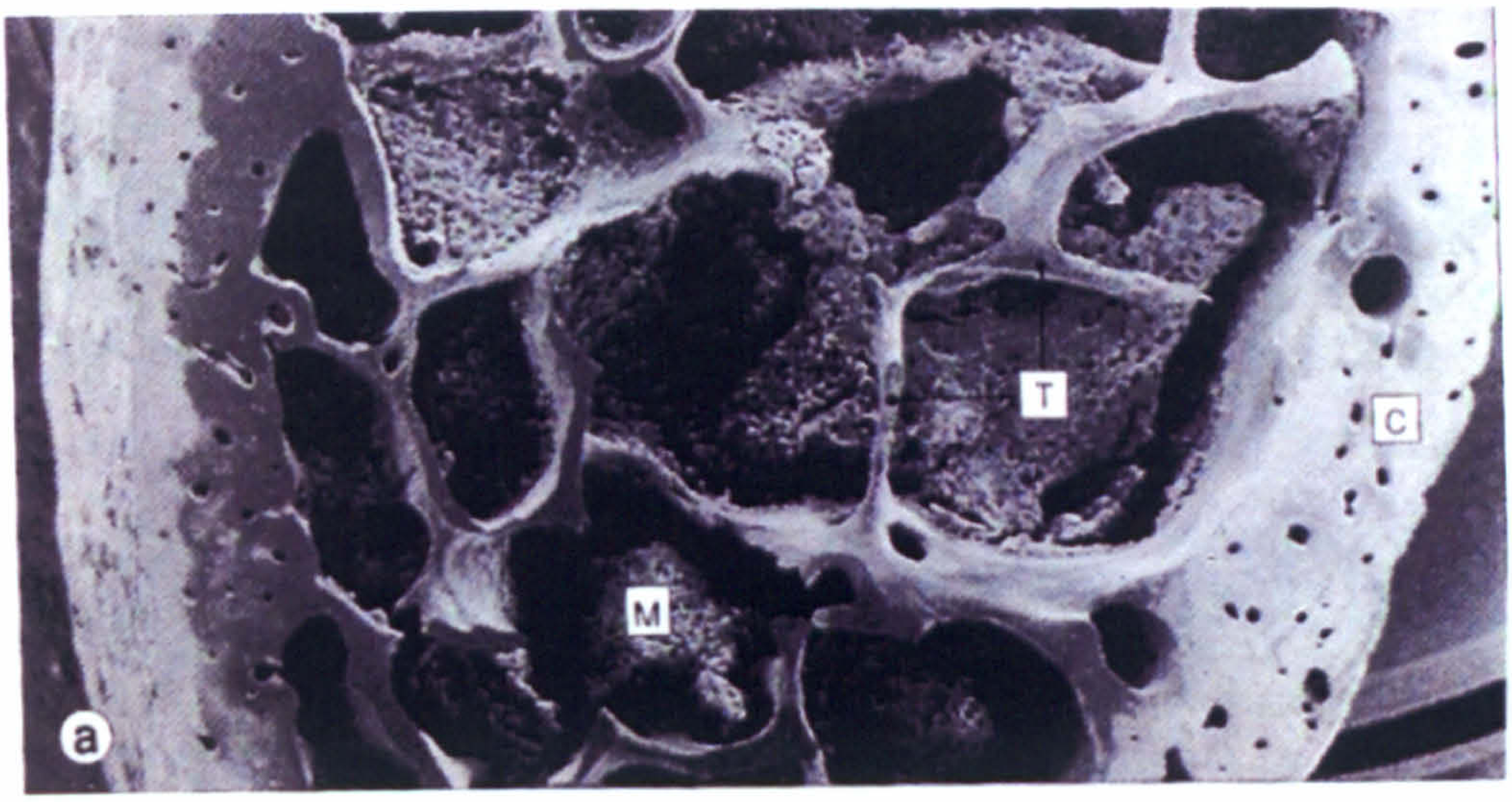

Figure 2.1.2 B – Low power scanning electron micrograph of a cross-section of human bone, showing the compact outer shell of cortical bone (C) bridged by interconnecting plates of trabecular bone (T) [Stevens and Lowe, 1993].

2.1.3 Mechanical Properties of Human Bone

The presence of hydroxyapatite (HA) crystals within the osteoid matrix results in a material with properties intermediate between those of collagen and those of the mineral crystals. The HA crystals give bone its characteristic hardness and rigidity, preventing damage to the bundles of collagen fibres. However, being ceramics, they are relatively inflexible, brittle and have poor impact resistance. They have good resistance to compression, but are susceptible to shattering when exposed to bending, twisting or sudden impacts. The organic components, particularly collagen, are responsible for the flexibility and good tensile strength of bone. They can easily withstand bending and twisting, but have poor compressive strength [Martini, 1995].

The exact mechanical properties of bone are difficult to define, being determined by a number of factors including orientation of collagen fibres, degree of mineralization, and porosity. Not only does the strength of bone depend, like most materials, on the loading regime (e.g. tension, compression, and flexion) and rate of loading, but bone is also anisotropic, i.e. its mechanical properties are dependent on the orientation of the bone structure with respect to the direction of the applied force. Bone is stronger and stiffer in the longitudinal direction, i.e. parallel to the long axis of the osteons, than in the transverse direction. Bone is stronger in compression than in tension, and is weakest in shear. Table 2.1.3A summarises the ranges of strengths of compact bone reported by Yaszemski *et al* [1996], compiled from a number of sources.

Loading Mode		Ultimate Strength (MPa)	Young's Modulus (GPa)
Longitudinal	Tension	78.8-151	17-20
	Compression	131-224	17-20
	Shear	53.1-70	3.3
Transverse	Tension	51-56	6-13
	Compression	106-133	6-13

Table 2.1.3 A: Strength of femoral cortical bone.

The material properties of bone are greatly influenced by its apparent density, that is the mass of bone divided by the bulk volume. Cortical bone has an apparent density of approximately 1.8gcm^{-3}, and is significantly stronger and stiffer than cancellous bone, whose density varies between 0.1 to 1.0gcm^{-3} [Yaszemski *et al*, 1996] and has a reported strength of 5-10MPa and modulus of 50-100MPa. However the modulus or strength of cortical bone is affected proportionally more by changes in porosity than cancellous bone.

Although the mineral content of bone is more consistent than its porosity, changes in mineralization have a greater effect on bone's mechanical properties. Loss of mineralization results in a weaker and less stiff structure with an increased risk of fracture (Wright and Hayes, 1977). The hardness of cortical bone has been linked to the extent of mineralization, and has been found to be 20-25% greater when the bone is tested longitudinally than when tested transversely [Amprino,1958].

Osteonal compact bone has been found to be weaker and less stiff than primary bone [Reilly *et al.*, 1974]. It is thought that this results from the formation of haversian systems which replace the highly mineralised bone matrix, and the subsequent increase in haversian canals also increases the porosity of the structure. However its fracture toughness and fatigue resistance are superior, which has been attributed to the interfaces between lamellae and osteonal cement lines trapping and dispersing cracks into longitudinal directions so as to prevent growth of traverse cracks which may have otherwise led to fracture [Piekarski, 1970].

Bone is viscoelastic, with the strength and modulus both being sensitive to the rate of loading. Increased strain rates have been shown to reduce the ductility of compact bone loaded in compression, but increase the modulus and strength [McElhaney, 1966].

The age and health of the individual may also affect the mechanical properties of their bones. One study found the tensile strength of the human femur to be around 120 MPa at the age of 20, but to decrease to around 65 MPa by the age of 95 [McCalden *et al.*, 1993]. The strength of the tibia however did not exhibit such a marked decrease with age [Burnstein *et al.*, 1976].

2.1.4 Bone formation and remodelling

Bone is formed by specialised cells known as osteoblasts, which are thought to derive from osteogenic stem cells. These cuboidal cells synthesise and release the proteins and other organic components of the bone matrix in a process known as 'osteogenesis'. Following production of osteoid, most osteoblasts return to an inactive state at the surface of the bone, having adopted a flattened and more spindle-like shape. Some osteoblasts however become trapped within the bone they were forming, and end up residing in small cavities (lacunae) in the bone (Figure 2.1.4A). These cells, which are then known as osteocytes, account for most of the cell population and are thought to be involved in the mineralization process. They may also participate in the repair of damaged bone. The lacunae are connected by canaliculi, narrow channels containing long cytoplasmic process that allow adjacent osteocytes to communicate with each other and receive nutrients.

Mineralised bone is resorbed by giant multi-nucleated cells called osteoclasts, which are thought to be derived from hemopoietic stem cells in the bone marrow. They secrete acids and proteolytic enzymes which dissolve the bone matrix and release the stored minerals in a process known as osteolysis.

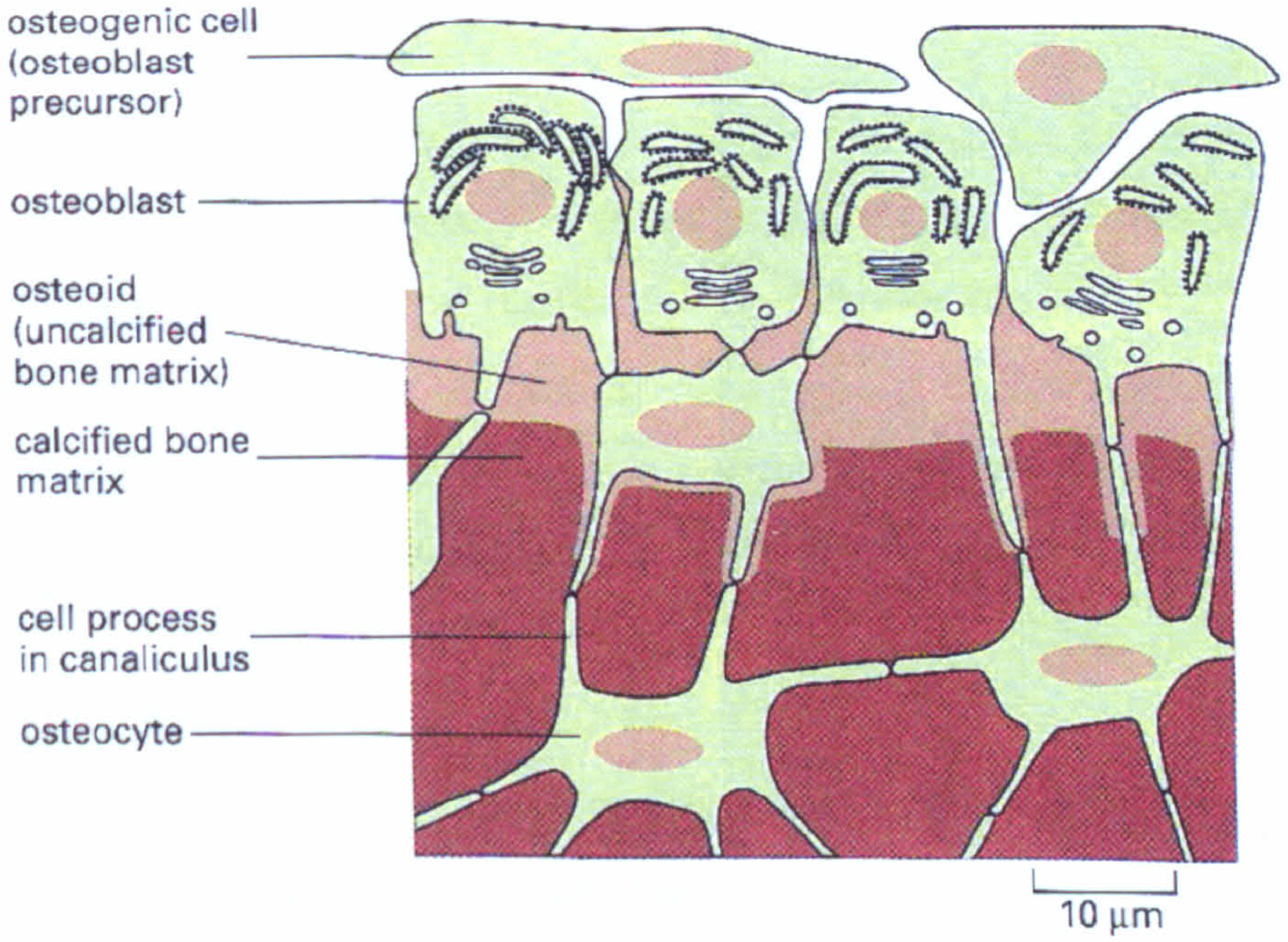

Figure 2.1.4 A: Deposition of bone matrix by osteoblasts [Alberts *et al.*, 1994]

In healthy, mature bone, a delicate balance between the activities of the osteoblasts and osteoclasts allows the organic and mineral components of the bone matrix to be continually recycled and remodelled, without affecting the overall mass of bone [Brighton, 1984]. This process allows bones to maintain or change their shape and size during growth. An imbalance in remodelling leads to metabolic bone diseases such as osteoporosis, which usually occur with ageing.

Bone remodelling is thought to be controlled by cytokines and growth factors which affect the production and activity of bone cells. These include transforming growth factor beta (TGFβ) and insulin-like growth factors (IGFs) that stimulate the formation and activity of osteoblasts, and interleukin-1, -3, and -6, that stimulate resorption. The equilibrium between the activities of the two types of cells can also be changed in response to systemic hormones and mechanical stimuli. If a bone remains immobile for a significant period of time, rapid bone loss occurs due to increased osteoclastic activity. However weight-bearing or other activities that cause more stress than normal to be applied, increases osteogenic activity and hence results in an increase in bone mass. This phenomenon is known as Wolff's law of bone remodelling [Bronzino, 1995].

2.1.5 Fracture Repair

A useful consequence of the constant remodelling of bone is its ability to repair itself following minor injury. The process of fracture healing can be thought of as three overlapping stages: inflammation, repair and remodelling [Ratner *et al.*, 1996]. The sequence and duration of each stage is influenced by local factors such as the degree of local trauma, type of bone affected, and presence or absence of infection as well as more general systemic factors such as age, hormones and nutrition.

Inflammation – Time of injury to 24-72 hours.

Immediately after fracture, extensive bleeding from the fracture site and surrounding tissues causes the formation of a large clot, or fracture haematoma. Platelets in the blood attach to the fibrin clot and release vasoactive mediators, growth factors and other cytokines, which attract inflammatory cells to the fracture site. Polymorphonuclear leucocytes, macrophages and mast cells remove necrotic bone and tissue debris. This is followed by the stimulation of proliferation of the cells necessary for repair of the bone.

Repair – 2 days to 2 weeks

During the reparative phase, osteoblasts derived from both the fracture site and from distant sites transported to it via the bloodstream proliferate and begin to lay down new bone matrix. A soft bridging callus of fibroblasts and proliferating osteoblasts in a collagen rich matrix forms into which new blood vessels grow. Ossification of the matrix leads to the formation of new woven bone.

Remodelling – Middle of repair phase to up to 7 years

Once continuity between the bone fragments has been re-established and the callus has stopped increasing in size, maturation and remodelling of the callus begins. This remodelling starts during the reparative phase, and may continue for up to seven years. During this phase the woven bone undergoes sequential resorption and deposition, gradually being converted to more organised lamellar bone. The balance of resorption and deposition according to the stresses placed on the bone result in the restoration of the bone's original configuration and shape (Wolff's Law).

2.2 Bone Replacement Materials

Bone loss due to surgery, disease, accidents, or normal ageing, can result in both a functional and cosmetic handicap. Although, as has been seen in the previous section, bones are able to regenerate themselves to repair voids up to a certain size, if the defect is too large, a soft connective tissue scar is produced, which impairs bone stability and can potentially lead to fracture of the bone. Therefore a bone replacement material is used to fill the fracture space and bridge the defect, thus regaining continuity between bone tissues. In some circumstances, such as chronic non-healing fractures or for correcting spinal curvature in scoliosis, these materials can also be used to stimulate bone fusion.

Bone is one of the most commonly transplanted materials, second only to blood transfusion [Bhan, 2003]. Bone replacement materials are biomaterials, which are defined as "any substance (other than drugs) or combination of substances synthetic or natural in origin, which can be used for any period of time, as a whole or as a part of a system which treats, augments, or replaces any tissue, organ or function of the body" [Williams, 1987].

Before we consider the materials currently used as bone replacement materials and discuss their suitability for this application, it is important to ascertain the properties that are important in a biomaterial specifically intended for use as a replacement for human bone.

2.2.1 Requirements of a bone replacement material

The most obvious requirement of any biomaterial is that it must be able to perform the function or functions that necessitated its insertion. It is not sufficient for the implant to simply reside or survive in the body. Implants designed to replace lost or damaged bone must regain the mechanical function of the bone by restoring skeletal continuity at the site of disease or injury. They must also stay functional for a reasonable period of time. Our expectations from implants are increasing, and it is no longer sufficient for an implant to alleviate pain and restore some function for a few years – 15 years or more are now generally expected [Jones and Hench, 2001]. As they are implanted in the body and thus only accessible by major surgery, they must be able to survive and remain functional for this time without maintenance.

A material should be selected that has adequate mechanical properties to cope with the forces applied to it, which will depend on the bone that it is intended to repair or replace. The main mechanical properties vital to the roles of bone in the skeleton are strength, toughness, fatigue resistance and lightness. Ideally the material should have similar mechanical properties to the natural bone that it is replacing. If its modulus is too low, it will not be able to withstand the stresses placed upon it; conversely, if it is too high, 'stress shielding' may occur [Bauer, 1999]. It was reported in section 2.1.4 that normal weight-bearing exercise encourages bone formation and if bones are not subjected to these stresses, they will weaken and deteriorate. When a replacement material is used that has a significantly higher modulus than that of natural bone it takes a disproportionate amount of the load, effectively shielding the surrounding bone from stress. This leads to bone resorption around the implant, which in turn can result in loosening of the implant. It was seen in Section 2.1.3 that the strength of bone can vary significantly due to a number of factors. However for the purpose of design goals for replacement materials, strengths of 5-10MPa or 100-150MPa and moduli of 100-150MPa or 10-20GPa are required for replacement of trabecular bone and cortical bone respectively.

Unlike engineering materials used in other applications, those intended for implantation must be able to maintain their mechanical properties in the extremely hostile environment of the human body. A neutral pH, low salt content, and modest temperature may suggest a relatively mild environment, but the body is surprisingly harsh, and resistance to corrosion is an essential requirement for bone replacement materials both to ensure a long life for the implant and to prevent potentially harmful substances from entering the bloodstream. The material must also be able to withstand attack by the body's immune system, which is designed to eradicate invading foreign substances and recognises biomaterials as such.

Another important requirement of any material or combination of materials implanted into the body is that they should be biocompatible. Biocompatibility has been formally defined as: "the ability of a material to perform with an appropriate host response in a specific application" [Williams, 1999]. A biocompatible material does not adversely affect the biological environment within which it is placed, either by irritating the surrounding structures, provoking an abnormal inflammatory response, inciting allergic or immunologic reactions, or causing cancer. At the same time the material itself is not adversely affected by the surrounding host tissues and fluids. However this does not mean that there should be no response, i.e. the material should be inert, as was previously thought. In fact, as we will see in section 2.2.2, no material when placed into the human body is completely inert – there will always be some kind of reaction between the implant and tissues. Moreover, many materials are currently being developed with the intention of producing an "appropriate" response. Whether the response that the material elicits is an appropriate one is dependent on the location of the material within the body, the physical form of the material, e.g. whether it is used in solid or particulate form, and the application for which it is intended [Ratner, 1996]. No material is universally biocompatible. For example, a material that exhibits good biocompatibility when in contact with bone may not do so when used in a blood-contacting device such as an artificial heart valve.

It is important that no particulate or corrosion debris is generated, which may cause local tissue reactions or, in some cases, induce malignant tumours [Revell *et al.*, 1997]. The material must be able to be sterilised before implantation to avoid infection, and the method carefully selected so as not to affect the properties of the material.

The methods used to manufacture the implants and secure them into the defect must also be considered. The replacement material should be easily formed into sometimes complex shapes, and must be able to be implanted quickly with minimal damage to the surrounding tissues or the surface of the material. Skeletal morphology can vary significantly between patients. Therefore in order for minimal skeletal adaptation to be necessary, the material must be readily modifiable either by the manufacturer prior to surgery or by the surgeon during implantation. Ideally a processing technique should be used that allows the production of an implant that exactly matches that of the defect in the bone of the patient, i.e. a custom made implant, a particular aspiration that the work presented in this thesis will be addressing.

Fixation of the material into the defect is very important as loosening between the material and surrounding bone is currently the main reason for skeletal implant failure. The methods presently used in the fixation of artificial materials and the developments being made to improve these will be discussed in detail in Section 2.2.3. The implanted material should allow bone to grow right up against it, a process known as 'osseointegration'. The chances of achieving secure fixation of the implant are increased by using a bioactive material. Bioactivity refers to the ability of certain materials to form a direct physicochemical bond with bone. Ideally, in order to ensure the implanted material is tightly secured into the defect, a material that acts as an osteoconductive scaffold is required [Çehreli *et al.*, 2003]. Osteoconduction supports ingrowth of bone into the three-dimensional structure, therefore providing maximum integration of the surrounding natural bone into the implanted material. To achieve this, a fully interconnected porous matrix conductive to resorption and new bone formation is required. By using a porous implant the interfacial area between the implant and the tissue is increased, thereby reducing the movement of the device in the tissue. Although still subject to much debate, pores in the approximate range of 100 to 600μm appear to be required for mechanically strong bone ingrowth [Klawitter *et al*, 1971]. The ideal pore shape and size has been shown to be specific for different cell types [Burg *et al*, 2000]. A minimum pore size of 100μm is necessary for cell penetration, tissue ingrowth and vascularisation. Re-establishment of a vascular supply is required for the delivery of nutrients, cellular precursors, and bioactive molecules to the regenerating bone, and for the removal of metabolic wastes and necrotic debris. High porosity can however adversely affect the mechanical strength and reliability of implants, which is an important consideration if the material is intended for use in load bearing applications.

Ideally the material should be resorbable, initially re-establishing the mechanical integrity of the injured skeleton, but then gradually resorbing as natural bone is produced. It is important however that the material resorbs in such a way that only non-toxic degradation products are produced that can be easily excreted or metabolised via normal physiological mechanisms.

2.2.2 Response of the body to implantation of a foreign material

When a biomaterial is implanted into the human body a sequence of events are initiated similar to the normal process of wound healing [Fig 2.2.2A]. A number of factors influence the duration and intensity of each of these events including the extent of injury caused by insertion of the implant, the chemical and physical properties of the material used, and the geometry of the implant [Anderson, 1998]. The degree to which these factors cause deviation from the optimal wound healing largely determines the biocompatibility of the material.

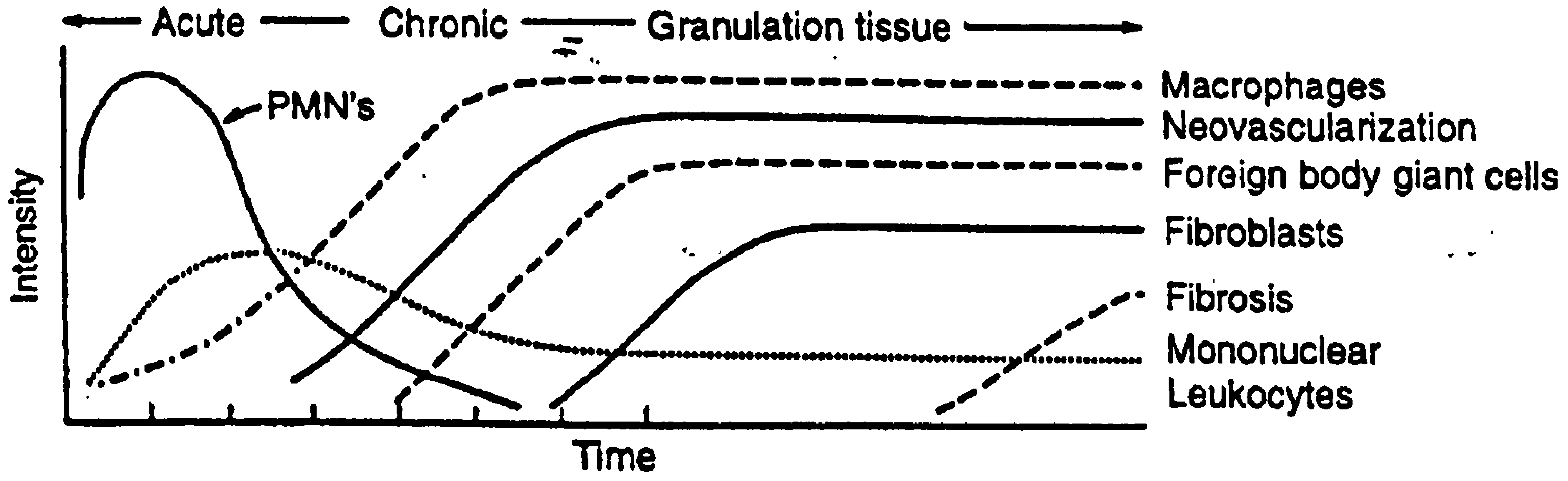

Figure 2.2.2 A: The temporal variation in the acute inflammatory response, chronic inflammatory response, granulation tissue development, and foreign body reaction to implanted biomaterials [Anderson, 1998]

Implantation of a biomaterial into bone causes extensive bleeding from the implantation site and surrounding tissues as a result of the surgical trauma [Anderson, 1998]. This triggers an inflammatory reaction which serves to isolate, dilute, or neutralise the article causing the injury. Acute inflammation, which depending on the severity of the injury lasts from minutes to days, is characterised by the exudation of fluid and plasma proteins, and migration of leukocytes (predominately neutrophils) to the implant site. Here activation of neutrophils and macrophages causes phagocytosis and enzyme release to occur. Generally they are not able to completely engulf and degrade biomaterials due to the disparity in their size, but the early processes of phagocytosis, such as recognition and neutrophil attachment still occur. In addition 'frustrated phagocytosis' may occur, whereby leukocyte products are released in an attempt to degrade the biomaterial even though they are unsuccessful in completely engulfing it.

Studies have suggested that the amount of such products released is dependent on the dimensions of the implant, and that greater amounts are released for materials in phagocytosable form, e.g. powder or particulate than when the same material is present in bulk [Henson, 1971]. Persistence of an inflammatory stimulus, either due to the chemical and physical properties of the biomaterial or from motion of the material in the implant site, gives rise to chronic inflammation. This response, characterised by the presence of macrophages, monocytes, and lymphocytes tends to be shorter in duration and confined to the implant site.

A reparative response follows two to three days after implantation, initiated by the action of monocytes and macrophages. Granulation tissue, so-called because of its pink, soft granular appearance, forms on the surface of the healing wound and is characterised by numerous small blood vessels and fibroblasts. The blood vessels are formed by budding of existing vessels in a process known as neovascularisation that involves the proliferation, maturation, and organisation of endothelial cells to form new capillaries. The fibroblasts proliferate and synthesise initially predominately proteoglycans, but later predominately collagen, mainly of type III, to form a fibrous capsule. Granulation tissue also usually contains macrophages and monocytes which fuse to form foreign body giant cells which attempt to phagocytose the implant.

The form and topography of the surface of the implanted material determines the type and amount of cells involved in the foreign body reaction. For example relatively flat and smooth surfaces have a foreign body reaction composed of a layer of macrophages one to two cells thick, whereas that of rough surfaces consists of macrophages and foreign body giant cells at the surface. These cells may remain permanently at the tissue-implant interface, although whether they remain activated or become quiescent is uncertain. The final event in the healing process is usually the formation of a fibrous capsule around the biomaterial, which isolates it from the surrounding bone. This occurs when adjacent parenchymal cells are replaced by connective tissue, as being permanent cells they are unable to reproduce themselves. A fibrous capsule does not form in all cases. Titanium alloys, for example, are able to become in direct contact with the regenerated bone without the formation of a fibrous capsule [Johansson *et al.*, 1989].

All materials implanted in living tissues elicit some kind of response. Four general categories of materials have been defined, depending on the type of interfacial reaction that occurs when they are implanted - toxic, biologically inactive (nearly inert), bioactive, and resorptive [Hench and Wilson, 1993].

Toxic – Materials that exhibit a toxic response are obviously unacceptable as implant materials. Toxicity may be acute or chronic. Acute toxicity occurs immediately following implantation, with the end result being either death or complete recovery. Chronic toxicity may not be immediately apparent and may not have a specific effect. It usually takes longer to develop and results in general prolonged illness. One way that chronic toxicity can arise is from prolonged or repeated administration of a toxic substance, as occurs with the gradual release of metal ions from a corroding metal implant. Highly toxic materials cause tissue necrosis. Rejection of the implant is normally signified by the presence of a large number of foreign body giant cells and phagocytes, whilst activation of the immune system is denoted by the propagation of lymphocytes. The *in vitro* evaluation of the toxicity of an implanted material using cell culture techniques is called cytotoxicity, the general principles of which are described in section 2.5.7.

Biologically inactive (nearly inert) – The tissue response to a biologically inactive, nearly inert implant is to encapsulate it with a non-adherent fibrous tissue which isolates it from the surrounding bone. The fibroblasts that lay down this tissue are affected by enzymes of activated macrophages, so as long as phagocytic activation is maintained, the thickness of the capsule will increase. The ideal scenario is for the material to be covered by bone tissue rather than a fibrous layer, but this is rarely the case. A thick fibrous capsule reflects poor biocompatibility. A number of factors influence the thickness of the fibrous layer including the conditions of the implant, host tissue, and motion and fit at the interface, and the mechanical load [Cao & Hench, 1995]. For example a chemical stable material such as alumina will be encapsulated by a very thin interfacial fibrous layer under an optimal mechanical fit, whereas more chemically reactive metallic implants will elicit layers of greater thickness. The presence of a fibrous layer prevents any chemical or biological bonds forming between the biomaterial and bone tissue, allowing movement at the interface. This movement, known as micromotion, causes further development of the fibrous capsule which eventually results in deterioration in function of the implant. When the fibrous capsule becomes several hundred micrometers thick, the implant can loosen in the defect which invariably leads to failure for example through fracture of the implant or the bone adjacent to it.

Bioactive - Certain compositions of glasses, ceramics, glass-ceramics, and composites have been shown not to form this fibrous tissue, but instead form a silica hydrogel layer on their surface that, fuelled by consuming calcium and phosphate ions from the surrounding body fluid, allows subsequent crystallisation of an apatite-like phase [Hench, 1994]. As the composition and structure of this apatite is very similar to that in bone, osteoblasts are able to preferentially proliferate and differentiate to produce both apatite and collagen on this layer thus allowing the bone to come in direct contact with the implant via its surface apatite layer, without the intervention of the fibrous tissue layer, and form tight chemical bonds with the bone. This allows the development of a much greater interfacial adhesive strength. The phenomenon of bioactivity will be discussed in more detail in Section 2.2.5.3.

Resorbable – Resorbable implants are degraded gradually by the biosystem of the organism and replaced by natural osseous tissue. This results in a very thin or even non-existent interfacial thickness. To be successful biomaterials, resorbable materials should be able to maintain the strength and stability of the interface during degradation and replacement, and have a similar resorption rate to the repair rates of body tissues. It is also important that dissolution occurs without toxicity or rejection. Examples of these materials include tricalcium phosphate, porous HA, calcium phosphate salts, certain bioglasses, and polyurethane.

It is worth noting however that biomaterials may be toxic, biologically inactive, bioactive or resorbable to various degrees and that a definite distinction between the four types of material does not always exist. This is demonstrated by variations in the thickness of the fibrous capsule forming around biologically inactive materials, with less bioinert materials such as stainless steel having a considerably thicker fibrous tissue layer than more bioinert materials such as alumina. The type of interfacial reaction that the material elicits upon implantation determines the means possible to achieve attachment of the implant to the surrounding bone.

2.2.3 Implant fixation techniques

A prerequisite for the success of a bone replacement material is permanent fixation of the implant into the defect. Achieving and maintaining a stable interface between the biomaterial and host tissue has proven to be a considerable challenge, with loosening currently being the main reason for skeletal implant failure. There are three main types of fixation technique – morphological, biological, and bioactive fixation.

2.2.3.1 Morphological fixation

Morphological fixation techniques are used for dense, non-porous, biologically inactive materials such as metals or alumina. Implants are secured through bone growth into surface irregularities either by press-fitting the implant into the defect [Cameron, 1994a], cementing it in using, for example, PMMA bone cement [Charnley, 1979], or by using threaded components [Albrektsson *et al.*, 1994]. These methods have the advantage that they provide instant stability and therefore allow immediate weight-bearing. As was reported in section 2.2.2, when implanted into bone tissue, biologically inert materials are encapsulated by a non-adherent fibrous layer. It is therefore imperative that a tight mechanical fit is achieved by this fixation method, as if any movement occurs at the implant-tissue interface, the fibrous layer thickens causing the implant to loosen which in turn can lead to failure of the implant. Bone cement functions as a grouting material, hence the strength of the cement-bone interface depends on the ability of the cement to penetrate between bone trabeculae resulting in a form of mechanical interlocking as no chemical bond between the cement and bone occurs [Charnley, 1979]. Its minimal adhesive properties also means that undercuts, holes or furrows are required in the implant material to achieve a secure attachment between the cement-implant interface. The use of bone cement creates both bone-cement and cement-implant interfaces, with the possibility of problems of mechanical failure and instability occurring at either one. An advantage however of these materials is that being viscoelastic polymers they can function as shock absorbers, allowing uniform transmission of loads between the implant and bone, thus reducing localised high-contact stress [Ramakrishna *et al.*, 2001]. The most widely used bone cement is based on poly(methylmethacrylate) PMMA, which is also known as acrylic bone cement. This self-polymerising material is made up of solid PMMA powder and a liquid MMA monomer. Concerns have been raised about the possible release of cytotoxic monomers into the blood stream and the highly exothermic reaction that occurs with the polymerisation of methylmethacrylate, which results in elevated temperatures in excess of 70°C in the tissues and may also induce local bone necrosis [Block *et al*, 1970]. Polymerisation can also cause undesirable shrinkage of the polymer. Due to poor fatigue strength, attempts have been made to improve the mechanical properties of bone cement by reinforcing it with fibrous materials such as UHMWPE [Wagner and Cohn, 1989] and carbon fibres [Saha and Pal, 1986]. However due to difficulties such as achieving uniform distribution of fibres, and the significant decrease in workability due to the increased apparent viscosity of bone cement, reinforced cements are not yet used in clinical practice.

2.2.3.2 Biological Fixation

Biological fixation is achieved by using materials with textured or porous surfaces that allow tissue ingrowth, thus stabilising the implant. This fixation method allows implants to withstand more complex stress states than if morphologically fixed. Ideally pores should be interconnected and greater than 100-150μm in diameter in order to provide a blood supply to the host tissues. The ingrown tissues should also be subjected to mechanical stresses to prevent resorption. The drawback of using this method as the sole fixation technique however is that the strength of the fixation is dependent on bone growth which usually takes at least twelve weeks before it can be completely weight-bearing. Also the higher porosity content results in implants with lower mechanical strength and reliability, reducing their ability to function as load-bearing components. Whilst the increased interfacial area between the implant and bone results in increased resistance to implant motion, if loosening does occur and the prosthesis is required to be replaced, porous ingrowth implants are notoriously difficult to remove and can cause considerable damage to the surrounding bone. Furthermore, ingrowth into porous implants is most successful in conditions where there is near normal bone mass. However replacement materials are commonly implanted into areas where the surrounding bone has been affected by disease or injury. For these reasons, some researchers believe that the use of bone cement is still presently the gold standard for fixation of implants into bone [Johnston, 1987].

2.2.3.3 Bioactive Fixation

Bioactive materials, which are discussed in more detail in section 2.2.6, achieve fixation by forming direct physiochemical bonds with the bone tissue without the formation of a fibrous capsule. Often the bonding is so strong that removal of the implant cannot be achieved without breaking the implant or bone [Strnad, 1992]. A number of bioactive materials are now known including bioactive glasses (e.g.Bioglass®), bioactive glass-ceramics (e.g. Ceravital®, AW glass-ceramic, or machinable glass-ceramics), dense hydroxyapatite (e.g. Durapatite® or Calcitite®), or bioactive composites (e.g. polyethylene-Bioglass®, polysulfone-Bioglass®, and polyethylene-hydroxyapatite (Hapex®) mixtures) [Hench, 2002]. For the various bioactive materials, the time dependence of bonding, the strength of the bond, the mechanism of bonding, and the thickness of the bonding zone are different [Hench, 1991].

2.2.4 Current bone replacement materials

The gold standard for replacement of human bone tissue is a type of tissue graft known as an autograft. This procedure involves taking bone fragments from an undamaged portion of the patient's body (usually the hip, pelvis, or ribs) and transplanting it into the damaged area. Although these materials exhibit good biocompatibility and can closely replicate the structure of human bone, they tend to be brittle and when sterilised, experience a significant loss of strength [Damien *et al.*, 1999]. Other drawbacks include the limited volume of available bone, the additional surgery required and pain caused by taking bone from an undamaged area, and the time required for the bone to heal. Often the newly formed bone will not take the exact shape of the original damaged bone.

The use of allografts, a similar procedure except the bone used is taken from a cadaver rather than the patient, overcomes many of these limitations, but introduces several of its own. There is a greater chance that the bone will be rejected by the body as a foreign tissue, as well as the risk of transfer of infectious diseases such as HIV and hepatitis.

Concerns over the use and availability of autogenous and allogeneic bone graft materials have resulted in the development of artificial materials. The most common of these are rigid internal metal plates, which have the advantages of a long clinical history, are reasonably cheap, and are easy to produce and shape [Gogolewski, 2000]. The plates are usually formed to the approximate morphology of the implant site prior to implantation, then adapted intra-operatively by the surgeon who manually bends the plate into the exact shape and fixes it to existing bone by means of retaining screws (Riden, 1998). Drawbacks of this procedure include the large difference in Young's moduli between metal implants and bone which can cause stress-shielding, the reduction of the blood supply at the implantation site, the potential for corrosion, wear and debris formation, the need for mechanical fixation, and the fact that the plates, by not actually replacing the removed bone tissue, do not possess the desired characteristic of filling the void with a structure that would encourage tissue re-growth and revascularisation [Gogolewski, 2000; Riden, 1998].

For these reasons, attention has turned towards bioceramics and glasses as alternative synthetic bone replacement materials. Examples of bioactive glass-ceramics currently available to surgeons include Cerabone® (apatite-wollastonite), Ceravital® (apatite-devitrite) and Bioverit® I (mica-apatite), and the most commonly used bioactive glass is Bioglass® which is used for middle ear devices and implants for the orbital floor [Höland and Beall, 2002]. The replacement materials are moulded to fit into the defect, and generally held in place by pins, plates or screws. The applications of Cerabone® A-W are shown in Figure 2.2.4A.

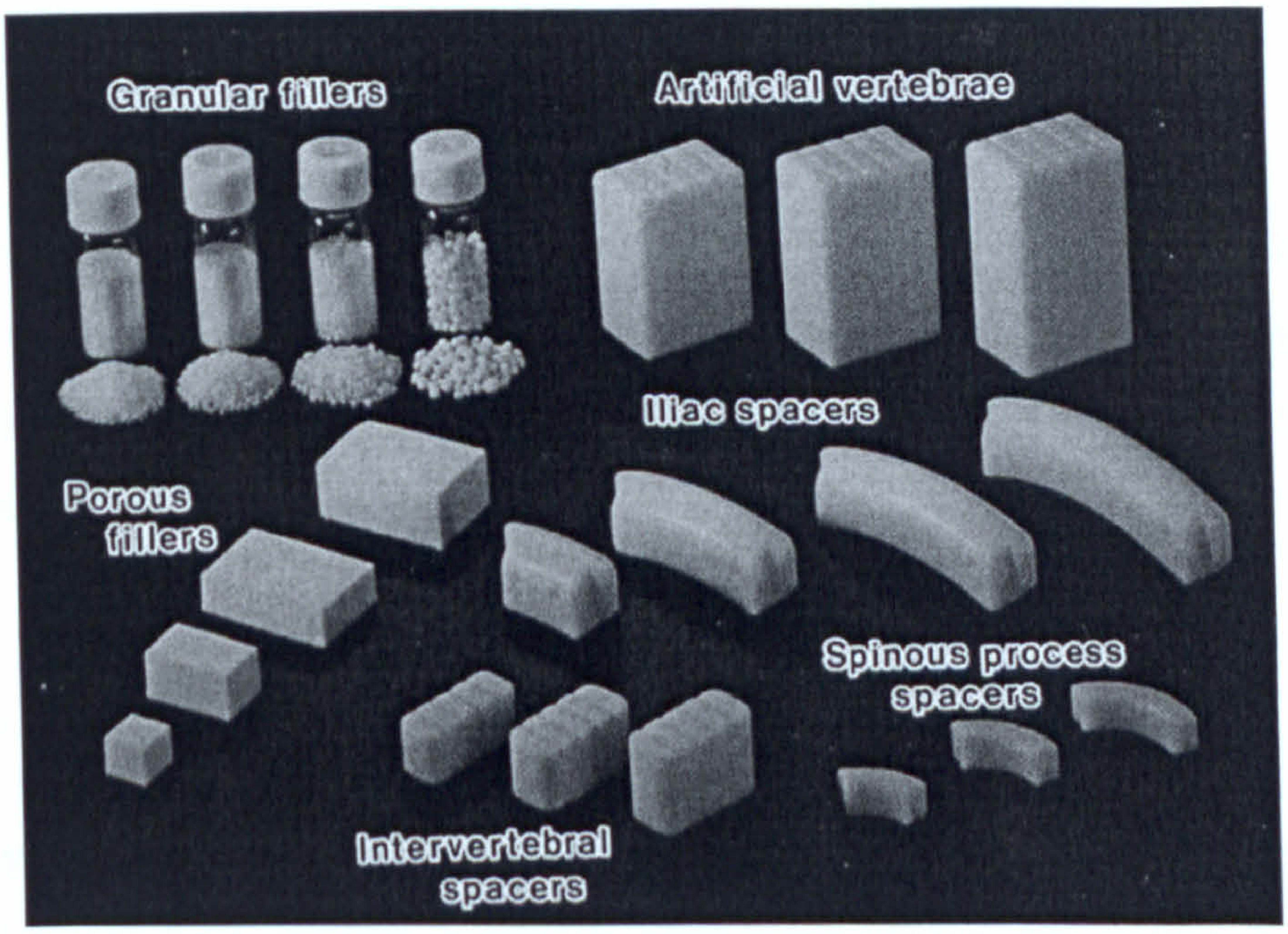

Figure 2.2.4 A: Artificial vertebrae, spacers, and fillers made from Cerabone® A-W [Holand and Beall, 2002]

2.2.5 Candidates for bone replacement materials

In deciding on a material for this work, it was necessary to consider the range of materials available to us, including both natural and synthetic materials.

2.2.5.1 Natural Materials

Autografts and allografts, the most obvious candidates for replacement of damaged bone are currently in use and their advantages and disadvantages have already been discussed. A third option is the use of xenografts, transplanted from the bone of another animal. In particular, researchers have looked at bovine apatite [Lin *et al.*, 1999], bovine and porcine collagen [Badylak, 2004], and sea coral, thermally converted into calcium carbonate [Merkx *et al., 1999*]. These materials are much more widely available than human bone and reduce the amount of surgery required. There are however significant drawbacks with xenografts, such as weak, unpredictable mechanical strength, a risk of transmission of infection, and strong immunological reactions by the patient to the transplanted tissue due to its foreign proteins.

2.2.5.2 Synthetic materials

The concerns over the use of natural materials have turned interest to the development of alternative synthetic substitutes. There are four general classes of synthetic materials from which an implant could be fabricated; these are metals, polymers, ceramics and glasses, and composites.

2.2.5.2.1 Metals

Metals have long been used as implant materials for orthopaedic applications due to their good mechanical strength, hardness, reasonable fatigue life within the body, and relative ease of manufacture. Metallic alloys are generally used rather than pure metals and are based on three alloy systems – cobalt chromium, stainless steels, and titanium alloys.

At present, metals are the only materials capable of withstanding the mechanical demands of load-bearing situations. However they generally cannot physically bond to bone tissue and therefore act as biologically nearly inert materials, with a fibrous capsule forming around the implant upon implantation. As was explained in Section 2.2.2 this can lead to loosening of the implant. Attempts have been made to improve their integration with natural bone by coating the metal implants with hydroxyapatite, a bioactive ceramic material similar in nature to bone tissue [Geesink *et al.*, 1988]. The thickness of this layer must be strictly controlled. The coating should be thick enough to provide sufficient material for forming a bond with the surrounding bone tissue, taking into account the possibility that the apatite surface may dissolve by 10-15 microns during the first few months whilst trying to achieve bone union. However the mechanical properties deteriorate with increasing coat thickness, with coatings greater than 100-150 microns at an increased risk of suffering from fatigue failure under tensile loading. In many cases, achieving a secure bond between the coating and the bulk material has proved very difficult, with poor adhesive strength leading to delamination and wear of the hydroxyapatite layer [Hardy *et al.*, 1991; Buma and Gardeniers, 1995].

Certain titanium alloys are exceptions and do not form a fibrous capsule but instead become fully integrated with natural bone due to an unreactive layer of oxide that forms on their surface [Adell *et al*, 1986]. Titanium alloys also have the advantage of a lower modulus than the other implant metals, reducing the effects of stress shielding. However there are great concerns about the significant amount of metallic wear debris produced by titanium alloys [Friedman *et al*, 1994].

The production of wear debris is one of a number of concerns with the use of metals as implants. Body fluids are extremely corrosive, which is of great concern for metal alloys, leading not only to an obvious loss in mechanical strength in the material, but the corrosion products when released into the tissue can have a number of adverse physiological effects such as metal sensitivity, allergic reactions and neoplastic effects. Wear debris, resulting from articulating surfaces can have similar effects. There is a considerable mismatch between the moduli of metal implants and that of bone, which leads to problems of stress-shielding and bone resorption around the implants.

For these reasons, metals are not considered ideal materials for use as bone replacement materials. However due to their mechanical strength they are currently, and will probably remain in the short to medium term, the primary materials to be used in load-bearing situations.

2.2.5.2.2 Polymers

Whilst polymers are easily shaped at low cost and many are biocompatible, their use in orthopaedic applications has generally been limited due to insufficient strength. However where they have proved useful is as one of the articulating surface components in joint prosthesis, and for fixation as a structural interface between the implant component and bone tissue.

Ultrahigh molecular weight polyethylene, UHMWPE, is used as the acetabular component in artificial hip joints and the tibial plateau component in artificial knee joints. A high density form of polyethylene is used as the low density material is unable to withstand the temperatures required for sterilisation of implants, and the high density form also exhibits superior wear characteristics. However whilst UHMWPE has excellent physical and chemical properties in the short term, it will creep and exhibits fatigue failure in the longer term. As a relatively soft material it is able to absorb some of the cyclic implant stresses that are placed on the joint and facilitates smooth articulation of the bearing surfaces. However with the opposing surface commonly constructed from a metal or ceramic, the mismatch in surface hardness leads to the generation of UHMWPE wear debris, which has been found in some cases to lead to osteolysis (bone cell death) and loosening of the implant [Kurtz *et al.*, 1999]. Whilst creep occurs significantly less in UHMWPE than in low molecular weight polyethylenes, it still occurs to a significantly greater extent than in metal or ceramic materials, or in cortical bone. In addition it may cause the patterns of stress transfer to change, affecting the body's ability to maintain appropriate bone density adjacent to the implant [Davidson and Schwartz, 1987]. UHMWPE is a biologically inactive material and thus is fixed in place using bone cement.

Self-curing acrylic bone cements based on poly(methylmethacrylate), PMMA, are the other major use of polymers in orthopaedic applications. The advantages and drawbacks of these materials have been discussed previously, in section 2.2.3.1.

The potential to use polymers as bone replacement materials arises from:

a) the ability to tailor their composition and structure to suit a specific need, thus providing great design flexibility, and
b) their ability to undergo controlled degradation.

The former can be achieved by combining different monomers to form copolymers, controlling the extent of polymerisation or cross-linking between adjacent polymeric chains, or from the incorporation of chemical additives [Brown *et al.*, 1999]. Biodegradation is "*the gradual breakdown of a material mediated by specific biological activity*" [Brown *et al.*, 1999]. A number of processes are involved including dissolution, hydrolysis, and enzyme degradation. It is essential that the breakdown products are non-toxic, and ideally they should be naturally occurring compounds. They must have high initial strength and a controlled reduction in mechanical properties. A large number of polymers have been investigated for potential use in this area, with the majority of current research focusing on three poly(α-hydroxy esters) – poly(L-lactic acid) (PLLA), poly(glycolic acid) (PGA), and poly(lactic-co-glycolic acid) (PLGA). These materials have proven biocompatibility and a long history as degradable surgical sutures. However their potential use as bone replacement materials is limited by their high flexibility and low strength.

2.2.5.2.3 Ceramics and Glasses

Ceramic materials were first used for bone substitution in 1963 [Damien and Parsons, 1990]. Since then they have been playing an increasing role in implant technology. This is hardly surprising since their composition is the most similar to the mineral component of bones. In addition they are well tolerated by tissues, with negligible foreign body reactions and demonstrate good resistance to the corrosive nature of body fluids [Jarcho, 1981]. They are low in density, hard-wearing and demonstrate high strength under compressive load. However it is primarily the brittleness of ceramics that precludes their wide use at present. Also, due to their generally extremely high melting points and limited ductility, they cannot be easily worked or shaped.

Ceramics used as biomaterials are termed bioceramics, and can be biologically inactive (e.g. alumina, zirconia), resorbable (e.g. tricalcium phosphate), bioactive (e.g. hydroxyapatite, bioactive glasses, and glass-ceramics), or porous for tissue ingrowth (e.g. hydroxyapatite-coated metals, alumina). A comparison of the relative rate of bioreactivity (A) of the different types of bioceramics, glasses, and glass-ceramics, and the time dependence of formation of bone bonding at the implant interface can be seen in Figure 2.2.5A.

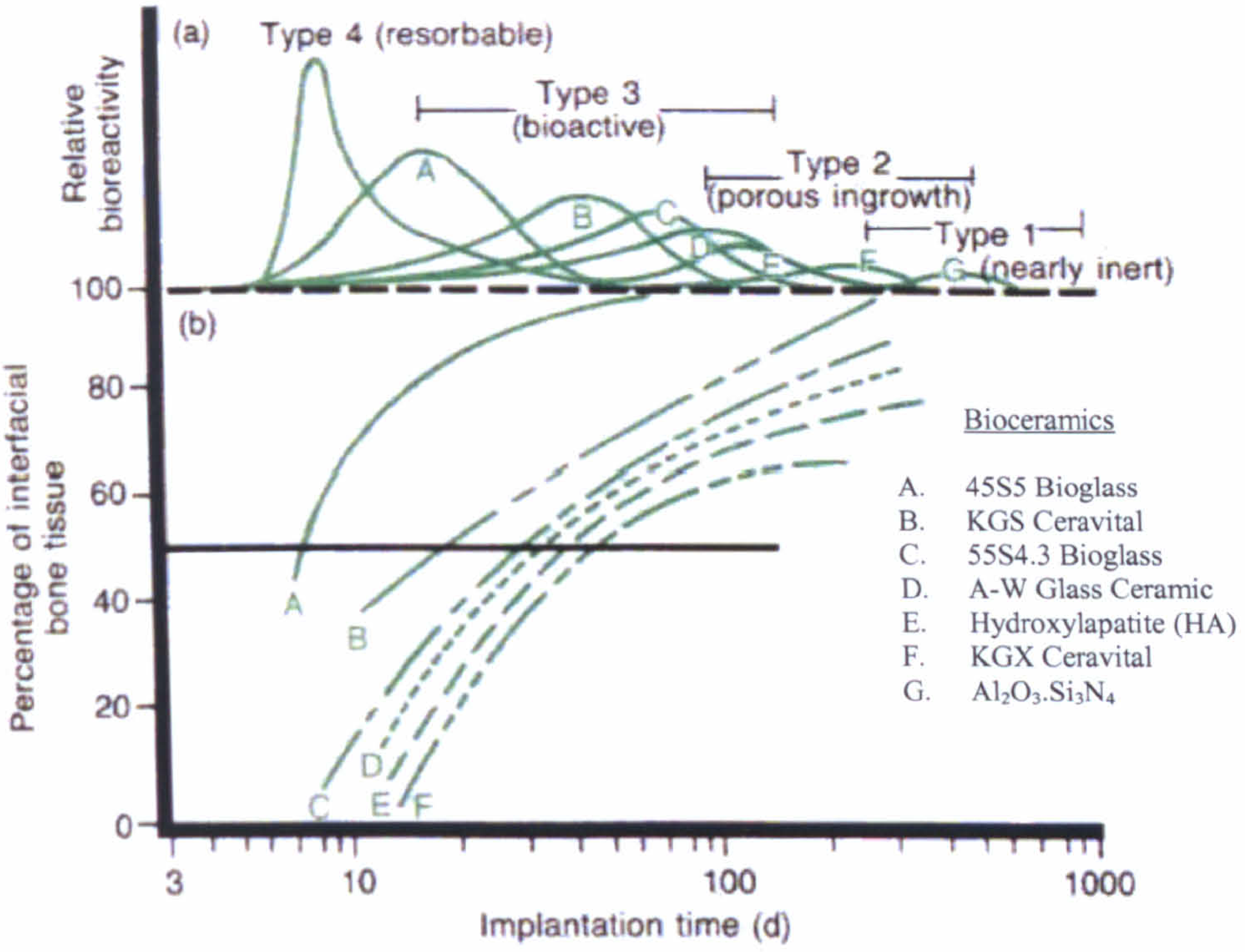

Figure 2.2.5 A: Bioreactivity of various bioceramic implants [Hench and Wilson, 1993]

Different thermal processing routes used to produce bioceramics result in five types of bioceramic each with different microstructures [Ratner, 1996]. They are:

1. Glass
2. Cast or plasma-sprayed polycrystalline ceramic
3. Liquid-phase sintered (vitrified) ceramic
4. Solid-state sintered ceramic
5. Polycrystalline glass-ceramic

The current work is concentrating on glass ceramics, so called because they are made in a glassy state and then converted to a polycrystalline ceramic by controlled devitrification.

2.2.5.2.3.1 Glass-ceramics

Glass-ceramics are a class of ceramic material formed through the controlled crystallisation of a base glass. Crystallisation is achieved by subjecting the base glass to a carefully regulated heat-treatment schedule, resulting in the nucleation and growth of crystal phases within the glass. The resulting glass-ceramic consists of at least one glass phase and one crystal phase and has superior mechanical properties to those of the base glass from which it was formed [Thompson, 1998]. The reason for this is that unlike in glass which is amorphous, crystalline ceramics contain structural discontinues or grain boundaries at points were the crystals meet, which act as an impediment for fracture propagation by causing deflection, branching, or splitting of the cracks.

Crystallisation is a nucleation and growth process. Submicroscopic nuclei are formed in the base glass and grow into macroscopic crystals to form a polycrystalline ceramic. Nucleation may be either homogeneous or heterogeneous. In homogeneous nucleation, the resulting crystals are of the same constitution as the nuclei that initiated their formation, whereas in heterogeneous nucleation the crystals are often chemically quite different. Homogeneous nucleation occurs when a new phase develops in the absence of any foreign boundaries (e.g substrates or phase boundaries) as a result of local fluctuations of density and kinetic energy. This is extremely difficult to achieve experimentally as there must be no dust particles or other foreign bodies in the material that would result in nucleation becoming heterogeneous. Homogeneous nucleation tends to occur at high degrees of supersaturation or supercooling of the liquid phase [McMillan, 1979]. Figure 2.2.5B shows the dependence of nucleation and crystal growth on the temperature to which the glass is heated.

The majority of crystallisation that occurs within glass-ceramics is heterogeneous, which involves phase boundaries, special catalysts, and foreign substrates that are distinct from the parent phase. This results from situations when the driving forces causing the formation of a new phase are stronger than those required by the parent phase for its transformation into a crystal [McMillan, 1979].

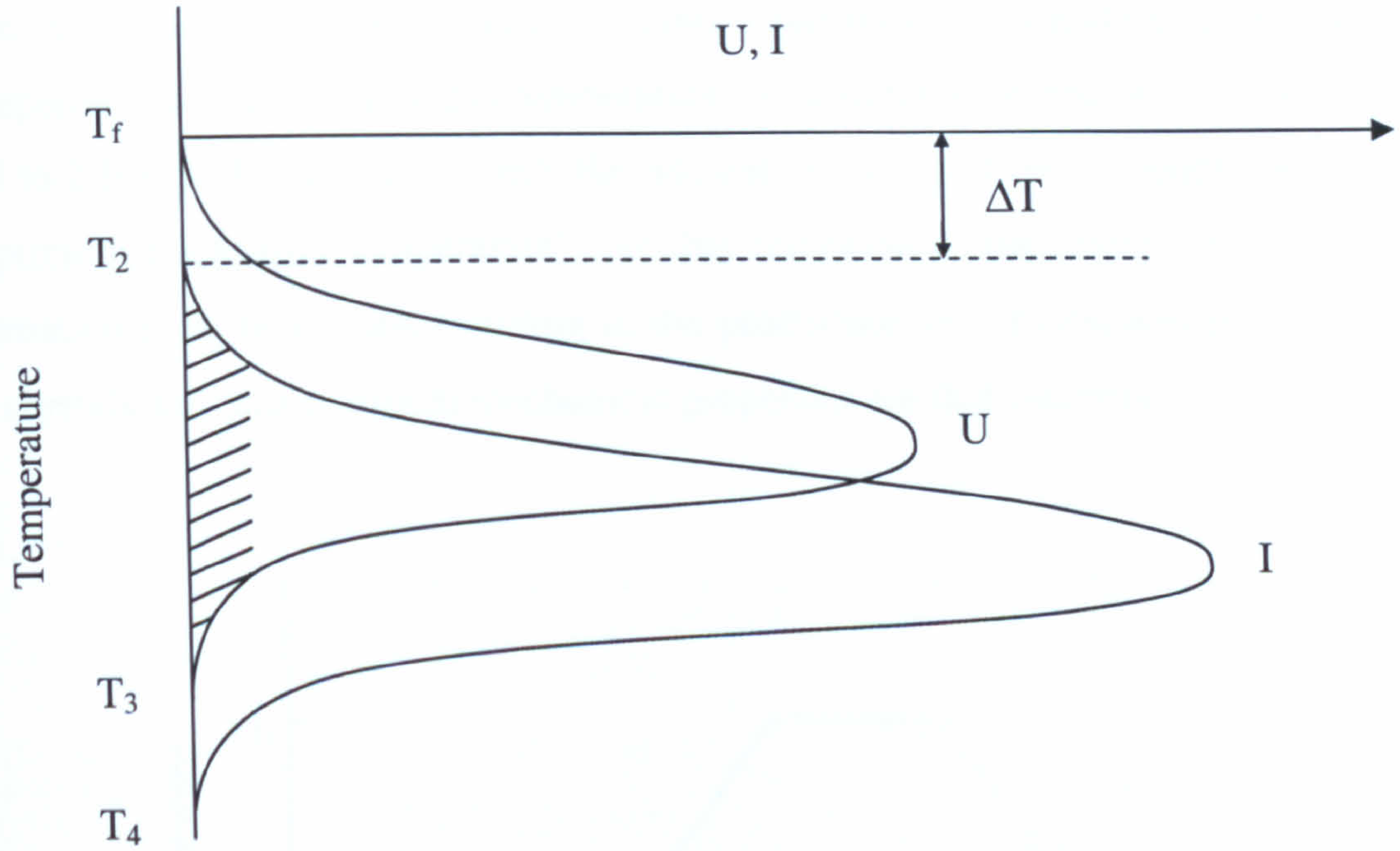

Where U is the rate of crystal growth, I is the rate of nuclei formation and Tf is the temperature at which fusion occurs.
Note the critical region for crystal growth is thus between T2 and T3.

Figure 2.2.5 B: The dependence of crystal growth and nucleation on temperature [Lorrison, 2003]

In order to produce a material with good mechanical strength, a fine-grained microstructure is usually required and therefore it is desirable to produce a glass-ceramic that contains small, closely interlocked crystals. To achieve this efficient nucleation is needed producing a large number of small crystals rather than a small number of relatively coarse ones. Once the glass has been nucleated, the temperature is raised to allow crystal growth on the nuclei. Careful control must be exercised over the rate of temperature rise as a heating rate that is too rapid may cause deformation or cracking of the glass-ceramic to occur. This results from the generation of stresses in both the glass phase and the crystal phases as a result of a difference in their densities and the volume change which accompanies crystallisation [McMillan, 1979]. With slower heating this should not occur since stresses are relieved by viscous flow of the glass phase.

An idealised heat-treatment schedule for a glass-ceramic is shown in Figure 2.2.5C. The initial stage involves heating the glass from room temperature to the nucleation temperature and holding at this temperature for a suitable period of time, usually from 0.5 to 2 hours. The point at which the nucleation rate is at its maximum is termed the "optimum nucleation temperature". At this temperature the degree of crystal nuclei formation is at its greatest resulting in the production of a maximum possible number of crystals and thus optimum mechanical properties for that material.

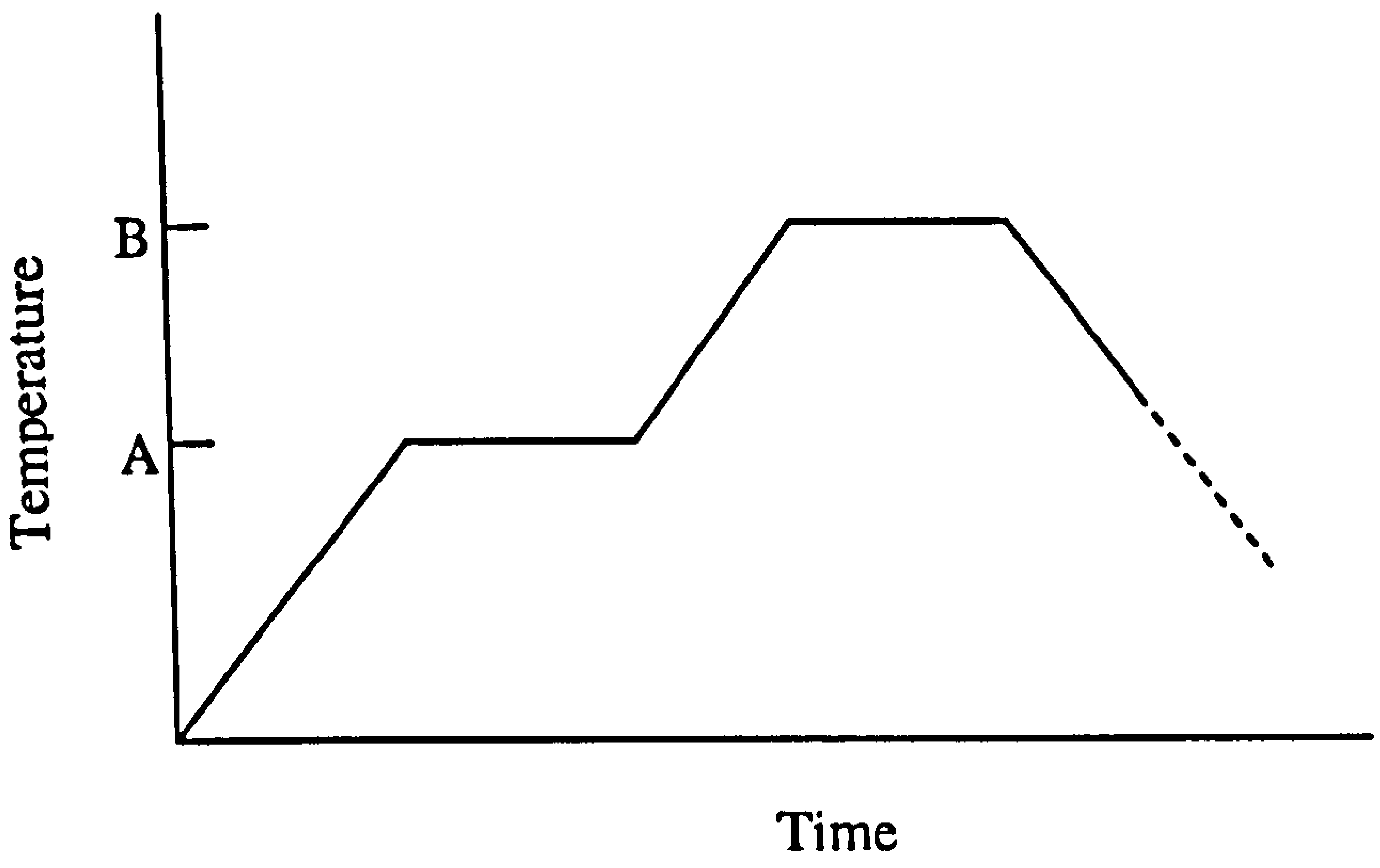

A. Nucleation Temperature
B. Maximum crystallisation temperature

Figure 2.2.5 C: Idealised heat-treatment schedule for a glass-ceramic

Following nucleation, the temperature of the glass is raised further to allow crystal growth to occur at a controlled rate up to a point where maximum crystallisation can be achieved without causing deformation of the material. It is held at this maximum crystallisation temperature for a period of at least one hour, although longer holds are often used to increase the degree of crystallinity in the glass-ceramic.

This two stage heating regime is considered optimum as it allows crystal nuclei to be generated in the glass at temperatures below those at which major crystalline phases could grow at a significant rate [McMillan, 1979].

The process of controlled crystallisation is termed ceramming. If uncontrolled crystallisation occurs, which is most likely on the surface, there will be a small number of large crystals due to a reduced number of nuclei available, and thus a decrease in mechanical properties [Stewart, 1972].

2.2.5.2.4 Composites

Composites have been developed in an attempt to solve the problem of elastic modulus mismatch and stress shielding of bone. Bioinert composites, such as carbon-carbon fibre composite materials, have a low modulus, good strength, and are lightweight. However under cyclic loading delamination can occur which causes the release of carbon fibres into the interfacial tissues resulting in chronic inflammation [Bronzino, 1995]

Attempts to mimic the natural structure of bone have led to composites containing hydroxyapatite with collagen to be studied by a number of groups [Du *et al.*, 1998; Marouf *et al.*, 1990]. Although these materials generally have good toughness, they tend to have lower strength than natural bone possibly due to the poor wet tensile strength of reconstituted collagen [Tenhuisen *at al.*, 1995]. Synthetic polymers, such as polyethylene, have been combined with bioactive ceramics, such as synthetic hydroxyapatite to produce bioactive composites with elastic moduli closer to that of natural bone [Bonfield, 1998]. However the material had less than optimal bioactivity due to the small surface area of hydroxyapatite available and the slow rate of bonding. The use of more bioactive materials, such as bioglass, combined with the use of resorbable polymers such as PLLA and alginate have therefore been investigated [Higashi *et al.*, 1986; Klein *at al.*, 1987]. Whilst these approaches are promising, improvements to the interfacial bonding between the phases and reductions in the size of the second phase particles need to be made in order to increase the composite material's strength and fracture toughness.

2.2.6 Bioactive Materials

The importance of achieving secure fixation of the implanted material into the bony defect was discussed in sections 2.2.1 and 2.2.3. The chance of achieving this is increased by using a bioactive material.

A bioactive material is defined as "a material that elicits a specific biological response at the interface of the material, which results in the formation of a bond between the tissue and that material" [Hench *et al*, 1972]. A number of compositions of glasses, ceramics, glass-ceramics, and composites have been shown to bond to bone.

Materials that exhibit bioactive behaviour can be divided into two distinct classes – Class A and Class B [Hench, 1994]. Class A materials are osteoproductive which has been defined by Wilson *et al* as "the process whereby a bioactive surface is colonised by osteogenic stem cells free in the defect environment as a result of surgical intervention" [Wilson *et al.*, 1994]. This type of bioactivity occurs when a material elicits both an intracellular and an extracellular response at its interface. Class B materials are osteoconductive, providing a biocompatible interface along which bone migrates. This type of bioactivity occurs when a material elicits only an extracellular response at its interface [Hench, 1994].

The bioactivity of a material is ranked using the Index of Bioactivity, I_B, which is 100 divided by the time taken for more than 50% of the interface between bone and an implant to chemically bond together [Hench, 1991]. If a material has an I_B value greater than 0 but less than 8 (class B) then it will bond to hard tissue, and if this value is greater than 8 (class A) then it will bond to both soft and hard tissue. An example of a class A material is 45S5 Bioglass®, and a class B material is synthetic hydroxyapatite [Hench, 1991].

The ability of certain $CaO-SiO_2$-based glasses and glass-ceramics to bond to bone has been attributed to the formation of a hydroxycarbonate apatite (HCA) layer in the surface of the material when in contact with body fluid. The mechanism of formation of this layer, which is similar to that of bone mineral, has been described by Jones and Hench [2001] as follows:

Stage 1. Rapid exchange of Na^+ and Ca^{2+} with H^+ or H_3O^+ from the solution causing hydrolysis of the silica groups, which creates silanols (Si-OH):

$$Si\text{-}O\text{-}Na^+ + H^+ + OH^- \longrightarrow Si\text{-}OH^+ + Na^+(aq) + OH^-$$

This stage is usually diffusion controlled and exhibits a t-1/2 dependence. The pH of the solution increases as a result of H+ ions in the solution being replaced by cations.

Stage 2. The cation exchange increases the hydroxyl concentration of the solution, which leads to an attack on the silica glass network. Soluble silica is lost in the form of $Si(OH)_4$ to the solution, resulting from the breaking of Si-O-Si bonds and the continued formation of silanols at the glass solution interface.

$$Si\text{-}O\text{-}Si + H_2O \longrightarrow Si\text{-}OH + OH\text{-}Si$$

This stage is usually controlled by interfacial reaction and exhibits a $t^{1.0}$ dependence.

Stage 3. Condensation and repolymerisation of the SiO_2-rich surface layer, depleted in cations:

$$\text{-}Si\text{-}OH + HO\text{-}Si\text{-} \longrightarrow \text{-}Si\text{-}O\text{-}Si\text{-} + H_2O$$

Stage 4. Migration of Ca^{2+} and PO_4^{3-} groups to the surface through the SiO_2 rich layer, forming a $CaO\text{-}P_2O_5$ rich film on top of the SiO_2 rich layer. Growth of this amorphous $CaO\text{-}P_2O_5$ rich film follows by incorporation of soluble calcium and phosphates from solution.

Stage 5. Crystallisation of the amorphous $CaO\text{-}P_2O_5$ film by incorporation of OH^-, CO_3^{2-}, or F^- anions from solution to form a hydroxyl, carbonate, apatite (HCA) layer.

These are the first five stages in the process of complete bonding of a bioactive material to bone, occurring on the material side of the interface and not depending on the presence of tissues. It has therefore been possible to study this sequence of events *in vitro* using a simulated body fluid (SBF) containing similar ion concentrations to that of human blood plasma. A schematic representation of the mechanism of apatite formation on the surface of $CaO\text{-}SiO_2$-based glass-ceramics in the human body can be seen in Figure 2.2.6A.

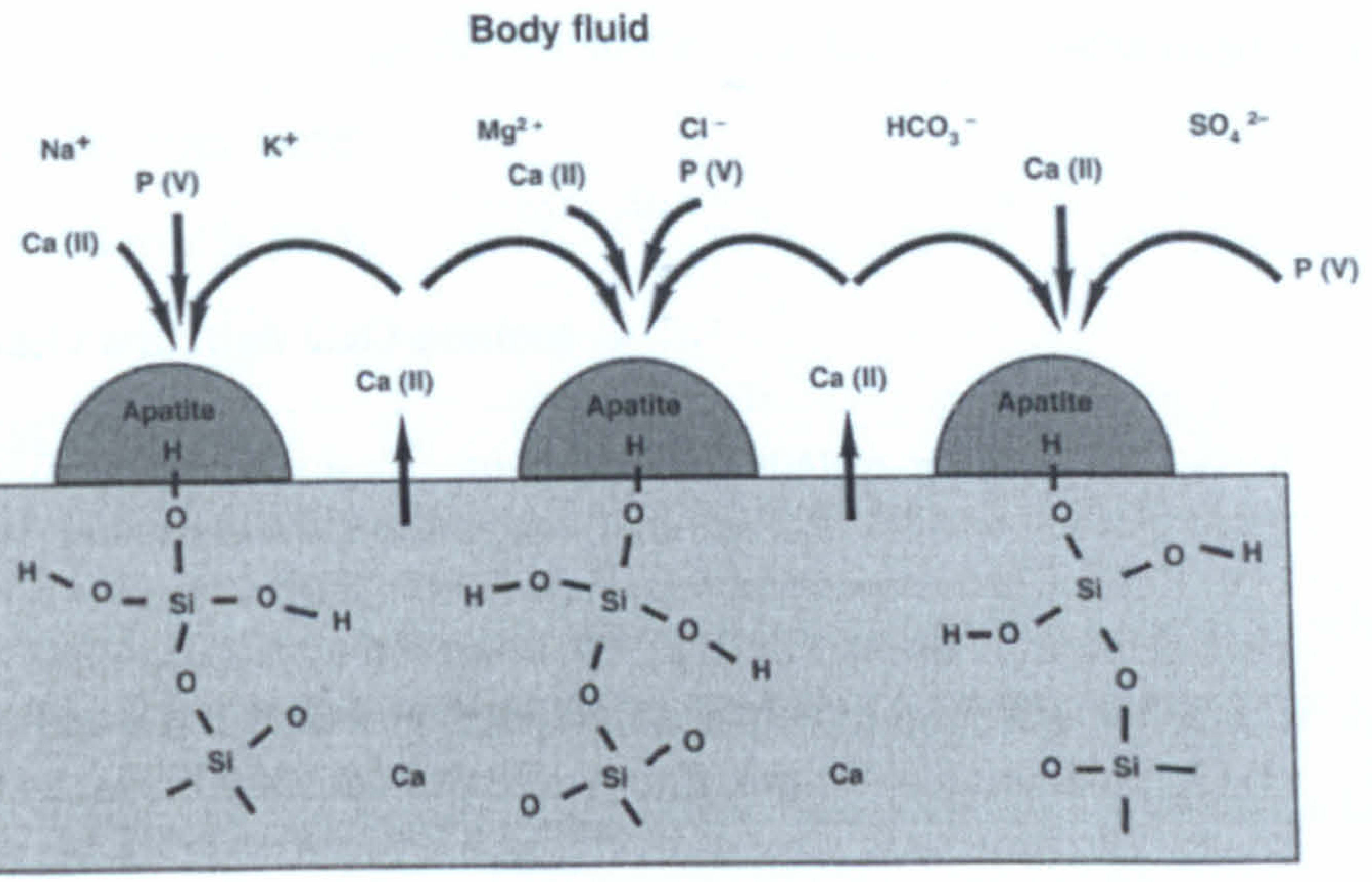

Figure 2.2.6 A: Schematic illustration of the mechanism of apatite formation on the surface of $CaO\text{-}SiO_2$-based glass-ceramics in the human body [Kokubo, 1993].

Stages 1-5 result in the formation of a hydroxyl carbonate apatite (HCA) crystal layer on the implant surface. However for the implant to bond to tissues, stages 6-11 are necessary, as described below [Jones and Hench, 2001]:

Stage 6. Adsorption and desorption of biological growth factors in the HCA layer to activate differentiation of stem cells.

Stage 7. Action of macrophages to remove debris from the site allowing cells to occupy the space.

Stage 8. Attachment of stem cells on the bioactive surface.

Stage 9. Differentiation of stem cells to form bone growing cells, such as osteoblasts.

Stage 10. Generation of extracellular matrix by the osteoblasts to form bone.

Stage 11. Crystallisation of inorganic calcium phosphate matrix to enclose bone cells in a living composite structure.

2.2.6.1 Bioactive glasses

A certain compositional range of bioactive glasses containing SiO_2, Na_2O, CaO, and P_2O_5 were the first materials to demonstrate this bioactive behaviour [Hench *et al.*, 1972]. Their key features were:

- less than 60 mol% SiO_2
- high Na_2O and high CaO content
- high CaO/P_2O_5 ratio

Many of the glasses in this system are based on the composition 45S5 in which there is 45 wt% SiO_2, S as the network former, and a 5 to 1 molar ratio of Ca to P. Glasses with Ca to P molar ratios that are significantly lower than this cannot bond to bone [Hench and Paschall, 1973]. The addition of as little as 3 wt% Al_2O_3 to the formula also prevents bonding to bone [Hench, 1991]. Produced under the brand name Bioglass®, these bioactive glasses have been used in the form of middle ear devices, implants for the orbital floor, endosseous ridge maintenance devices and particles for injection [Höland, 1997]. Whilst bioactive glasses undergo rapid surface reaction which leads to fast tissue bonding, their mechanical properties are relatively poor, demonstrating low strength and fracture toughness due to an amorphous three-dimensional glass network.

2.2.6.2 Bioactive Glass-ceramics

Higher strengths and improved mechanical properties can generally be achieved by using glass-ceramic materials as opposed to glasses. A number of bioglass-ceramics have been developed, containing apatite as a crystal phase. Two of these are apatite-wollastonite (A-W) developed by Kokubo *et al.* [1982], and apatite-mullite (A-M) developed by Hill *et al.* [1991]. Whilst the presence of an apatite phase allows tissue bonding to occur, both glass-ceramics contain at least one other crystal phase designed to act as a reinforcing agent to improve the mechanical properties of the material. The majority of the glass-ceramics tissue bonding properties is acquired from the uncrystallised glass remaining in the body of the material [Strnad, 1992].

2.2.6.2.1 Apatite-Wollastonite (A-W)

Apatite-wollastonite (A-W) glass-ceramic was developed by Kokubo and is produced by Nippon Electrical Glass Co., Ltd. under the trade name of Cerabone®. The material contains crystalline apatite ($Ca_{10}(PO_4)_6(O, F_2)$ and β-wollastonite ($CaO{\cdot}SiO_2$), with its high strength being attributed to the presence of the chain phase wollastonite. A-W glass-ceramics have a reported bending strength of 215MPa, compressive strength of 1080MPa, and fracture toughness of 2MPa√m [Höland and Beall, 2002]. However due to the tendency of wollastonite to surface nucleate, processing can be difficult, as A-W glasses cannot be cast and therefore it is difficult to produce complex or customised geometries.

2.2.6.2.2 Apatite-Mullite (A-M)

Apatite-mullite glass-ceramics were developed in 1991 as a result of research into improved ionomer glasses for incorporation into glass (ionomer) polyalkenoate cements [Hill *et al*, 1991]. Based on the system $SiO_2{\cdot}Al_2O_3{\cdot}P_2O_5{\cdot}CaO{\cdot}CaF_2$, these glasses were shown to crystallise to fluoroapatite and mullite, resulting in a microstructure of interlocking needle-like apatite crystals with a high length to diameter aspect ratio, as seen in Figure 2.2.6B. As a result, apatite-mullite glass-ceramics have demonstrated high strength and fracture toughness, with one composition when cerammed demonstrating strength of 260MPa and fracture toughness of 2.7MPa√m [Ref. 8 in Clifford *et al*, 2001]. The high fluorine content in these glasses facilitates amorphous phase separation, leading to bulk nucleation. They therefore have an advantage over apatite-wollastonite glass-ceramics as the two-stage crystallisation process of crushing and sintering is not required.

The nucleation and crystallisation behaviour of this set of materials is affected by both the fluorine content and the calcium to phosphate ratio of the glass. If fluorine is not present, no apatite phases are formed. Fluorine reduces the glass transition and peak crystallisation temperatures by disrupting the glass network and replacing bridging oxygens with non-bridging fluorines [Rafferty *et al.*, 2000]. Glasses with a calcium to phosphate ratio of 1.67, which corresponds to apatite, have been shown to undergo bulk

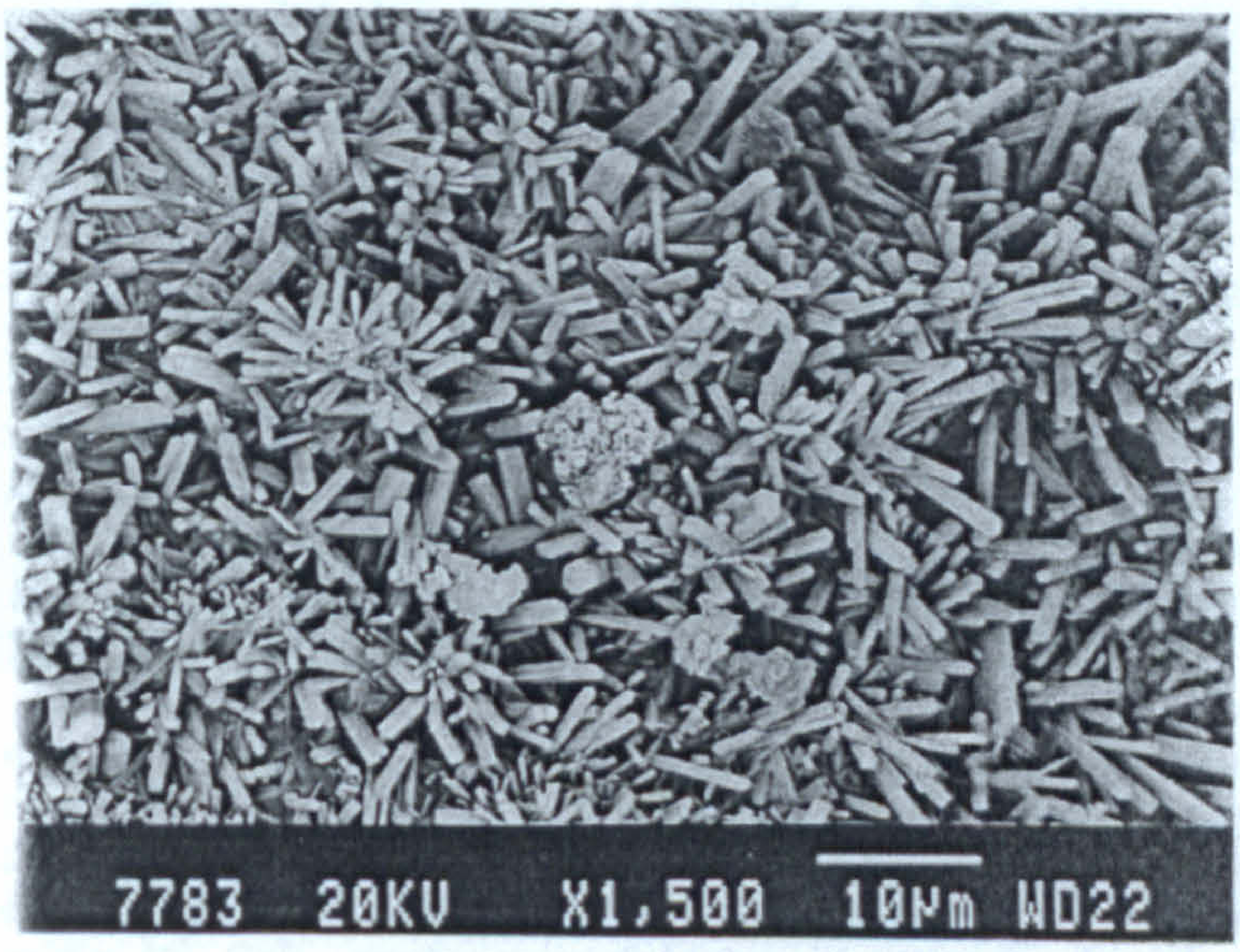

Figure 2.2.6 B: SEM of a fracture surface of an apatite-mullite glass-ceramic [Rafferty *et al.*, 2000]

nucleation, whilst compositions either side of the apatite stoichiometry exhibit surface nucleation. However by holding the latter glass compositions for an hour at a temperature close to the glass transition temperature, bulk nucleation can be made to occur [Clifford et al., 2001]

LG112 (University of Limerick Glass 112), an apatite-mullite glass-ceramic that has been shown to be the most bioactive of a series of glasses based on the general formula $4.5SiO_2 \cdot 3Al_2O_3 \cdot yP_2O_5 \cdot 3CaO \cdot 1.51CaF_2$ has been implanted into a rat femur to assess its ability to bond to bone tissue [Hatton, 2000]. Both the base glass and the resulting glass-ceramic were implanted into bone, and backscattered images of the implanted materials that were taken are shown in Figures 2.2.6Ca and b respectively. In Figure 2.2.6Ca, a fibrous capsule layer can be seen around the implanted material. However in Figure 2.2.6Cb, excellent osteointegration is seen with the formation of mineralised bone in direct contact with the implant. It was therefore concluded that although neither sample showed any signs of an adverse reaction, prior to heat treatment the glass demonstrates no signs of bioactive bonding. However following heat treatment and crystallisation, this composition of apatite-mullite glass-ceramic is bioactive.

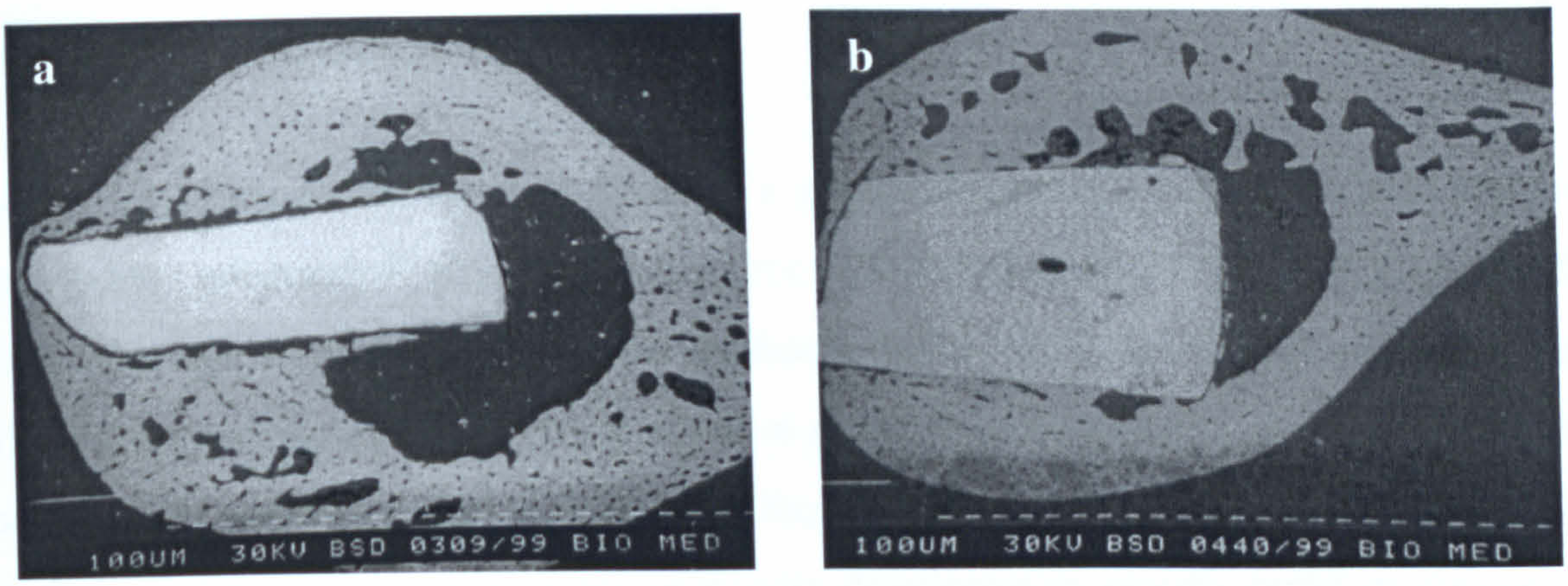

Figure 2.2.6 C: Backscattered image of LG112 implanted without heat treatment (a) and after heat treatment (b) [Hatton, 2000]

2.2.6.3 Bioactive Metals and Polymers

Until recently, the only materials considered to exhibit bioactivity were certain compositions of glasses and glass-ceramics. However, through research into the mechanisms of bioactivity and advanced understanding of the formation of bone-like apatite on their surfaces it has now become possible to even form this layer on the surfaces of metals and organic polymers *in vitro* [Kokubo, 1996]. When titanium metal and its alloys are subjected to alkaline solution and heat treatments, a thin alkali titanate layer forms on their surfaces. On subsequent soaking in SBF, hydrated titania is formed and induces apatite nucleation. The apatite layer is tightly bonded to the substrates as it is integrated through the hydrated titania and titanium oxide later. When these chemically treated titanium substrates are implanted into rabbit tibia, they directly bond to living bone [Yan *et al.*, 1997]. Similar success was experienced by chemically processing the titanium with hydrogen peroxide solution containing tantalum chloride [Ohtsuki *et al.*, 1997]. Organic polymers also form apatite nuclei on their surfaces when placed on CaO-SiO_2-based glass grains soaked in SBF. The period for which the polymers are soaked in solution determines the thickness of the apatite layer.

2.3 Layer Manufacturing

Layer manufacturing is the term given to a group of related technologies that are used to produce geometrical objects directly from CAD data sources without part specific tooling or human intervention. These methods, which were commercialised in the mid 1980's, are unique in that they use additive rather than subtractive techniques to build parts on a layer-by-layer basis. The term "Rapid Prototyping" is also commonly applied to these technologies as they were originally developed to rapidly build prototypes of new products for design approval and part verification, although this terminology is now considered to be a little dated. Whilst these processes are still frequently used for the production of prototypes for design evaluation, the direct production of final parts is also now achieved. In addition, 'rapid' is misleading as although the process could reduce the design cycle by weeks or even months, individual objects may still take hours to produce, thus speed is only relative. "Solid Freeform Fabrication" is an alternative commonly-used term for these processes.

All of the layer manufacturing technologies begin with a three-dimensional computer solid model of the part, which is mathematically sliced into a series of parallel cross-sectional layers. Each of these layers are then successively converted into physical layers, with new material being deposited on and bonding to the previous layer. Thus the part is built up layer by layer, from the bottom upwards.

The most common layer manufacturing processes include stereolithography, thermal phase change inkjets, fusion deposition modelling, laminate object manufacturing, three dimensional printing and selective laser sintering, each of which will be described in more detail in the following section. These techniques are defined by the method used to form the physical layers, for example stereolithography uses light (photopolymers) to convert liquids into solids, fusion deposition modelling involves the extrusion of thermoplastics, laminate object manufacturing the stacking of web materials, and selective laser sintering the bonding of powders. In addition, new layer manufacturing technologies continue to be developed, as well as improvements made to the equipment and materials of current technologies.

Layer manufacturing exhibits a number of advantages over traditional methods such as milling or turning that use subtractive techniques:

- It allows solid parts to be formed with little or no dependence on the geometry of the tools being used to achieve the net form or the features on the part to be machined.
- As layer manufacturing is not a contact process there are no cutting forces, thereby allowing smaller and more detailed features to be created.
- Complex parts can be fabricated in one set-up that might otherwise require several operations from different machines using traditional methods.
- These technologies help shorten the time required to go from design to manufacture, thus reducing the cost of the product and consequently increasing competitiveness.
- Objects can be formed from multiple materials or as composites.
- It is more economical to produce one-off prototypes for testing fit and function for specific applications.
- As additive processes, they do not produce the large amount of waste material that subtractive methods do.

General limitations of layer manufacturing include the high capital costs of the machines used in some of the processes, and whilst they may be useful for small production runs it may prove more economical to use conventional methods for long production runs. The materials available for use with these technologies are limited and dependent on the process chosen.

2.3.1 Stereolithography (SLA)

Stereolithography (SLA) was the first layer manufacturing technique to be developed and is still currently the most widely used. Parts are built by tracing a laser beam on the surface of a vat of photosensitive monomer resin, causing it to polymerise and solidify in areas where the laser strikes. Most of the photopolymer materials used require an ultraviolet light, but some resins that work with a visible light are also used.

A schematic diagram of the apparatus used in SLA can be seen in Figure 2.3.1. The part is built on a moveable platform which is initially situated just below the surface of the vat of resin. A laser beam, directed by a scanner system consisting of galvanometer-controlled mirrors, traces a cross-section of the desired part using information obtained from a 3D CAD solid model file.

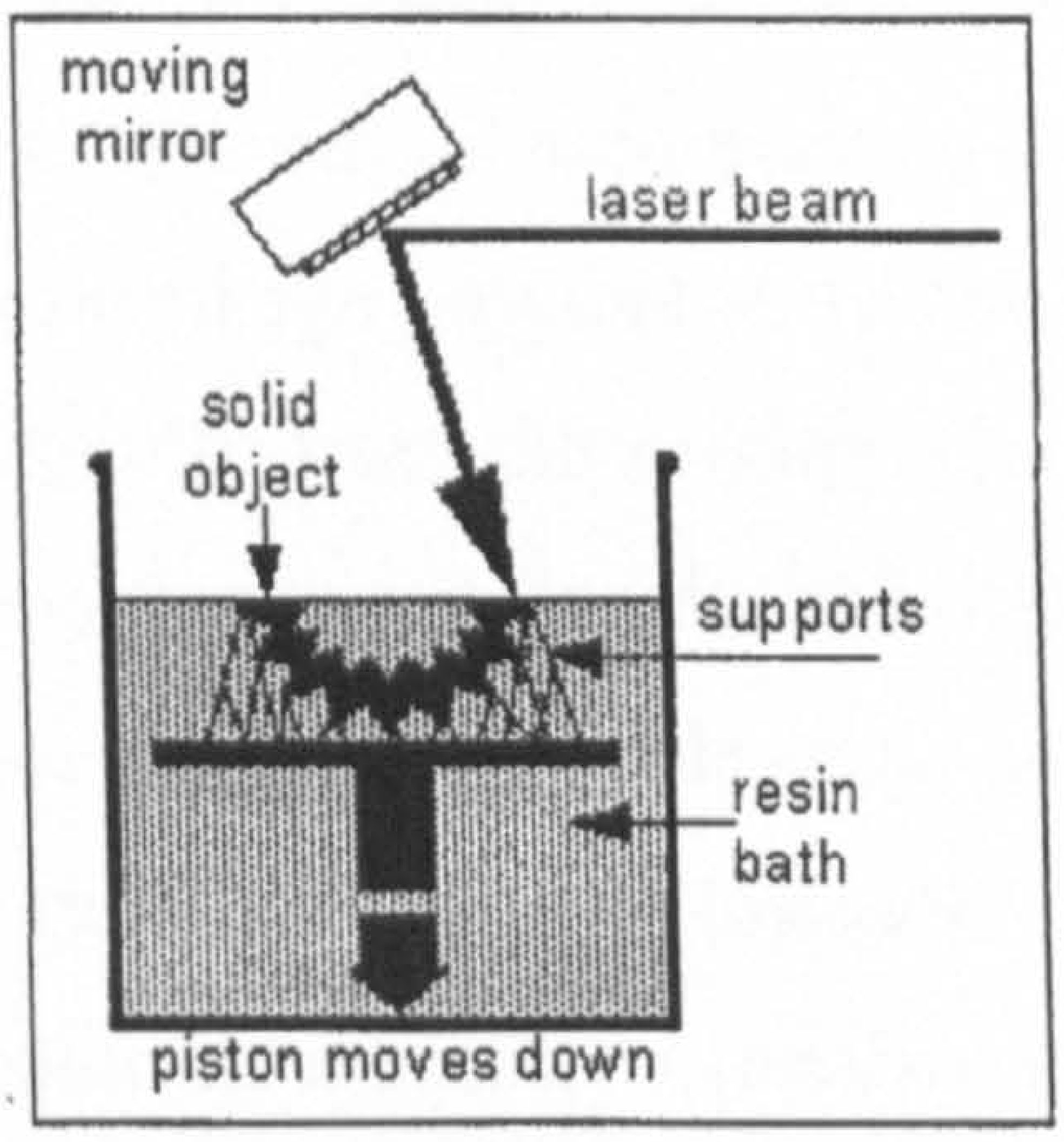

Figure 2.3.1 A: Schematic diagram of SLA [www.jtap.ac.uk, 2002]

The boundaries of the layer are scanned and then, if the part is required to be solid, the interior is either hatched or solidly filled. If possible, parts are often left hollow to reduce material costs.

Following completion of this layer, the platform is lowered into the vat slightly, and a new layer of liquid flows in over the top. The liquid is allowed to settle in order to ensure a level surface and to inhibit bubble formation, often using a wiper blade or pump driven recoating system to facilitate this. Subsequent layers are then scanned in a similar process with the layers bonding to each other due to the self-adhesive property of the photopolymer. Once the complete, three-dimensional object has been formed, it is removed from the vat and allowed to drain, before being post-cured in an UV oven to ensure that no liquid or partially cured resin remains.

Objects with overhangs or undercuts require support structures in order to prevent swaying or deformation of the overhangs during the fabrication process. These supports are constructed by the same process and at the same time as the main object, then removed at the end of the process.

SLA is generally considered to offer the greatest accuracy of all the layer manufacture processes, with an average accuracy of ±0.1mm [Dickens, 1994]. It is reasonably fast and provides a surface finish comparable to that of NC milling. On the negative side, the resin is expensive, messy, toxic, and must be shielded from light to avoid premature polymerisation. There is a limited choice of resins that can be used, although research is currently being conducted into developing new materials for use with this technology [Nee *et al.*, 2001]. Conversion from a monomer to a polymer causes about 3% shrinkage, with a further 2% shrinkage possible if the final part is post-cured. However this can be corrected automatically from the original CAD solid model file. The need for support structures for overhangs and undercuts introduces problems with their removal if the part has internal cavities with little or no access. The removal of too little support or too much of the part can result in tolerance deviations. These drawbacks, added to the fact that the materials currently available are organic resins which aren't suitable for use as implant materials eliminate this method as an ideal way of producing bone replacement materials.

2.3.2 Thermal Phase Change Inkjets

This technology, which was originally known as Ballistic Particle Manufacturing (BPM), creates three-dimensional parts by printing cross-sectional layers of liquid or molten material onto a substrate. Droplets of the material are ejected from jetting heads which are moved under computer control in the required geometry for a particular layer of the part. When the droplets contact the substrate, they immediately cold weld to form a solid part.

Figure 2.3.2A illustrates a typical system for this technique. Separate jets are used for the plastic build material and a wax-like support material, which are held in a melted liquid state in heated reservoirs. The supports are usually made from a different material in order to facilitate their removal from the part at the end of the process.

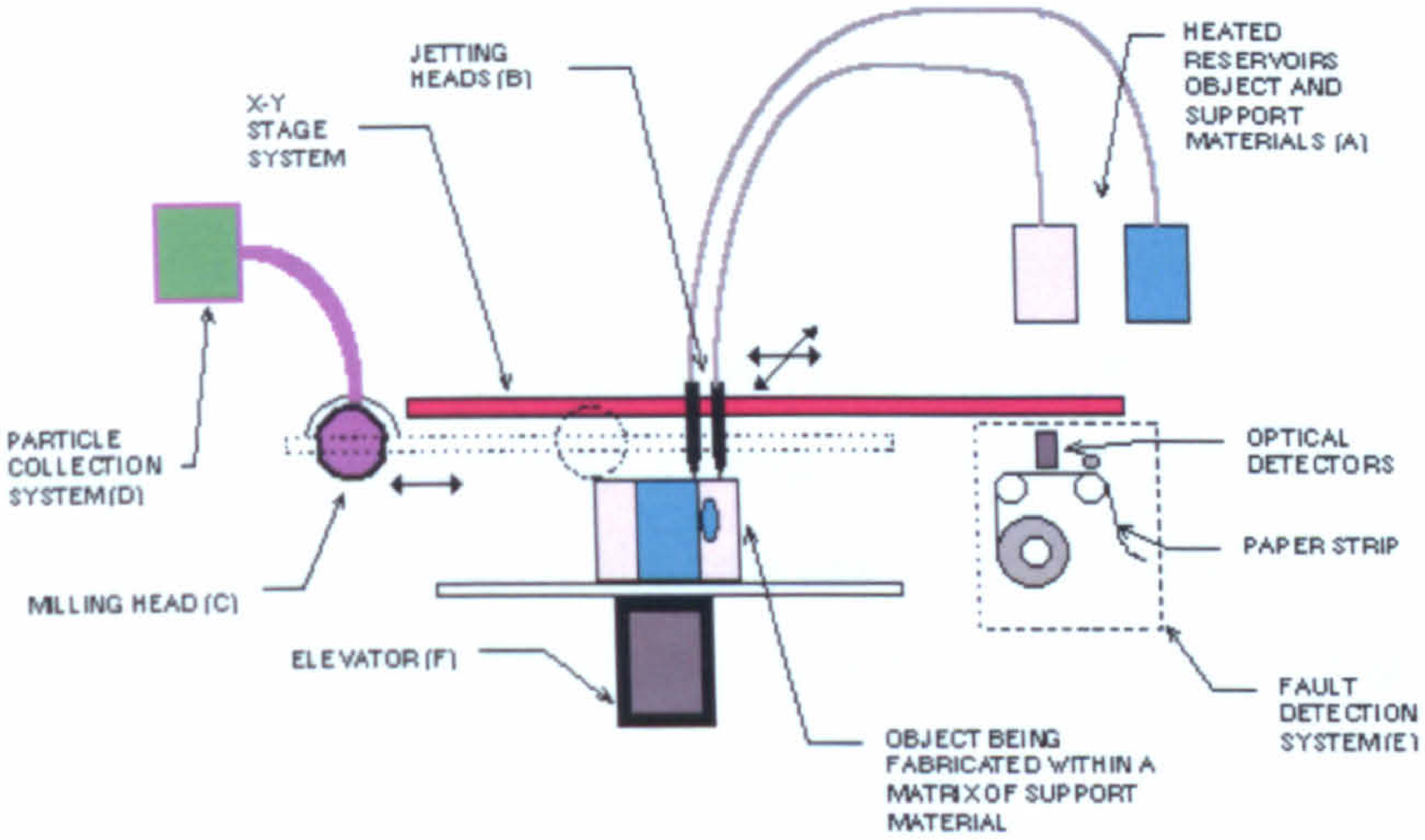

Figure 2.3.2 A: Schematic diagram of a thermal phase change inkjet [Castle Island, 2004]

Once a layer has been completed, a milling head is passed over the layer to ensure it is of uniform thickness, and the process is repeated to produce the next layer of the part.

The temperature of the droplets needs to be controlled carefully. If they are too cold they will solidify mid-flight and will therefore not weld to the part; if they are too hot, the part will lose shape. The deformation and placement accuracy of the droplet depend on its velocity. If it is moving too slowly, placement accuracy will be poor, if it moves too quickly the droplets will be highly deformed on impact.

The main advantage of thermal phase change inkjets is the ability to produce extremely fine resolution and surface finishes. However the technique is very slow for large objects, and there is a very limited selection of materials that can be used with this technique.

2.3.3 Fusion Deposition Modelling (FDM)

Fusion Deposition Modelling (FDM) was developed by S. Scott Crump in 1988 (patented in 1989) and is the second most widely used layer manufacturing technology, after SLA.

A continuous thread of thermoplastic filament material is forced out through a small temperature-controlled extrusion nozzle which is guided over a build platform in the required geometry by a robotic device. As the material is passed through the nozzle it is heated to just above its melting point so that when it makes contact with the previous layer it immediately cold welds to form a solid part. Following the completion of each layer, the extrusion head is raised by a programmed distance in the z-axis to allow deposition of the subsequent layer, the process repeating until all layers have been deposited and the solid model has been produced. A schematic diagram of FDM is shown in Figure 2.3.3A.

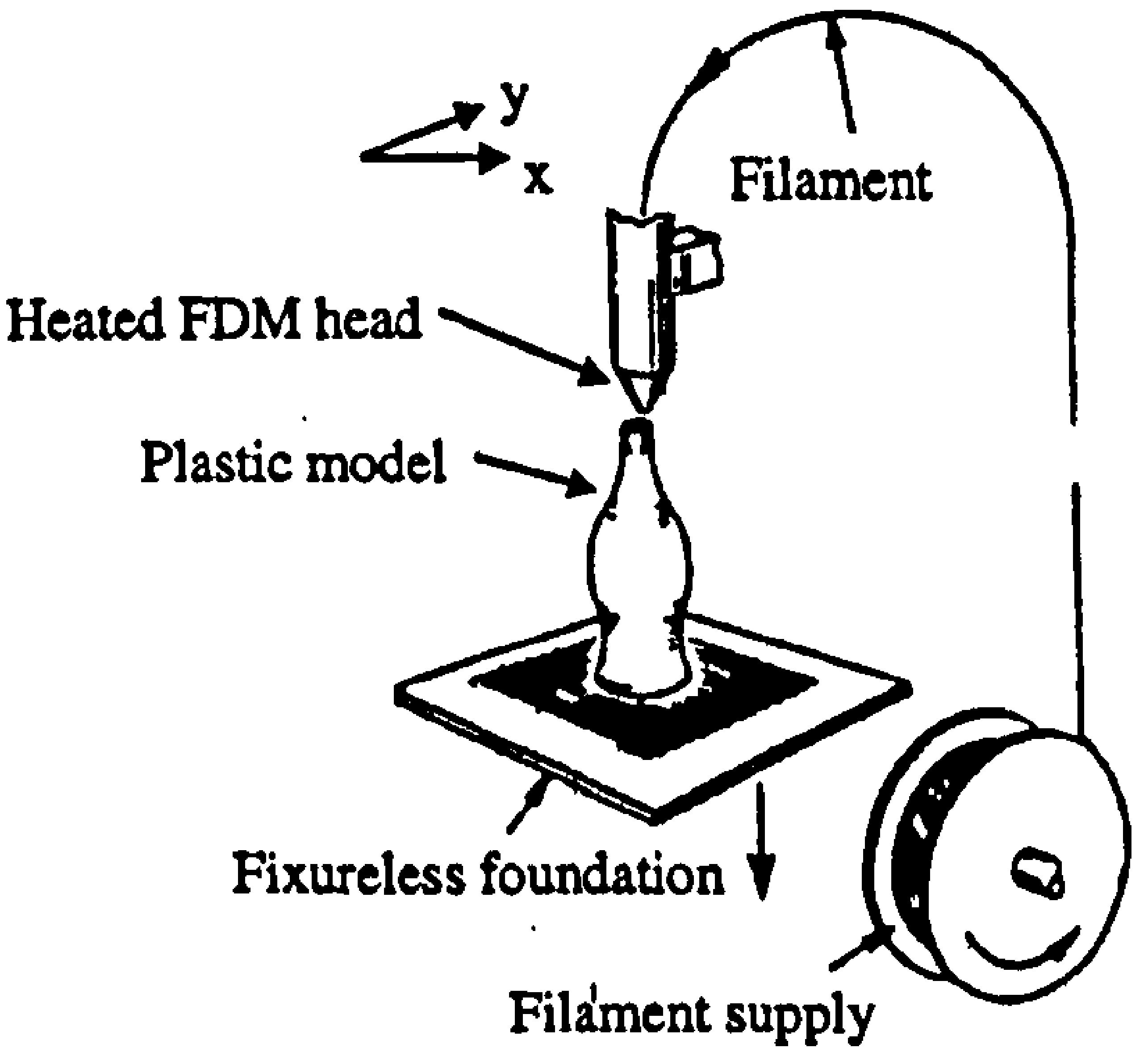

Figure 2.3.3 A: Schematic diagram of the apparatus used in FDM [Jacobs, 1992].

If a support structure is required it is provided by a second nozzle and can be made from the same material as the part, usually in a different colour for easier identification when separating the two at the end of the build process, or from a different material which can be more easily removed due to weaker bonds with the part.

A variety of materials are available for this process, those most commonly used include a tough, nylon-like polymer, and both machinable and investment casting waxes. A number of other polymers, as well as ceramic and metallic materials are currently being investigated for potential use with this technique. Water soluble support materials have also been developed that are simply washed away allowing easier removal.

The advantages of FDM are attributed to the simplicity of the machine, the ease of changing materials, and the relatively large variety of materials available for use with the process. Although much improvement has been made to the surface finish of produced parts, it is still not comparable to that of stereolithography, as the resolution of the process is dictated by the thickness of the filament material which is generally 1.27mm. Support structures are often required, producing similar problems to those experienced by SLA. Parts with wide cross-sections can be slow to produce.

2.3.4 Laminated Object Manufacturing (LOM)

Laminated Object Manufacturing (LOM) uses a laser beam to cut out the outline of each layer of an object from thin sheets of material, usually paper, but polymers, metals, or composites may also be used [Klosterman *et al.,* 1998]. The undersides of these sheets are coated with a heat-sensitive adhesive that bonds them to the previous layer when a heated roller is passed over.

Figure 2.3.4A illustrates this process. The material is unwound from a feed roll (A), and is pulled across a base plate, before being fixed in place when the heated roller (B) passes over it and activates the glue. The laser beam, controlled by a CAD system, then scans over the surface, cutting the layer to its required shape. The laser intensity is carefully modulated to cut though the material at a depth of exactly one layer thickness. Any material that is not required for the model is heavily cross-hatched with the laser so that it can be easily removed at the end of the build. During the process however, this material acts as a support to the rest of the part.

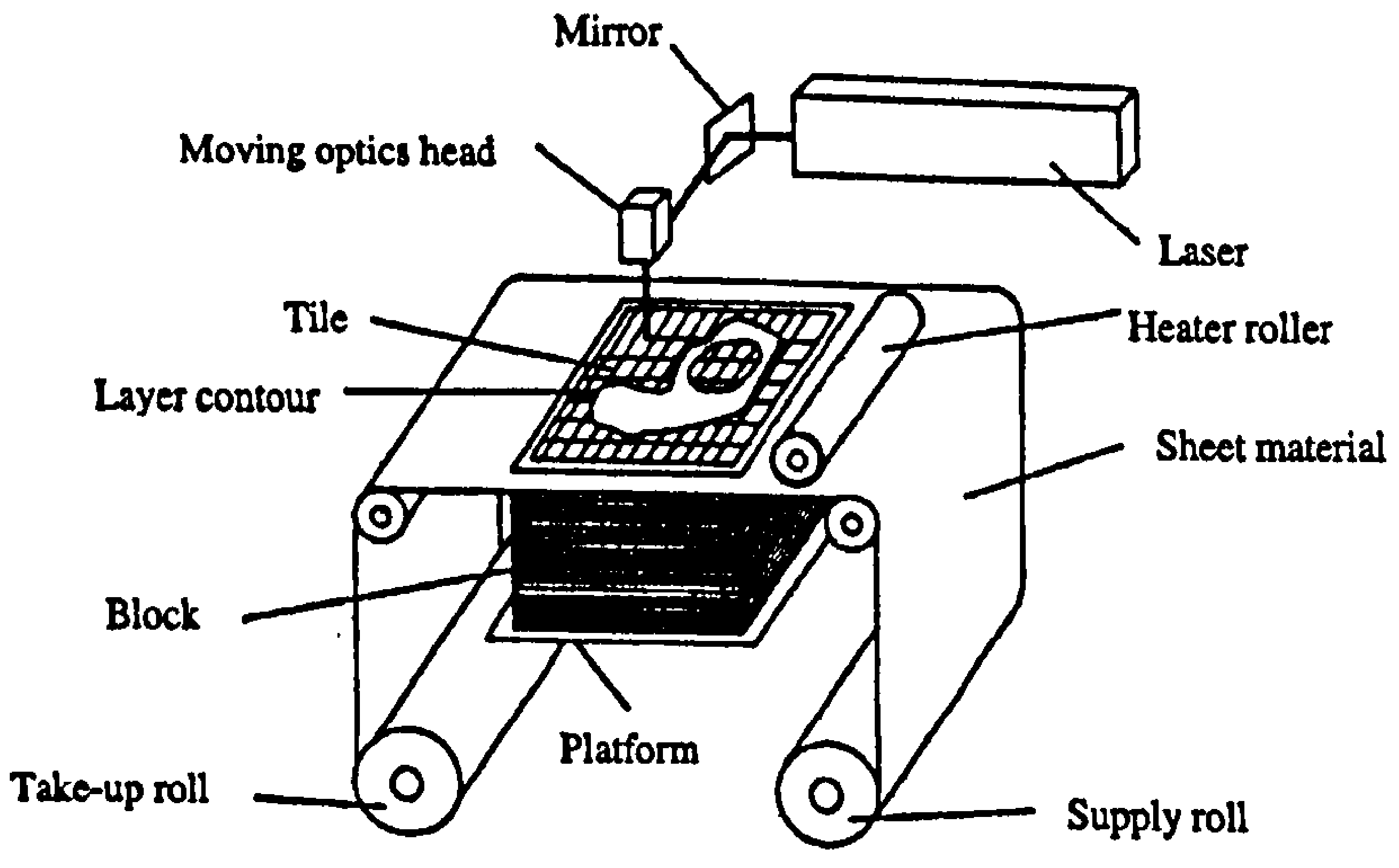

Figure 2.3.4 A: Schematic diagram of LOM [Jacobs, 1992]

By using a sheet of material that is wider than the build area, when the cross-section of the part has been cut, any material not being used to support the model can be wound onto a second roller as the edges of the sheet remain intact. As it does so, new material is pulled across the base plate which moves down one layer thickness and the whole process begins again.

As it is only necessary for the laser to scan the contour rather than the entire cross section, LOM is a relatively high speed process. Due to the use of sheet material, models do not shrink or distort [Yan and Gu, 1996]. However, difficulties arise in the production of hollow parts or parts with undercuts and re-entrant features. There is also a large amount of scrap generated. The produced parts have limited applications as functional prototypes due to poor shear strength resulting from the layering of adhesive and material.

2.3.5 Three Dimensional Printing (3DP)

Three dimensional printing was developed at Massachusetts Institute of Technology and is shown schematically in Figure 2.3.5A. The process uses powdered materials which are thinly spread over the surface of a powder bed and levelled by a roller. A multi-channel jetting head selectively deposits a liquid adhesive onto the layer of powder according to data from a computer model, and the powder particles become bonded in these areas. On completion of a layer, the piston that supports the powder bed lowers the work piece by a distance equivalent to one layer thickness, and the next layer of powder is spread over the previously formed layer. The process is repeated until the entire part is formed within the powder bed. Any overhangs, undercuts, or internal volumes in the part are supported during the build cycle by the surrounding unbound powder. Once all layers have been completed, the object is elevated and any unbound powder is removed leaving a relatively low-density "green part". Heat treatment is used to enhance the bonding of the glued powder.

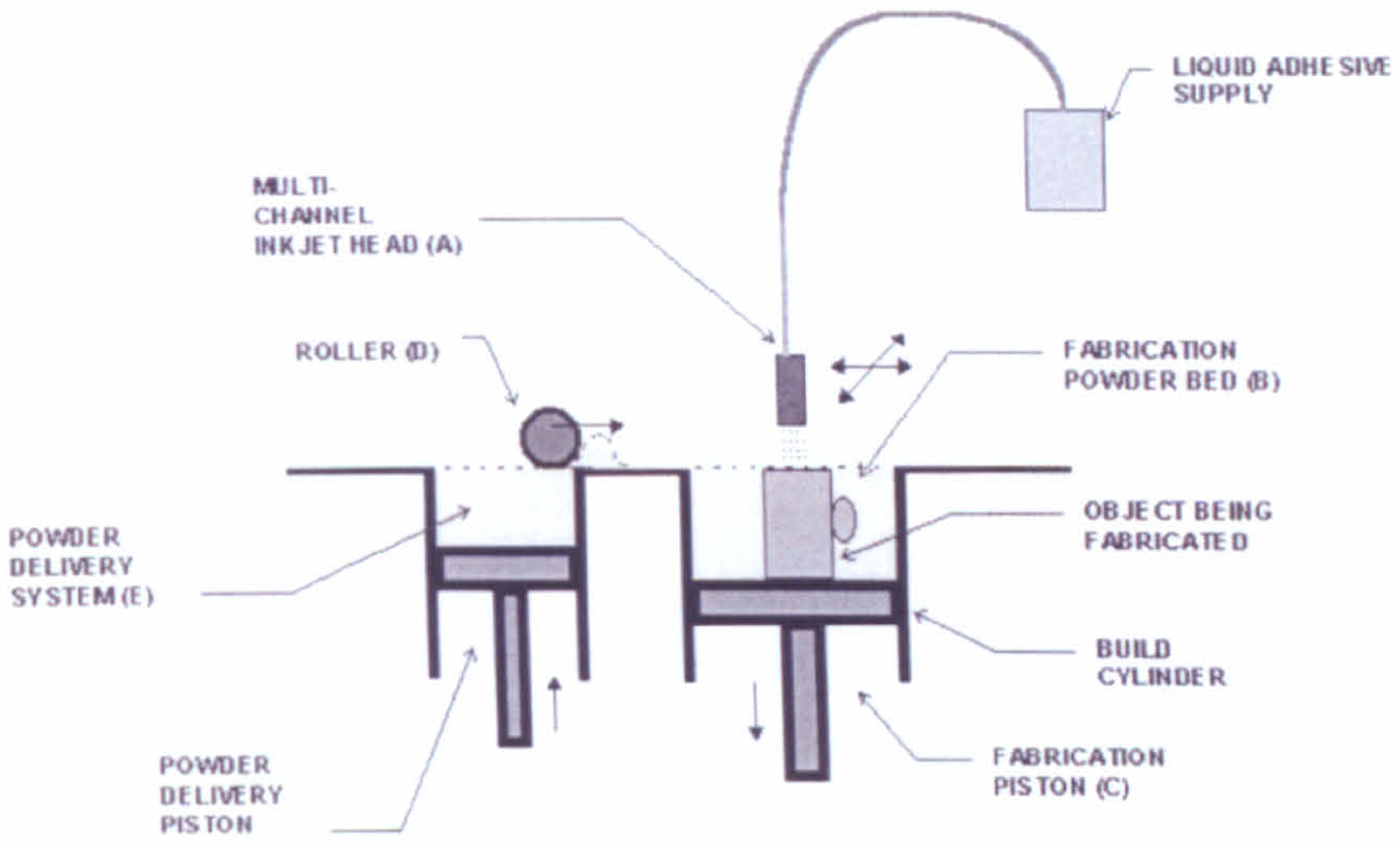

Figure 2.3.5 A: Schematic diagram of 3DP [Castle Island, 2004].

3DP is a particularly versatile method as it can be used to process any material that can be obtained as a powder, including ceramics, metals, polymers and composites. There is also the ability to control local material composition, as different materials can be dispensed from different print heads. There are limitations however on resolution, fragility of parts, surface finish and materials available.

2.3.6 Selective Laser Sintering (SLS)

Selective Laser Sintering was first developed at the University of Texas, USA, and has since been commercialised by DTM Corporation. Three-dimensional objects are produced using heat generated by a focused laser beam to selectively sinter layers of powdered material together.

The process of selective laser sintering consists of eight stages:

1. The object to be produced is defined by a CAD solid model file which is sliced into mathematical layers that represent the cross-section of the part.
2. A thin layer of powder is uniformly spread over the build platform by a roller.
3. A laser beam scans across the layer of powder only scanning the areas required for that particular slice of the desired object, as specified by the CAD data file.

4. The selected powder particles are heated by the energy from the laser to a temperature above the melting or softening temperature so that they coalesce into a solid mass.
5. Once the laser has scanned the entire cross-section the platform lowers and the next layer of powder is spread over the previously sintered layer.
6. Selected areas of this layer are sintered and bond to the previous layer, making up the next slice of the part.
7. The process is repeated until the entire part is fabricated.
8. The sintered object is then lifted out of the machine and brushed off to remove any loosely attached material. The unsintered material can be sieved and used again.

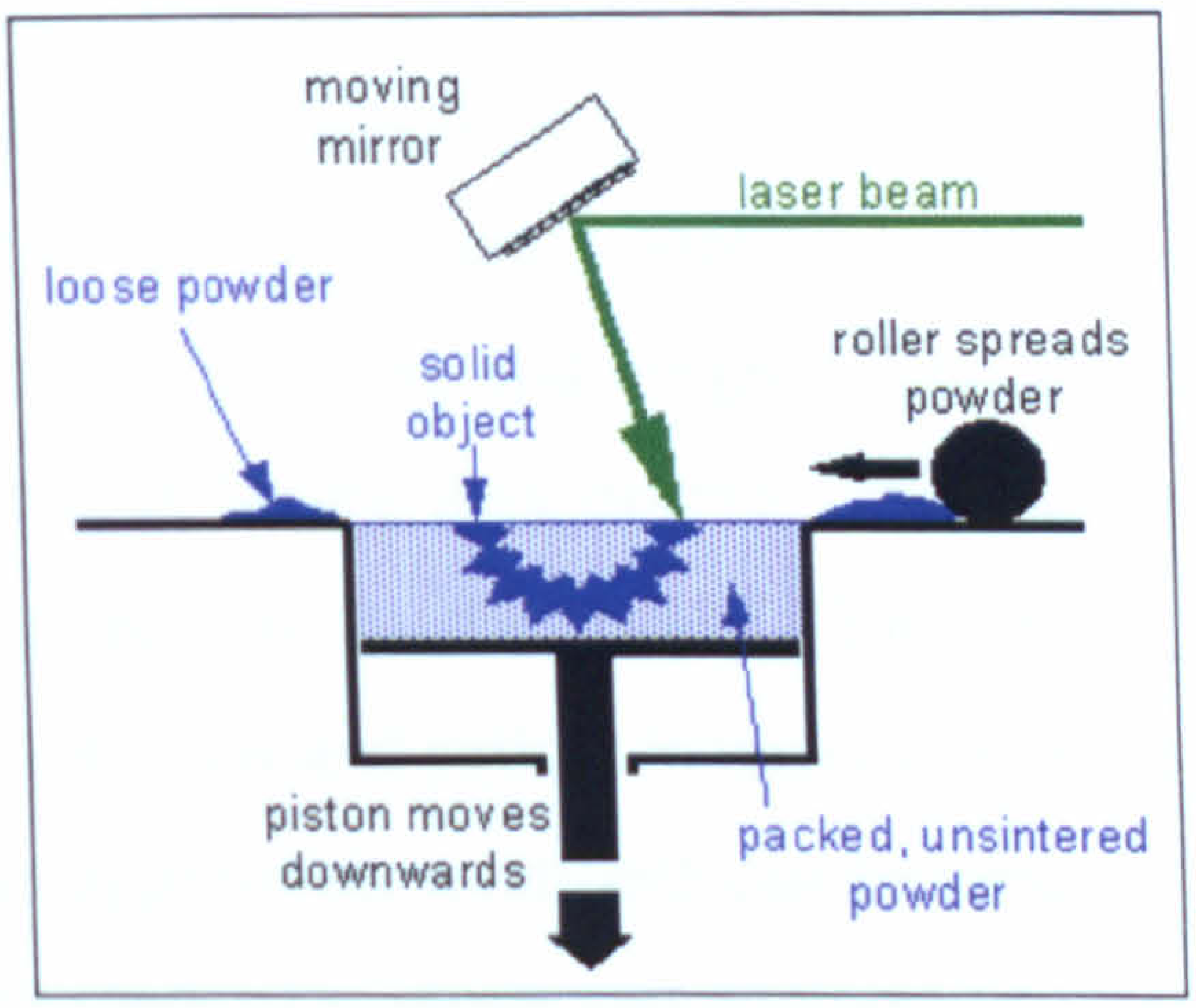

Figure 2.3.6 A: Schematic diagram of SLS [www.jtap.ac.uk, 2002]

The completed part is then either used as it is, or if necessary, post-processed to achieve required properties such as improvements to surface finish or decreasing surface porosity.

The major advantage of SLS over the other layer manufacturing techniques is the variety of materials that can potentially be used to make parts, as theoretically any powder that can be fused is capable of being transformed into a model.

In addition, SLS has an inherent advantage over other layer manufacturing methods such as stereolithography and fused deposition modelling in that there is no need for external supports for overhangs or unconnected parts as the model is supported during the build cycle by the tightly packed unsintered powder. Since there are no supports to interfere with each other, more parts can be built in a single machine run and parts can be oriented so that surfaces that need to be smooth are scanned in the build plane, thus minimising the need for post processing.

As SLS was the process chosen for processing of the glass-ceramic in this work, it will be discussed in more detail in section 2.4.

2.3.7 Use of Layer Manufacturing in Medical Applications

At present the main medical application of layer manufacturing techniques is the construction of physical models of patient's bones from CT or MRI data. These models can be used for preoperative planning and surgical simulation, and allow surgeons to practice complex procedures before they operate, thus saving time during the actual procedure and reducing the risk to the patient [Yay *et al.*, 1995]. Communication between the physician, surgeons and patient is improved as the damage to the bone can be seen clearly and thus appropriate treatment can be agreed. The models may also be used as teaching aids for medical students and doctors.

Layer manufacturing techniques are also increasingly being used to produce a number of external medical devices such as SLS fabricated sockets for below-the-knee amputees [Rogers, 2000], and custom-fit masks that reduce scarring on burn victims [Grimm and Wohlers, 2002].

Layer manufacturing techniques are increasingly being investigated for the production of scaffolds for tissue engineering applications. FDM has been used by Zein *et al* [2002] to produce poly(ε-caprolactone) (PCL) scaffolds with fully interconnected porous channels of 160-700μm diameter and 48-77% porosities. A number of different laydown patterns for each consecutively deposited layer were used to produce a variety of honeycomb-like designs, which demonstrated compressive strengths and yield strengths ranging from 4 to 77MPa and 0.4 to 3.6MPa respectively, depending on the pattern used.

Kim *et al* [1998] have looked at using 3DP with a particulate leaching technique to create porous scaffolds using polylactide-coglycolide (PLGA) powder mixed with salt particles and a suitable organic solvent. Distilled water was used to leach the salt particles to create scaffolds with pore sizes of 45-150μm and 60% porosity. 800μm diameter longitudinal channels were printed and horizontally stacked, and arranged in parallel throughout the scaffolds height.

This work is looking at the possibility of applying layer manufacturing technology to the fabrication of bioactive ceramics for bone replacement and simulation of bone ingrowth. Fabrication of small hydroxyapatite objects have previously been attempted using SLA [Griffith et al, 1996], although due to the large volumes of organic resins, concerns have been raised over the potential toxicity of the parts if complete removal of the resin decomposition products is not achieved. In addition, problems were experienced with maintaining dimensional tolerances and structural integrity during densification. An indirect SLA method has also been attempted using a 40 vol% flowable suspension to produce controlled porosity hydroxyapatite parts [Chu et al, 2001]

Darsell *et al* [2003] have used an indirect fused deposition process to fabricate controlled porosity alumina bone grafts. This process first required a polymeric mould or negative of the desired structure to be fabricated, before infiltrating the structure with the desired material. A binder removal and sintering cycle was then used to remove the mould polymer and densify the ceramic structure. An average compressive strength of 130 ± 13 MPa was reported for samples with 29 vol% porosity with a pore size of 300μm, although increasing porosity was found to degrade the mechanical properties of the implants.

As we saw in section 2.3.6, there are a number of factors that make selective laser sintering one of the ideal techniques for the production of bioceramic implants for bone replacement applications. As the technique uses powdered materials, there is inevitably going to be a certain degree of porosity in the powder bed which will be passed on to the produced parts. This allows a relatively porous, open structure to be produced, which allows bone to grow inside it, improving the integration of the artificial material with the natural tissue. Attempts to process bioceramics using a direct laser sintering method has proven to be unsatisfactory, producing parts with poor structural integrity from very small processing windows. Using a direct method, the apatite-mullite glass-ceramic used in this work can only be sintered at low speeds of around 1 and 2mm/sec and at powers around 2-3W and even then consolidation is poor – see Figure 2.3.7A. This has been attributed to high surface tensions experienced upon melting, a large viscosity change at the glass transition temperature and intra-process crystallisation [Lorrison, 2003].

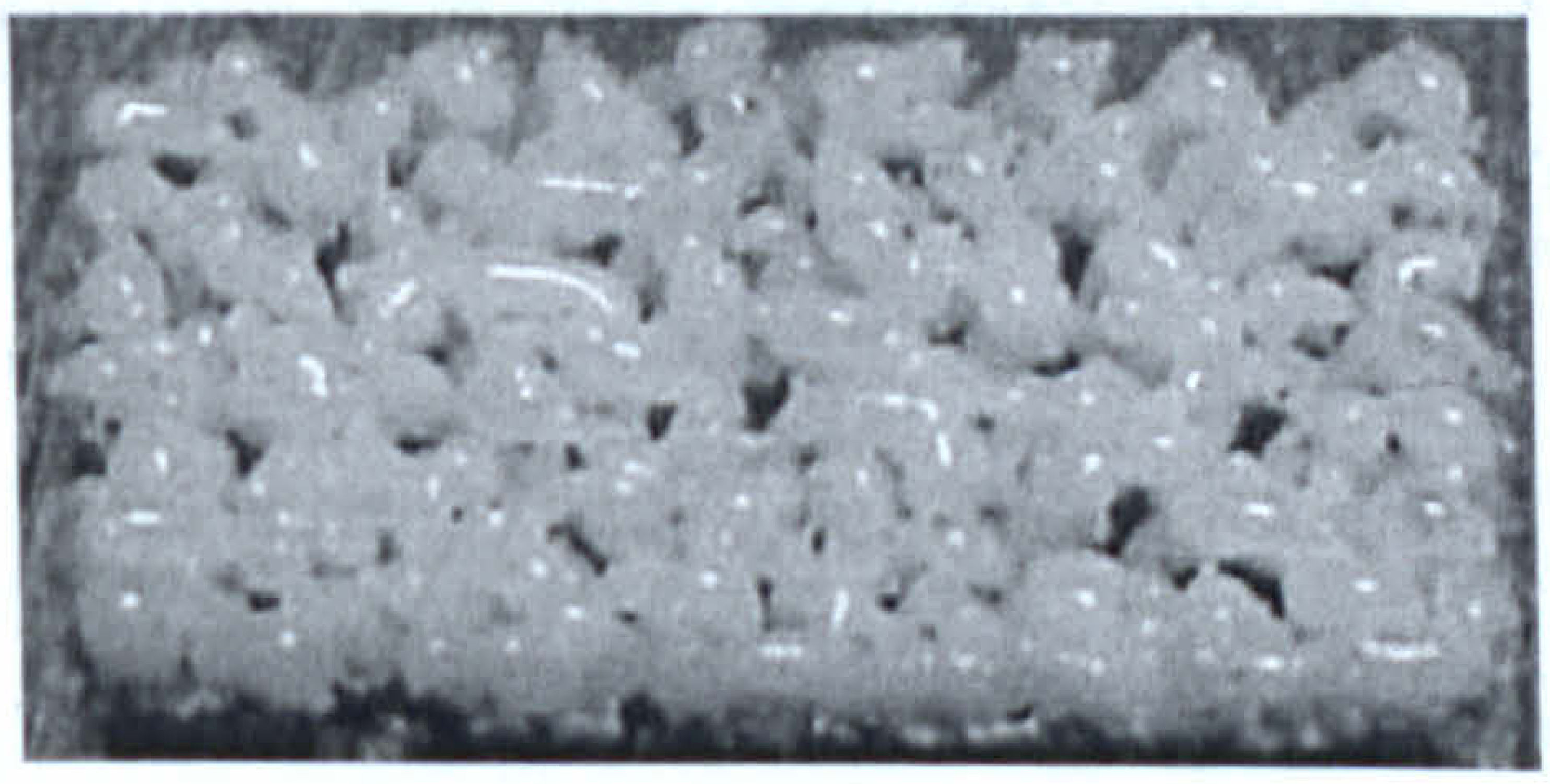

Figure 2.3.7 A: An 8x15mm monolayer produced by direct SLS of an A-M glass-ceramic [Lorrison, 2003].

However it is thought that by adopting an indirect method where a low melting temperature binder is blended with the relatively high melting temperature glass, green parts with superior structural integrity may be produced when laser sintered. These parts can subsequently be post-processed to burn off the binder and sinter the glass.

2.4 Principles of SLS

In the last section it was reported that SLS involves the sintering of powder particles to produce solid three-dimensional objects. In order to understand some of the events that may be occurring during the laser sintering process therefore, it is important to have an understanding of the principles of sintering and grain growth and the factors involved in the processing of powders.

2.4.1 Sintering

Sintering has been defined as "*a thermal treatment for bonding particles into a coherent, predominantly solid structure via mass transport events that often occur on the atomic scale. The bonding leads to improved strength and a lower system energy*" [German, 1996].

The driving force for the sintering process is the reduction in total interface energy, with surface energies being larger in magnitude than grain boundary energies. Surface energies are therefore lowered during sintering by a reduction in total particle surface area associated with pores with concomitant formation of interparticle bonds.

The bonds grow by various mechanisms that occur at the atomic level and which can be categorised in terms of the solid-liquid-porosity diagram shown in Figure 2.4.1A.

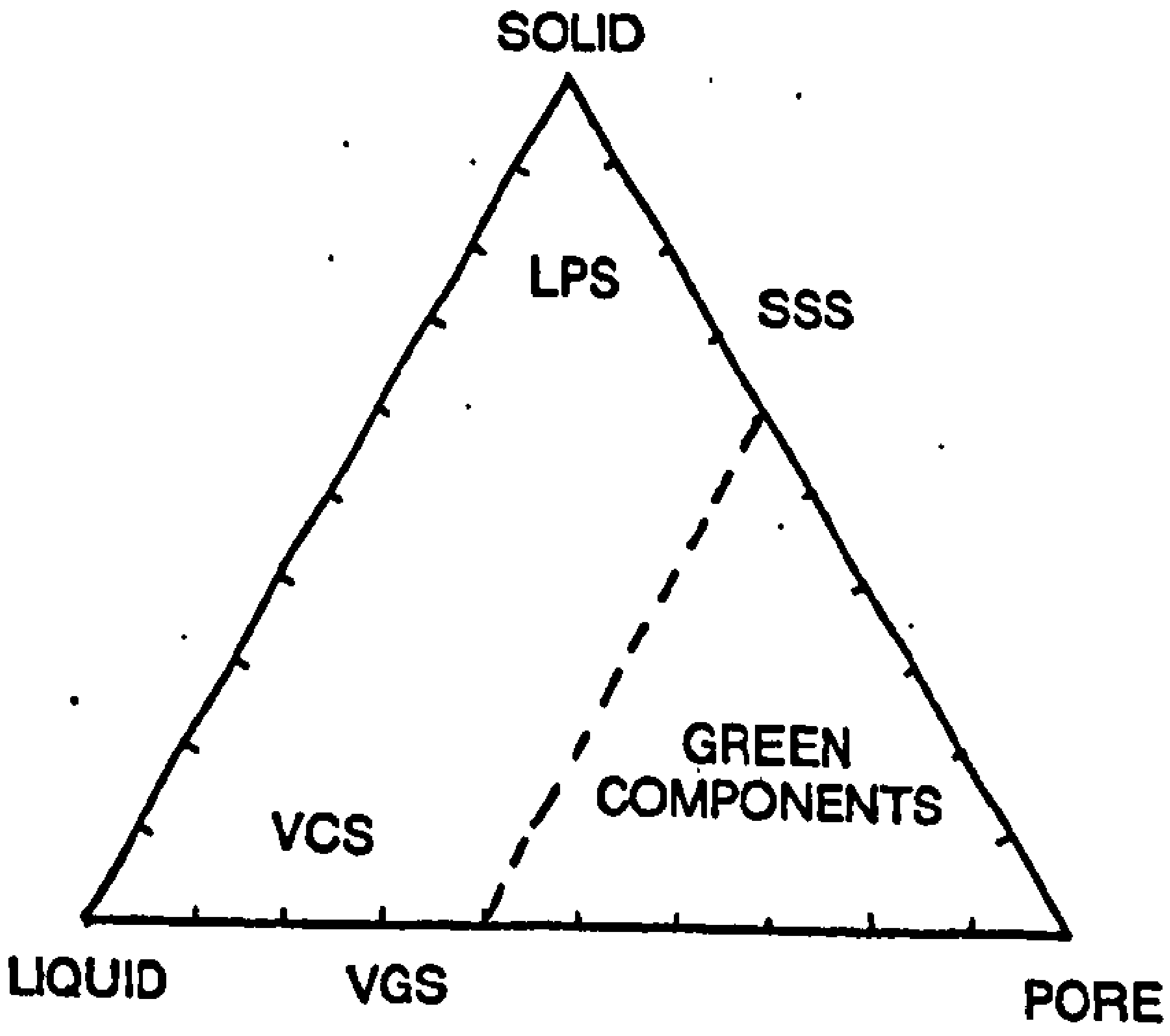

Figure 2.4.1 A: Ternary diagram illustrating the various types of sintering [Lee & Rainforth, 1994]

1. Solid State Sintering (SSS): Bonding is by solid-state diffusion and as only solid and pores are involved it is covered by the right-hand edge of the diagram.
2. Liquid Phase Sintering (LPS): Particle melting results in a solid-liquid mixture during the thermal cycle. All three components are involved but as most material is solid (<20% liquid) it is concentrated at the solid apex on the diagram.
3. Viscous Glass Sintering (VGS): This is the mechanism by which glass powders densify as occurs in glazing and enamelling. As only liquid (molten glass) and pores are involved it is covered by the bottom edge of the diagram.
4. Viscous Composite Sintering (VCS): Densification occurs in the presence of a viscous liquid, differing from LPS by the much greater amount of liquid present (>20% liquid). Also know as vitrification, this is the process that takes place in the sintering of many whitewares such as porcelains.

The following sub-sections will concentrate on the two main sintering mechanisms – solid state and liquid-phase sintering.

2.4.1.1 Solid State Sintering (SSS)

The SSS process can be broadly divided into three overlapping stages – initial, intermediate, and final.

Loose particles in contact with each other adhere as a result of weak forces such as van der Waals forces and agglomeration forces from liquids. Particles rotate and repack where possible in order to obtain a higher packing density and lower energy grain boundary structure [ref 29 in German, 1996].

The initial stage of SSS, illustrated in Figure 2.4.1B is characterised by the formation of a sinter bond at the points of contact between particles leading to initial neck formation.

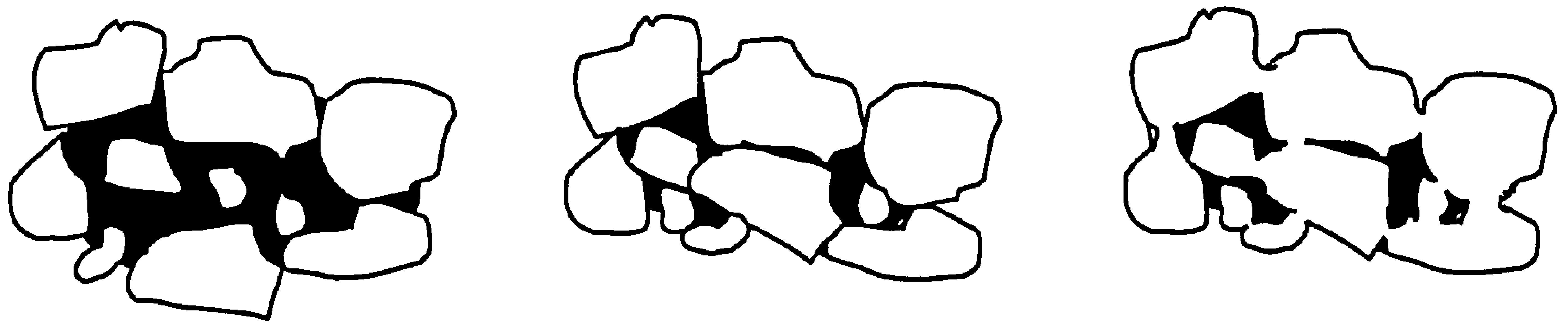

Starting particles Rearrangement Neck formation

Figure 2.4.1 B: Schematic diagram illustrating the initial stage in the sintering process [Ref.90 in Georgiou, 2002]

In this stage the size of the necks is small enough for neighbouring necks to grow independently of each other, particles do not lose their individuality, and no significant shrinkage of the compacted powder is observable. The pores are mostly interconnected (open porosity) and irregular in shape. The stage is considered to have ended when the necks begin to impinge at an approximate neck size ratio X/D of 0.3 – See Figure 2.4.1C [German, 1996].

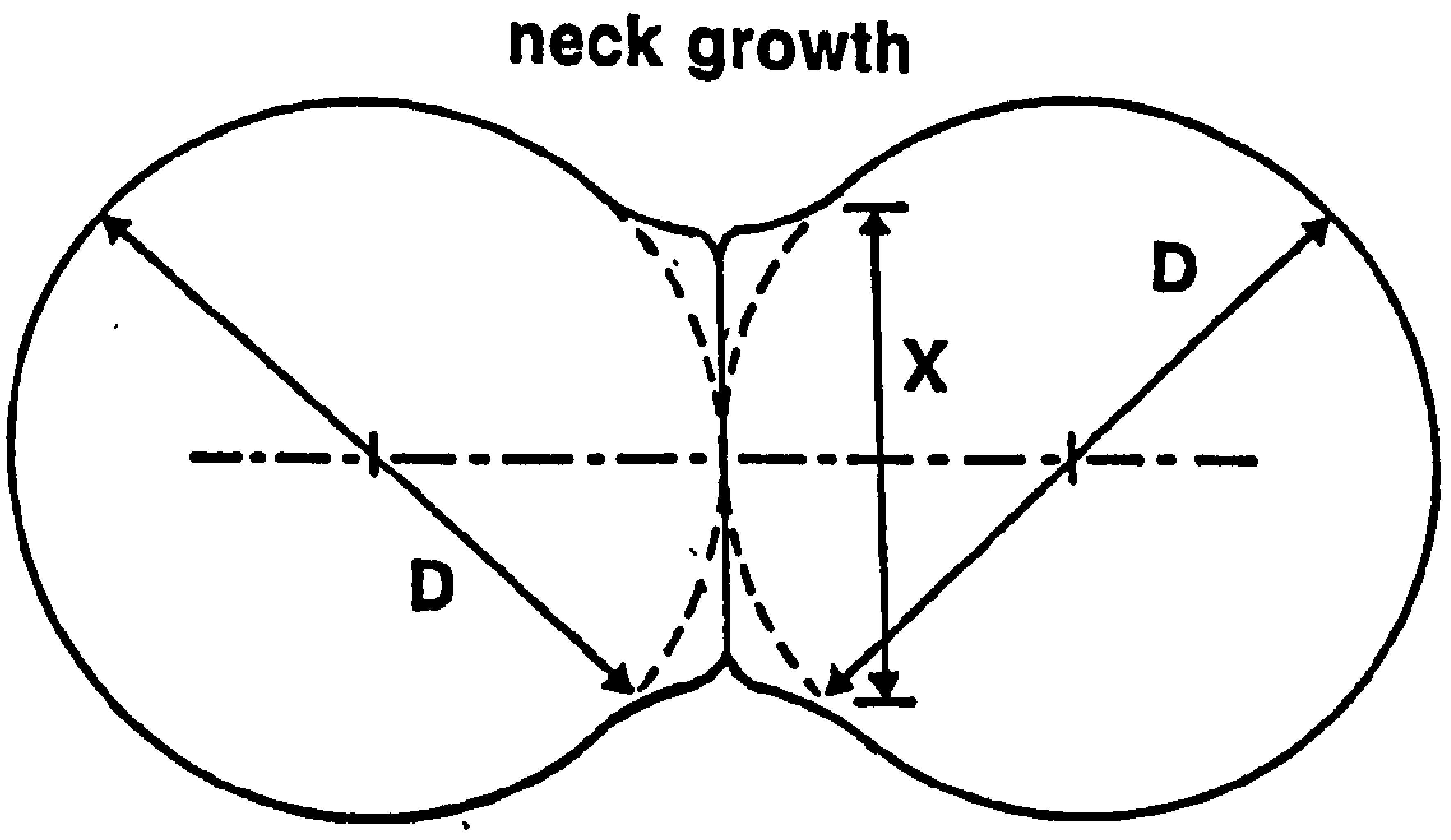

Figure 2.4.1 C: Sintering profile for two spherical particles with a neck diameter of X and sphere diameter of D [German, 1996].

During the intermediate stage, the size of the necks between particles grow, leading to a substantial decrease in the amount of porosity, and as the particles move closer together, shrinkage occurs. This is illustrated in Figure 2.4.1D. Pores become more spherical and open porosity decreases with more and more becoming closed off to leave isolated voids (closed porosity). Materials requiring a porous structure are only sintered to this stage. As the pores shrink and occupy less grain boundary area, grain growth becomes increasingly active.

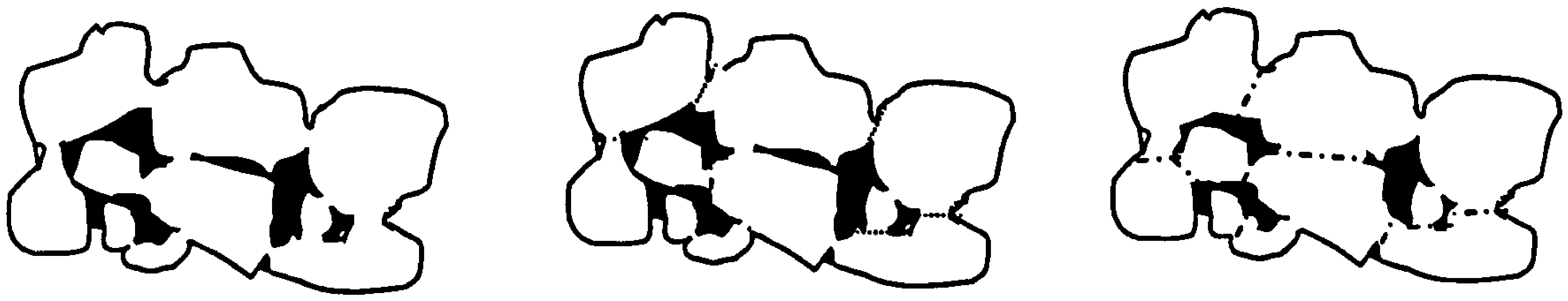

Neck growth and volume shrinkage.

Lengthening of grain boundaries.

Continued neck growth and grain boundary lengthening, volume shrinkage, and grain growth.

Figure 2.4.1 D: Schematic diagram illustrating the intermediate stage in the sintering process [Ref.90 in Georgiou, 2002]

In the final stage of sintering, the pores spheroidise and become closed. Densification is slow and relatively minimal as it is impeded by extensive grain growth. The endpoint density is limited by gas in the pores, but can often be eliminated by vacuum sintering to produce high final densities.

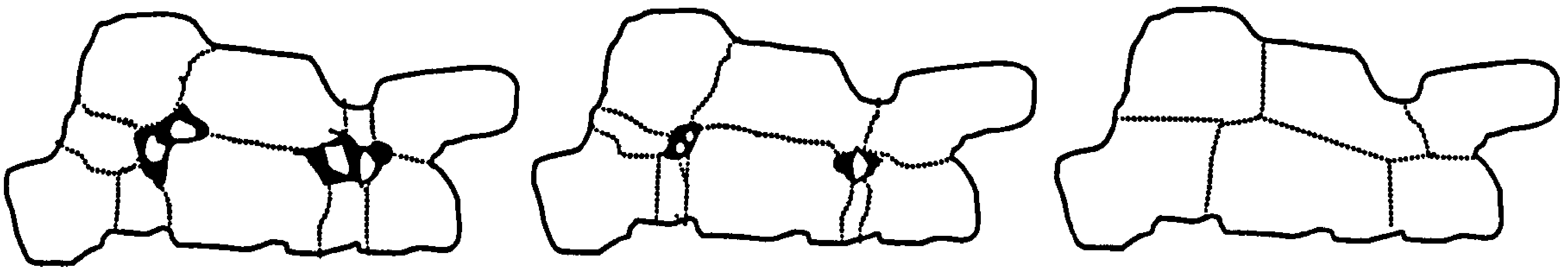

Grain growth with discontinuous pore phase

Grain growth with porosity reduction

Grain growth with porosity elimination

Figure 2.4.1 E: Schematic diagram illustrating the final stage in the sintering process [Ref.90 in Georgiou, 2002]

There are a number of different transport mechanisms which determine how mass flows in response to the driving force for sintering, i.e. reduction in surface area. The two main classes of mechanism, surface transport and bulk transport, are depicted in Figure 2.4.1F.

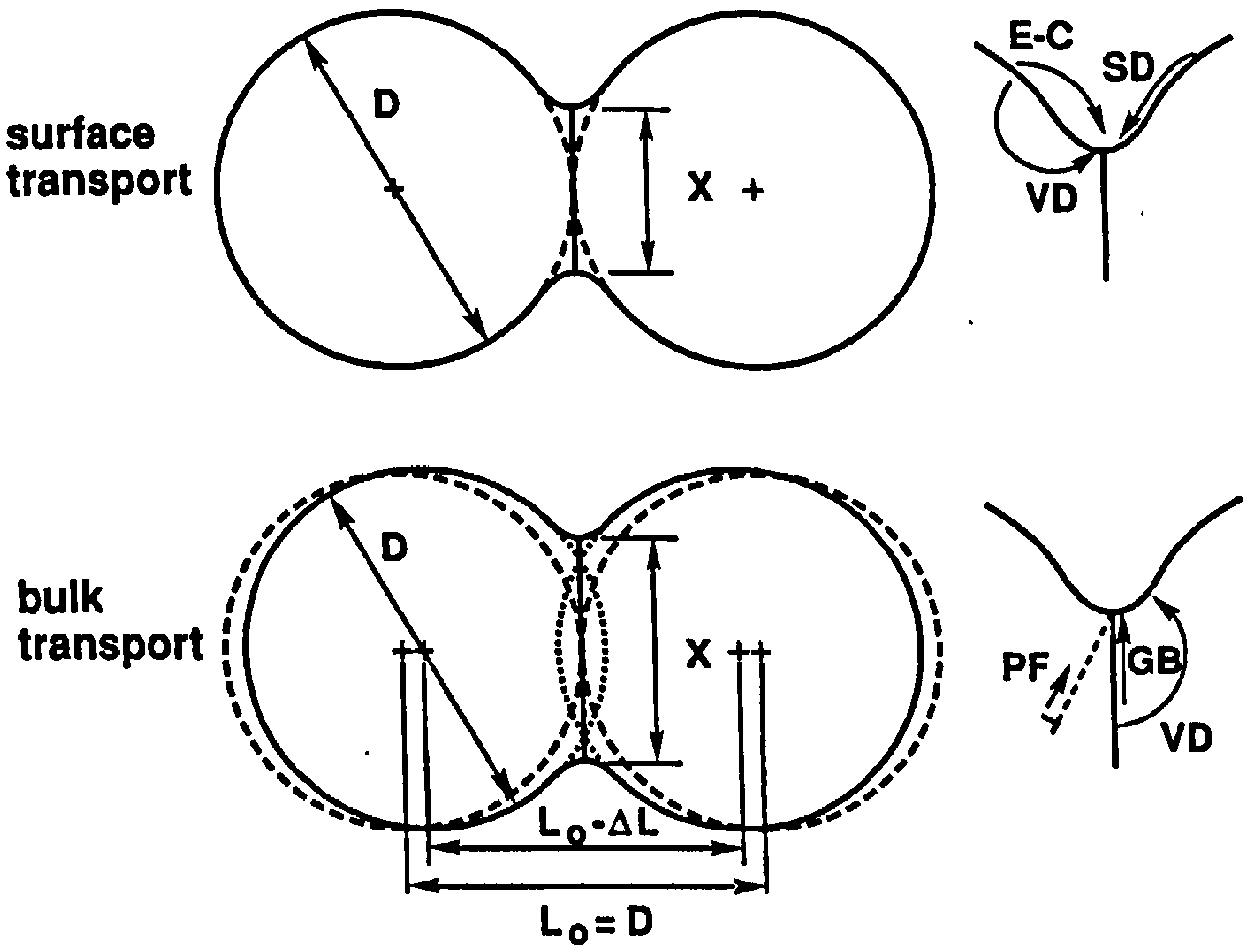

(E-C, evaporation-condensation; SD, surface diffusion; VD, volume diffusion; PF, plastic flow; GB, grain boundary diffusion; VD, volume diffusion)

Figure 2.4.1 F: Schematic illustration of two classes of sintering mechanism – surface transport and bulk transport [German, 1996]

In surface transport processes such as evaporation-condensation, surface diffusion, and volume diffusion, mass flow originates and terminates on the particle surface and thus neck growth occurs without a change in particle spacing. As a result there is a loss of surface area during neck growth, but no densification or shrinkage occurs. Surface diffusion is an initial contributor to the sintering of many materials and involves the motion of atoms between defect sites such as ledges and kinks. As both the population of these sites and the motion between them are thermally activated, surface diffusion is greatly influenced by temperature with highly curved surfaces and high temperatures leading to more diffusion. As the activation energy for surface diffusion is usually less than that for other mass transport processes, it tends to initiate at lower temperatures. Surface diffusion very rarely dominates the mass flow and its importance declines as sintering progresses. However for producing materials with high open porosity these sintering mechanisms are important as they result in well grown necks that provide good mechanical strength without densifying and thus loosing the open pore structure [German, 1996].

In bulk transport processes such as volume diffusion, grain boundary diffusion, and viscous flow, mass flow originates in the interior of a pair of particles and terminates at the neck region. It is these processes that are responsible for densification during sintering. Amorphous materials tend to sinter by viscous flow, with viscosity decreasing with increasing temperature. Crystalline materials however sinter by grain boundary or volume diffusion. Interparticle grain boundaries form due to misaligned crystals and allow mass flow along a narrow transport path to be deposited at the bond between particles. Grain boundary diffusion appears to be the dominant mechanism for many common ceramics [Lee and Rainforth, 1994]. In volume diffusion vacancies (sites where an atom is missing) migrate through the crystalline structure along a diffusion pathway of which there are three main types. These are illustrated in Figure 2.4.1G. The first pathway, termed volume diffusion adhesion, involves vacancy flow (and thus atomic flow in the opposite direction) from the neck surface to the particle surface through the interior of the particle, resulting in the deposition of mass at the neck surface. The second pathway, termed volume diffusion densification, is from the neck surface to the interparticle grain boundary, causing densification and shrinkage of the material to occur. The final pathway, termed dislocation climb, allows vacancies to be emitted or annihilated by dislocations, which also results in densification as the vacancies did not originate at the surface. The process is particularly common in compacted powders [German, 1996].

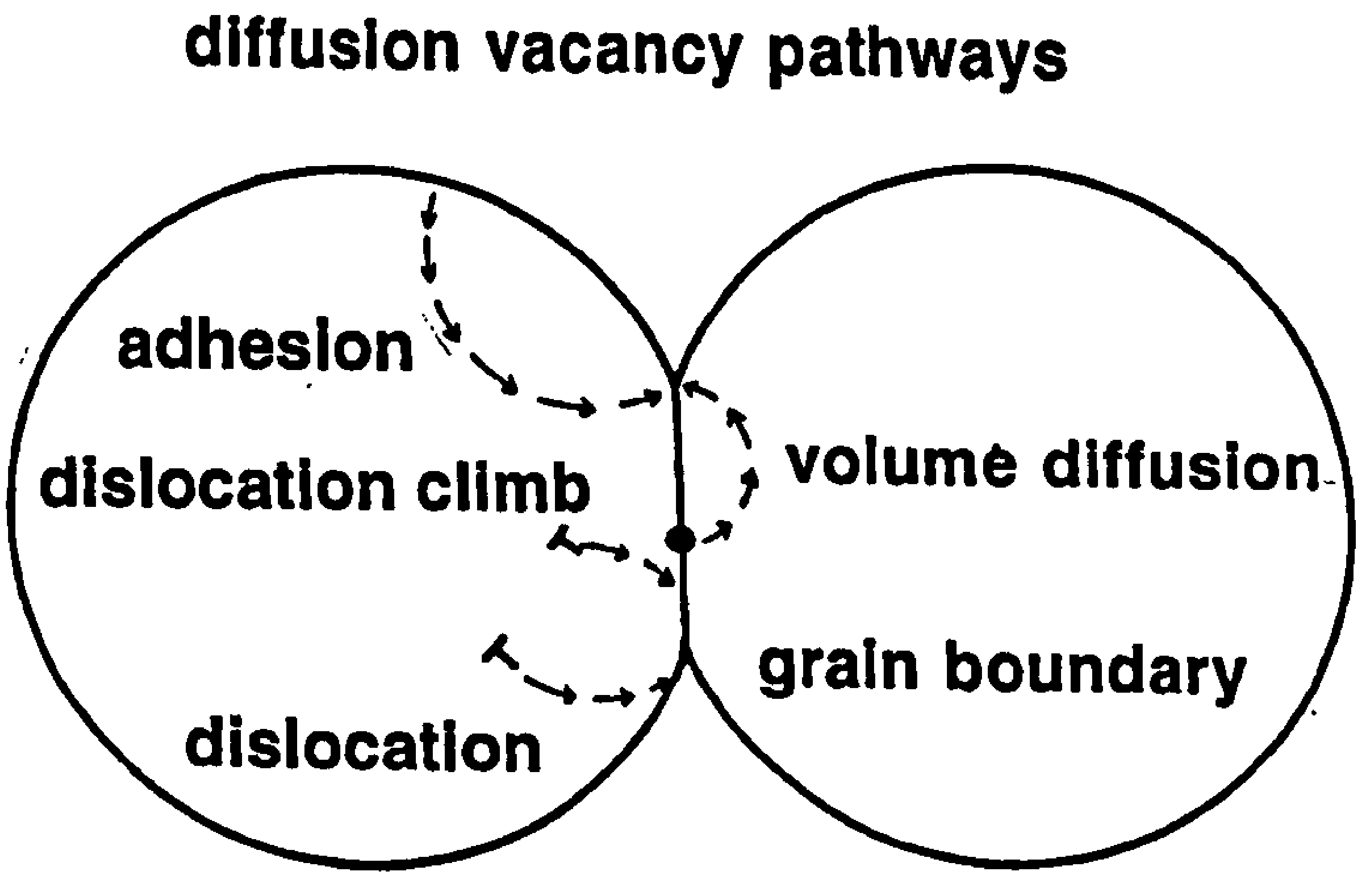

Figure 2.4.1 G: Volume diffusion pathways [German, 1996].

2.4.1.2 Liquid Phase Sintering (LPS)

Whilst SSS occurs in some important bioceramics such as specialised forms of alumina and zirconia [Lee and Rainforth, 1994], the majority of commercial ceramics are densified in the presence of a liquid phase. This phase is usually formed by design, but it may also form as a by-product of incidental impurities. The liquid coats the powder particles and causes more rapid densification at temperatures considerably lower than required for SSS. Liquid phase sintering may therefore occur in ceramics where solid state sintering is not possible e.g. covalently bonded Si_3N_4.

Like SSS, the driving force for LPS is a reduction in surface energy. The stages of LPS are depicted in Figure 2.4.1H.

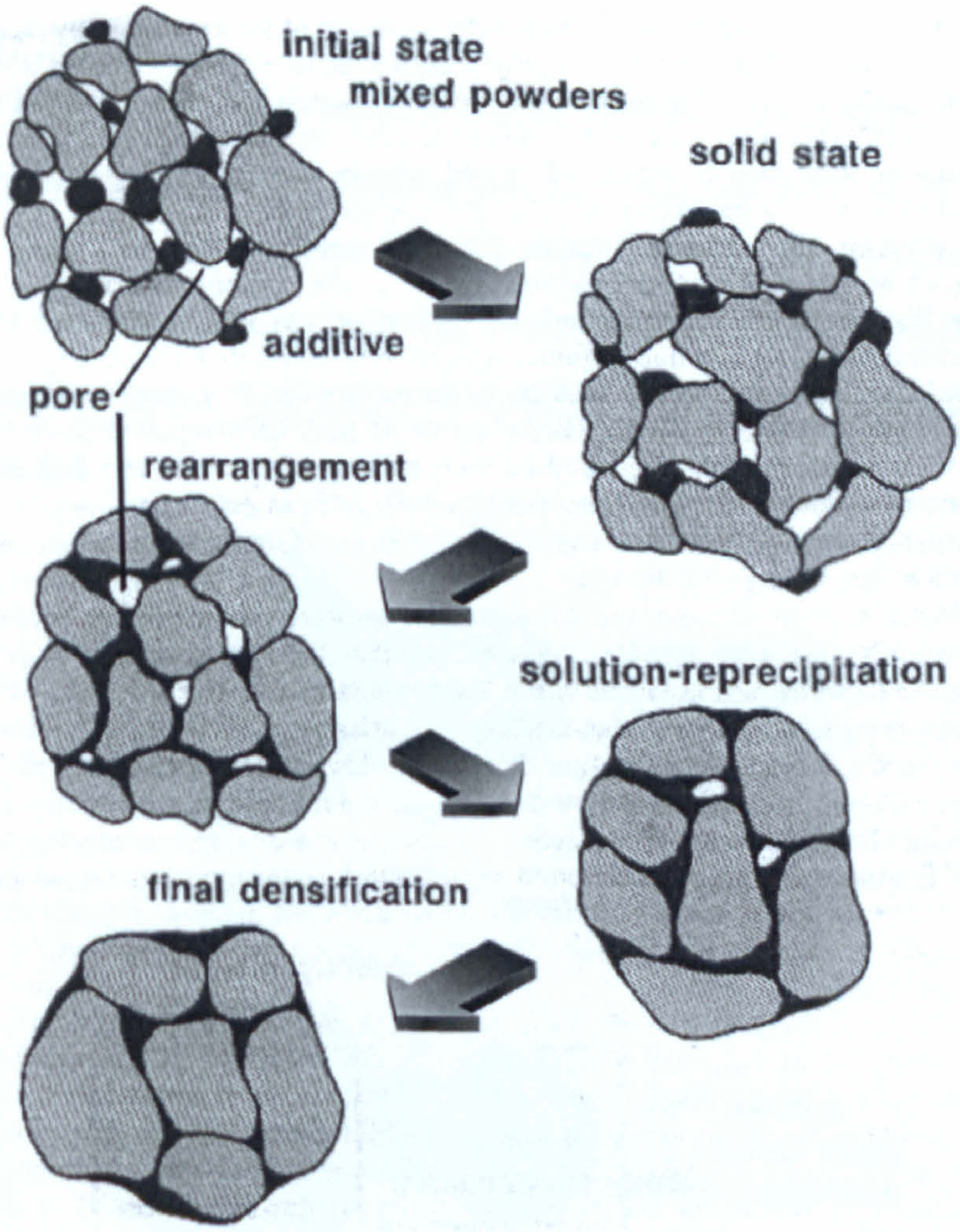

Figure 2.4.1 H: Stages of liquid phase sintering [German, 1996].

As the powder is heated some densification may occur even before the first liquid forms, as a result of solid-state sintering driven in part by the chemical concentration gradient in the microstructure. Subsequent densification is determined by the amount of liquid phase present. The liquid phase normally forms by one of two methods – composite sintering or solid solution sintering. Composite sintering occurs when the powdered material is comprised of two different materials with one having a lower melting temperature which forms the liquid phase upon heating. Solid solution sintering occurs when the material is of one composition but has a mixture of particle sizes, with the smaller particles melting first to form the liquid phase.

Three stages of densification are encountered after the initial formation of the liquid phase: rearrangement, solution-reprecipitation, and final-stage sintering.

Rearrangement

The presence of a liquid promotes particle rearrangement via capillary forces that draw the particles together and cause densification. In order for LPS to be successful the liquid must be able to sufficiently wet the solid surface, characterised by a small contact area θ. If the liquid poorly wets the surface, swelling occurs and liquid may be extruded from surface pores. The affect of wetting on particle attraction/separation can be seen in Figure 2.4.1I .

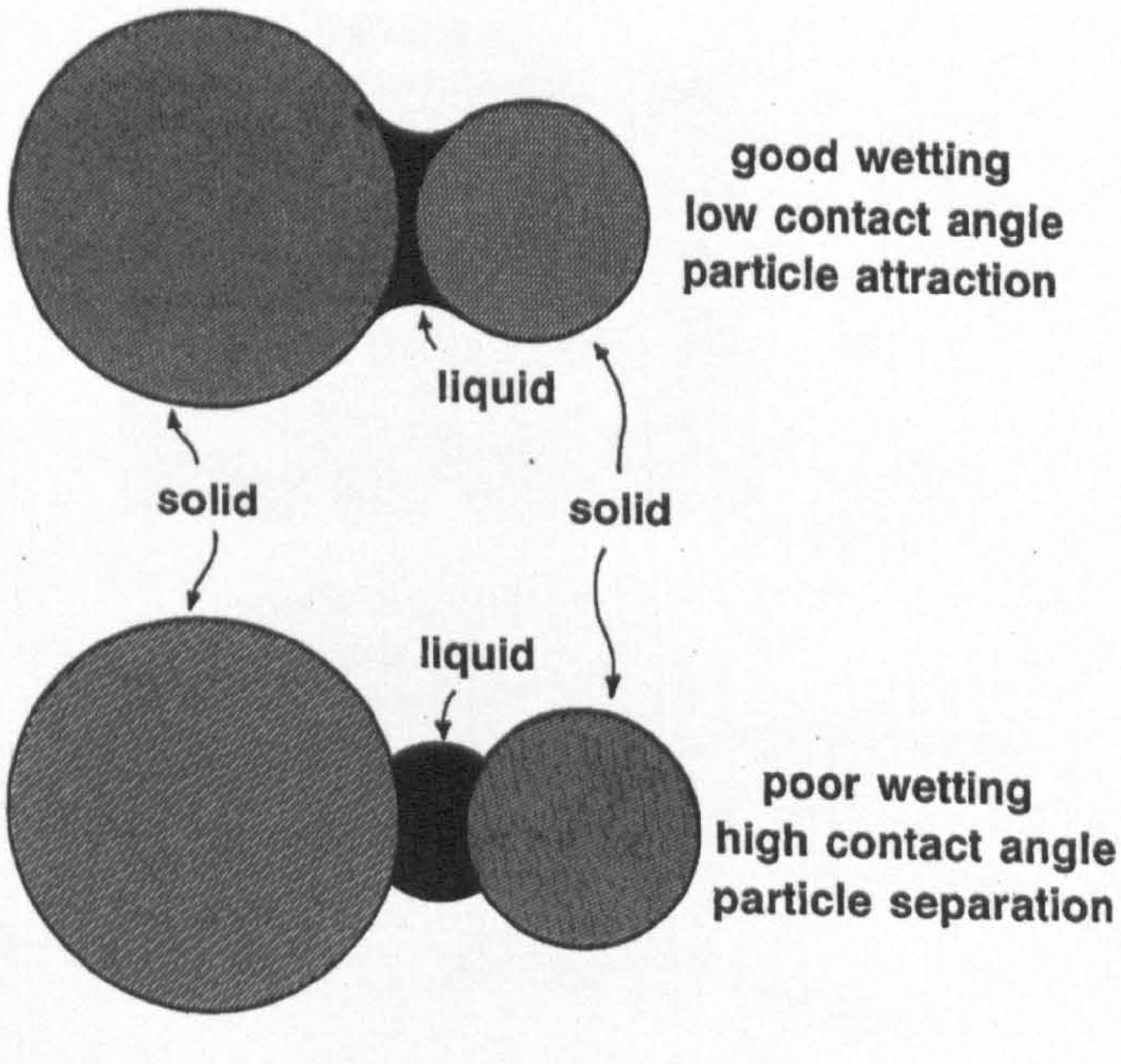

Figure 2.4.1 I: Affect of good and poor wetting on particle attraction and separation [German, 1996]

The range of pore shapes and sizes in a typical powder create a range of capillary conditions, with the smaller capillaries having higher energy per unit volumes. As a wetting liquid occupies the lowest-energy position it preferentially flows into these smaller capillaries leaving the larger ones empty. If there is insufficient liquid to fill all the pores the particles are pulled together by the liquid to minimise the energy, resulting in rearrangement densification. Small particle sizes and smooth particles aid rearrangement densification as the capillary force is higher [German, 1996].

If enough liquid is formed, full density can be achieved via rearrangements. However in most liquid-phase sintering systems there is insufficient liquid and therefore solution-reprecipitation events are required.

Solution-reprecipitation

As the particles continue to be heated, the solid phase dissolves into the liquid, causing the volume of liquid to increase until it becomes saturated with the solid component. As the solubility of solid grains varies inversely with grain size, the smaller solid particles preferentially dissolve in the liquid phase and precipitate on the solid surfaces of large particles as depicted in Figure 2.4.1J. This process is termed Ostwald ripening and causes the particles to decrease in number but increase in size. Densification is aided by a large amount of liquid and high solid solubilities in the liquid.

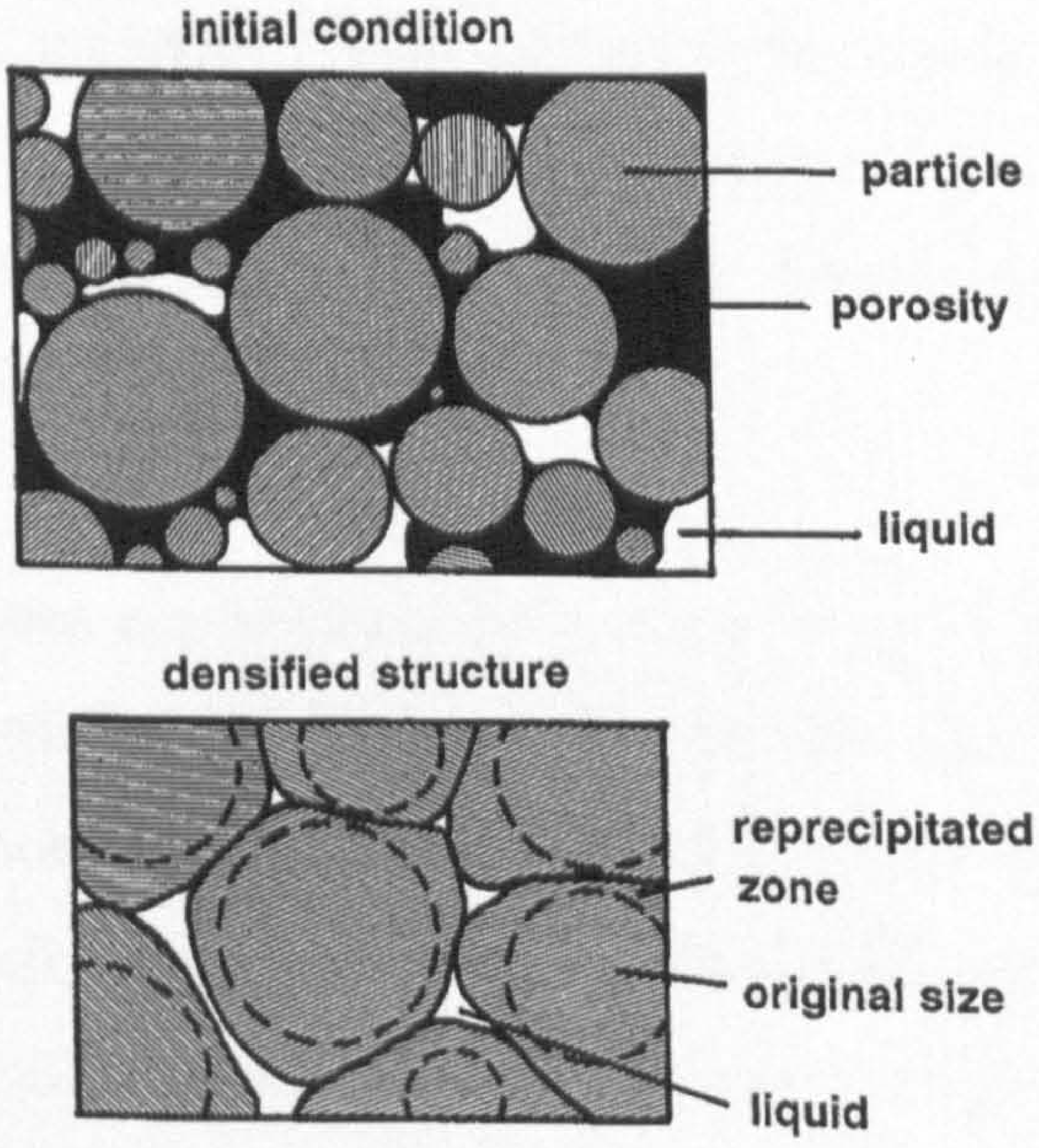

Figure 2.4.1 J: Schematic illustration of pore elimination via grain shape accommodation through solution-reprecipitation [German, 1996]

Besides contributing to grain coarsening, the process of solution-reprecipitation provides densification via grain size accommodation. Growing solid grains are allowed to deviate from a minimum energy spherical shape to provide better packing and release liquid to fill any remaining pores. Grain size accommodation is favoured as although spherical shapes have lower solid-liquid surface areas, the adjusted grain shapes eliminate porosity and the high interface energy associated with pores. By the end of the intermediate stage, pores have generally been eliminated or become stabilised by trapped gas.

Final-Stage Sintering

The final stage of liquid-phase sintering is characterised by continued grain growth with slow densification controlled by solid-state diffusion. A prolonged final stage can result in degradation of the properties of most liquid-phase sintered materials due to problems such as the entrapment of gas in residual pores which can lead to compact swelling. Therefore short sintering times are generally preferred in practice.

2.4.2 Powder and Particulates

The morphology and size of the powder particles are important variables in the laser sintering process since they influence packing, flow and compressibility [German, 1994]. They also affect uniformity and homogeneity during sintering, and help to explain many processing characteristics. Maximum particle packing and uniformity is generally desired as it results in a high sintered density and superior mechanical strength [Lee and Rainforth, 1994].

Improved packing densities are achieved by using a range of particle sizes, where the gaps between larger particles are filled by smaller ones [Lee and Rainforth, 1994]. Optimum packing of monosized spherical particles results in 30% porosity [Figure 2.4.2A], which is usually undesirable in the production of parts requiring good mechanical strength since the large amount of porosity results in an increased critical flaw content. However by adding smaller particles that are the size of the interstices, the porosity can be reduced to 26%, and adding even smaller particles in the then remaining gaps reduces porosity even further to 23%. However some applications, including that being considered in this work of producing a material favourable for the ingrowth of bone, may require a certain degree of porosity to remain. In these situations strict control of the porosity must be achieved to ensure that sufficient porosity is retained, whilst at the same time ensuring that the mechanical strength is adequate for the application. This can be achieved by controlling the particle size distribution by, for example, using a lower proportion of smaller particles, thereby allowing gaps between particles to remain.

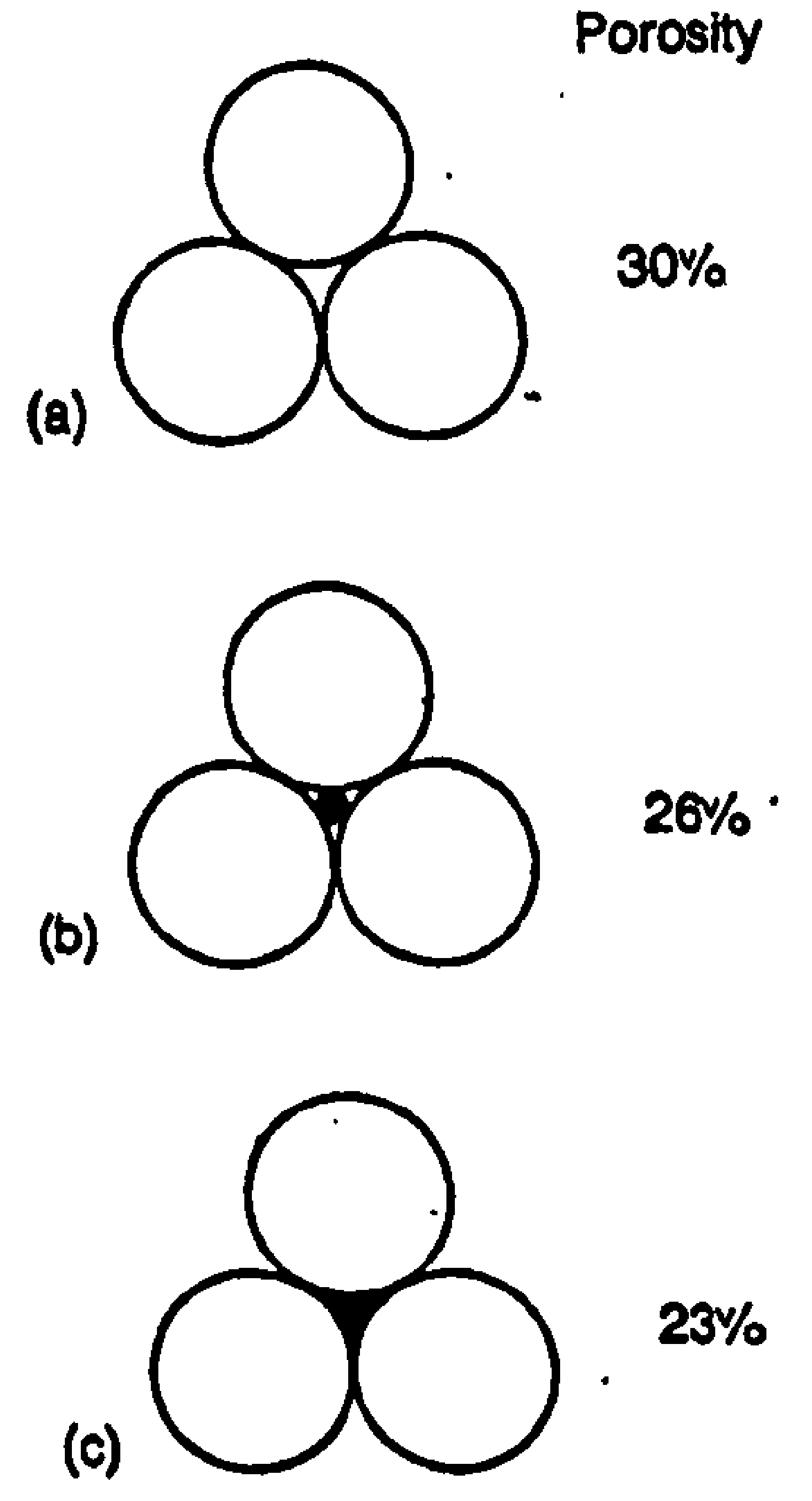

Figure 2.4.2 A: Illustration of the reduction in porosity that results from the use of multisized particles [Lee and Rainforth, 1994]

The above theory on particle size distributions and packing arrangement is based on the assumption that the powder particles are idealised spheres or circles. This is very rarely the case, the exception being powders produced through atomisation techniques. Most milled ceramic powders have a broad size distribution and a range of complex particle shapes [German, 1994]. The various particle size fractions can be separated out by sieving or controlled segregation techniques such as sedimentation. However particle morphology is very difficult to quantify due to the highly complex and irregular particle shapes that result from different manufacturing techniques. Therefore qualitative descriptors are often used, a collection of which are given in Figure 2.4.2B.

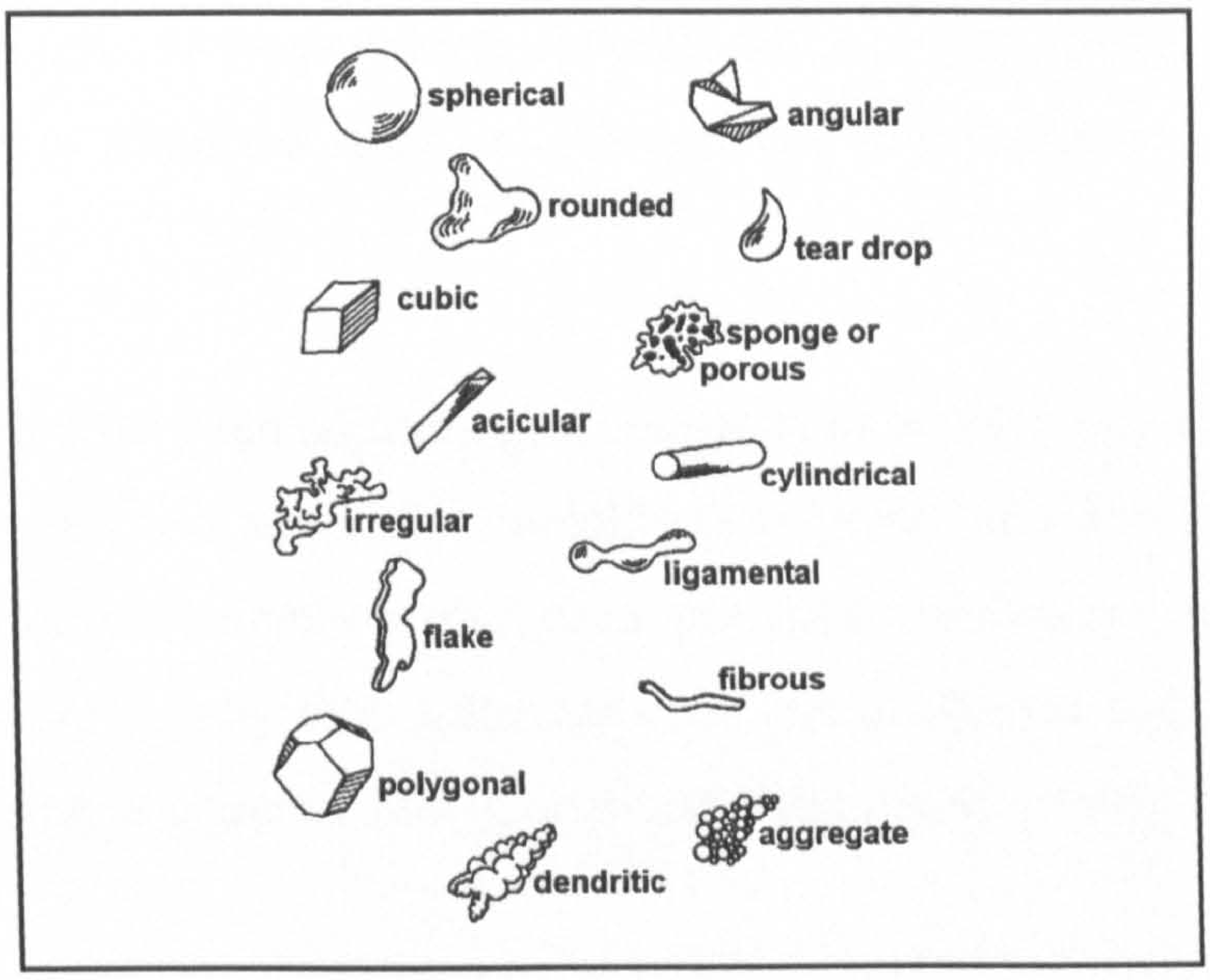

Figure 2.4.2 B: A collection of possible particle shapes and the suggested qualitative descriptors [German, 1994]

Particle morphology has an effect on the packing density, as the more irregular the particle shape or the greater the surface roughness, the less efficient particle packing becomes. As can be seen in Figure 2.4.1C, for monosized particles differing in shape, the closer they are to the idealised sphere, the higher the packing density.

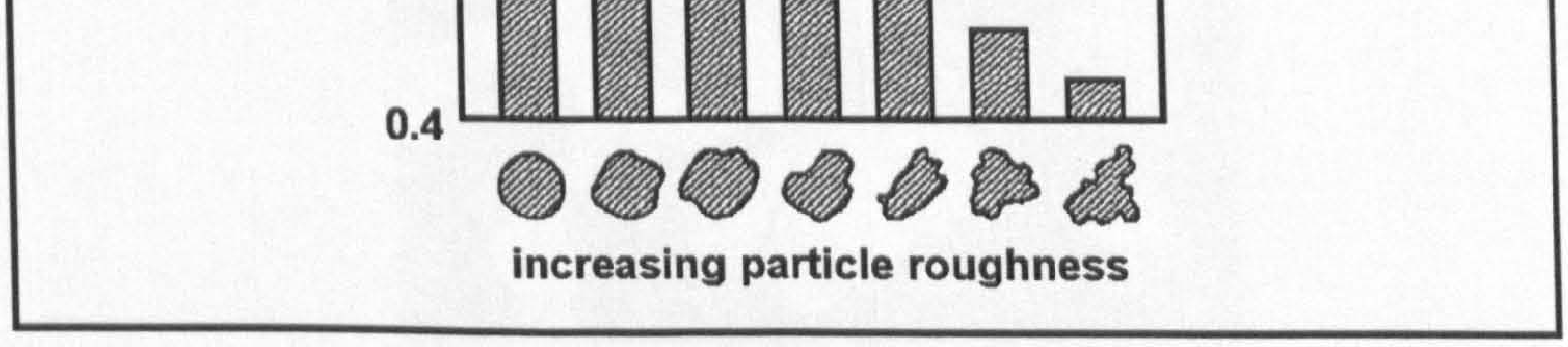

Figure 2.4.2 C: A plot of fractional packing density for monosized powders versus particle irregularity [German, 1994]

An increase in particle surface area due either to an increase in particle size or deviation from a spherical shape results in an increase in the amount of friction in a powder mass. Consequently, the particles exhibit less efficient flow and packing. By reducing the particle size, the ability of the powder to flow can be improved up until the point where the particles start to acquire a static self charge, and thus become difficult to spread evenly.

The rate of sintering between adjacent powder particles is determined by their size and shape. Small particles will sinter more quickly than larger ones due to a higher energy per unit volume, more available surface area, and higher curvature. Irregularly shaped particles sinter more rapidly than spherical ones due to sharper radii at the points of contact which shrink at a greater rate [Cutler and Henrichsen, 1960].

2.4.3 Porosity

Pores can be classified into two major types – open pores, which connect to the outside of the material, and closed pores, which do not have an opening on the surface of the material and may contain a fluid. Open pores may be penetrating, in which case they have two or more openings located on two sides of a porous material, or non-penetrating when there is only an opening on one side of the material. A schematic diagram of the different morphology of pores can be seen in Figure 2.4.3A.

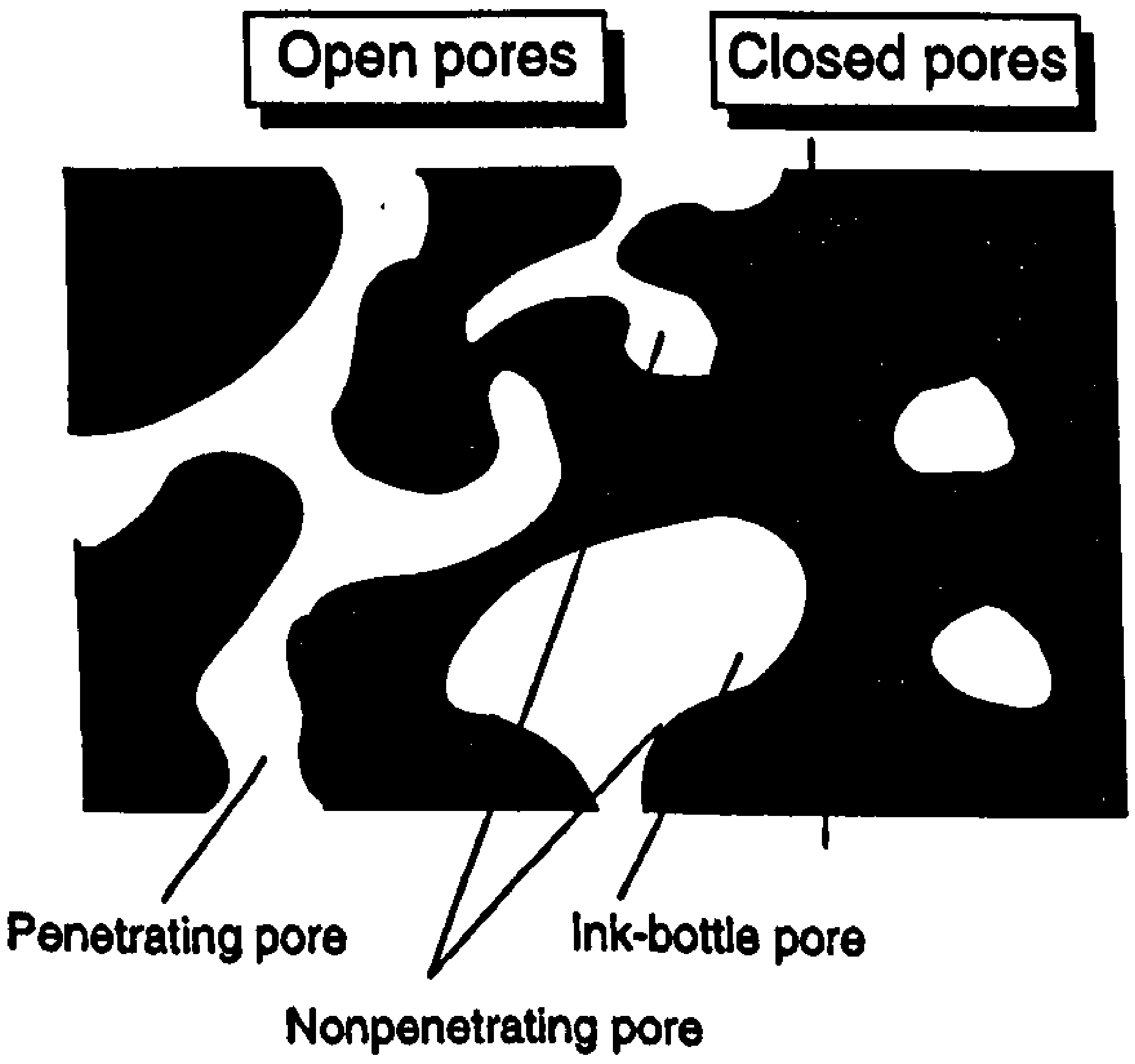

Figure 2.4.3 A: Schematic illustration of open and closed porosity [Ishizaki *et al.*, 1998].

The presence of open porosity in a material results in a decrease in density and an increase in specific surface area. In many applications high open porosity is desirable to generate useful properties such as fluid permeability, filtration effects, and for the purpose of producing bone replacement materials, bone ingrowth. However an increase in porosity generally results in a decrease in mechanical strength [Ishizaki *et al.*,1998].

2.4.4 SLS Processing Parameters

SLS is unique in its ability to convey strength to a part through the control of its parameters. The key operational parameter in the SLS process is energy density which is assigned a dimension known as the Andrew number. Nelson *et al.* [1993] has shown energy density to be composed of three operating parameters:

$$EnergyDensity = \frac{P}{\pi\omega^2} \times \frac{2\omega}{SS} \times \frac{2\omega}{ScSp} \cong \frac{P}{SS \times ScSp}$$

where ω = effective laser beam radius, P = laser power, SS = scan speed, ScSp = scan spacing

1st term = power density of laser beam
2nd term = approximates time that a circle with radius ω is under the laser beam during one pulse of laser power
3rd term = estimates number of pulses received by the same circle

Scan spacing (i.e. the distance between two adjacent parallel scan lines) is usually less than the laser beam diameter in order to allow each point on the surface to receive several pulses of laser power. If scan spacing is too great, the cross-section may not be completely sintered. Scan speed, measured in mm per second, is the speed at which the laser beam moves on the part bed. As the amount of energy absorbed is dependent upon the duration of radiation from the laser on a unit area, increasing the scan speed will mean less energy is absorbed and thus the degree of sintering will be reduced. Consequently the porosity within the samples will increase [Leong *et al.*, 2001].

Another fabrication parameter to be considered is the layer depth, i.e. the depth that the part piston lowers for each layer and hence the thickness of the layer of powder to be scanned. This factor has a great influence over both building time and surface roughness. A balance is required between decreasing surface roughness using smaller slice thickness, whilst at the same time maintaining large enough slices for reasonable speed to be used in the production of the part.

Tensile strength and part density increase with decreasing scan speed, scan spacing and increasing laser power [Gibson and Shi, 1997]. Tensile strength is proportional to part density, and thus in order to obtain good mechanical properties, fully dense parts are usually favoured. High energy density can cause curling and distortion of the parts, and thus an optimal energy density should be sought in order to achieve good mechanical properties whilst maintaining accuracy.

In theory, it should be possible to use a SLS process to replace the complete sequence of steps in the fabrication of the implant. Currently however this does not happen, as the green parts produced by SLS have relatively low densities, and thus in practice SLS is generally only used for shaping, with post processing steps then being required to increase density and impart strength to the part.

2.4.5 Direct versus Indirect

Successful sintering of particles during SLS is dependent on adequate absorption or coupling of the laser energy. Ideally a direct laser sintering method is desired, both to increase the sintered density and decrease the processing time. This involves forming a dense layer by the melting and solidification of the individual powder particles. Sintering occurs by the formation of a neck between adjacent solid particles. However this process can be very slow and difficult to realise in practice [Fuesting *et al.*, 1996].

Alternatively an indirect method may be used, so called because a polymeric binder is added to the glass powder and during the SLS process behaves like a low temperature phase, bonding the substrate particles into a contiguous part. The resulting 'green part' is then post-processed in a furnace to either burn the binder out of the system [Barlow and Vail, 1994], or chemically convert the binder to a higher melting point component [Lee and Barlow, 1993]. Both polymers and inorganic materials have been used as binders for several years, but polymers have the advantage of being able to be completely eliminated from the green part following post-processing.

2.4.6 Factors Affecting Accuracy

STL Files: Like most layer manufacturing systems, SLS machines use a standard STL input file format. An STL file approximates the surface of the three-dimensional CAD model with multiple facets (usually triangles) – as shown in Figure 2.4.6A. On curved surfaces facets are difficult to avoid and will often be transferred to the final model. Reducing the size of the facets may allow smoother surfaces to be produced, but will result in large data files that may cause storage and computing problems [Yan and Gu, 1996].

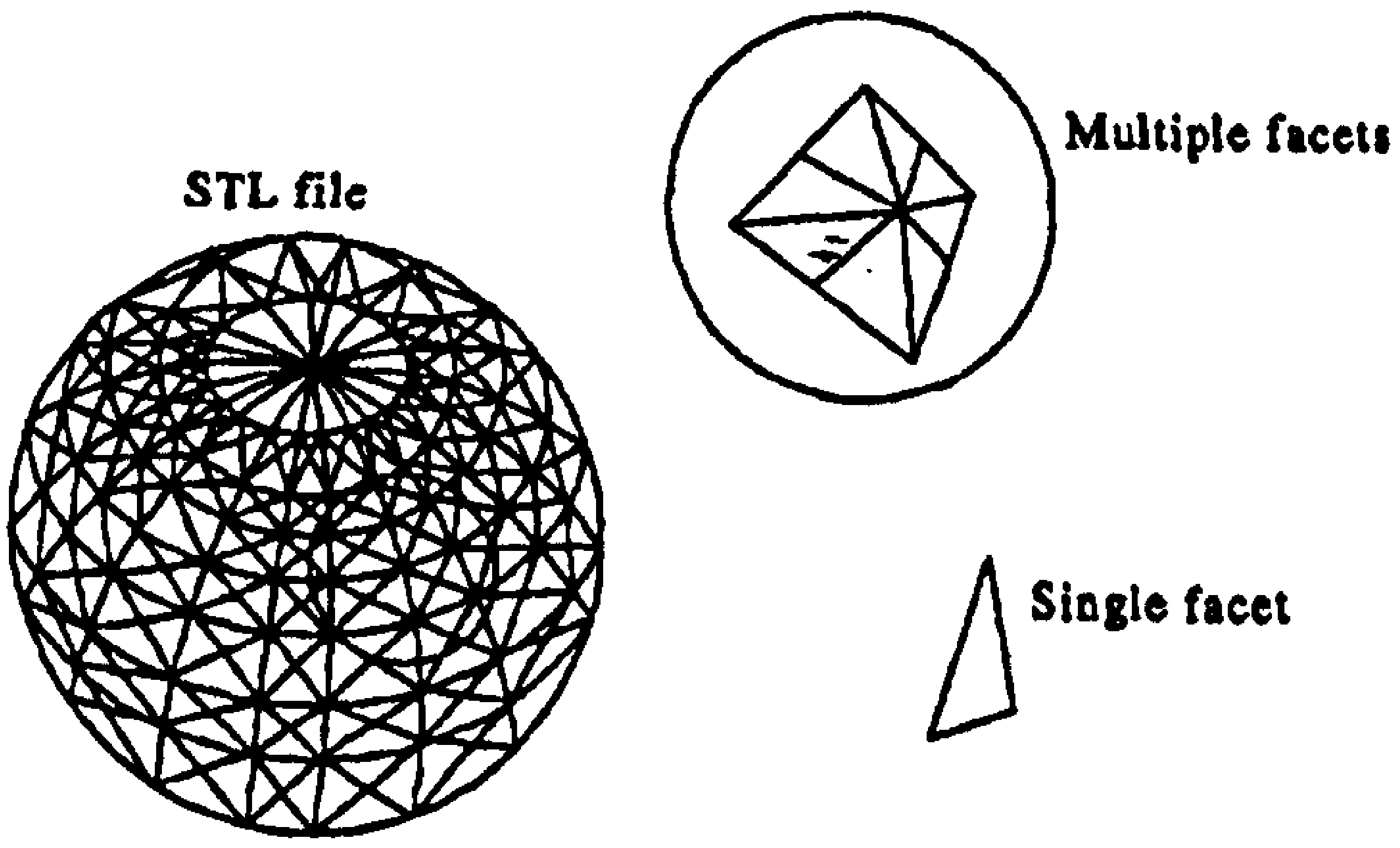

Figure 2.4.6 A: Approximation of the surface of a sphere with multiple facets [Yan and Gu, 1996].

Stairstepping: As with all layer manufacturing techniques, selective laser sintering produces a "stairstepping" effect as a consequence of the addition of material in layers which have a finite thickness and as the laser only cuts the part perpendicular to the plane. Parts with slight slopes are particularly affected. The problem can be alleviated by reducing the thickness of the layers which for SLS is usually achieved by reducing the particle size. However there is a limit to how small the powder can be ground to as there becomes a point when the smaller particles begin to acquire a static self-charge that makes spreading of the powder increasingly difficult. Thin layers also make the build process very slow. A partial solution to this problem is the use of adaptive slicing where variable slice thicknesses are used depending on the local slope of the part - See Figure 2.4.6B [Pham *et al.*, 1999].

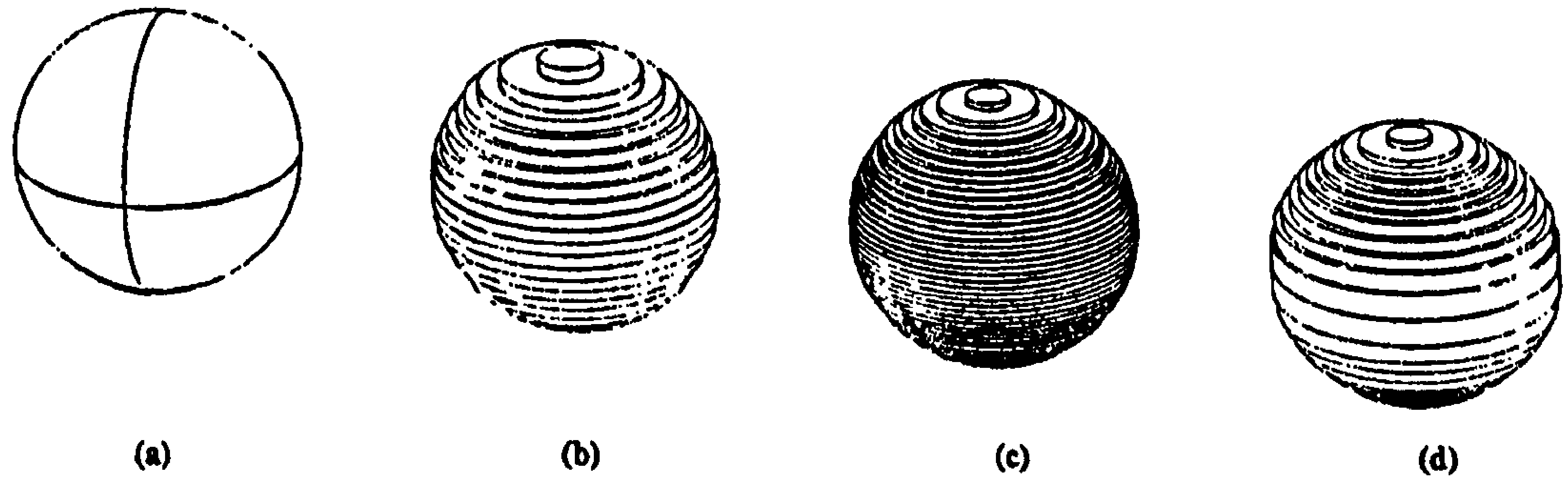

Figure 2.4.6 B: Slicing of a ball: a) no slicing, b) thick slicing, c) thin slicing, d) adaptive slicing [Pham *et al.*, 1999]

Material-related Errors

The major material-related errors are shrinkage and distortion. Shrinkage results from solidification during the cooling down of the material. Dimensional shrinkage can often be predicted and can be compensated for by scaling the CAD model. However shrinkage is not always uniform in the x, y, and z axis – for example if shrinkage of a new layer is constrained by the existing part substrate or by powder trapped within enclosed areas. Variations in the temperature of different areas can also result in non-uniform shrinkage [Pham *et al.*, 1994].

X and Y Errors

In addition to shrinkage effects, the accuracy in the x and y directions can be affected by the scanning system used and its ability to accurately generate the intended laser path [Pham *et al.*, 1994]. Mirror galvanometers are used to position the laser beam and therefore errors are often as a result of the time required to accelerate and decelerate them.

Z Errors

When STL files are sliced into layers, there will be some round-off error, and if either the top or bottom surface of a feature does not coincide with a specified layer then its height will be adjusted. If both surfaces are rounded-off then the height may be adjusted by a whole layer thickness [Pham *et al.*, 1994]. Dimensions in the z-axis can also be affected by "z-growth". This occurs during scanning of successive layers when additional energy is imparted to the layers below causing them to thicken. As this growth is sensitive to geometry and operating parameters it is difficult to predict.

2.5 Experimental Analysis Techniques

A number of experimental techniques were used in this work to determine the mechanical and biological properties of parts produced by SLS. The principles of some of the more important of these are explained below in order for readers that are unfamiliar with them to gain an insight into their functions.

2.5.1 Differential Thermal Analysis (DTA)

Differential Thermal Analysis (DTA) is a technique which enables investigation of the crystallisation of glasses and determination of the temperatures at which different crystals are formed. When a glass crystallises, an exothermic reaction occurs as the free energy of the regular crystal lattice is less than that of the disordered liquid state. Conversely, an endothermic reaction occurs when the crystal melts. A schematic diagram of a DTA apparatus is shown in Figure 2.5.1A.

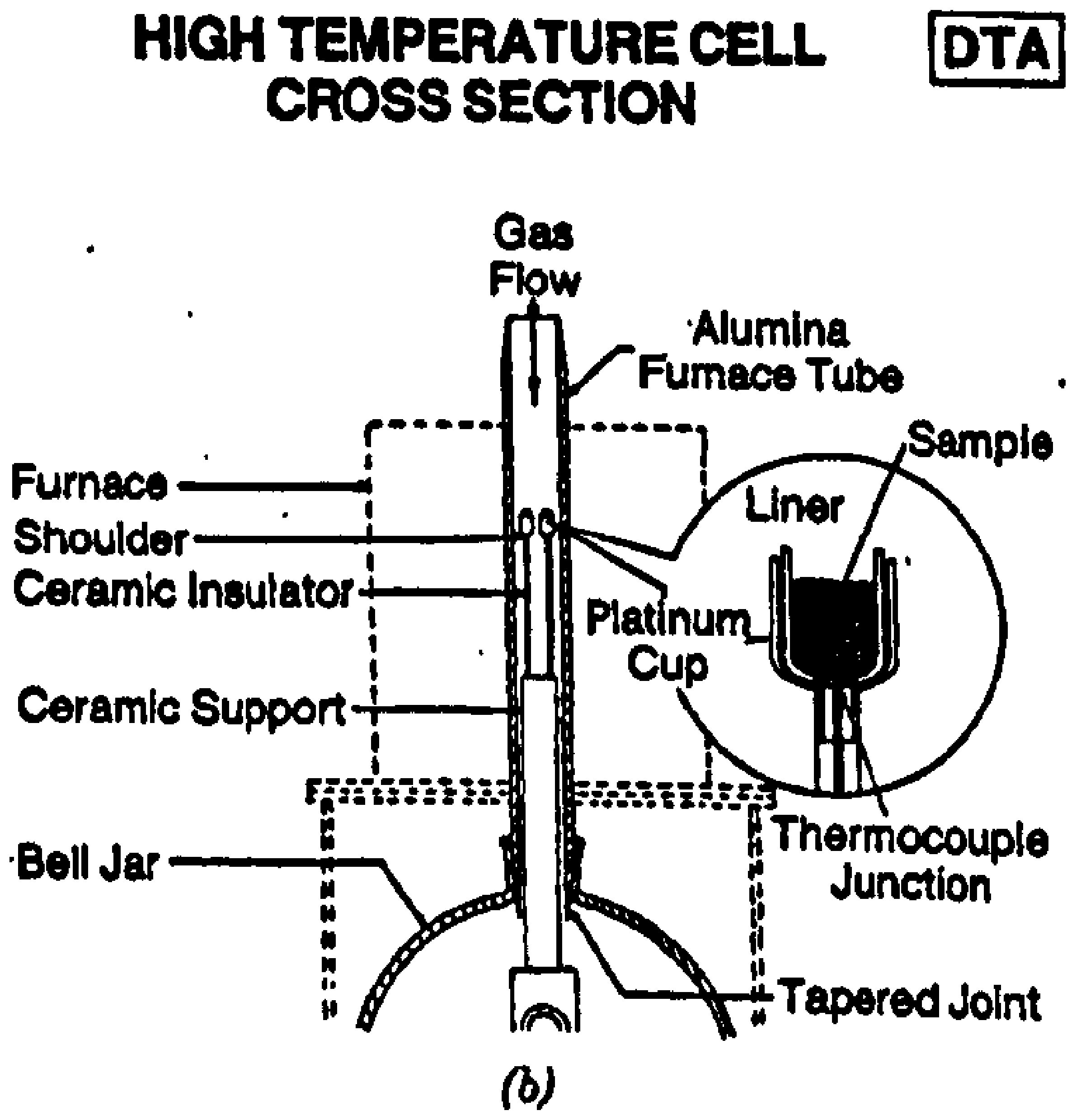

Figure 2.5.1 A: Schematic diagram of DTA apparatus [Bundle *et al.*, 1992]

The material to be tested is placed in powder form, into a small sample holder, usually made from platinum or other refractory metal. An inert reference material, such as aluminium oxide is placed in an adjacent sample holder. The two samples are heated together at a constant rate and the difference in temperature between them is measured during heating. As DTA is a comparative method, the heating of the two samples must be symmetrical.

The differential temperature between the two samples is plotted against the actual temperature, as a line of best fit. A typical DTA curve can be seen in Figure 2.5.1B.

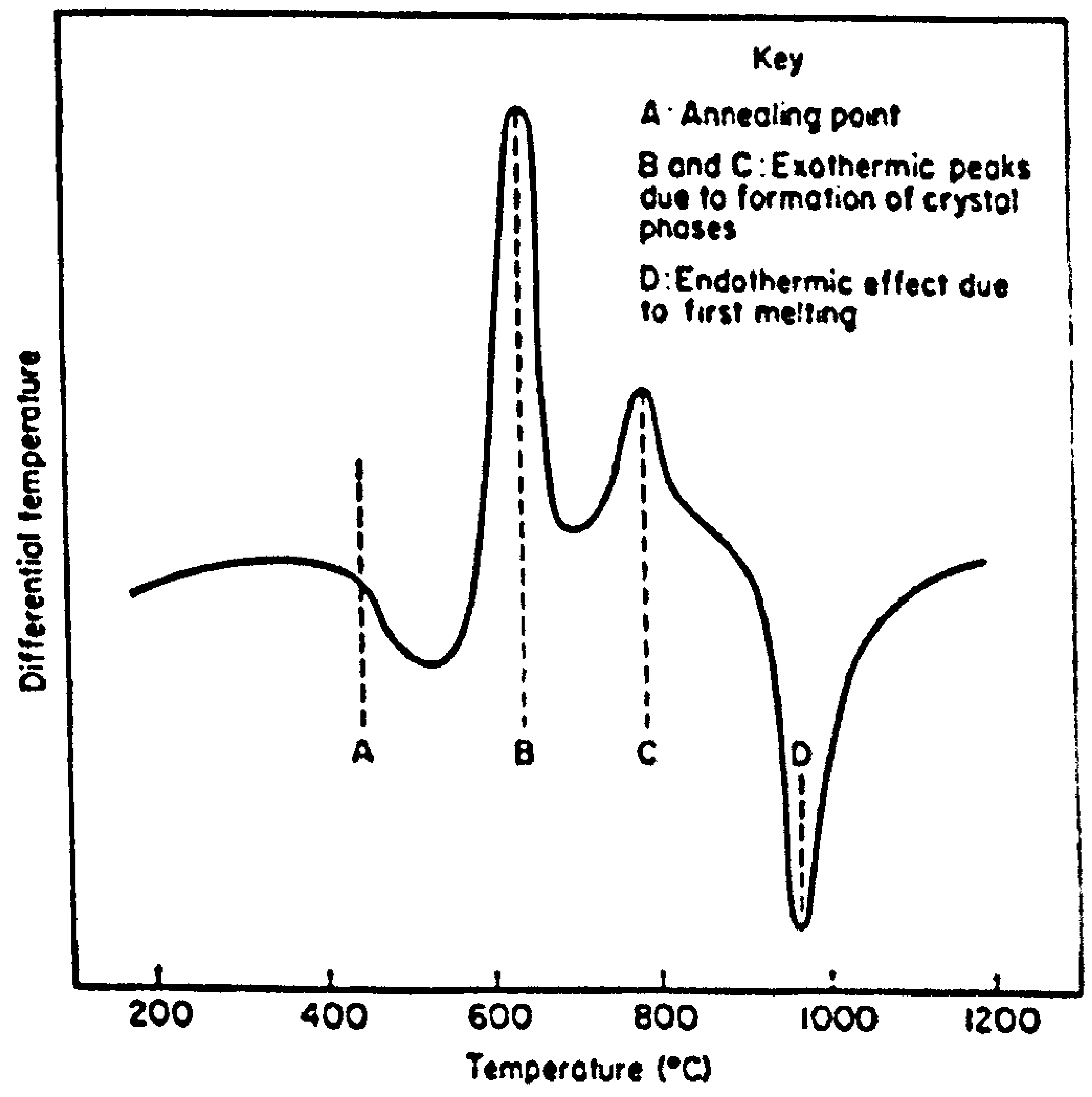

Figure 2.5.1 B: Differential thermal analysis curve for a devitrifiable glass [McMillan, 1964]

As the material is heated the curve dips due to a slight absorption of heat which occurs when the annealing point of the glass is reached. Following further heating, sharp peaks and dips are observed, as a result of exothermic and endothermic events respectively occurring. DTA is therefore useful when devising suitable heat-treatment regimes for glass-ceramics as it is possible to determine both the temperature ranges in which crystallisation occurs and the maximum temperature to which the glass-ceramic can be heated without deformation resulting from melting of crystal phases [McMillan, 1964].

2.5.2 X-ray Diffraction (XRD)

X-ray diffraction is a versatile, non-destructive analytical technique for the identification and quantitative determination of the various crystalline phases present in solid materials and powders and for analysing structural properties (such as stress, grain size, phase composition, crystal orientation, and defects) of the phases.

X-rays are electromagnetic radiation of wavelength about 1Å (10^{-10}m) which is comparable to the size of an atom. In this technique specimens are bombarded with x-rays from various angles which interact with the electrons in the atoms, resulting in scattering of the radiation. If the atoms are organised into parallel planes, as is seen in crystalline materials, the rays will be diffracted back to a detector at an angle related to the arrangement of the particular crystal structure, as shown in Figure 2.5.2A.

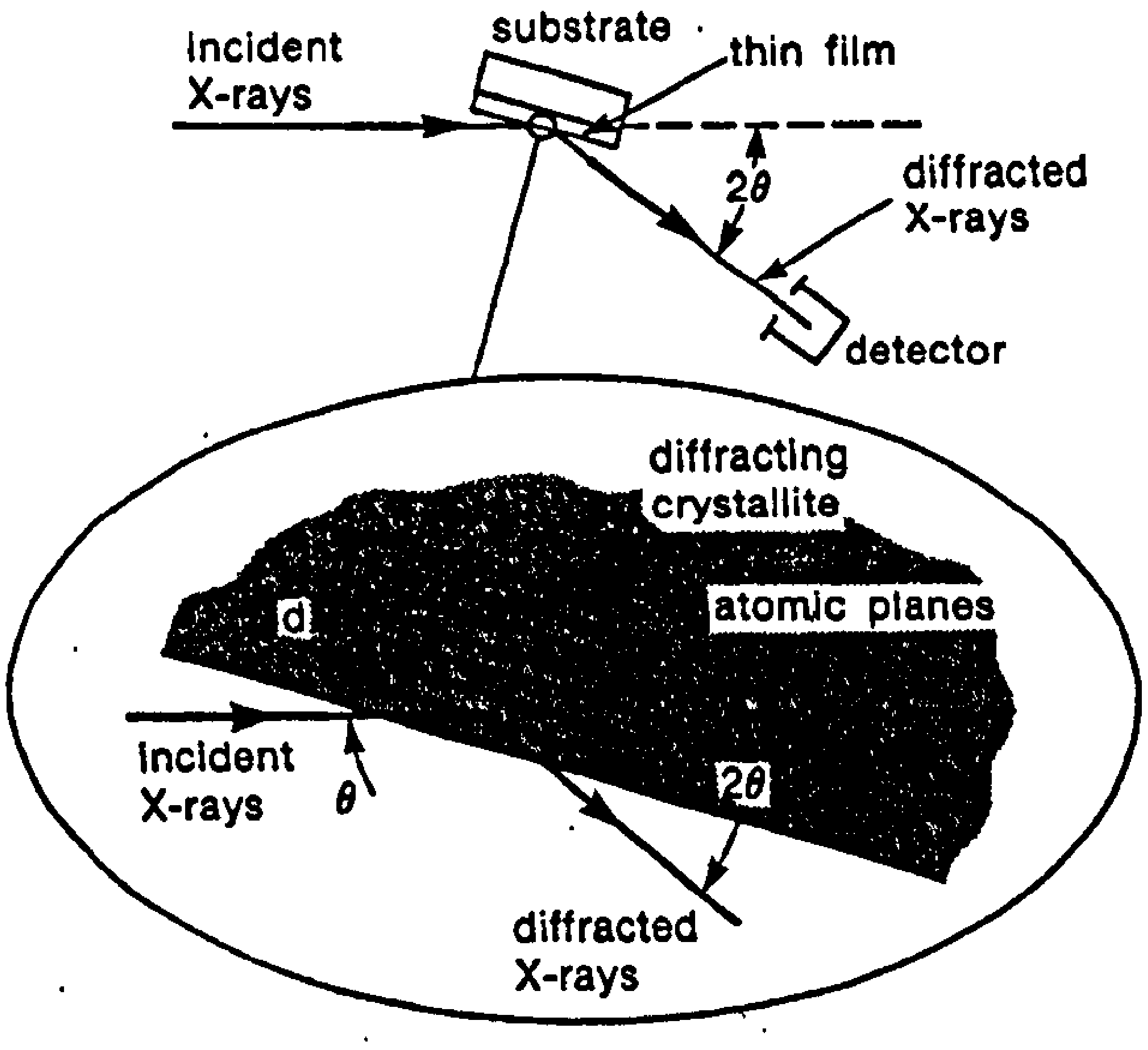

Figure 2.5.2 A: Basic Features of a typical XRD experiment [Bundle *et al.*, 1992]

The relationship between the wavelength of the x-ray λ, atomic spacing d and the scattering angle θ can be expressed as the Bragg equation which has the formula: $n\lambda = 2d\sin\theta$ (n is an integer representing the order of the diffraction peak). By varying the angle of incidence, a diffraction pattern emerges that is characteristic of the sample and can be identified by comparing it with an internationally recognised database of reference patterns. The positioning of the peaks in a particular pattern indicate the phase(s) present and the height of these peaks the relative concentration of that phase(s). The widths of the peaks provide an indication of the average crystallite size, with the peak width narrowing as the crystallite size increases. The background hump shows the amorphous content.

X-ray diffractometers consist of an x-ray generator, a goniometer and sample holder, and an x-ray detector such as photographic film or movable proportional counter. X-rays are produced by either x-ray tubes or synchrotron radiation, and whilst x-ray tubes are more common, synchrotron facilities are increasingly becoming the preferred sources for x-ray diffraction measurements. In an x-ray tube, x-rays are generated when a focused electron beam bombards a stationary or rotating solid target with high energy (10-100keV) electrons that knock out inner shell electrons in atoms. A free electron in an outer shell fills the hole in the inner shell and emits an x-ray photon with energy characteristic of the target material. Common targets include Cu and Mo, which have strong K(alpha) x-ray emission at 1.54 and 0.71Å, respectively. A continuous spectrum of x-rays is emitted by this source and therefore a monochromator is required to select a single wavelength. Synchrotron radiation is emitted by electrons or positrons travelling at near light speed in a circular storage ring. They are very powerful sources, thousands to millions of times more intense than average x-ray tubes.

There are three main types of x-ray diffraction – single crystal, powder and thin-film. In single crystal diffraction the crystal is usually cut in such a way that a particular set of reflecting planes of known spacing is parallel to its surface. The crystal is positioned so that its reflecting planes make a particular angle θ with the incident beam and D, the counter which measures the intensity of the diffracted x-rays, is set at the corresponding angle 2θ. When an entire crystal is measured, a sharp x-ray diffraction spectra is produced, unique to that particular crystal type.

However single crystals are extremely difficult to produce, extract and handle, so powder x-ray diffraction is usually employed. Powder XRD provides less information than single crystal diffraction but is much simpler and faster in confirming the identity of a solid material and determining crystallinity and phase purity. The sample to be examined is reduced to a fine powder and packed into a shallow cup-shaped holder which is rotated with respect to the beam by an angle theta. The diffracted beam is detected by using a moveable detector such as a Geiger counter, which rotates at twice the rate of the sample and is at an angle 2θ with respect to the incoming x-ray beam. In powder XRD the crystalline domains are randomly oriented in the sample. Some of the crystals will be correctly oriented so that their primary crystallographic planes can reflect the incident beam, while others will be correctly oriented for reflecting from their secondary planes, etc. [Cullity, 1978]. Therefore the produced two-dimensional diffraction pattern shows concentric rings of scattering peaks corresponding to the various d spacings in the crystal lattice. The phases of the material can be identified from the positions and intensities of these peaks. As this method identifies crystallographic compounds rather than just elements, complex ceramic materials can be characterised. Either transmission or reflection geometry can be used to collect powder diffraction data, with both methods generating the same data as a result of the particles being randomly oriented. A transmission method is more commonly used for liquid phase samples. Reflection geometry is used for thin-film diffraction measurements as the substrates are generally too thick for transmission. The diffracting power of thin films is small, so the instrumentation and techniques used are designed to maximise diffracted intensities and to minimise background. There are two main measurement techniques – the first uses photographic film, which provides fast, preliminary information, but is considered somewhat out-dated, and the second uses diffractometers, where the diffracted x-rays are detected with photon counters which provide more accurate, quantitative data and have superior signal-to-noise ratios [Bundle *et al.*, 1992].

2.5.3 Scanning Electron Microscopy (SEM)

Scanning electron microscopy provides topographical information which is useful for examining the microstructure of parts and determining any evidence of sintering. The SEM process uses a stream of relatively high-energy electrons (typically 5-100keV) which are focused into a fine probe that is rastered over the surface of the sample. This results in the emission of low-energy secondary electrons from each spot that the focused beam strikes. A proportion of these emitted electrons are collected by detectors that interpret the stream into an image. Only secondary electrons generated near the surface of the specimen can be detected due to the shallow penetration depth of the electrons produced by the primary electron beam, and thus this technique can only be used for surface analysis.

A schematic diagram of a scanning electron microscope is shown in Figure 2.5.3A, the main features of which are an electron column containing the electron source (i.e. the gun), magnetic focusing lenses, a specimen vacuum chamber and an electronics console containing a control panel, electronic power supplies and scanning modules.

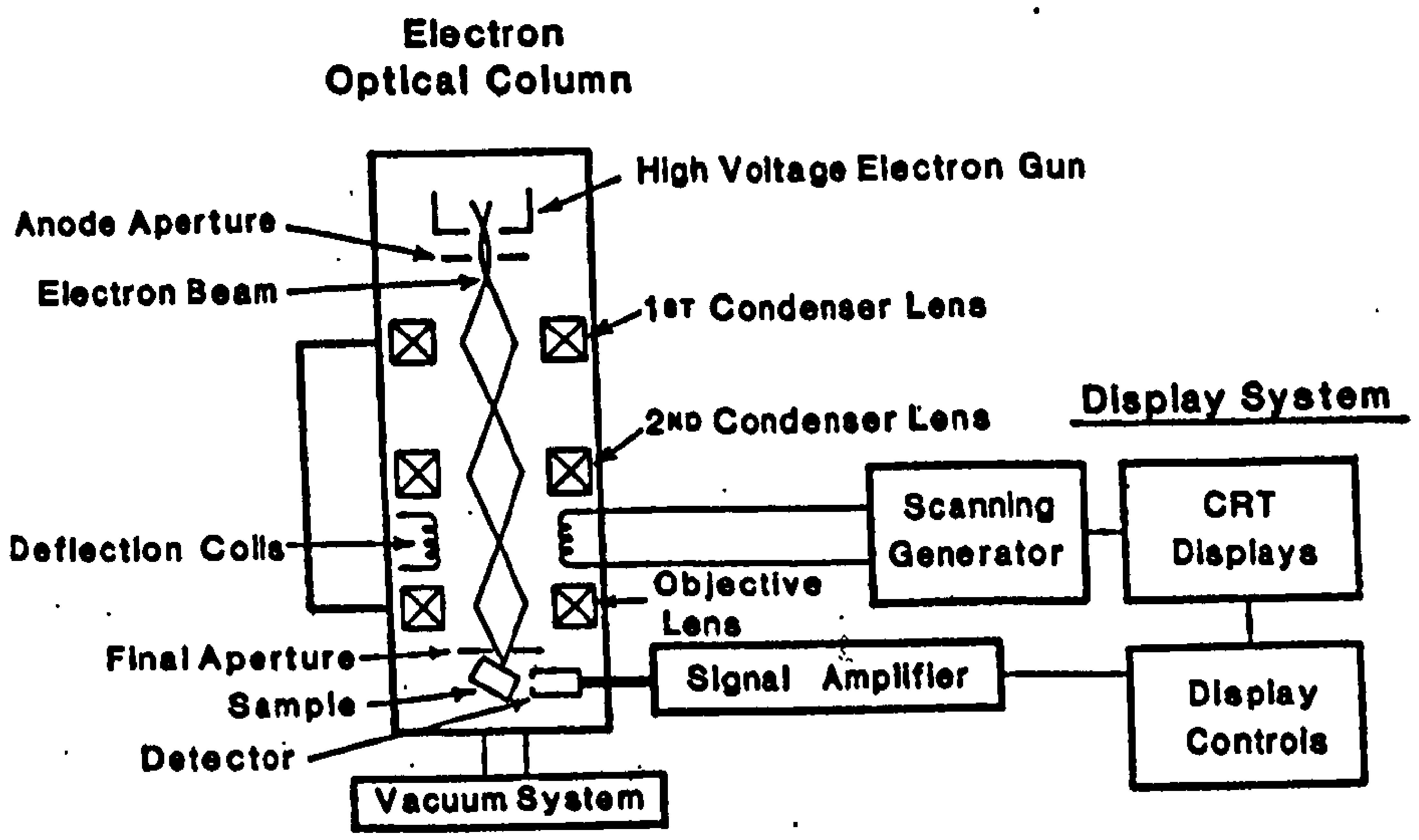

Figure 2.5.3 A: Schematic diagram of a scanning electron microscope [Bundle *et al.*, 1992].

There are three main types of electron sources: thermionic tungsten, lanthanum hexaboride (LaB_6), and hot and cold field emission, although tungsten filaments are most commonly used. Increasing the heating current passed through the filament increases the filament temperature and consequently the electron emission, up to a saturation point where electron emission is concentrated uniformly over the tip of the filament.

The electron gun produces an electron beam that is subsequently defocused by a series of magnetic lenses. When the current that is passed through the top condenser lens is increased, the focal length is decreased and the divergence increases [Bundle *et al.*, 1992]. The size of the produced image is reduced, explaining why the term ‘spot size’ is used for this control. Smaller spot sizes are attained with less current and a smaller signal-to-noise ratio, and thus images become increasingly noisy as the magnification is increased.

The electron beam is then passed through the final lens-aperture combination which focuses the beam onto the surface of the sample. The sample is attached to a specimen stage that can be moved in the x and y-directions, can be tilted with respect to the beam diameter, and can be moved in the z-direction for adjustment of the 'working distance', which is the distance between the final lens and the sample's surface.

Samples for analysis by SEM require very little preparation, particularly if they are conducting materials. Insulating materials however need to be coated with a thin (approximately 10-nm) conducting film of carbon, gold, or some other metal.

2.5.4 Micro Computed Tomography (μCT) Analysis

Micro computed tomography is a non-destructive x-ray imaging method for examining the internal structures of three-dimensional objects. It is based on the principle that x-rays are attenuated to different degrees as they pass through objects of varying density. The transmitted x-rays pass through a collimator and a scintilltor (which converts the x-rays into light), then into a one-dimensional array of detectors to reveal an image of the interior of the object. During the image acquisition the sample is rotated step at a time through 180 degrees, with a two-dimensional image or *slice* being recorded at every rotation. A series of contiguous two-dimensional images are acquired by incrementally translating the sample in the axial direction, which can then be stacked to form a three-dimensional image of a section, or, if the entire part has been scanned, a full volumetric image can be performed. Resolutions in the range of 15 to 30μm are typically achieved in commercial scanners, allowing a wide range of samples to be suitable for structural analysis.

2.5.5 Inductively Coupled Plasma Atomic Emission Spectroscopy (ICP-AES)

Inductively Coupled Plasma (ICP) Atomic Emission Spectroscopy is a technique for elemental analysis, where samples in liquid form are passed through a plasma source causing the emission of electromagnetic radiation. The frequency of this radiation is characteristic of the element that emitted it, and can be calibrated against standards to provide a quantitative analysis of the original sample.

A schematic diagram of a typical ICP instrument, which consists of three main sections – a nebuliser, a torch, and a detection system, is shown in Figure 2.5.5A.

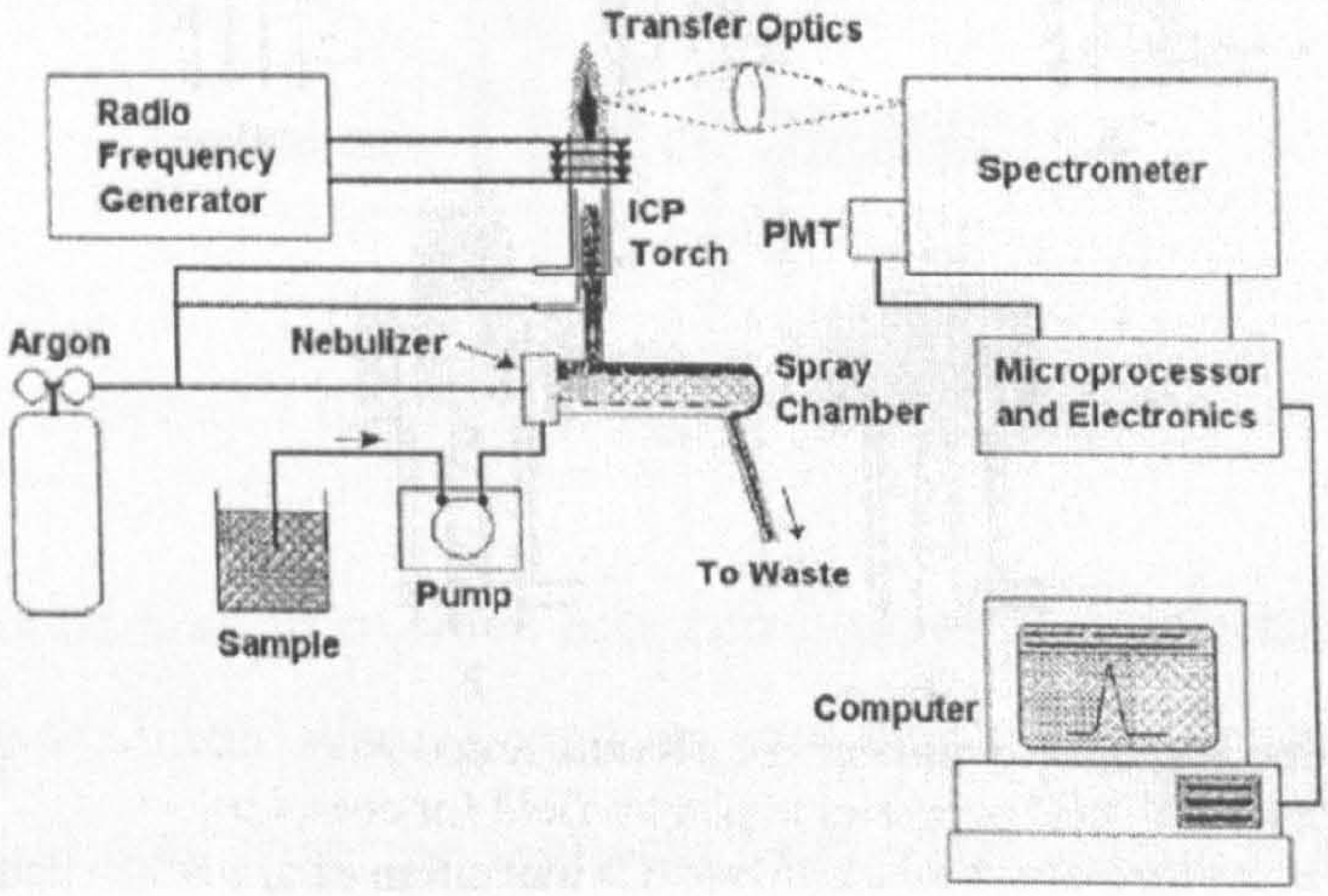

Figure 2.5.5 A: Schematic diagram of a typical ICP instrument [Arcinas, 2001]

A continuous flow of analyte liquid is drawn into the nebuliser through a capillary tube using a peristaltic pump. Here a flow of plasma support gas, typically argon, converts it into a fine aerosol, with particle size diameters between 1-10μm. If the liquid was directly injected into the plasma it would either extinguish the plasma or cause the atoms to be insufficiently desolvated, making excitation and emission less efficient. The aerosol is separated by size - the droplets that are too large to be vaporised effectively in the plasma are drained, and the smaller drops are directed through the centre of an argon plasma at a temperature of approximately 8000°C. Plasma is a high-temperature, partially ionised gas, sometimes described as the fourth state of matter. Although argon is most commonly used, helium, nitrogen, oxygen, and mixed gas plasmas have also been used. The inductively coupled plasma is formed and maintained using a torch and induction coil [Figure 2.5.5B].

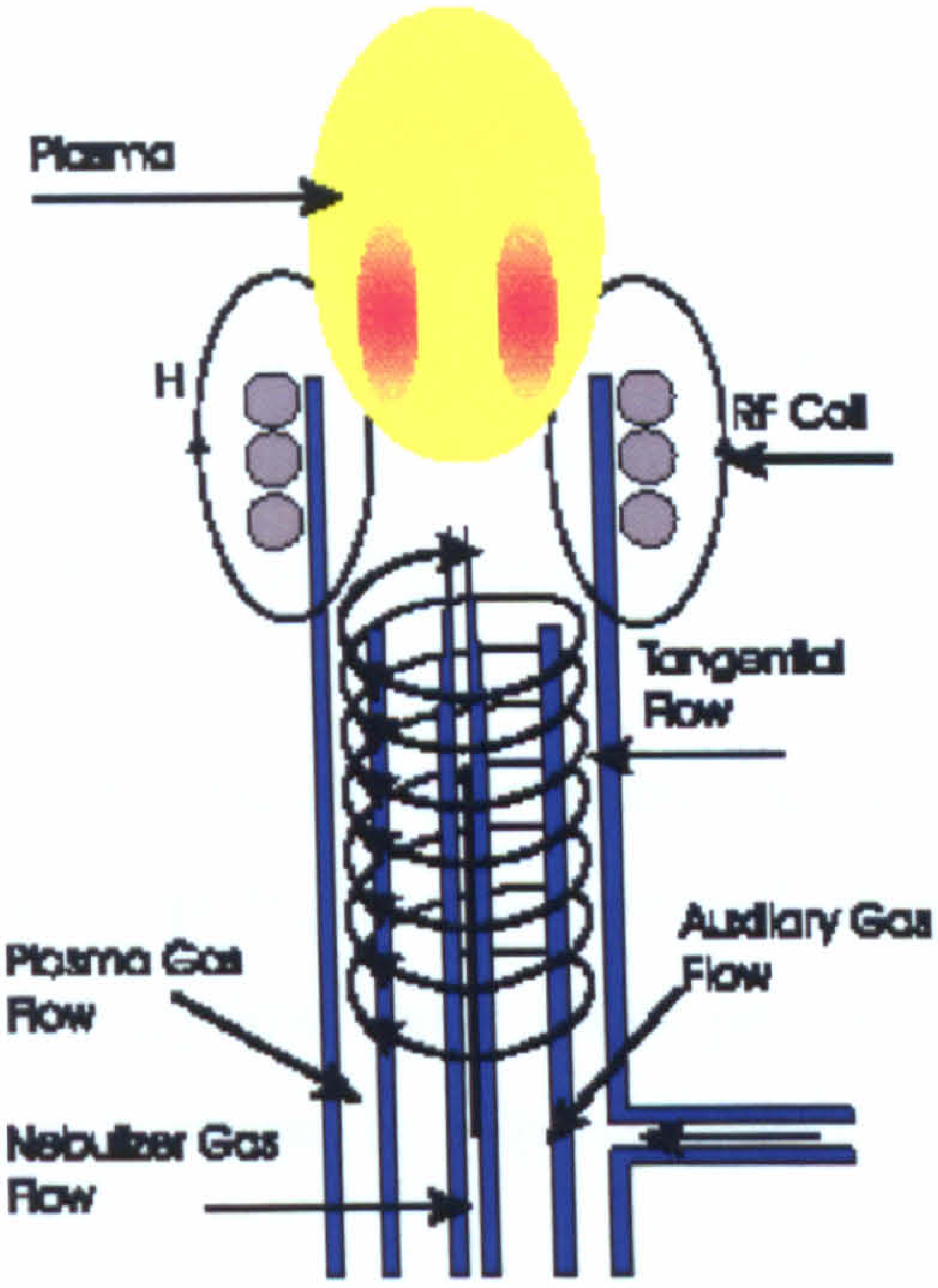

Figure 2.5.5 B: Schematic diagram of an ICP torch [Manning and Grow, 1997].

The plasma torch is composed of three concentric glass or quartz tubes. The outer tube provides argon gas for initial plasma ignition, and then maintains the gas flow in order to keep the load coil cool from the immense heat. The sample is introduced into the plasma via the innermost tube, with the middle tube ensuring that the plasma doesn't come too close to the nebuliser flow. The plasma is generated using a radiofrequency generator, typically at 27 or 40MHz. Current is carried through an induction coil that is wrapped two or three times around the ICP torch and sets up an annular magnetic field region within the coil and above the torch, where the plasma is maintained.

Upon reaching the high temperature plasma, thermal collisions cause the sample atoms or ions to lose an electron and reach an excited state. When the excited electrons return to a lower or ground level state, they emit element specific electromagnetic radiations normally in the form of light in the UV-visible region of 160 to 800nm. The emitted light is collected by an optical spectrometer and passes through a diffraction grating which separates the light into a spectrum of its constituent wavelengths. The diffracted light is then focused onto a solid-state detector, which identifies each wavelength and its relative intensity. The spectrum of light frequencies is unique to the element that emitted it and therefore can be used to identify the presence of that element in the sample. The intensity of the emitted light is proportional to the concentration of that element within the sample solution and therefore can be compared to calibration standards for quantitative purposes. Calibration is usually achieved by running known solution standards containing the elements of interest in a number of different concentrations, generating calibration curves equilibrating instrument response with known concentration. The unknown data can then be plotted on these curves, thus allowing the amount of each element of interest to be calculated.

An advantage of this method is the ability to determine many elements simultaneously in a single sample analysis since the plasma ionises all atoms in the sample and emits the spectra for each one. Very low levels (parts per billion) of most elements in a solution can be detected, and data can be acquired rapidly.

Some elements however cannot be easily identified using this method. Argon, for instance, cannot be measured due to it being used as the carrier gas. Oxygen, carbon, hydrogen and nitrogen are very difficult to measure due to their natural abundance within the system. Although halides such as Br, Cl and I can be measured, difficulties often arise as a result of their high ionisation energies. Problems can also arise if the wavelength of the element of interest if very close to that of another element. An example of this is phosphorus which shares a main wavelength with both copper and aluminium.

2.5.6 Cytotoxicity Testing

Considering the application to which these produced parts are intended and the number of possible adverse reactions to artificial materials that were discussed previously in this chapter, assessment of their biocompatibility is essential. The most common way of assessing biocompatibility is through the *in vitro* evaluation of the toxicological risks of the material using cell culture, which is known as "Cytotoxicity Testing". In these tests the ability of the material, or extracts from it, to interact with fibroblasts from standard cell lines without causing cell death is compared with positive and negative controls. There are three types of cytotoxicity tests that provide information on cell viability and death – direct contact, agar diffusion, and elution (also known as extract dilution) [Nicholson, 2002].

In direct contact assays a near-confluent monolayer of mammalian fibroblast cells is prepared. Following removal and replacement of the culture medium with fresh medium, the test material is placed on the culture and incubated for 24 hours at 37°C in a humidified incubator. The culture medium and sample are removed, and the cells fixed and stained with a cytochemical stain such as hematoxylin blue. As dead cells can no longer adhere to the culture plate, they are lost during the fixation process, leaving only living cells to adhere and be stained by the cytochemical stain. Thus the toxicity of the material is determined by the absence of stained cells under and around the periphery of the sample [Ratner *et al.*, 1996]. This method has the advantages that no extraction preparation is needed and the target cell comes in direct contact with the material. The period of time that the cells are exposed to the material can be extended by adding fresh culture media. However the major disadvantage with this method is the possible risk of physical trauma to the cells from either movement of the sample or crushing by the weight of a high-density sample [Ratner *et al.*, 1996].

When the culture medium is removed in agar diffusion assays it is replaced with a culture medium containing 2% agar. The test material is placed on the solidified agar and incubated as in direct contact assays. Vital stains, such as neutral red, are added to the agar and taken up and retained by healthy, viable cells, allowing them to be easily visualised. As dead cells cannot retain the dye, they remain colourless [Ratner *et al.*, 1996]. Not only does the layer of agar between the test material and the cells act as a diffusion barrier to enhance the concentration gradient of toxicants, but it also protects the cells from the risks of physical trauma seen with the direct contact method.

In elution assays an extract of the test material is prepared and placed on a prepared, near confluent monolayer of mammalian fibroblast cells. Following incubation at 37°C for 48hours, histochemical or vital stains are used to distinguish between living and dead cells.

In vitro methods cannot replace the use of *in vivo* procedures as many adverse effects *in vivo* cannot be predicted by using *in vitro* systems. However they are useful for initial screening of new materials particularly when large numbers of materials need to be investigated due to rapidity of assessment and the reduction in the number of animals that need to be sacrificed. As human cells and tissues can be used there is no need to extrapolate data from animals to humans and thus the results obtained are directly relevant to humans.

2.5.7 Assessment of Bioactivity

It was seen in Section 2.2.6 that the ability of certain CaO-SiO_2-based glasses and glass-ceramics to bond to bone is due to the formation of a hydroxycarbonate apatite (HCA) layer in the surface of the material when in contact with body fluid. This layer is also formed when the material is soaked in simulated body fluid (SBF), an acellular aqueous solution with an ion concentration and pH almost equal to those of human blood plasma [Kokubo *et al.*, 1990] – see Table 2.5.7A.

Ionic composition of SBF and Human Blood Plasma (mM)

	Na^+	K^+	Mg^{2+}	Ca^{2+}	Cl^-	HCO^{3-}	HPO_4^{2-}	SO_4^{2-}
SBF	142.0	5.0	1.5	2.5	147.8	4.2	1.0	0.5
Plasma	142.0	5.0	1.5	2.5	103.0	27.0	1.0	0.5

Table 2.5.7 A: Comparison of the ionic composition of SBF and Human Blood Plasma.

When a sample is soaked in SBF three events occur – release of ions, pH modifications, and growth of an apatite-like layer on the material surface [Vallet-Regí, 2001]. The bioactivity of a material can therefore be assessed *in vitro* by monitoring and characterising the modifications that occur in the fluid and on the material surface. As there is no cell content in the solution, the layer that grows on the surface of a bioactive material is a carbonate hydroxyapatite – see Figure 2.5.7A. However under *in vivo* conditions, cells will produce collagen which forms an adherent interface with the bioactive material, allowing osteoblasts to deposit bone.

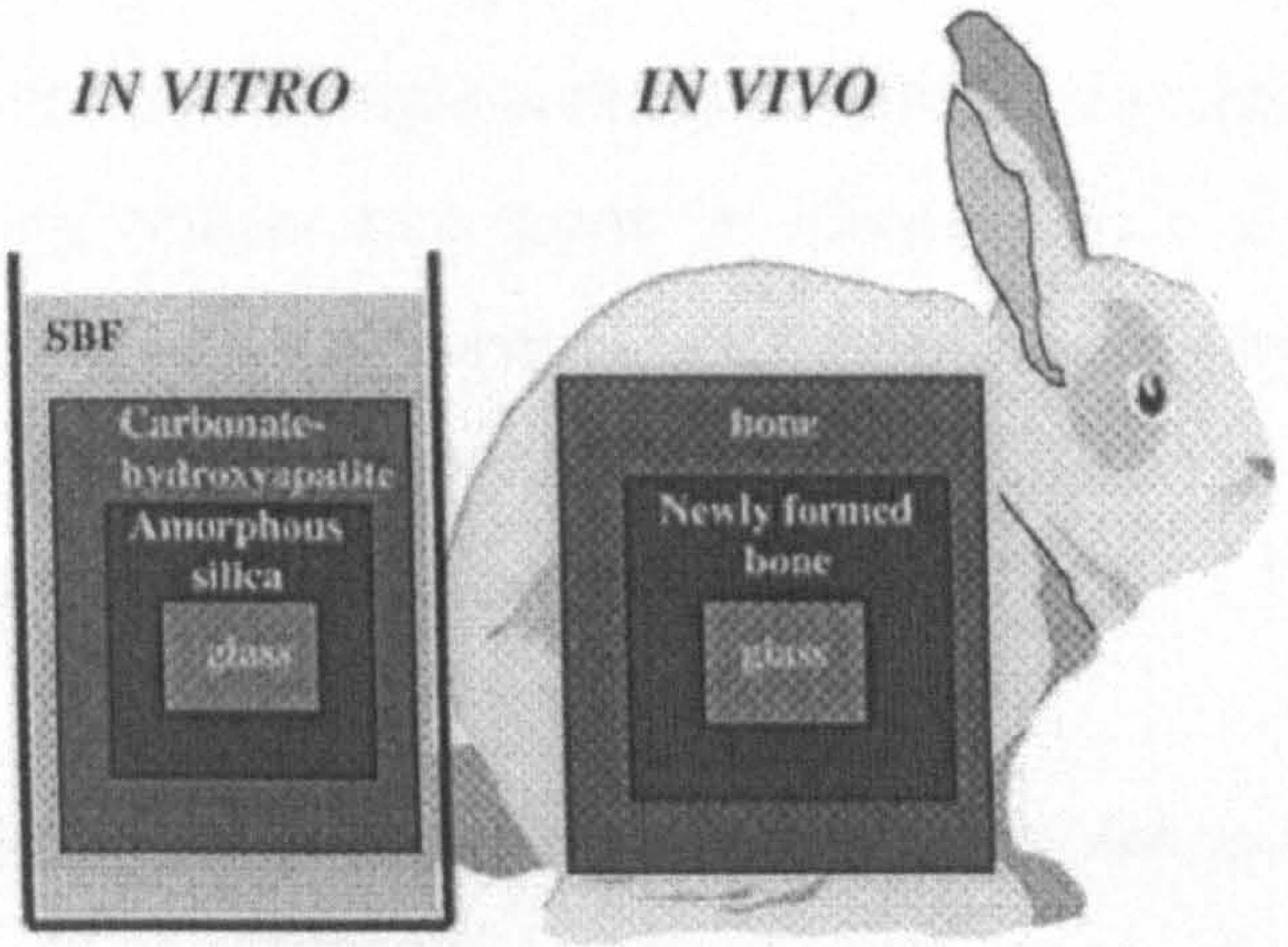

Figure 2.5.7 A: Comparative diagram of *in vitro* and *in vivo* assays of a bioactive glass [Vallet-Regí, 2001].

2.6 Aims and Objectives

The principle aim of this work was to determine the feasibility of using an indirect selective laser sintering process to produce porous three-dimensional glass-ceramic implants for use in bone replacement applications.

A number of layer manufacturing techniques have been discussed in this chapter, but most have limited use in this application due to the lack of materials that can be used with them, with very few allowing ceramic materials to be processed. The two techniques that were most suitable therefore were SLS and 3DP, both established methods that allow parts to be produced from a wide range of materials, as theoretically any material that can be obtained as a powder can be used with these techniques. In addition neither require external supports for overhangs or unconnected parts as the part is supported during the build cycle by the unsintered powder, thus allowing greater potential for parts to be produced with the complex geometry often required for medical implants. The expertise in RP at Leeds University is in the SLS process, and thus it was chosen for this study.

Direct SLS of bioceramics has previously been attempted with limited success [Lorrison, 2003]. This was attributed to high surface tensions experienced upon melting, a large viscosity change at the glass transition temperature and intra-process crystallisation. However it is thought that by adopting an indirect method where the relatively high melting temperature glass is blended with a low melting binder, polymer-bound "green parts" with superior structural integrity may be produced when laser sintered. These parts can subsequently be post-processed to thermally remove the binder and sinter the higher melting temperature glass.

Powder properties and fabrication parameters are both known to significantly influence the mechanical properties and surface qualities of parts produced by selective laser sintering. Different applications have different requirements and often a trial-and-error method needed to be used to determine the conditions required for a specific application. Thus the initial aim of this work was to obtain an understanding of the relationship between the powder properties, SLS fabrication parameters, and post-processing conditions in order to obtain an optimum part for the application of bone replacement.

Production of parts for bone replacement requires a compromise between optimising the mechanical strength so that it is similar to that of trabecular bone, and retaining sufficient porosity for the ingrowth of fibrous tissue. Therefore following successful production of these parts, their biochemical behaviour upon implantation needs to be studied, to evaluate not only the biocompatibility of the material, but also the subsequent regeneration of bone.

Chapter 3 Material Selection and Production

This chapter provides a rationalisation of the materials chosen for this work and details the methods used to produce them. It is intended as a reference for the experiments involving these materials that are described in subsequent chapters.

The first section, 3.1, considers the reasons for selecting the apatite-mullite glass ceramic, LDIG105, as the material for processing by SLS, and describes the procedures carried out to produce the starting glass and prepare it for laser sintering. The grounds for adopting an indirect laser sintering method and for selecting an acrylic binder are outlined in section 3.2.

Section 3.3 considers the rationale for infiltration of the laser sintered parts and explains the choice and production of the materials used. The actual process of infiltration will be described later, in Chapter 5.

The final section, 3.4, details the production of materials used as controls for the assessment of the biological properties of the materials produced by SLS, which will be described in Chapter 6.

The majority of the materials were produced by the author, specifically for this work. However the phosphate glass used for infiltration, as well as some of the cast apatite-mullite samples used for cytotoxicity and *in vitro* bioactivity testing were prepared by J.Lorrison at the University of Leeds, UK.

3.1 Selection of Material for SLS

From the materials available for use in biomedical applications, discussed in Chapter 2.2.5, it was decided that a glass-ceramic would offer the greatest potential for use with selective laser sintering. For optimum integration of the implanted material with natural bone a material that forms a direct bond with bone is desirable, which provides us with the choice of a bioactive glass, glass-ceramic, metal or polymer. Ceramics and glasses are widely preferred as bone replacement materials due to their low density, chemical inertness, and similar composition to human bone tissue. Glass-ceramic materials generally have higher strength and superior mechanical properties than glasses. They also have a longer history than bioactive metals and polymers, whose ability to be made bioactive either by reacting the surface with an alkaline solution and heat treatment, or placing on CaO-SiO_2-based glass grains soaked in SBF is only a recently discovered phenomenon and is in the very early stages of understanding and development. Glass-ceramics have the additional benefit of considerable flexibility in tailoring materials with specific properties either by the selection of an appropriate composition of the base glass or by the design of the glass ceramic microstructure via a carefully controlled crystallisation procedure.

It is generally agreed that for a glass-ceramic material to demonstrate bioactive properties, an apatite phase must be present. This provided three main options – hydroxyapatite, apatite-mullite (A-M), or apatite-wollastonite (A-W). Apatite-mullite was chosen over hydroxyapatite and apatite-wollastonite as experience regarding its production had been built up over the past few years in other research at the University of Leeds. Apatite-wollastonite had proven more problematic to produce with the facilities available. Therefore for the purpose of simply determining whether it is possible to process glass-ceramics by indirect SLS, it was considered rational to start with an apatite-mullite glass-ceramic. The particular composition, $4.5SiO_2{\cdot}3Al_2O_3{\cdot}1.6P_2O_5{\cdot}3CaO{\cdot}2CaF_2$, known as LDIG105 (Leeds Dental Institute Glass 105), was selected by slightly modifying another A-M glass, LG112 (University of Limerick Glass 112). As was seen in Chapter 2.2.7.1.2, LG112 has been shown to exhibit bioactive properties following heat treatment and crystallisation, forming a direct physical bond with bone tissue *in vivo*. The modification gave an increased fluorine content in LDIG105, which changed the Ca:P ratio to 1.56, bringing it closer to that of the apatite stoichiometric value of 1.67. This was done in an attempt to further increase the bioactivity of the material by increasing the potential for apatite crystallisation to occur during post-processing.

3.1.1 Preparation of LDIG105

A castable glass, LDIG105, with the composition $4.5SiO_2 \cdot 3Al_2O_3 \cdot 1.6P_2O_5 \cdot 3CaO \cdot 2CaF_2$ (molar ratio) was prepared in batches of approximately 500g. To calculate the required mass of each reagent, these molar ratios were multiplied by the molar masses of each reagent (given in Table 3.1A) to give a total mass which was then multiplied by a scaling factor of 0.44338. This scaling factor was calculated by dividing the required total mass, 500g, by the sum of the total masses for each reagent, 1127.7g.

Reagent	Molar Mass (g)	Total Mass (g)	Scaled Mass (g)
SiO_2	60.08	270.36	119.9
Al_2O_3	101.96	305.88	135.6
P_2O_5	141.94	227.104	100.7
CaO	56.08	168.24	74.6
CaF_2	78.08	156.16	69.2

Table 3.1.1A: Molar masses of glass reagents and the total masses to make one batch of LDIG105.

Whilst most of the reagents are available in the form specified, CaO is formed by the carbonate decomposition of $CaCO_3$ during heating, and therefore the change in mass of $CaCO_3$ needed to be taken into account in order to maintain the correct weight ratios. This required adjustment was calculated as follows:

For a batch of 500g, the final glass should contain 74.6g of CaO.
The molar weight of CaO is 40.078 + 15.9994 = 56.1g
The number of moles of CaO in 74.6g is therefore: 74.6 / 56.1 = 1.33
The molar weight of $CaCO_3$ is 40.078 + 12.011 + (3 x 15.9994) = 100.1g
Assuming 1.33 moles of CaO comes from 1.33 moles of $CaCO_3$,
1.33 moles of $CaCO_3$ is 1.33 x 100.1g = 133.1g

Therefore for a 500g batch of LDIG105, the final reagent masses required are:

Reagent:	SiO_2	Al_2O_3	P_2O_5	$CaCO_3$	CaF_2
Mass:	119.9g	135.6g	100.7g	133.1g	69.2g

Each reagent was weighed out (Sartorius Roughing balance, 3.1kgx0.1g, PT3100) and placed in a plastic container with P_2O_5 being added last due to its reactivity with air. An agitating bar was added to the closed container, and the reagents were mixed in a rotary mill for one hour. The resulting powder was transferred to a mullite crucible with lid and placed in a furnace (1600°C, I Temp 15/16, Pyrotherm) heated to 1450°C. After 1½ hours the crucible was briefly removed from the furnace, and the glass swirled around to aid homogenisation, before being returned to the furnace for a further thirty minutes. After this time, the crucible was removed and the glass melt poured in a slow circling motion into a large metal tank of cold water (Figure 3.1.1A). This shock quenching was used to rapidly cool the material before it had the chance to crystallise, and the circular motion helped to spread out the glass so that large masses of glass which would have taken longer to cool down and may have then crystallised, were prevented from forming.

Figure 3.1.1 A: Shock quenching of molten LDIG105 into cold water

A suction pump was used to retrieve the resulting glass frit from the water tank and catch it in a sieve which was left in a drying cabinet overnight to remove all moisture from the glass. The dried glass was placed in batches into a 250ml puck and mill in a Gy-Ro Rotary Mill and pulverised for approximately 120 seconds. The resulting glass powder was sieved through a series of mesh sizes, placed on a shaker (Octagon Digital) for 100 minutes, to separate it out into five particle sizes – 0-45µm, 45-90µm, 90-125µm, 125µm-1mm and >1mm. Zirconia beads were included within the sieves to reduce particle agglomeration.

In order to attain a sufficient amount of glass powder of each size range for laser sintering, several batches of glass needed to be mixed together. To ensure therefore that each batch had the same characteristics, differential thermal analysis (DTA) was carried out on each batch of glass in a modified Stanton Redcroft 673/4, using α-Al_2O_3 powder as a reference. Data was collected over a range from 400°C to 1250°C at a uniform heating rate of 10°C/min. To allow comparisons to be as accurate as possible between batches as well as to ensure consistency with other similar work being carried out in the department, only glass of particle size 90-125µm was used for DTA. However it has previously been shown that in similar glasses, DTA data is independent of particle size, since crystallisation proceeds by a bulk nucleation mechanism [Hill *et al.*, 1991].

A typical DTA trace can be seen in Figure 3.1.1B. From this trace, the glass transition temperature, Tg, is seen to occur at approximately 640°C, and the first peak, representing the apatite crystal phase, at around 735°C. The second peak, representing the mullite phase, occurs around 940°C. Similar values were seen on the DTA traces for the other batches, and this was considered sufficient to justify blending the powder together for sintering.

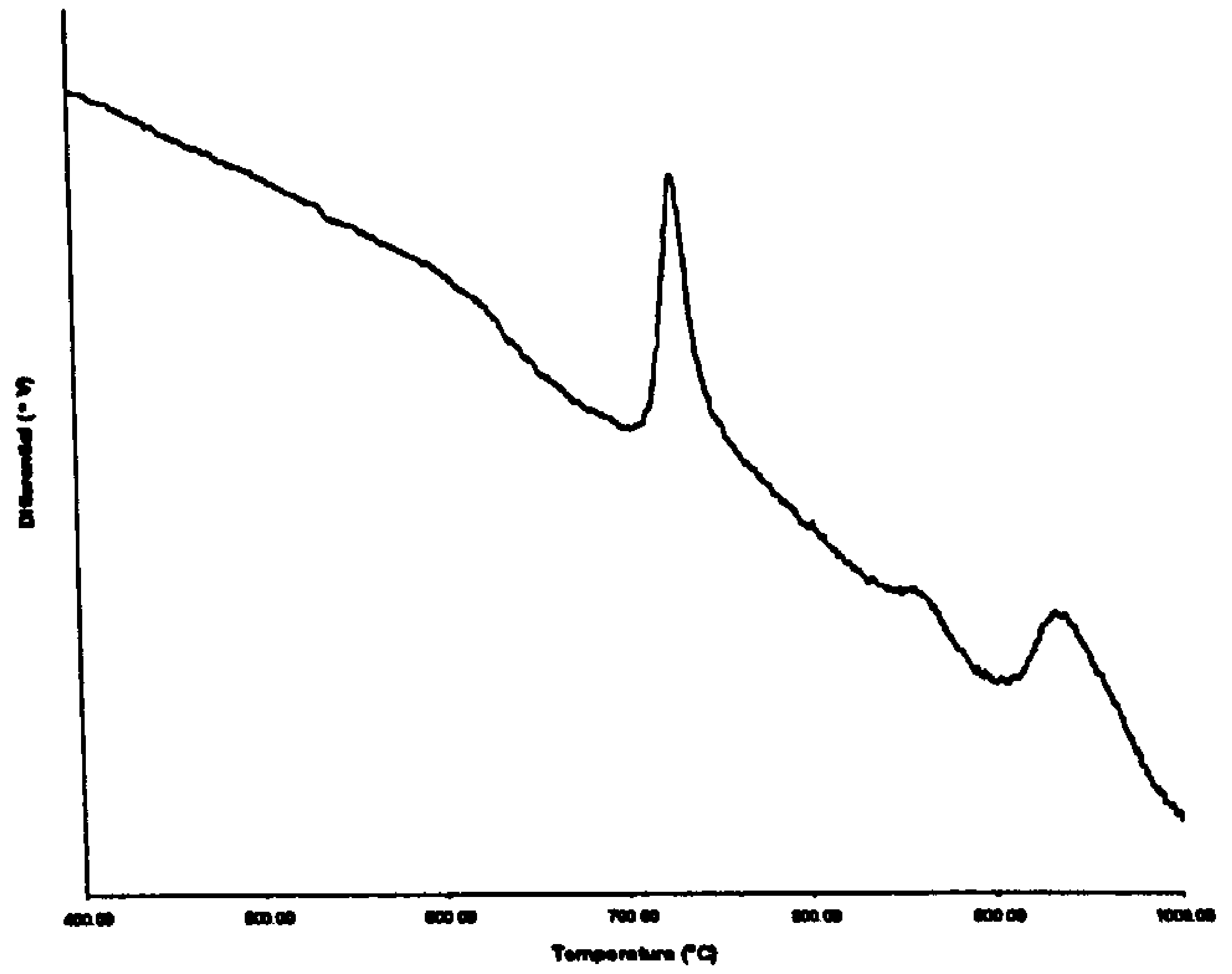

Figure 3.1.1B: DTA trace for unsintered LDIG105 (90-125μm)

Batches of glass were made up from all the separate glass-particle sizes, as well as mixtures of 45-90μm and <45μm glass particle size in ratios of 50:50 and 75:25 by mass.

3.2 Selection and use of a binder

As discussed in chapter 2.3.7, attempts at processing glass-ceramics by direct laser sintering has proven to be unsatisfactory, producing parts with poor structural integrity from a very small processing window. This has been attributed to high surface tensions experienced upon melting, a large viscosity change at the glass transition temperature and intra-process crystallisation [Lorrison, 2003]. It is thought however that by adopting an indirect method where a low melting temperature binder is blended with the relatively high melting temperature glass, green parts with superior structural integrity may be produced when laser sintered. These parts can subsequently be post-processed to burn off the binder and sinter the higher melting temperature glass.

Both polymers and inorganic materials have been used as binders for selective laser sintering for several years, but a polymer binder was favoured in this work as theoretically it is able to be completely eliminated from the green part following post-processing. This is important considering the desired application of the part, since the binder does not have proven biocompatibility and thus could prove toxic when implanted into the body.

The binder used for this work was an acrylic resin, obtained from DTM Corporation. As it was a commercial binder, the company would not divulge any further details. It was mixed in closed plastic containers with glass of each particle size range in a rotary mill for one hour. Batches containing 1, 3, 5, 10 and 15% binder were produced, calculated by mass. The glasses of mixed particle size were mixed with 5% binder by mass.

3.3 Preparation of materials for infiltration

Infiltration of the parts produced by SLS was carried out in an attempt to increase their strength. It was considered ideal for a resorbable material to be used, which would contribute to the strength of the implant immediately following implantation, but would then gradually resorb and be replaced by bone tissue which would grow into the re-forming pores and form a secure interlocking bond with the glass-ceramic material.

The first material to be attempted was a soluble phosphate glass, whose composition was obtained from a personal communication with the Eastman Dental Institute [Knowles, 2002], and was chosen due to indications from this research group that it possessed suitable strength and bioactivity to suit our requirements. It was proposed that not only would it increase densification and thus the mechanical strength of the parts, but it would also enhance bioactivity through the combination of two bioactive phases.

Infiltration with a polymer was also attempted. Bioresorbable polymers were considered ideal materials for temporary infiltration of the laser sintered parts since they can be engineered in such a way that their resorption rate in the body matches the formation rate of new tissue. Synthetic polymers were chosen over natural materials since they can be tailored to give a wider range of properties, have more predictable consistency between batches, and do not process the immunogenecity concerns associated with some materials from natural sources. A huge variety of synthetic resorbable polymers are available, with particular attention being currently paid to polyesters such as poly(lactic acid) (PLA), poly(glycolic acid) (PGA) and poly(lactic acid-co-glycolic acid) (PLGA). However for this work, polymethylmethacrylate (PMMA) were used. Although PMMA is not resorbable, it was thought that this more readily available material would be adequate for the purpose of simply determining whether it would be feasible to infiltrate the laser sintered parts with a polymer. In addition, PMMA has a long history of use as a biomaterial.

3.3.1 Phosphate Glass

The phosphate glass had a molar percentage of $50\%P_2O_5 \cdot 40\%CaO \cdot 10\%Na_2O$, and was prepared using a similar method to that used for the production of LDIG105, described in section 3.1.1. However the temperature of fusion was reduced to 1100°C, and instead of shock quenching the molten glass into cold water, it was poured directly onto a steel plate. The glass was cooled in this way as phosphate glasses can react strongly with moisture. This method also allowed the glass to cool with a speed sufficient to prevent crystallisation, due to the large thermal mass of the steel plate which absorbed the majority of the thermal energy relatively quickly, and the fluidity of the glass which allowed it to spread thinly over the surface of the plate. Following processing of the phosphate glass to a sub 20μm particle size, the material was stored in a desiccator prior to use [Lorrison, 2003].

3.3.3 Polymethylmethacrylate (PMMA)

PMMA was produced via a reaction between methylmethacrylate (+0.01% hydroquinone) and 2-5% benzoyl peroxide. Further details of this will be provided in Chapter 5.

3.4 Preparation of control samples for biological assessment

Previous assessment of the biocompatibility and bioactivity of glass-ceramics produced from glass in the system $SiO_2 \cdot Al_2O_3 \cdot P_2O_5 \cdot CaO \cdot CaF_2$ has been performed on samples produced by a conventional cast-crystallisation process. Therefore it was considered necessary to test samples of LDIG105 that had been cast in addition to those produced by laser sintering, in order to determine whether anything was happening during laser sintering or the subsequent post-processing route that was altering the bioactivity of the parts. As the cast material was intended as a control, the process for producing it was taken from that developed by Lorrison [2003] who had optimised and built up knowledge on its production, rather than adopting the heat treatment regime developed for post-processing the laser sintered components.

Bioglass®-type glass, a known bioactive material, and a non-bioactive commercial silica glass were used as controls.

3.4.1 Cast Apatite-Mullite

Glass was produced with the same composition and by the same method as for the SLS experiments (Section 3.1). The glass frit was ground into a powder with a particle size of sub 45μm in an attempt to reduce any inhomogeneous regions that may have affected the properties of the final material. The ground glass was transferred to a mullite crucible and placed in a furnace preheated to 1450°C. After one and a half hours the temperature of the furnace was raised to 1500°C for an additional half hour in a further attempt to eliminate any remaining inhomogeneous regions and to make the glass more fluid, hence facilitating its subsequent pouring into a mould. A carbon mould with a diameter of 30mm and 100mm in length was used, preheated to 631°C, 50°C below the optimum nucleation temperature (ONT) of LDIG105. The molten glass was carefully poured into this mould, as shown in figure 3.4.1A, and placed in a furnace at the same temperature for one hour. This temperature was chosen as it was sufficiently below the ONT to prevent any nuclei formation, but also high enough to allow the glass to anneal and thus prevent any thermal fracturing [Lorrison, 2003].

Figure 3.4.1 A: Photograph of molten glass being poured into a carbon mould.

The rod was left to cool at the natural rate of the furnace, before being removed from the mould to undergo post-processing. For this, the glass rod was coated with an investment material, then placed in a furnace and heated up to 681°C (the ONT for LDIG105) at a rate of 10°C/min. After an hour hold at this temperature, the furnace continued to be heated up at 10°C/min to 1100°C, for a further one hour hold, before cooling the rod back down to room temperature at the natural rate of the furnace. This two-tier heating regime was used to allow the formation of nuclei during the hold at the ONT, before heating further to provide the opportunity for maximum crystal growth and development. Once cool, the cerammed rod was removed from the investment material, and cut into approximately 2.2mm thick discs using a Struers Accutom 5 cutting rig at a rotor speed of 1500rpm and a feed rate of 0.05mm/s. The discs were then ground with a diamond grinding wheel (Imptech 302 DVT Grinder Polisher) to a thickness of 2mm±0.1mm, before being polished with successively finer grades of silicon carbide papers until a surface roughness of 1200 grit was achieved [Figure 3.4.1B]

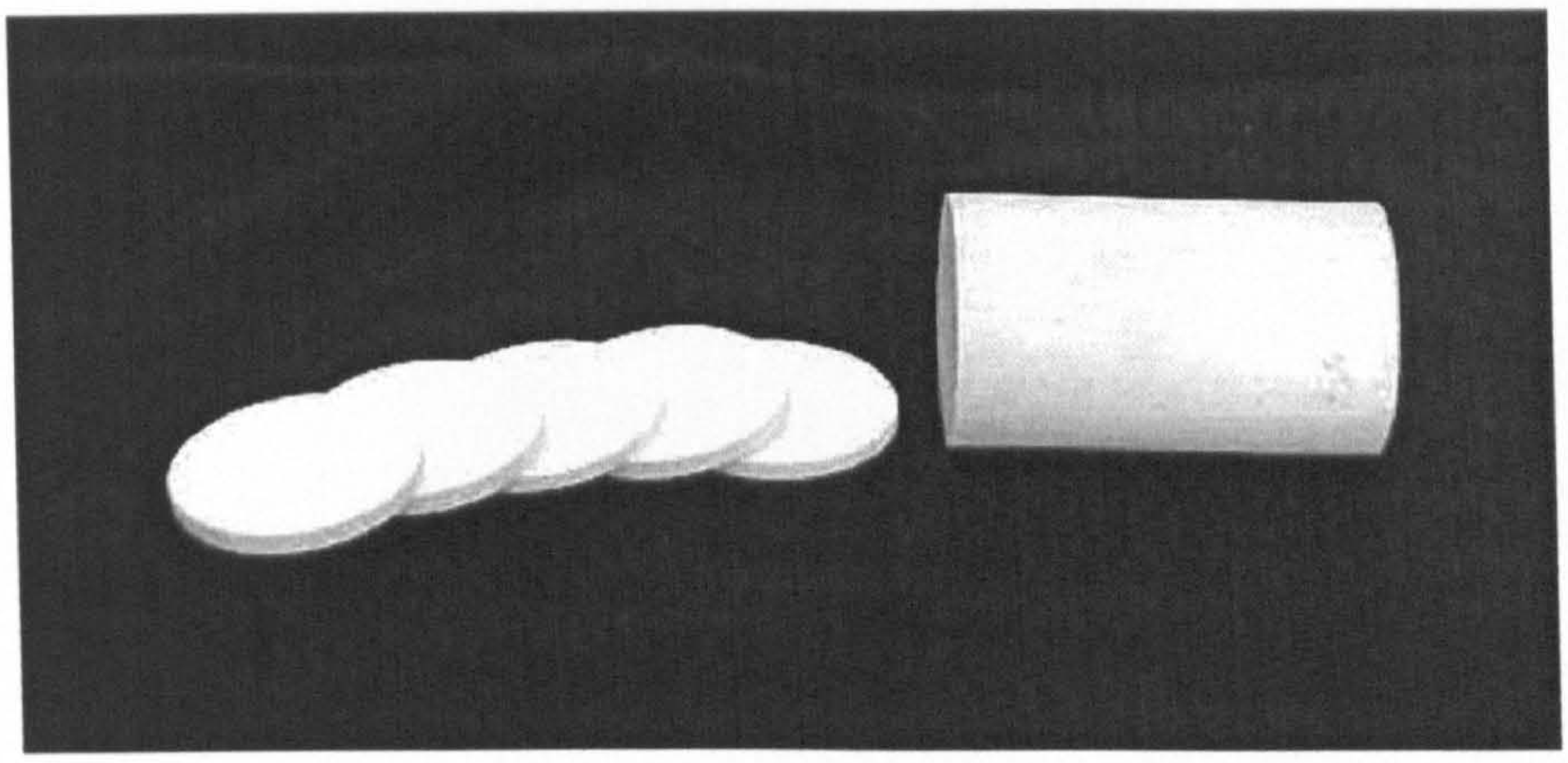

Figure 3.4.1 B: Photograph of a cerammed LDIG105 rod

The method described above was used to produce cylindrical rods with a diameter of 30mm. Whilst these were suitable for *in vitro* testing, samples for *in vivo* testing required a diameter of around 4mm, and due to the small size of the samples a number of modifications to the method used to produce them needed to be made. The main problem was getting the molten glass to flow down into the carbon mould. The mould was made with tapered holes in an attempt to overcome this, but was insufficient by itself in solving the problem (Figure 3.4.1C-left). The mould was then placed on a vibrating table during pouring, but this also proved unsuccessful. Finally a vacuum pump was attached to the base of the mould, as shown in figure 3.4.1C-right, which was successful in drawing the molten glass down into the mould.

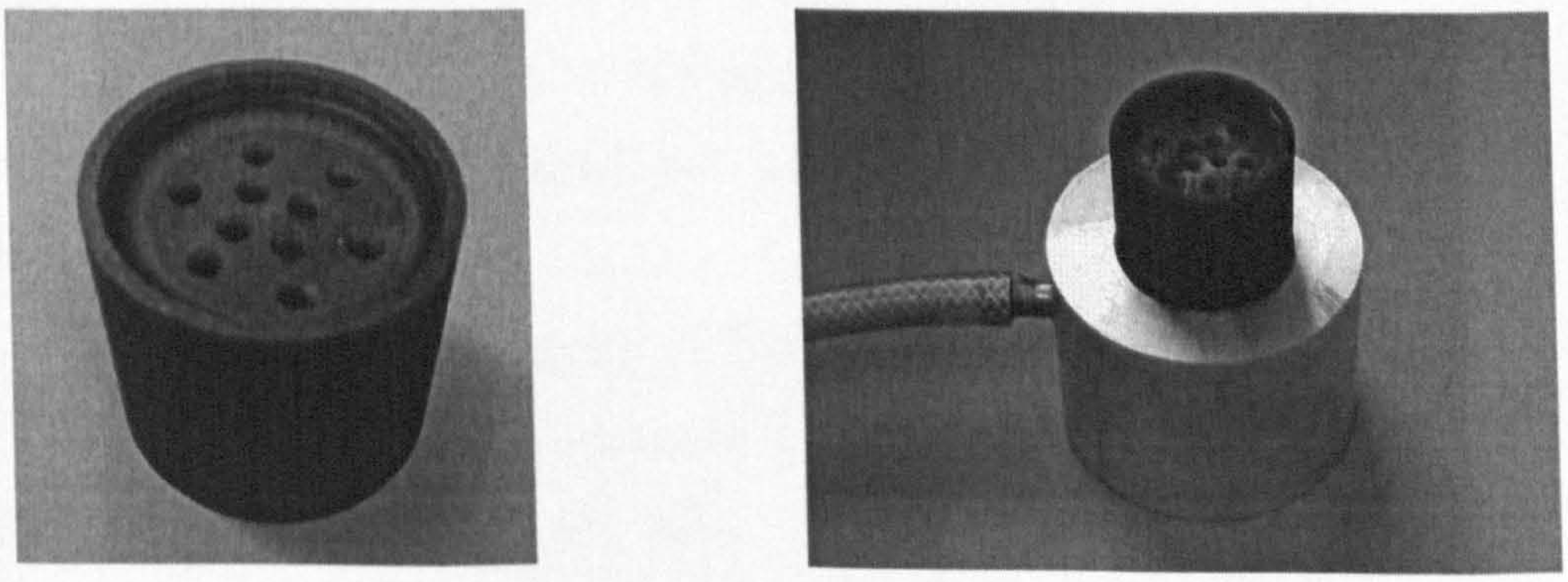

Figure 3.4.1 C: Equipment used for production of small diameter glass rods.
Left – carbon mould. Right – carbon mould with vacuum apparatus

The resulting glass rods (Figure 3.4.1D) were coated with an investment material and cerammed in a similar way to the larger rods.

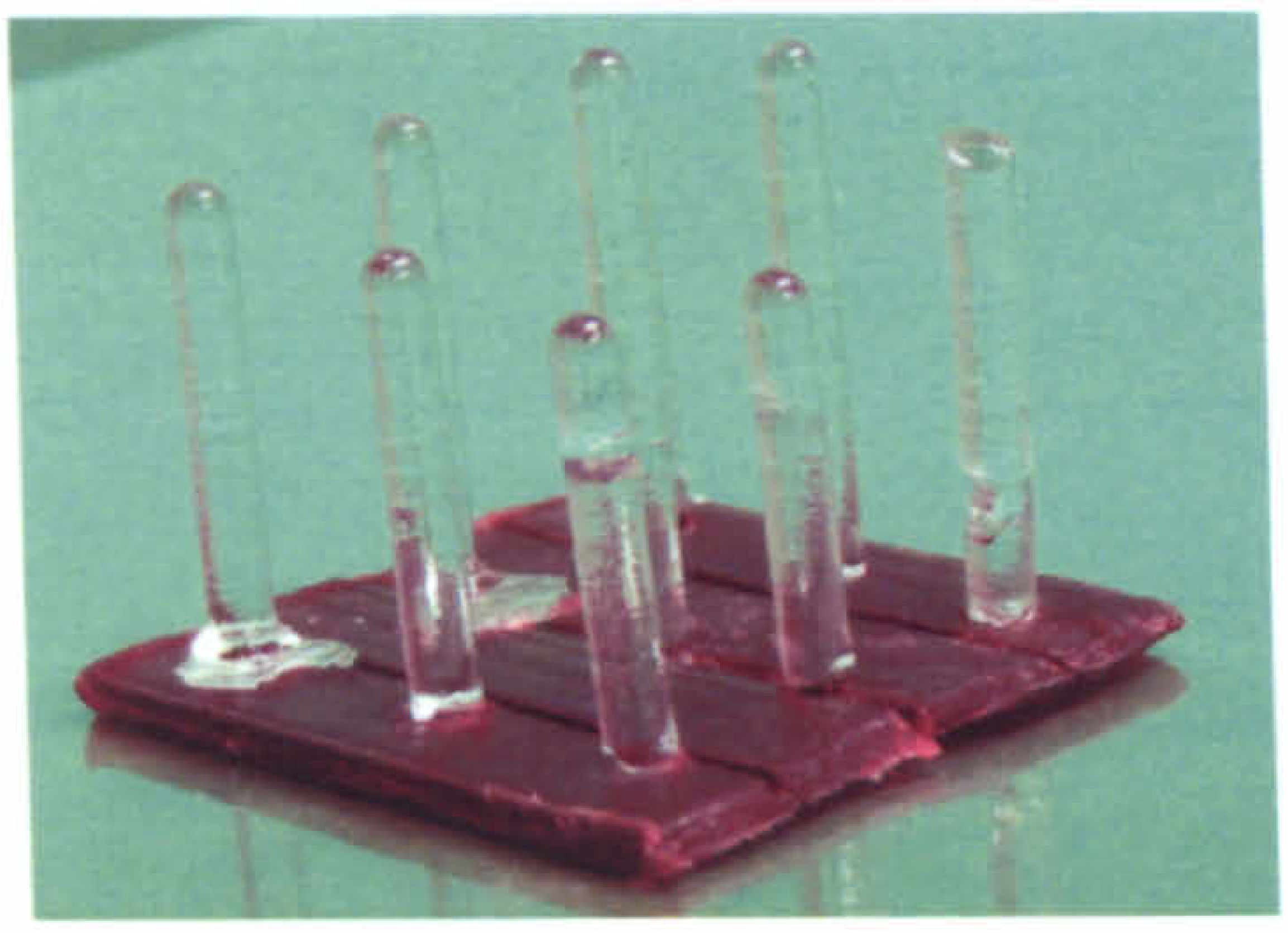

Figure 3.4.1 D: Small glass rods prior to ceramming.

3.4.2 Bioglass®-type glass

Bioglass®-type glass, with the composition $46.1SiO_2 \cdot 24.4Na_2O \cdot 26.9CaO \cdot 2.6P_2O_5$ (molar ratio) was prepared from reagent grade Na_2CO_3, $CaCO_3$, $Ca_2P_2O_7$, and SiO_2. The required mass of each reagent was calculated from the following reactions:

$$
\begin{aligned}
Na_2CO_3 &\rightarrow Na_2O + CO_2\uparrow \\
Ca_2P_2O_7 &\rightarrow 2CaO + P_2O_5 \\
CaCO_3 &\rightarrow CaO + CO_2\uparrow
\end{aligned}
$$

The molar masses of Na_2CO_3 and CO_2 are 105.99 and 44gmol^{-1} respectively.

Therefore 24.4mol% of Na_2O requires $24.4 \times 105.99 - (44 \times 24.4) = 1512.56$g of Na_2CO_3.

The molar mass of $Ca_2P_2O_7$ is 254gmol^{-1}.

Therefore 2.6mol% of P_2O_5 requires $2.6 \times 254 = 660.4$g of $Ca_2P_2O_7$.

This reaction also provides $2.6 \times 2 = 5.2$mol% of CaO.

The molar mass of $CaCO_3$ is 100.9gmol^{-1}.

26.9mol% of CaO is required, but 5.2mol% has already been produced in the above reaction.

Therefore a further 21.7mol% of CaO is required, which requires $21.7 \times 100.09 - (44 \times 21.7) = 1217.143$g of $CaCO_3$.

The molar mass of SiO_2 is 60gmol^{-1}.

Therefore 46.1mol% of SiO_2 requires $46.1 \times 60 = 2766$g of SiO_2.

These masses can be scaled down to a 30g batch from the following equation:

$$(1512.556)a + (1217.143)a + (660.4)a + (2766)a = 30\text{g}$$

$$a = 4.873 \times 10^{-3}$$

Therefore for a 30g batch of Bioglass®-type glass, the final reagent masses required are:

Reagent:	SiO_2	Na_2CO_3	$CaCO_3$	$Ca_2P_2O_7$
Mass:	13.499g	7.371g	5.931g	3.218g

The starting materials were weighed out and blended together manually for thirty minutes with a porcelain pestle and mortar. A platinum crucible was filled to approximately 80% with the powder and placed in a furnace preheated to 1450°C for 10 minutes. After this time the crucible was temporarily removed from the furnace for some of the remaining powder to be added, then returned to the furnace for a further 10 minutes. This process was repeated until the whole batch had been added and melted. The glass was kept in the furnace for a further two hours, being taken out briefly after an hour to be swirled around to aid homogenisation. After this time, the crucible was removed from the furnace, and the glass melt poured onto a stainless steel plate and pressed with another plate of stainless steel to form a transparent glass plate with a thickness of around 2-3mm. This was then annealed in a furnace (Electric Furnace $MoSi_2$ SB-2025D, Motoyama Co., Ltd) preheated to 650°C for four hours, before being allowed to cool to room temperature at the natural rate of the furnace. A band saw was used to cut the plate into squares with dimensions of approximately 10x10mm. All surfaces of the samples were polished with successively finer grades of silicon carbide papers until a surface finish of 6μm was achieved. The samples were washed with acetone in an ultrasonic cleaner for 5 minutes, wiped dry, then washed with ion-exchanged water in the ultrasonic cleaner for a further minute. Due to the reactivity of bioglass®-type glass with water, the samples were stored in a dessicator.

3.4.3 Commercial A-W (Cerabone®) (*in vivo* tests)

Glass-ceramic A-W supplied by Nippon Electrical Glass Co., Ltd was cut and ground into cylinders, 4mm in diameter, for *in vivo* testing.

3.4.4 Commercial Non-bioactive Glass

A commercial glass supplied by Matsunami Glass Ind., Ltd, Japan was used with a composition in weight percent of $72.6SiO_2{\cdot}1.8Al_2O_3{\cdot}3.8MgO{\cdot}7.9CaO{\cdot}12.1Na_2O{\cdot}0.1Fe$.

Chapter 4 Selective Laser Sintering

4.1 Equipment

Selective laser sintering was carried out on an experimental sinterstation in the School of Mechanical Engineering, University of Leeds, UK. The sinterstation, depicted in figures 4.1A and B, consisted of four principal subsystems [Hauser, 2003]:

1. **Laser and focusing optics:** A synrad 250W "Duo-Lase®" CO_2 laser with a wavelength of 10.6μm was used. The laser head (supplied by Laser Lines, Banbury, UK) comprised two 60-1 series 125W laser tubes that were mounted in juxtaposition and the two linearly polarised beams were combined by an optical beam collimator to give a maximum theoretical power output of 250W. The beam was focused onto the powder bed by a BEZ 10 beam expander (supplied by V&S Scientific Ltd, London, UK) giving a spot size of 1.1mm at the surface. The laser was water cooled by a closed loop NESLAB CFT-300 re-circulating chiller unit. Laser power was controlled manually using a Synrad UC-1000 Laser controller with added potentiometer and integral 1000 division counter.

2. **X-Y scan head:** A G325DT scan head (supplied by General Scanning Inc, Banbury, UK) consisting of two orthogonally positioned mirrors each with a scan angle of 40° peak to peak, was used to control the movement of the focused beam over the powder bed surface. The lower mirror directed the laser in the x-axis, then the larger upper mirror reflected it in the y-direction, whilst at the same time translating the beam through 90° and onto the powder bed surface. The movement of the mirrors was controlled by limited rotation closed loop galvanometers which were driven by a digital scanner controller and controlled by the PC based software PC-Mark MT.

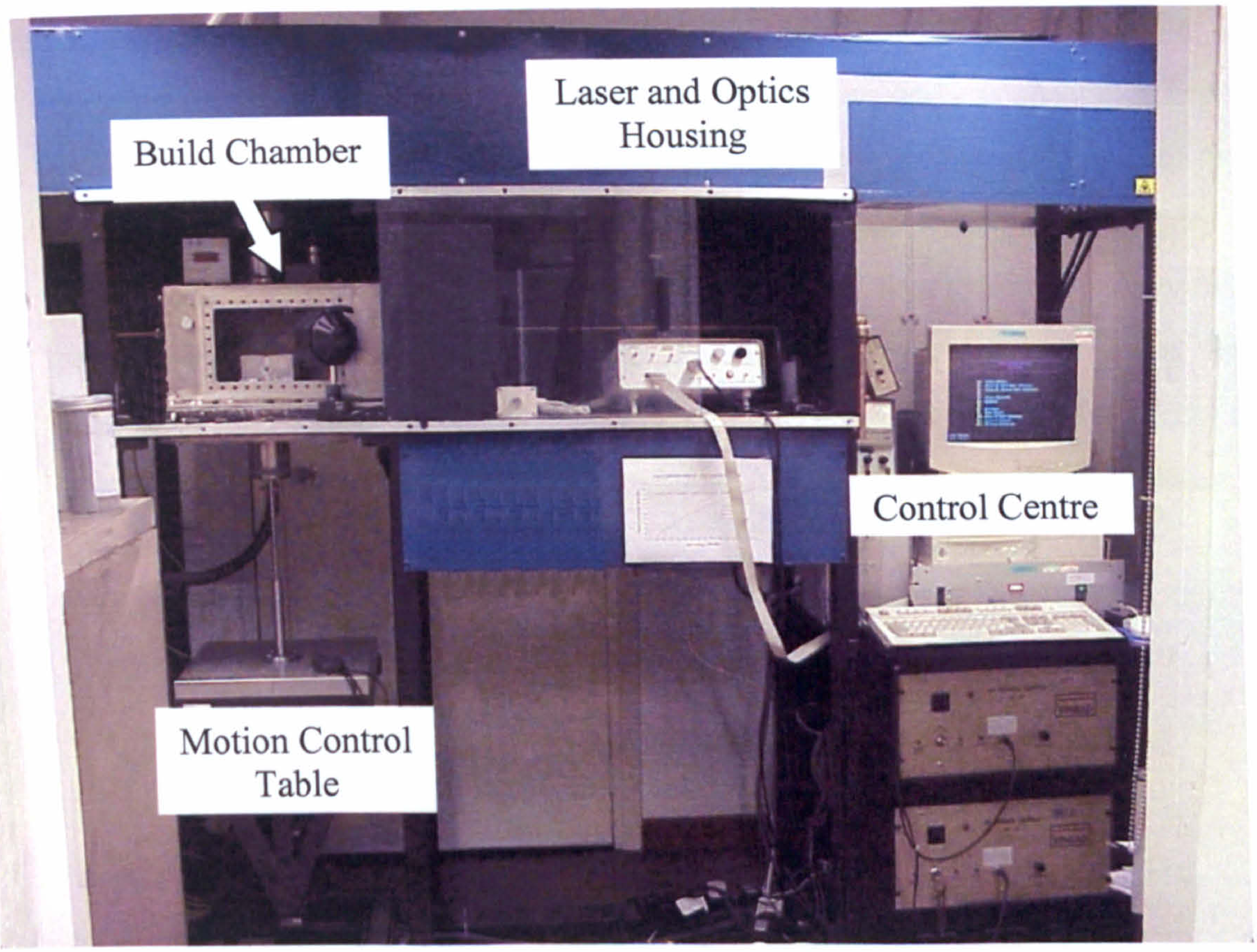

Figure 4.1 A: Photograph showing the arrangement of the experimental sinterstation

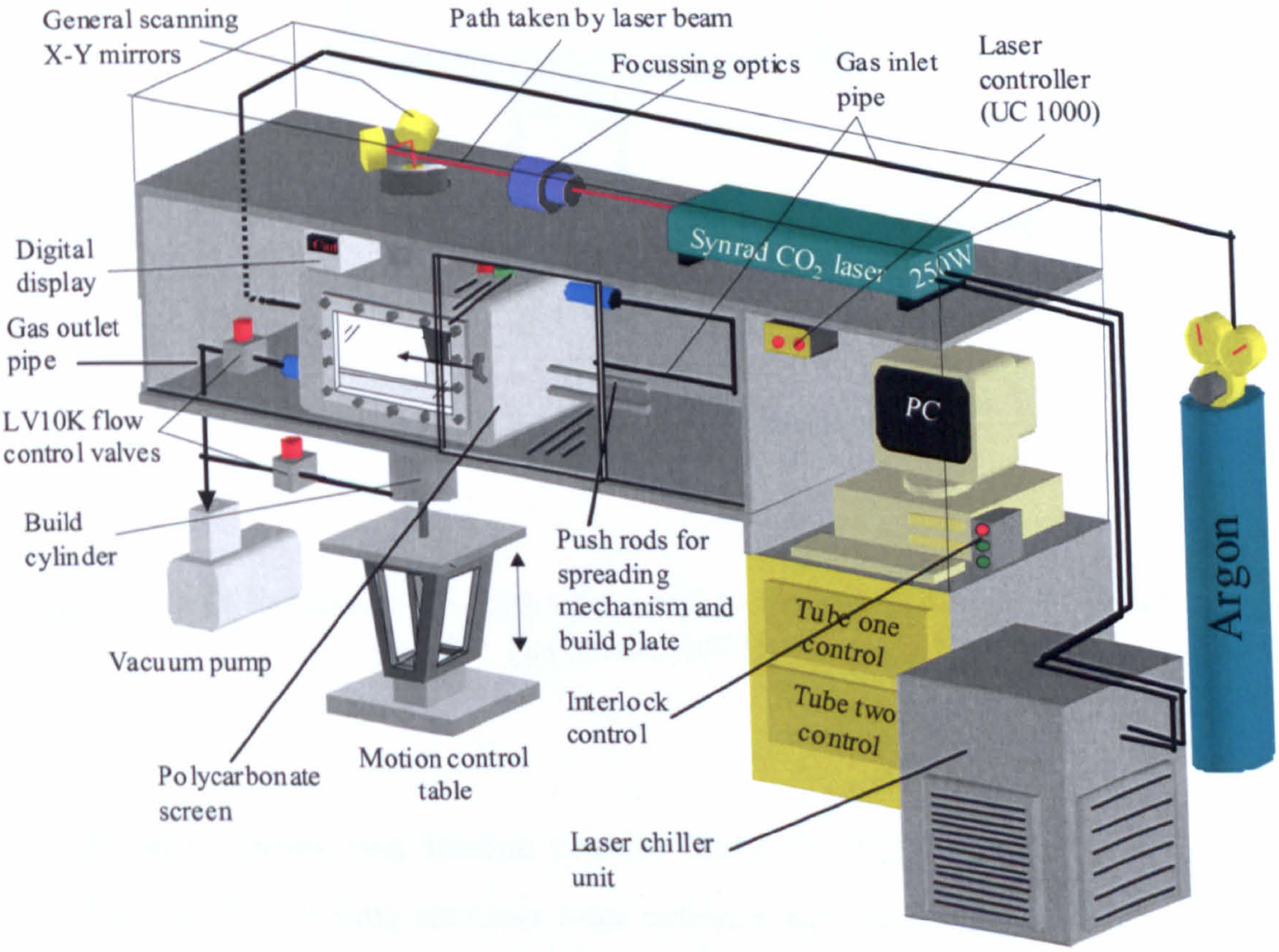

Figure 4.1 B: Schematic diagram of the experimental sinterstation [Hauser, 2003].

3. **Build chamber:** A schematic diagram of the stainless steel build chamber, an air tight cavity 460mm long, 260mm high and 250mm deep, is shown in Figure 4.1C. Access into this cavity was possible via a 250mm long and 150mm high portal machined into the front wall, which was sealed during sintering by an access plate fitted with a polycarbonate viewing window secured to the chamber wall by eight equally spaced M8 cap head bolts. 75mm diameter holes were machined in the base plate and roof of the chamber on the same centre line, the former to give access to the build cylinder and piston unit, and the latter to allow the laser beam to enter the chamber.

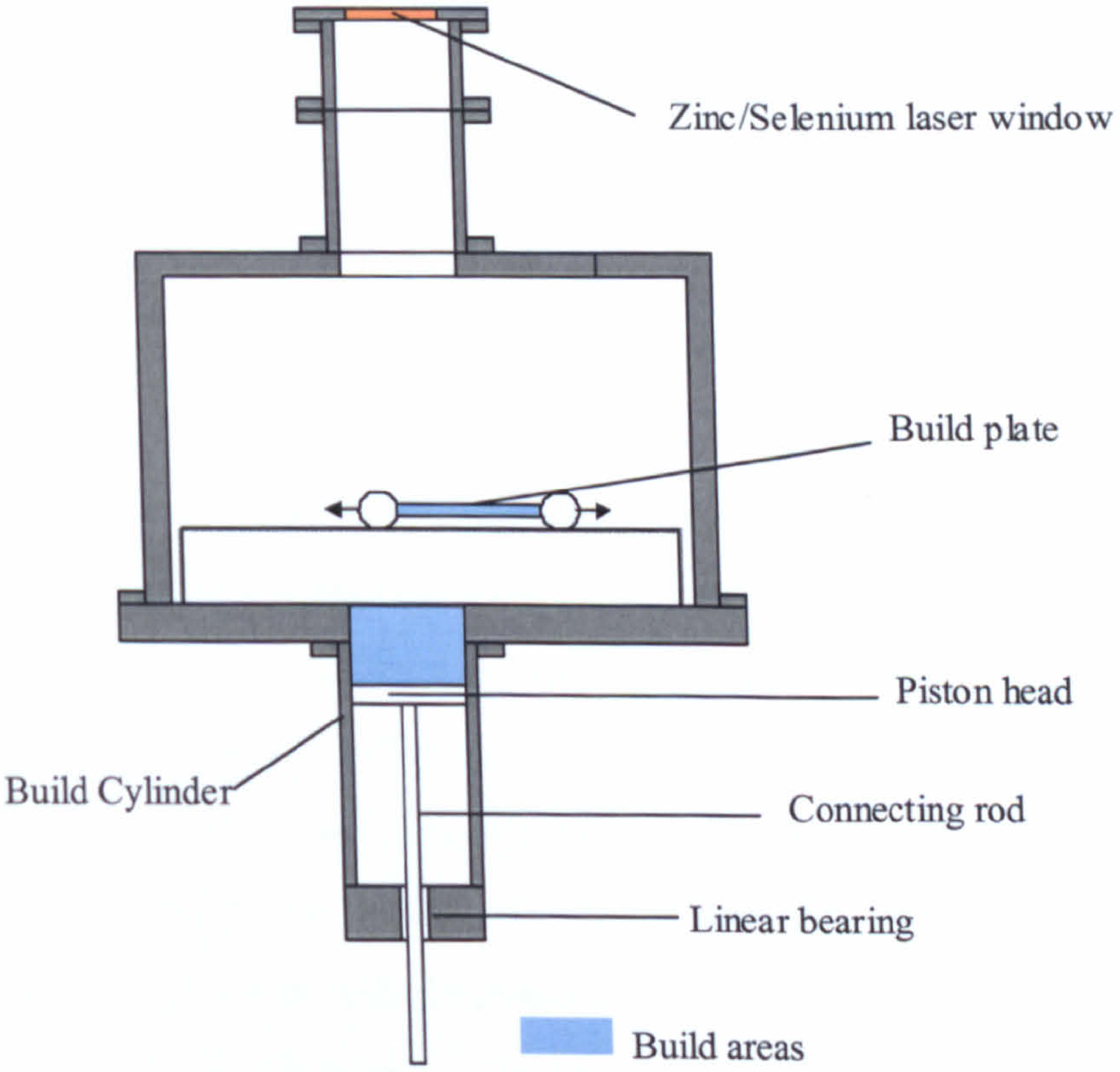

Figure 4.1 C: Schematic diagram of the build chamber showing the build areas [Lorrison, 2003].

4. **Build Cylinder and Motion control table:** The build cylinder was constructed from a 150mm long stainless steel cylinder with an internal diameter of 75mm and a wall thickness of 6mm. Its purpose was to house the piston assembly and

store the deposited powder and sintered components during multiple layer construction. The upper end of the cylinder was connected to a machined surface on the underside of the build chamber via a stainless steel flange, whilst the lower end of the cylinder was sealed using a threaded end cap and vacuum seal. The stainless steel end cap housed a sealed linear bearing, positioned axially, that moved the piston head via a connecting rod attached to the motion control table. The motion control table consisted of a 400mm^2 mounting platform attached to a NC2000 series linear translation stage (supplied by Naples Coombe Ltd, Chaddleworth, UK) capable of indexing a load of 150kg over a vertical distance of 250mm while maintaining an accuracy of ±0.1mm per 50mm travelled. The stage was driven by a servo motor through a gearbox and its position tracked by an encoder. The table, and thus the piston and the level of the powder bed, was controlled by a DOS based software programme called talk2bus.

The laser power output was calibrated against the control dial position using a P200C laser power probe (supplied and pre-calibrated by L.G. Products Ltd, Slough, UK) over a range of 0-200W. The power output for a given control dial position was measured by placing the heat sink of the probe into the path of the laser beam approximately 150mm above the build zone. This positioning was not critical since the total energy output at any point in the laser path would be the same, but it was important that the probe was located sufficiently away from the focal point of the laser where the high heat intensities may have damaged the surface coating on the heat sink, compromising the accuracy of the probe. The probe was exposed to the stationary beam for 20 seconds, momentarily removed, then exposed for a further 15 seconds before taking the reading. This was done to allow for the large thermal inertia of the heat sink. The reading was multiplied by a factory set calibration factor of 1.032 to give an accuracy of ±5%. Readings were taken for every 50 units on the numerical counter and plotted after correction against the control dial position with a 3rd order polynomial line of best fit. This calibration process was carried out several times during the duration of this work in order to maintain consistency between experimental results. A calibration graph made for the University of Leeds sintering machine is shown in Figure 4.1D.

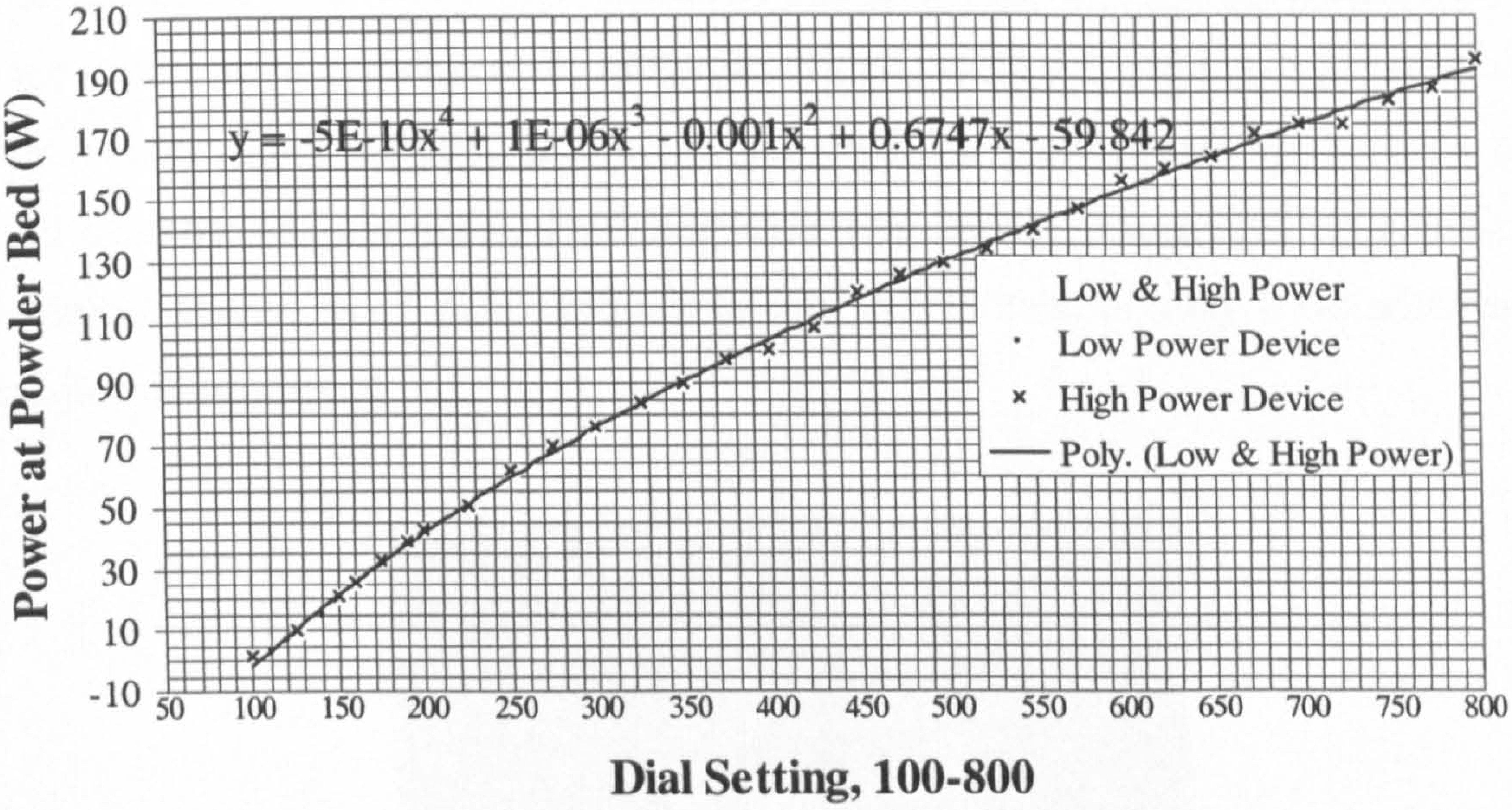

Figure 4.1 D: Powder calibration curve for the CO_2 laser on the University of Leeds sintering machine [Taylor, 2001].

For multiple layer scanning the powder was deposited onto the piston head which was lowered for each new layer by the motion control table. However single layer scans did not require the use of the piston, so instead a shallow tray consisting of a 170mm x 140mm x 10mm thick stainless steel plate with a 140mm x 130mm x 7mm deep recess was used (Figure 4.1E). The tray was filled with powder and levelled with a metal rule before being located on rails within the build chamber by four flanged wheels. Movement of the tray across the exposure range was achieved by a push rod and whilst limited to the x-direction increased the effective powder layer area.

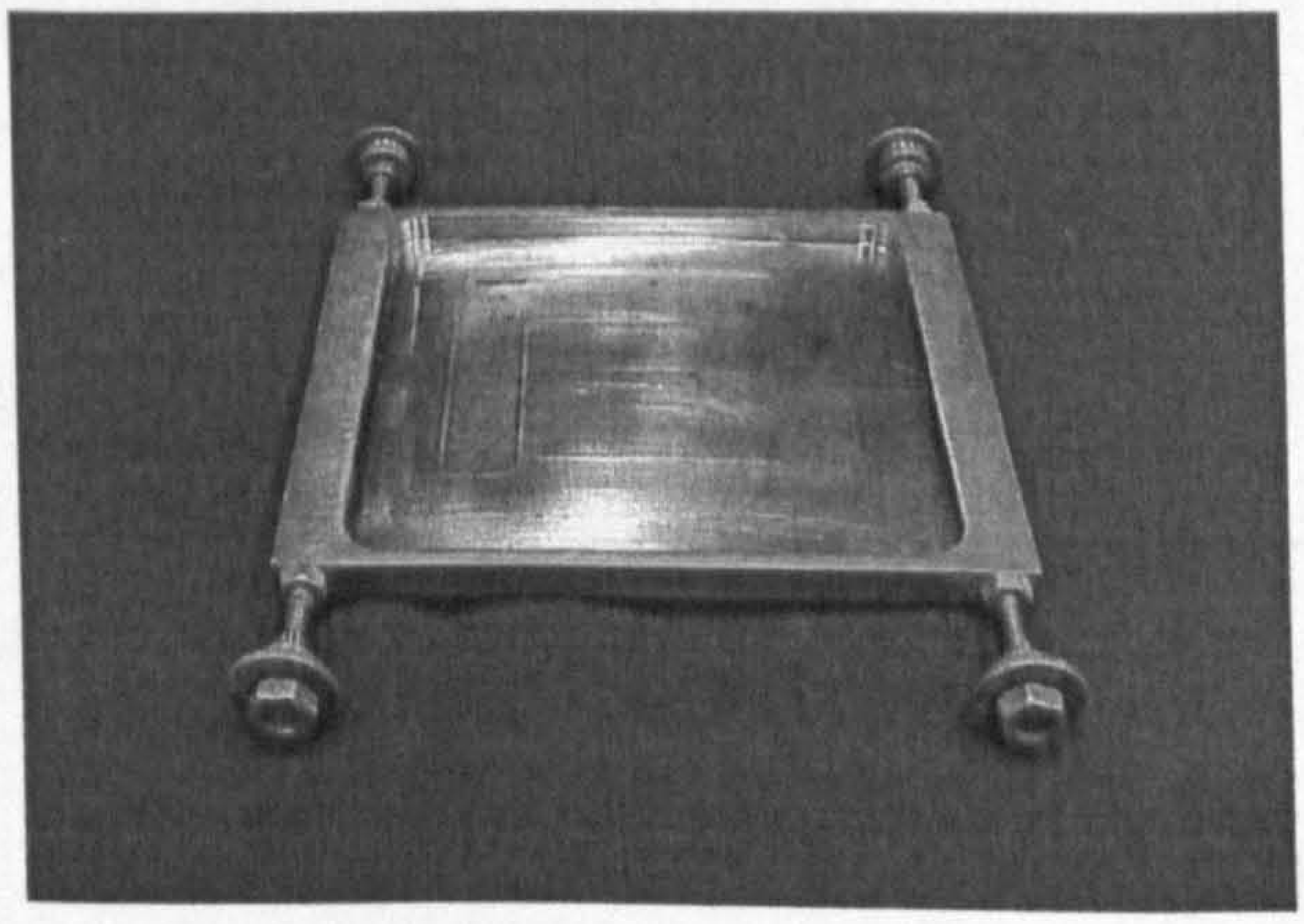

Figure 4.1 E: The stainless steel tray used for single layer scans.

In an attempt to eliminate contamination of the glass powder with other materials used in the sinterstation, a stainless steel liner was fitted inside the build cylinder and used in combination with a modified piston and polyurethane sheet placed on the floor of the build chamber (Figure 4.1F). Particular care was taken when preparing samples for biological testing as contamination with any other material may have affected the outcome of these experiments.

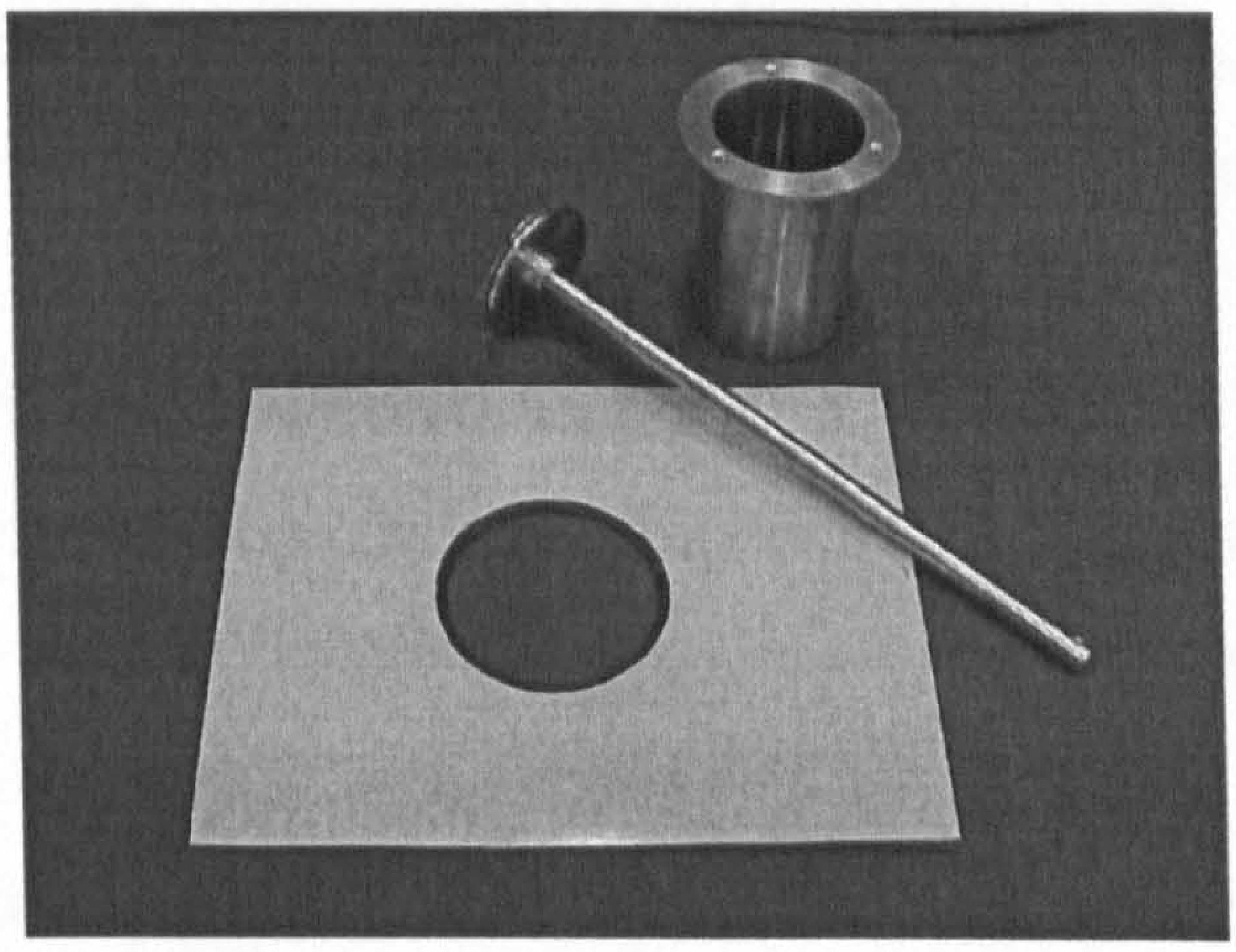

Figure 4.1 F: The liner used to prevent contamination of the glass-ceramic powder [Lorrison, 2003].

Experiments were generally carried out in air at normal atmospheric pressure, since the glass used does not oxidise, and therefore it was considered unnecessary to provide an inert atmosphere. However a small amount of scanning needed to be carried out in an argon rich atmosphere due to problems experienced with ignition of the samples. This was achieved by evacuating the build chamber to approximately 50mbar gauge pressure, then purging with argon gas (supplied by BOC; bottled with a 99.9% purity) until local atmospheric pressure was re-established. Entry of argon into the build chamber was regulated using a flow control valve, and exhaust flow using a RV3 rotary vane vacuum pump and fine leak control valve. A pressure sensor connected to an active digital display unit was used to monitor the pressure inside the chamber (all supplied by Edwards High Vacuum International, Sussex, UK).

4.2 Production of monolayers & determination of process diagrams

LDIG105 was produced, ground to a powder and mixed with an acrylic binder as described in Chapter 3.1.1. The glass-binder powder mix was placed in the stainless steel tray and levelled off with a metal ruler so as to obtain a flat powder surface. The thickness of the powder was maintained at approximately 5mm. As the purpose of these initial experiments was simply to establish the SLS fabrication parameters that could be used to process the material, monolayers, i.e. single layer scans, were produced with dimensions of 15 x 20mm. A number of processing parameters were explored including laser scan rate, laser power, and degree of scan line overlap. In addition the effect of different powder properties was examined including powder particle size and amount of binder used. The scanned monolayers were removed from the powder bed and lightly brushed to remove any loosely attached material. The success of the parameters used was determined by visual inspection and physical handling of the layers. Process maps depicting the scan speeds and laser powers at which the glass-binder mixes will sinter satisfactorily were produced for the various percentage binder and powder particle size combinations prepared in Chapter 3.

4.2.1 Effect of laser power and scan speed on the processing window

Monolayers were produced from LDIG105 with glass particle size 90-125μm and a binder content of 5wt%. The laser scan speed was varied between 50-500mm/sec and the laser power between 5-120W. The overlap between successive scan lines was kept constant at ½ of the beam diameter for all samples.

The process map produced for this material is shown in Figure 4.2.1A. The points plotted represent the combinations of laser scan speed and laser power used to produce monolayers. Successfully scanned layers are indicated by diamond shaped points. Above certain laser powers the material ignited during scanning, presumably due to the presence of the binder. The laser power at which this occurred for each of the scan speeds is depicted by square points, and a best fit line has been drawn from these values.

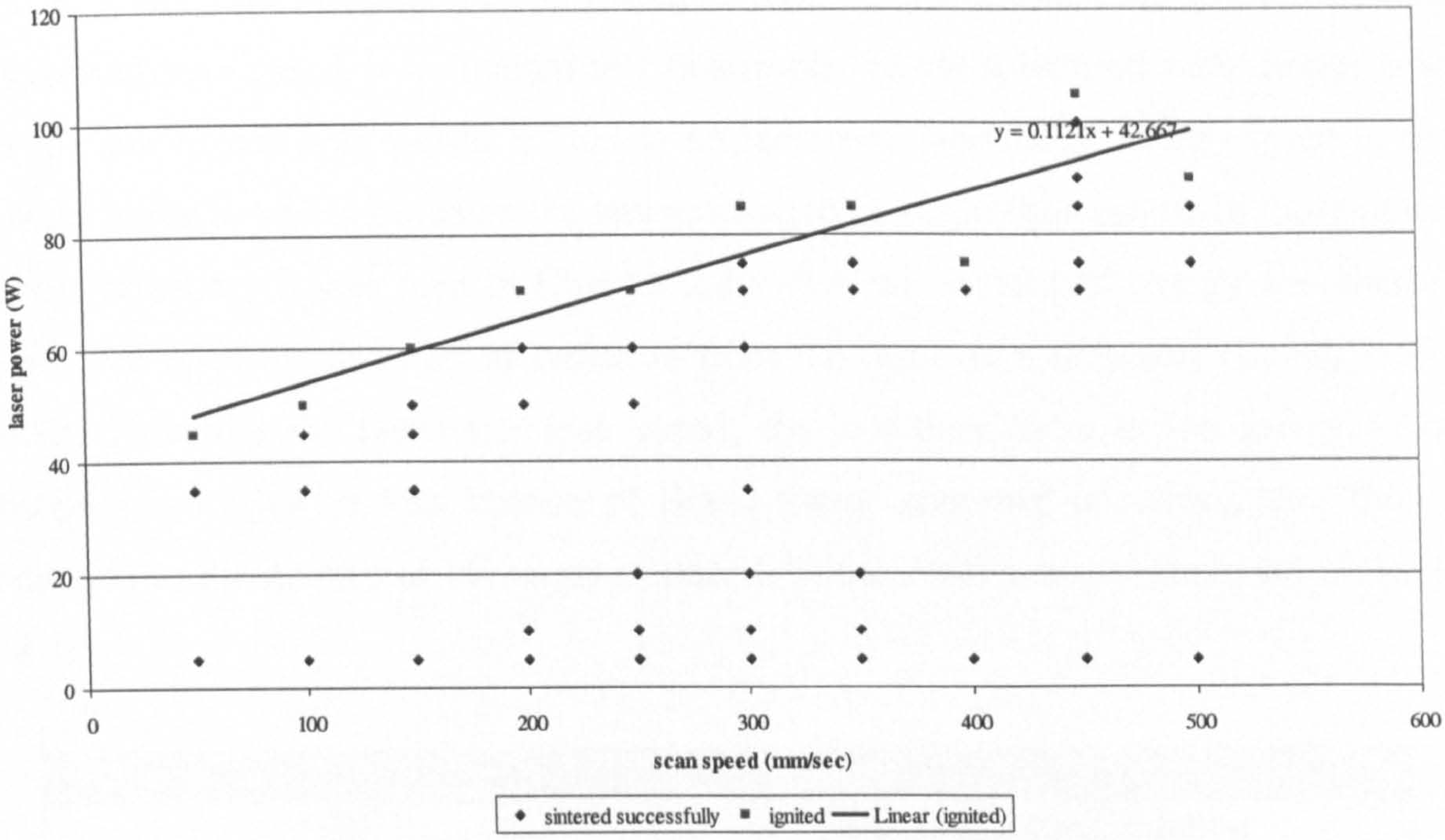

Figure 4.2.1 A: Process Map for LDIG105 (90-125μm) with 15% binder

For a given laser scan speed, the produced monolayers showed poor consolidation at very low powers of 5 or 10W and tended to disintegrate on handling. However as the laser power was increased the fragility of the monolayers continually decreased until they reached the point where the layers ignited during processing. In order to prevent the samples igniting, some sintering was carried out in an argon rich atmosphere, as described in section 4.1. However these samples tended to exhibit a significant amount of bonus-z and therefore attention turned to samples sintered at slightly lower powers that were well defined and which did not require sintering in an inert atmosphere. Table 4.2.1A summarises these results.

Laser Power (W)	Material Appearance
5	Weakly sintered
10	Increasing consolidation ↓
20	
45	
60	
≥70	Ignited during sintering

Table 4.2.1 A: Sintering quality of LDG105 (90-125μm) with 15% binder scanned at 250mm/sec

For a given laser power, the structural integrity of the samples increased with decreasing scan speed. It is thought that this improved consolidation with slower scan speeds and higher laser power is due to an increased amount of energy input to the powder surface, which increases the temperature locally and thus results in more liquid phase formation. It was seen in Chapter 2.4.4 that the amount of energy absorbed is dependent upon the duration of radiation from the laser on a unit area [Leong *et al.*, 2001]. Therefore the faster the scan speed, the less time there is for energy to be absorbed, resulting in less chance of liquid phase sintering occurring, and thus a reduction in the quality of the parts produced. These results are summarised in Table 4.2.1B.

Laser Beam Scan Speed (mm/sec)	Material Appearance
50	Reasonable consolidation
100	| Decreasing consolidation ↓
150	
200	
250	
300	
350	
400	
450	
500	Very little consolidation / weakly sintered

Table 4.2.1 B: Sintering quality of LDG105 (90-125μm) with 15% binder scanned at a laser power of 5W

For certain laser powers, decreasing the scan speed too far resulted in the sample igniting during sintering, the likelihood increasing with increasing laser power used. It appears therefore that there was a critical value of energy at which the polymer ignited. "Energy density", the key operational parameter in the SLS process was defined in Chapter 2.4.4 as:

$$EnergyDensity \cong \frac{P}{SS \times ScSp}$$

where P is the laser power, SS the scan speed, and ScSp is the spacing between adjacent raster scans.

The resulting "Andrew Number" is used to quantify the energy applied per unit area of power per unit time. Figure 4.2.1B shows the Andrew numbers for the combinations of laser power and scan speed used in this work. The shaded grey boxes indicate the values of energy density which caused the glass-binder to ignite, for LDIG105 (90-125μm) with 15% binder.

		Scan Speed (mm/sec)									
		50	100	150	200	250	300	350	400	450	500
Laser Power (W)	5	0.18	0.09	0.06	0.05	0.04	0.03	0.03	0.02	0.02	0.02
	10	0.36	0.18	0.12	0.09	0.07	0.06	0.05	0.05	0.04	0.04
	15	0.55	0.27	0.18	0.14	0.11	0.09	0.08	0.07	0.06	0.05
	20	0.73	0.36	0.24	0.18	0.15	0.12	0.10	0.09	0.08	0.07
	25	0.91	0.45	0.30	0.23	0.18	0.15	0.13	0.11	0.10	0.09
	30	1.09	0.55	0.36	0.27	0.22	0.18	0.16	0.14	0.12	0.11
	35	1.27	0.64	0.42	0.32	0.25	0.21	0.18	0.16	0.14	0.13
	40	1.45	0.73	0.48	0.36	0.29	0.24	0.21	0.18	0.16	0.15
	45	1.64	0.82	0.55	0.41	0.33	0.27	0.23	0.20	0.18	0.16
	50	1.82	0.91	0.61	0.45	0.36	0.30	0.26	0.23	0.20	0.18
	55	2.00	1.00	0.67	0.50	0.40	0.33	0.29	0.25	0.22	0.20
	60	2.18	1.09	0.73	0.55	0.44	0.36	0.31	0.27	0.24	0.22
	65	2.36	1.18	0.79	0.59	0.47	0.39	0.34	0.30	0.26	0.24
	70	2.55	1.27	0.85	0.64	0.51	0.42	0.36	0.32	0.28	0.25
	75	2.73	1.36	0.91	0.68	0.55	0.45	0.39	0.34	0.30	0.27
	80	2.91	1.45	0.97	0.73	0.58	0.48	0.42	0.36	0.32	0.29
	85	3.09	1.55	1.03	0.77	0.62	0.52	0.44	0.39	0.34	0.31
	90	3.27	1.64	1.09	0.82	0.65	0.55	0.47	0.41	0.36	0.33
	95	3.45	1.73	1.15	0.86	0.69	0.58	0.49	0.43	0.38	0.35
	100	3.64	1.82	1.21	0.91	0.73	0.61	0.52	0.45	0.40	0.36
	105	3.82	1.91	1.27	0.95	0.76	0.64	0.55	0.48	0.42	0.38

Figure 4.2.1B: Andrew Numbers used in this work with shaded boxes showing values which caused LDIG105 (90-125μm) with 15% binder to ignite during laser sintering.

If the above model had applied completely then the energy density which caused the powder to ignite would have been identical for all laser power : scan speed combinations. However it can be seen that these number are not consistent and instead the powder tends to ignite at lower energy density values when higher laser powers and/or faster scan speeds are used. This indicates that laser power has a larger influence than the Andrew number suggests. There is an inbuilt assumption in the Nelson model that there is an even distribution of energy emitted from the laser beam and thus the value stated for laser power is an average distribution, whereas it is more likely to be a Gaussian distribution with more energy resulting from the centre of the beam.

In addition, if a faster scan speed is used then there will be shorter delay between successive pulses applied to each point on the surface where there's overlap between adjacent scan lines. This may lead to higher surface temperatures and increased loss of polymer, as there is less time for loss of energy between pulses. Therefore ignition would occur at lower energy density values.

4.2.2 Effect of binder content on processing window

Process maps depicting the scan speeds and laser powers at which LDIG105 powder with glass particle size 45-90μm will sinter satisfactorily were produced for the various percentage binder combinations prepared in Chapter 3. These can be seen in Figures 4.2.2A-D. All demonstrated similar trends to those seen previously with 15% binder i.e. increased consolidation with increasing laser power and decreasing scan speed up to the point of ignition.

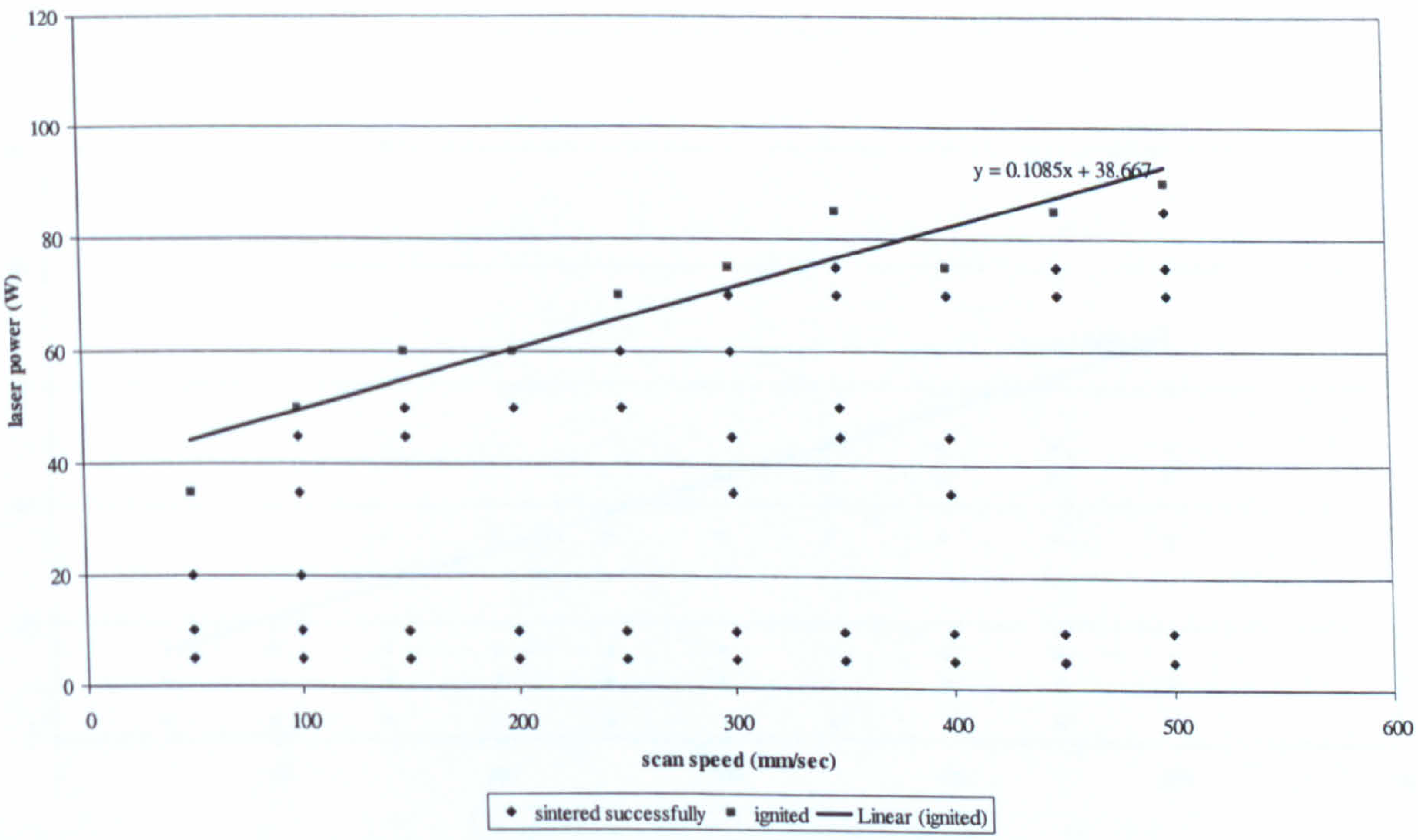

Figure 4.2.2 A: Process Map for LDIG105 (90-125μm) with 10% binder

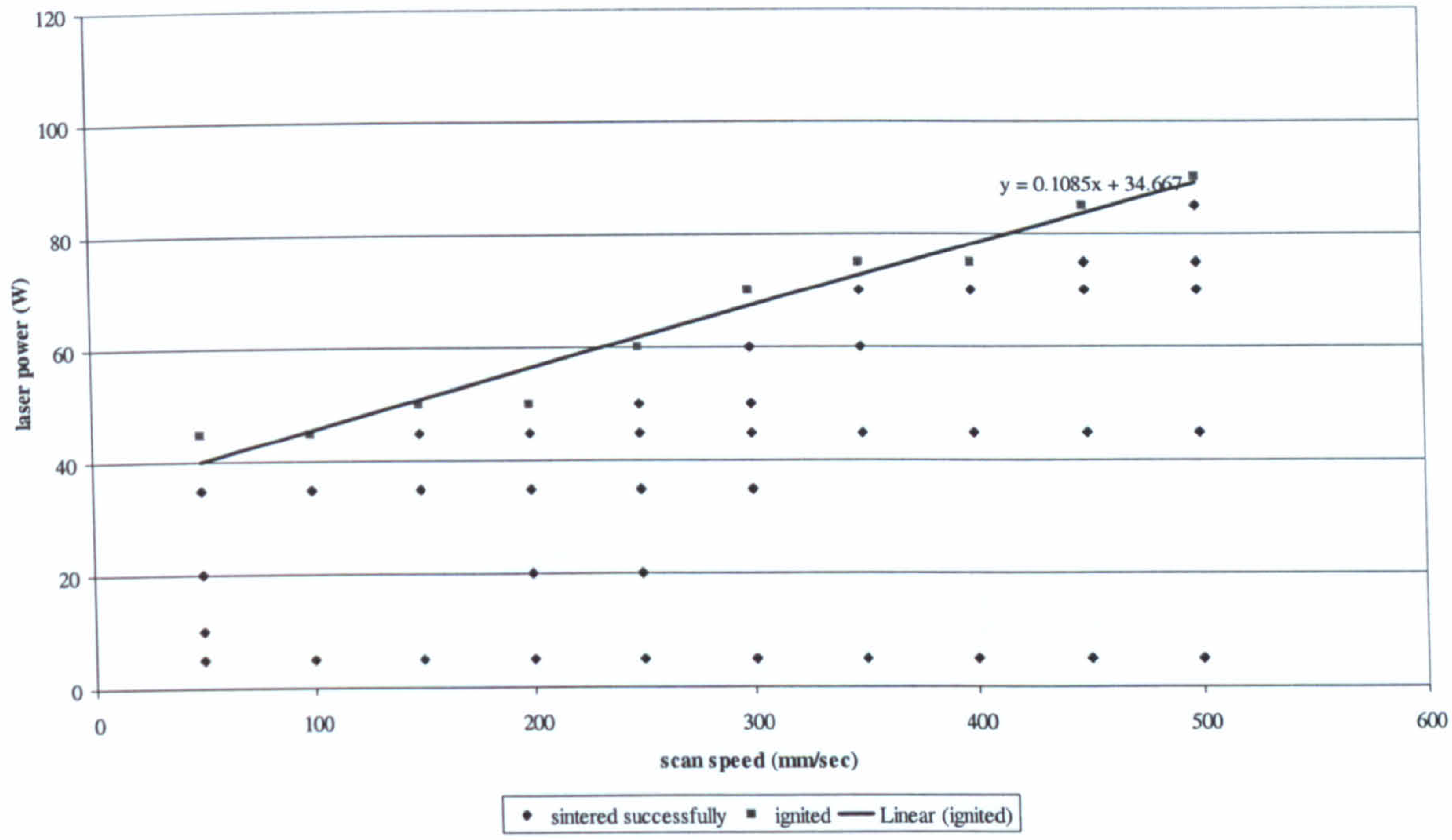

Figure 4.2.2 B: Process Map for LDIG105 (90-125μm) with 5% binder

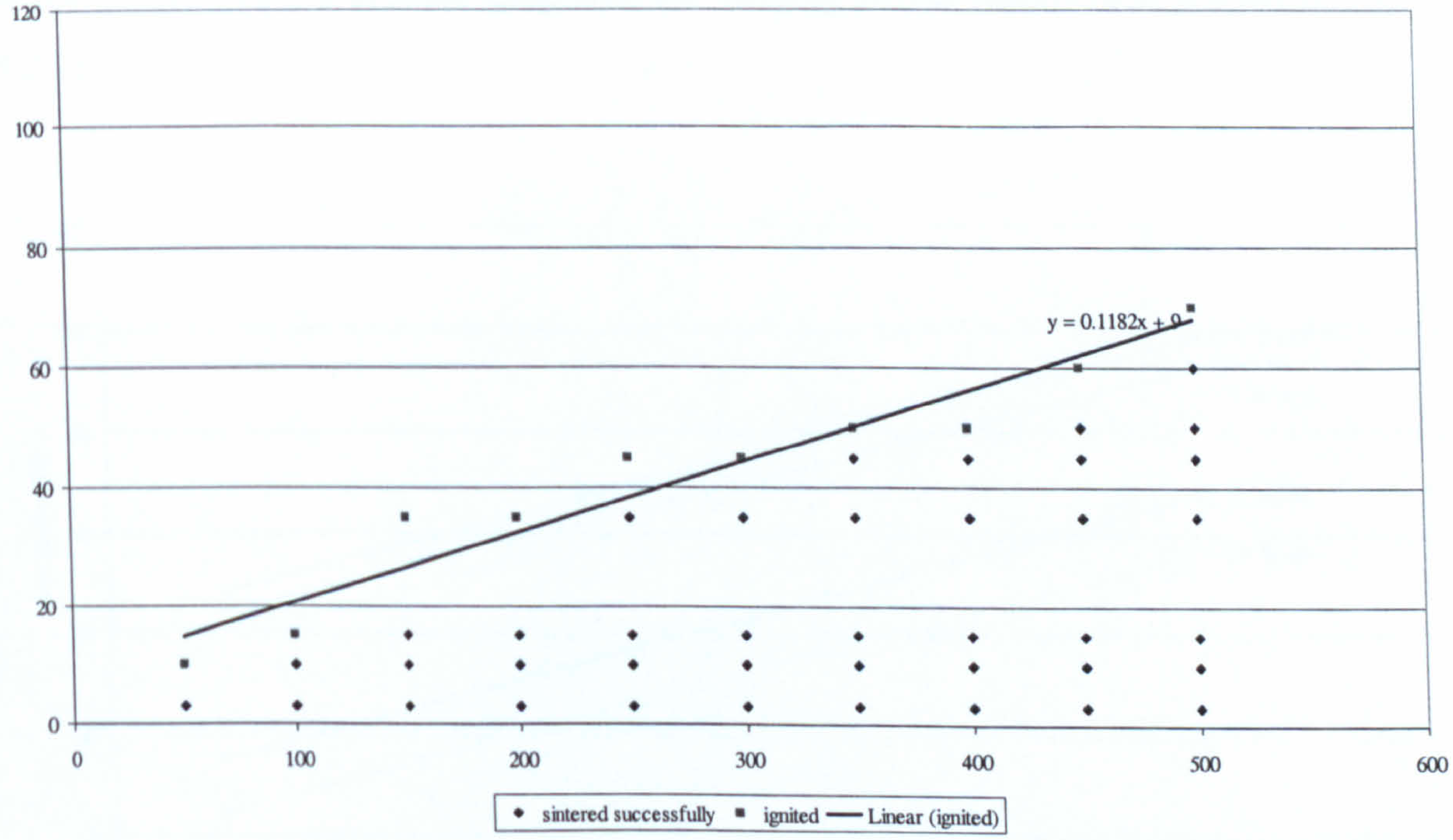

Figure 4.2.2 C: Process Map for LDIG105 (90-125μm) with 3% binder

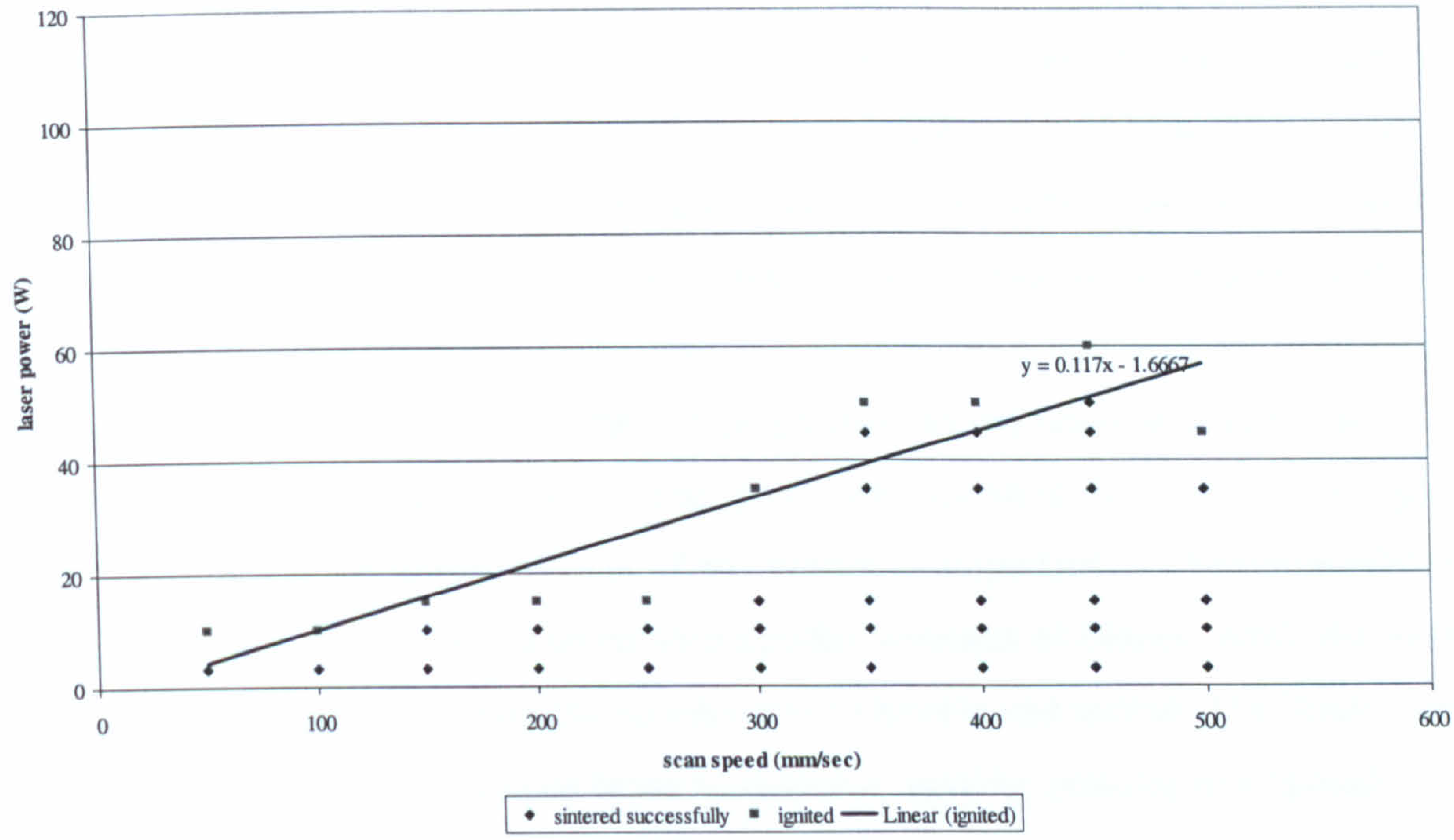

Figure 4.2.2 D: Process Map for LDIG105 (90-125μm) with 1% binder

A comparison of the process diagrams for varying binder contents is shown in Figure 4.2.2E.

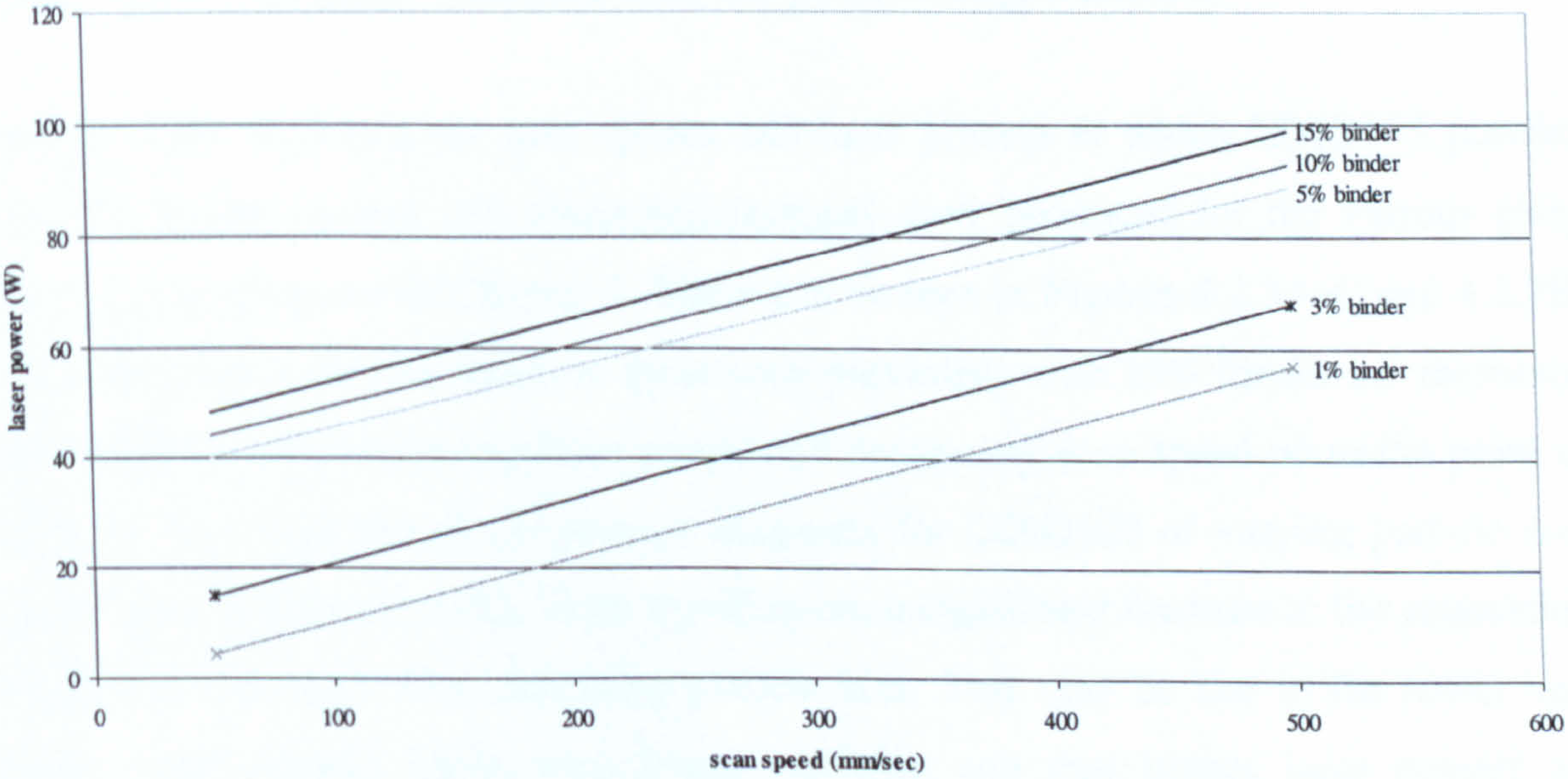

Figure 4.2.2 E: Maximum laser power:scan speed combinations for varying ratios of glass:binder (90-125μm)

As the binder content is decreased, a reduction in the processing window can be observed, with the glass-binder mix igniting at lower laser powers and scan speeds. This is probably due simply to less polymer being present and thus less energy is required before the samples ignite. The glass-ceramic has higher absorptance than the acrylic binder and thus when more ceramic/less binder is present the powder will heat up quicker. Lower binder contents are desirable because the porosity of the final object and consequently its strength and the shrinkage that occurs upon post-processing are proportional to the binder content. The parts are intended for use in biological applications where complete removal of the binder is important for biocompatibility, and this is more likely to be achieved with smaller amounts of binder. Also, the lower the percentage binder, the easier the powder was to handle and spread. The binder used is very fine, and in large amounts tends to disperse, making pouring and spreading of the powder more difficult. However samples produced from 1 and 3% binder mixes were very fragile, presumably due to not enough binder being present to bind the glass particles together. Therefore a compromise of 5% binder was used in further work, due to its large processing window, ease of handling, and ability to produce parts with sufficient structural integrity.

4.2.3 Effect of glass particle size on processing window

Process maps depicting the scan speeds and laser powers at which LDIG105 powder with 5% binder content will sinter satisfactorily were produced for the various glass particle sizes prepared in Chapter 3. These can be seen in Figures 4.2.3A-C and 4.2.2B. All demonstrated similar trends to those seen previously with 15% binder i.e. increased consolidation with increasing laser power and decreasing scan speed up to the point of ignition. A comparison of the process diagrams for LDIG105 of varying particle size can be seen in Figure 4.2.3D. From this diagram a significant increase in the processing window is observed with increasing particle size. This may be due to the lower heat transfer into powder layers with larger particles, and thus higher laser powers are required before the polymer binder ignites.

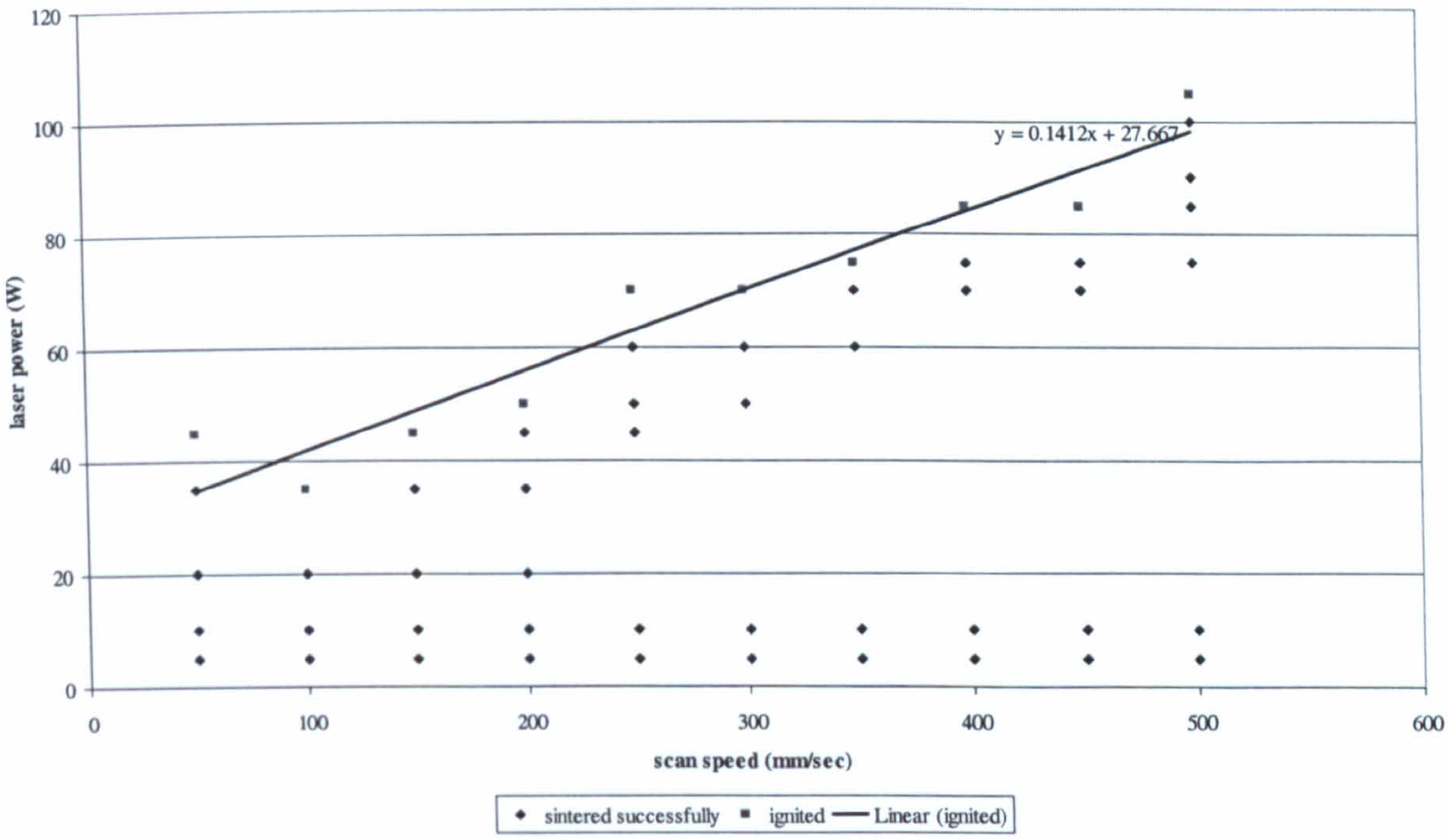

Figure 4.2.3 A: Process Map for LDIG105 (125μm-1mm) with 5% binder

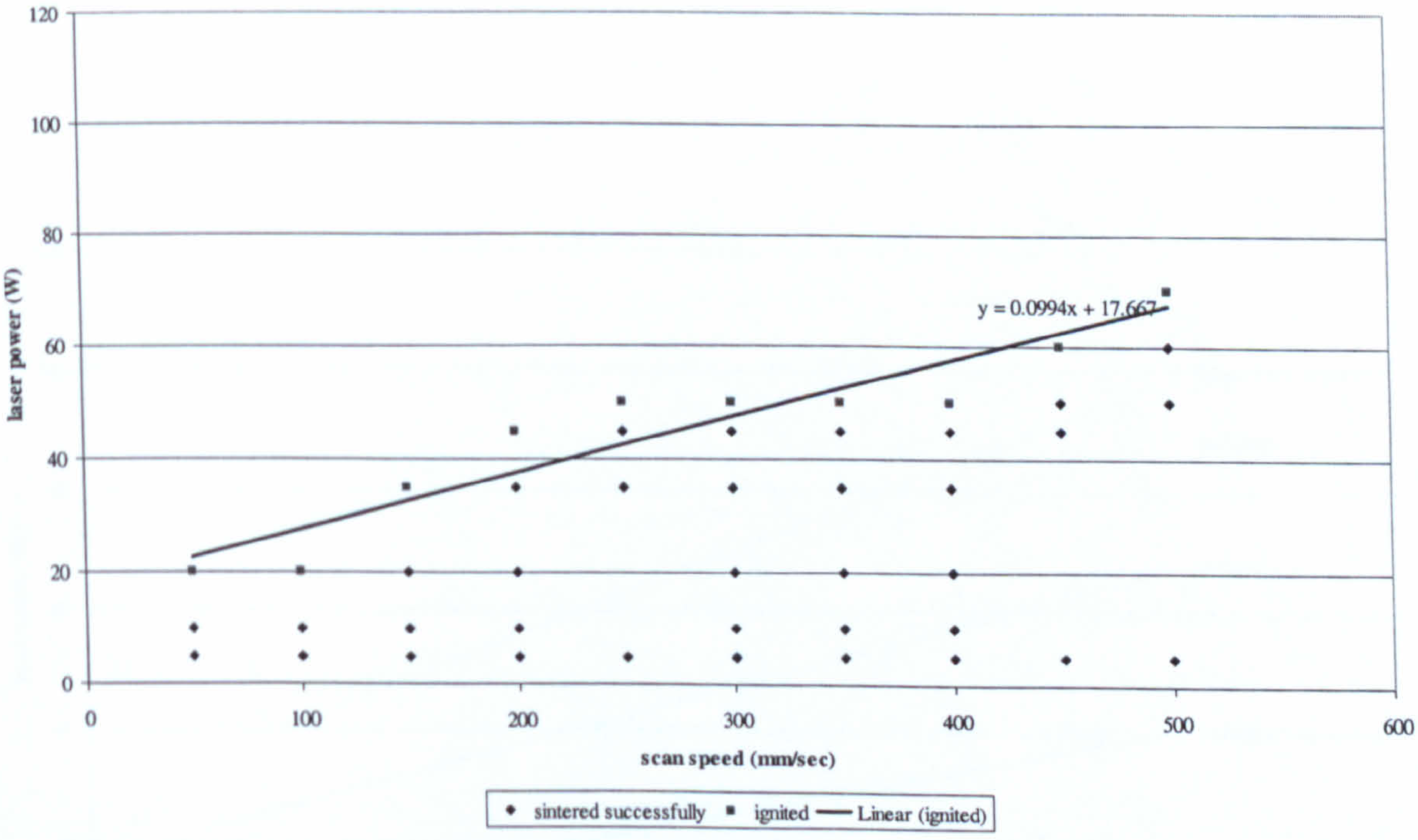

Figure 4.2.3 B: Process Map for LDIG105 (45-90μm) with 5% binder

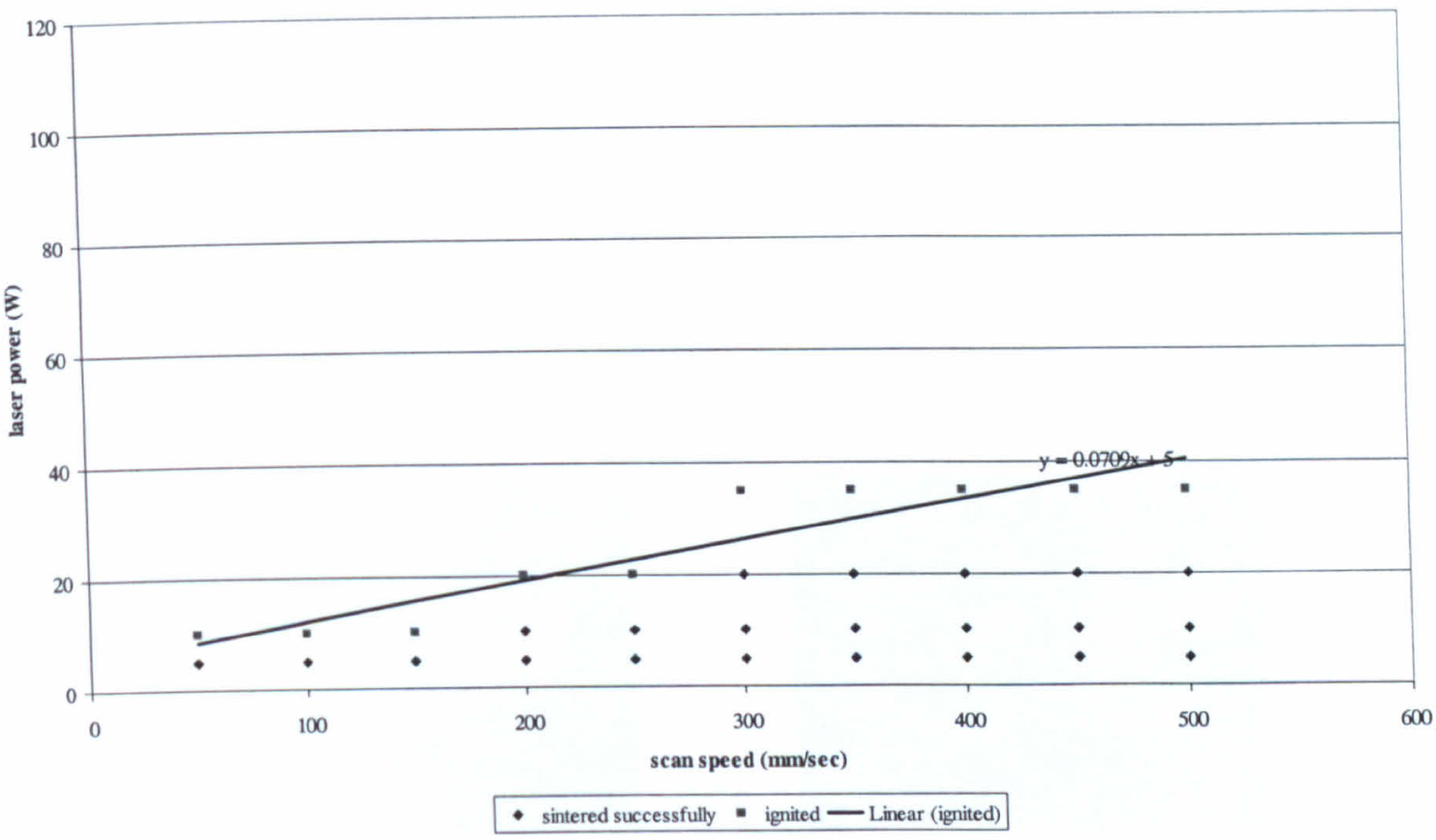

Figure 4.2.3 C: Process Map for LDIG105 (<45μm) with 5% binder

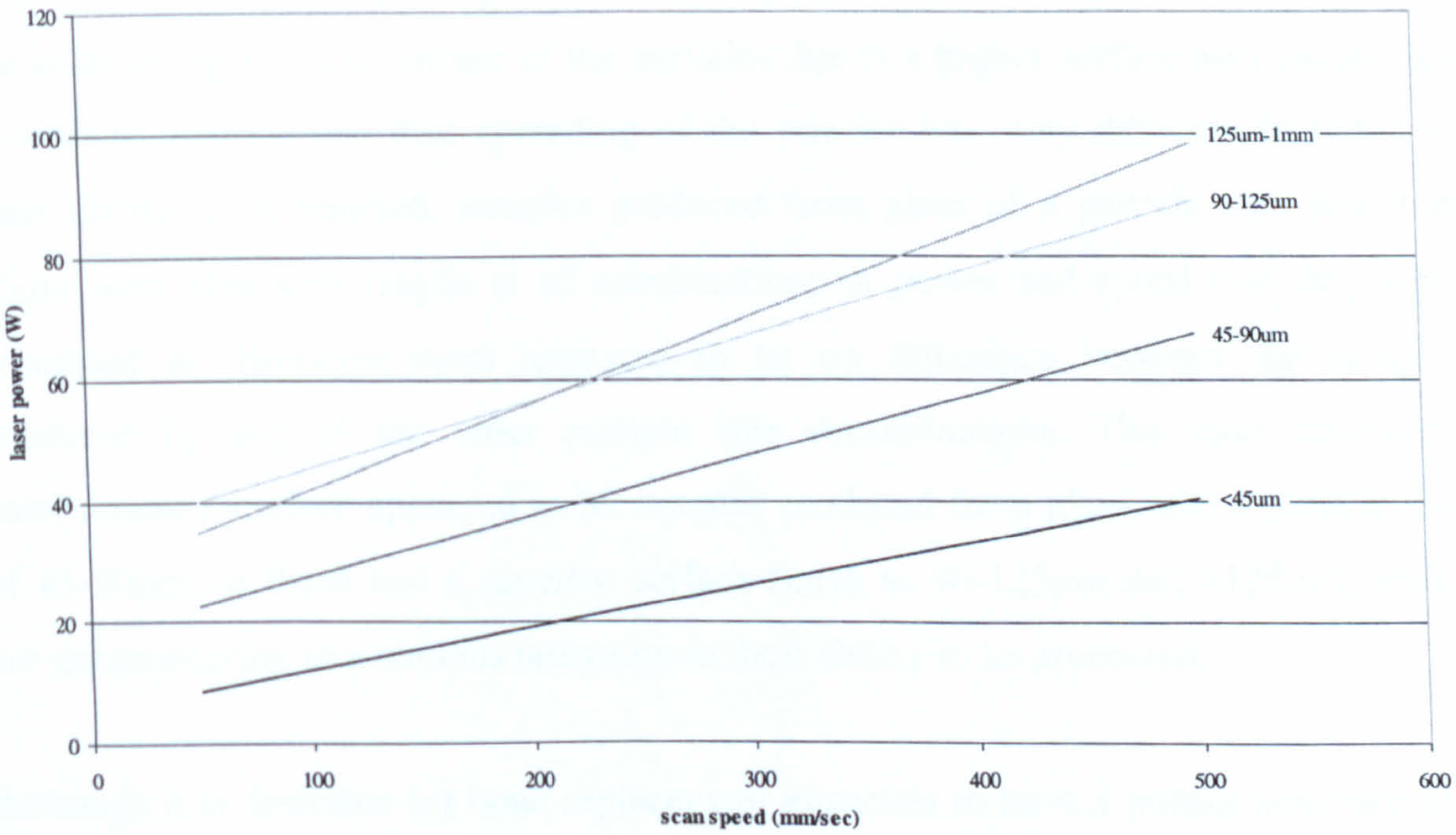

Figure 4.2.3 D: Maximum power:speed combinations for varying glass particle sizes (5% binder)

The size of the powder particles also affects the surface roughness and feature definition of the produced parts, and the porosity of the powder bed and hence the porosity of the final part. A significant improvement in surface finish and definition was seen with decreasing particle size as is illustrated by the photographs of monolayers pictured in Figure 4.2.3E a and b, which were produced from glass of particle size 90-125μm and 45-90μm respectively.

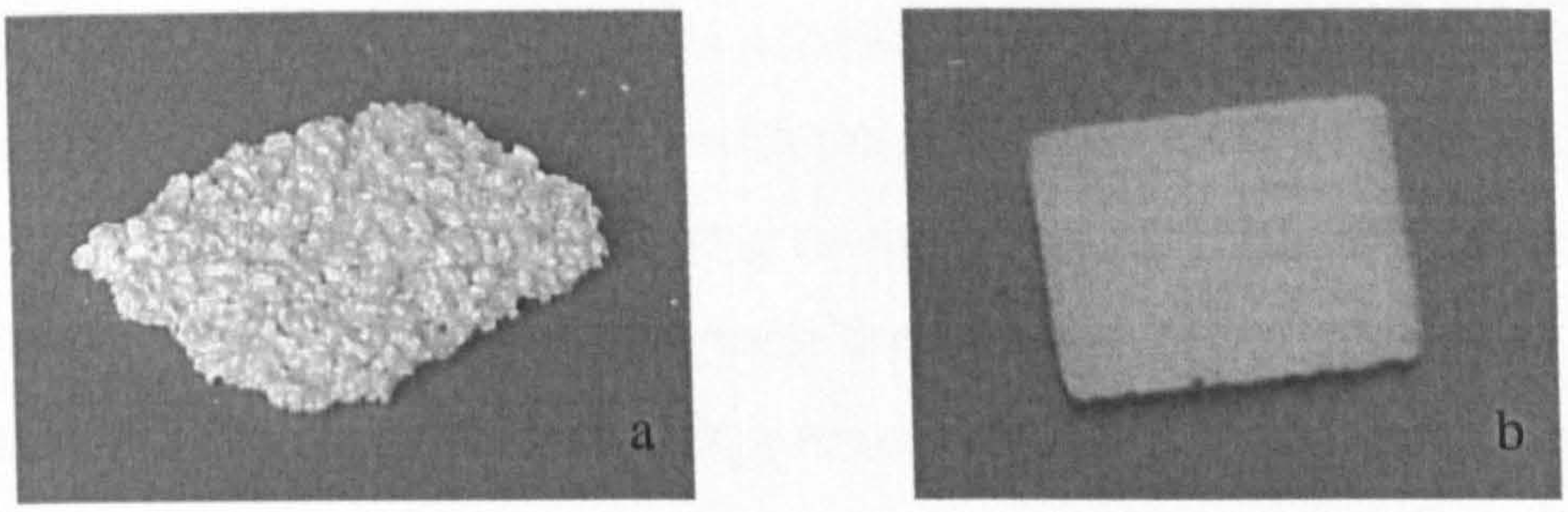

Figure 4.2.3 E: Samples produced from glass of particle size 90-125μm (a) and 45-90μm (b)

As the particle size was decreased, the thickness of the resulting monolayer was reduced. This should allow parts to be built from thinner layers, thereby improving accuracy and edge definition by reducing the effects of stairstepping. The particle size also influenced how easy the powder was to spread over the build area. Below 45μm the static charges on the surface of the particles due to a higher surface area caused the powder to disperse and thus spreading of the powder was very difficult. In terms of their ability to be handled, samples produced from glass of a particle size less than 45μm were also very fragile at all combinations of power and speed that they were processed at. However there appeared to be no difference between the samples produced by any of the other particle size denominations. The most promising compromise therefore appeared to be samples produced from glass with a particle size of 45-90μm, as these had a superior surface finish to 90-125μm and >125μm, whilst not demonstrating any obvious reduction in their ability to be processed.

Although it is desirable for bone replacement materials to have a porous structure, the more porous a material is the lower its mechanical strength tends to be and the greater shrinkage will occur on subsequent heat treatment of the part. Therefore attempts were made to increase the density of the powder bed, as it was thought that this would in turn result in a greater sintered density and thus allow a higher strength material to be produced. It was seen in Chapter 2.4.2 that improved packing densities are achieved by using a range of particle sizes, where the gaps between larger particles are filled by smaller ones. Therefore a combination of 45-90μm and <45μm glass particle sizes were blended together in ratios of 50:50 and 75:25, as described in Chapter 3.1.1. Process maps depicting the scan speeds and laser powers at which LDIG105 powder with 5% binder content will sinter satisfactorily were produced for the mixed glass particle fractions. These can be seen in Figures 4.2.3F and G. Once again they demonstrated similar trends to those seen previously with other glass particle sizes. In Figure 4.2.3H, it can be seen how these two processing maps compare to those of the single glass particle fractions. It appears that the greater the density of the powder bed, the smaller the processing window, i.e. the less energy required to cause the powder to ignite.

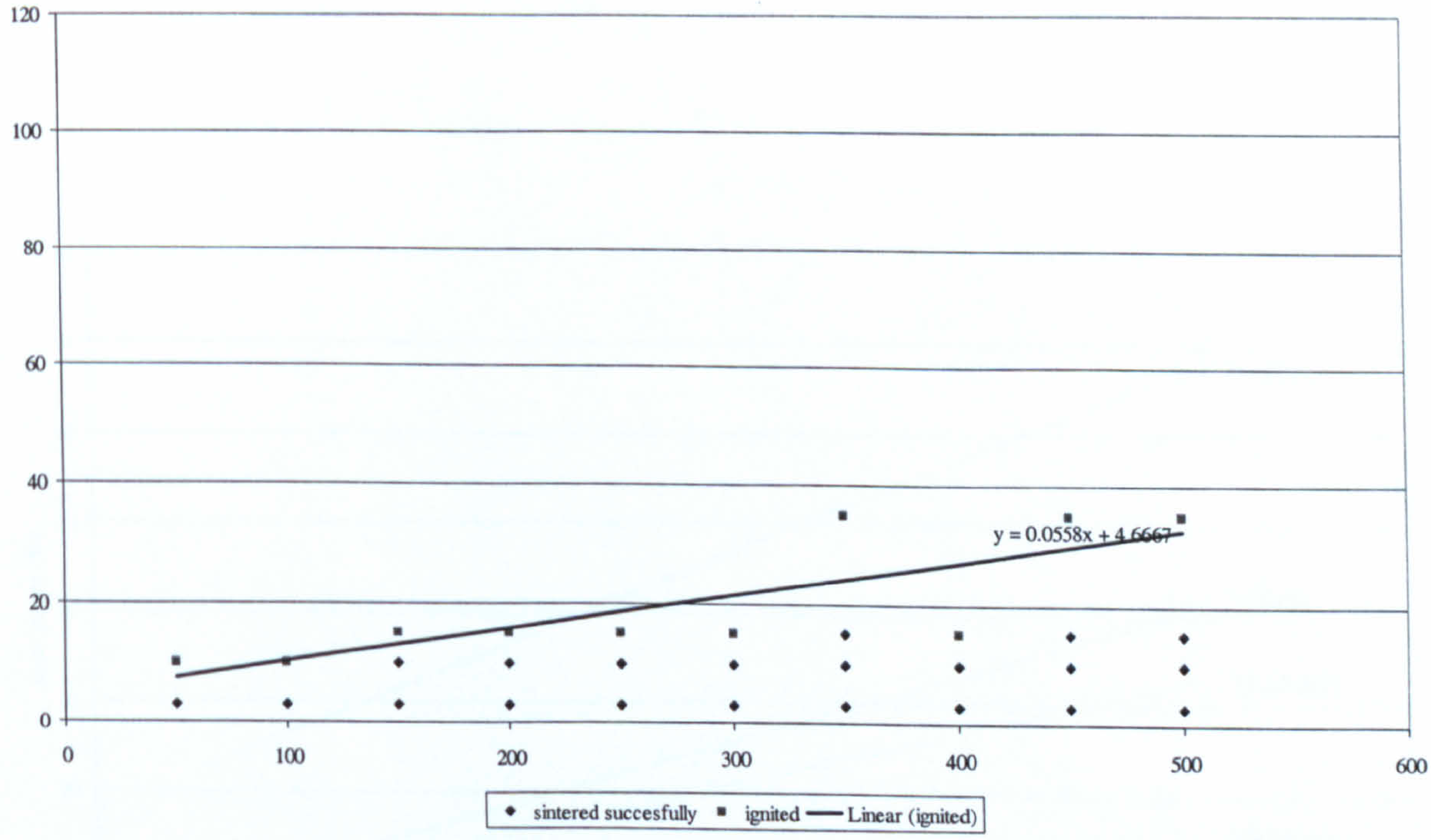

Figure 4.2.3 F: Process Map for LDIG105 (75% 45-90μm, 25% <45μm) with 5% binder

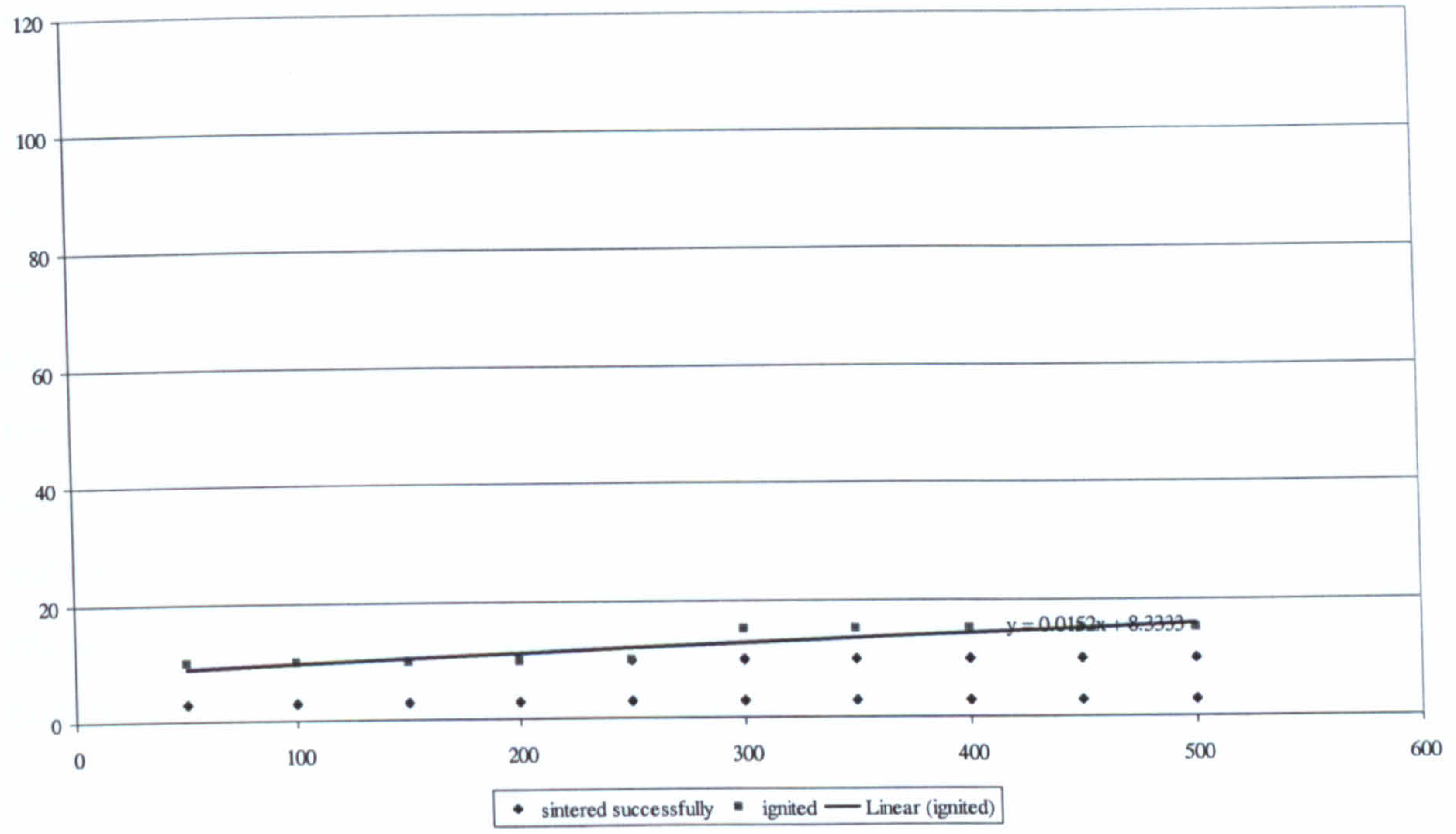

Figure 4.2.3 G: Process Map for LDIG105 (50% 45-90μm, 50% <45μm) with 5% binder

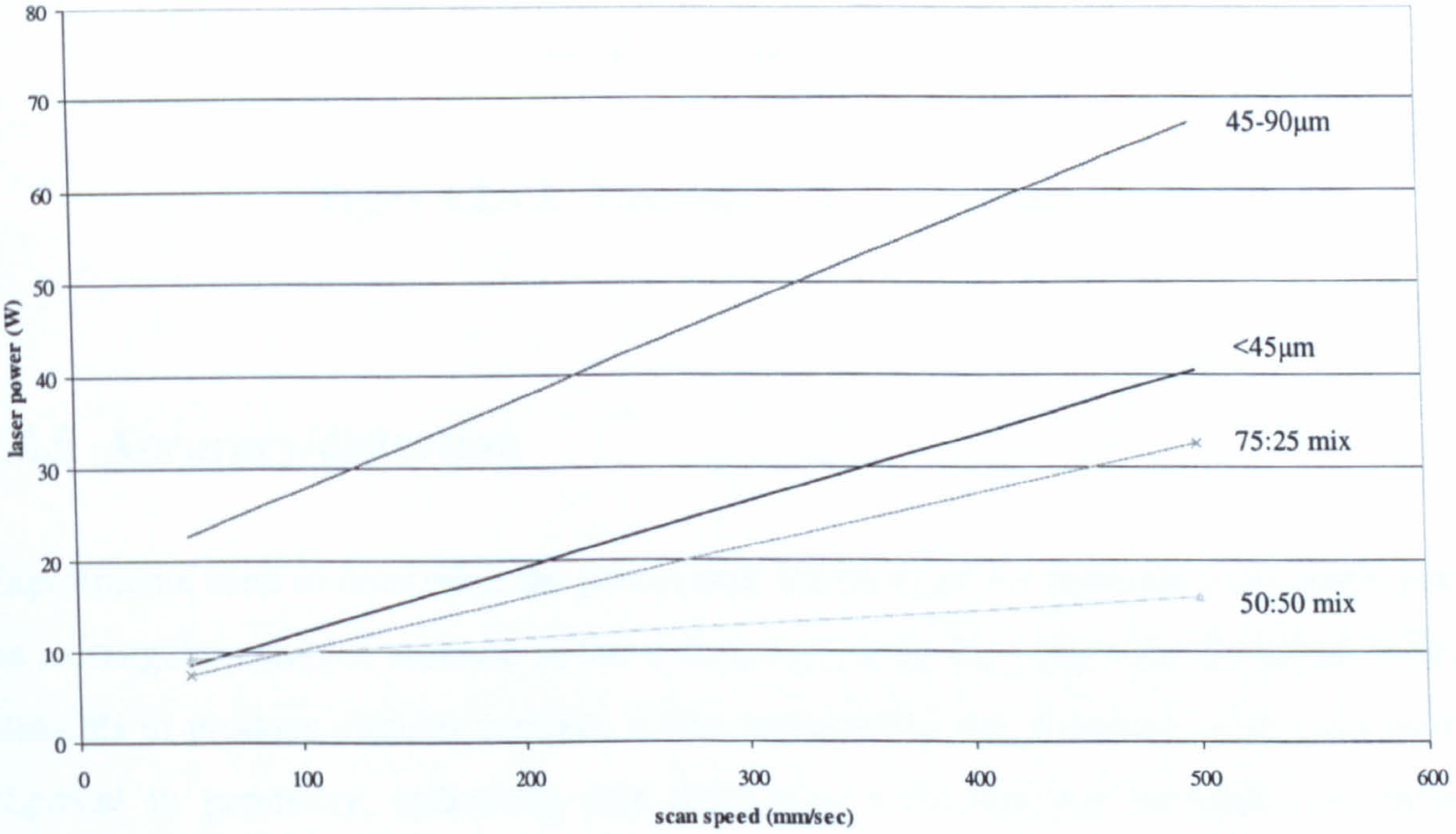

Figure 4.2.3 H: Maximum power:speed combinations for multisized glass particle sizes (5% binder)

4.2.4 Effect of scan overlap on the processing window

When scanning LDIG105 powder with glass particle size 45-90µm and a binder content of 5wt%, the degree of overlap between successively scanned lines was varied between ¼, ½ and ¾ of the laser beam diameter, which was 1.1mm – see Figure 4.2.4A. Whilst all three showed some signs of bonding, monolayers produced using a ½ or ¾ overlap had superior structural integrity to those with only a ¼ overlap. No obvious difference could be observed between those with a ½ overlap and those with ¾ overlap. As increasing the overlap increases the time needed to produce the part, a ½ overlap was chosen for future experiments as the production time could be reduced without compromising the structural integrity of the part.

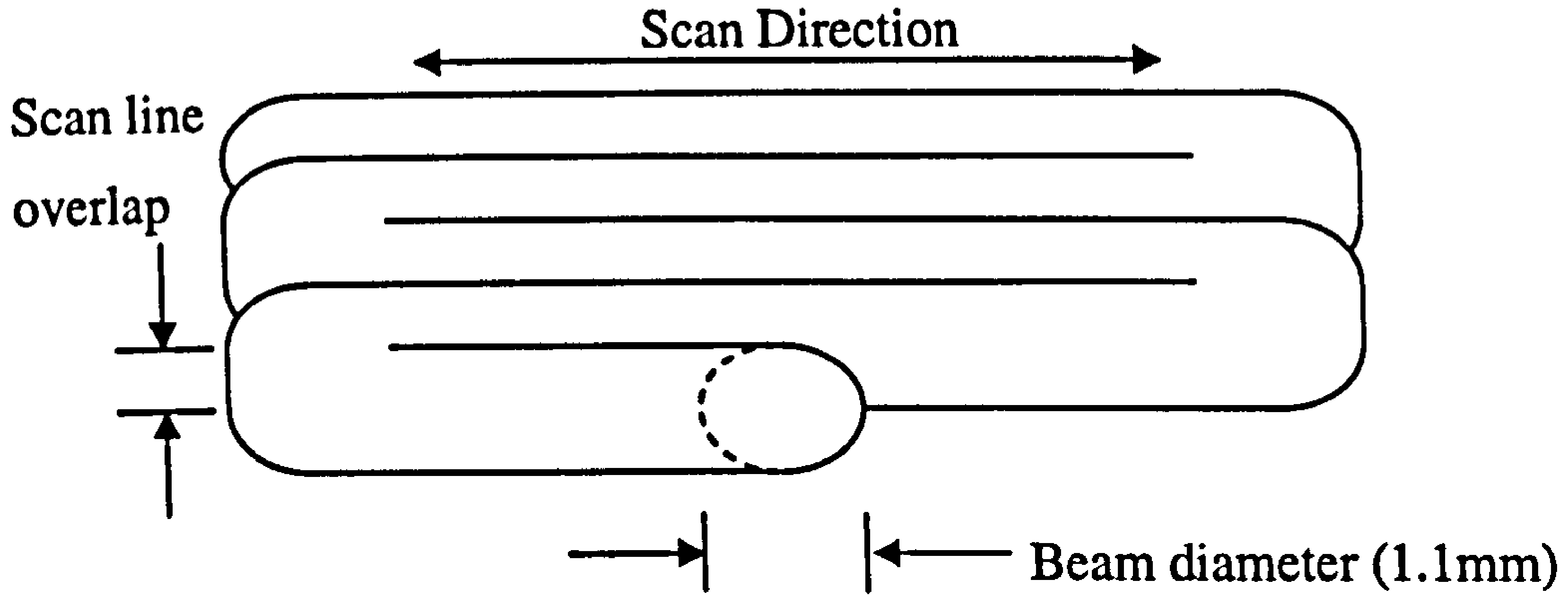

Figure 4.2.4 A: Schematic of scanning process

4.2.5 Accuracy/distortion

Experiments used to determine the processing windows of the material were performed on rectangular samples scanned in the x-direction along the long axis. However during attempts to produce circular samples it was noticed that the produced parts were more elipsical in geometry, indicating that there was a discrepancy between the vector lengths in the x and y direction – see Figure 4.2.5A. It is probable that this is as a result of different alignments / scaling factors in the x and y scanning mirrors.

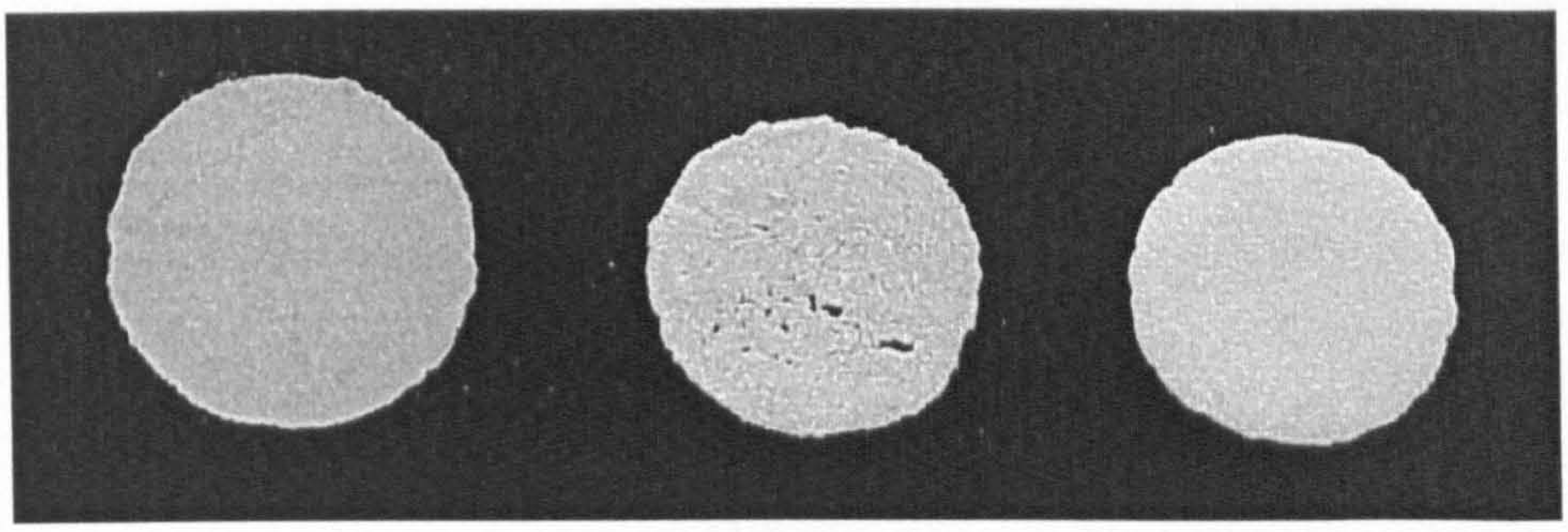

Figure 4.2.5 A: Circular monolayers demonstrating inaccuracies in x and y directions.

It was therefore considered necessary to determine the degree of inaccuracy of laser scanning in the x and y directions. This was established by producing rectangular monolayers of a range of intended lengths and widths, and measuring their actual dimensions following laser sintering. All these monolayers were produced from glass of particle size 45-90µm with 5% binder. As shown in Figure 4.2.5B, scanning in the x-direction was divided into x-lines and y-gaps, and scanning in the y-direction into y-lines and x-gaps.

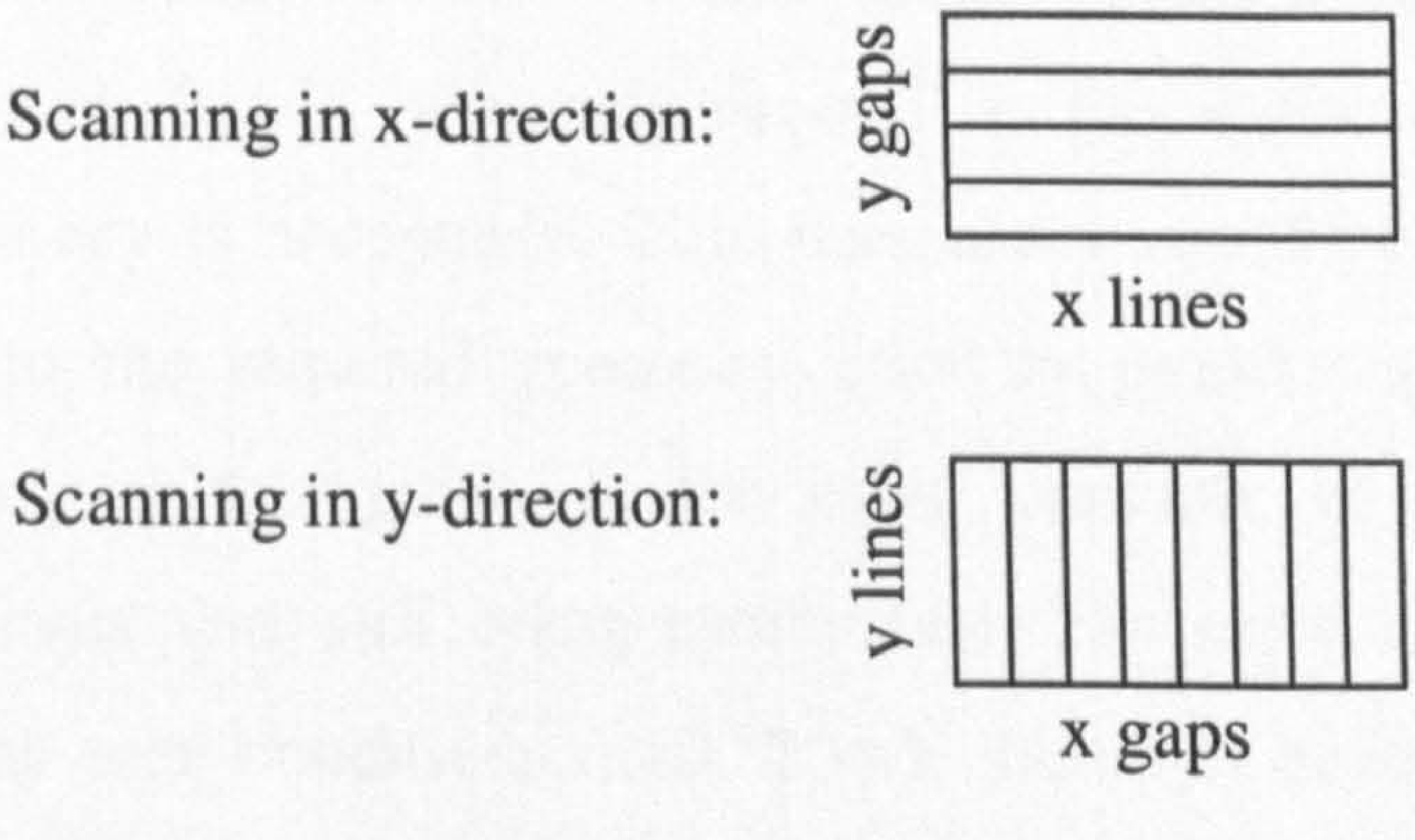

Figure 4.2.5 B: Illustration of nomenclature assigned to scanning parameter

These experiments were performed for a variety of laser powers and scan speeds, although the scan overlap was kept constant at ½ the beam diameter. A typical graph for one set of conditions (150mm/sec scan speed, 3W laser power) is shown in Figure 4.2.5C.

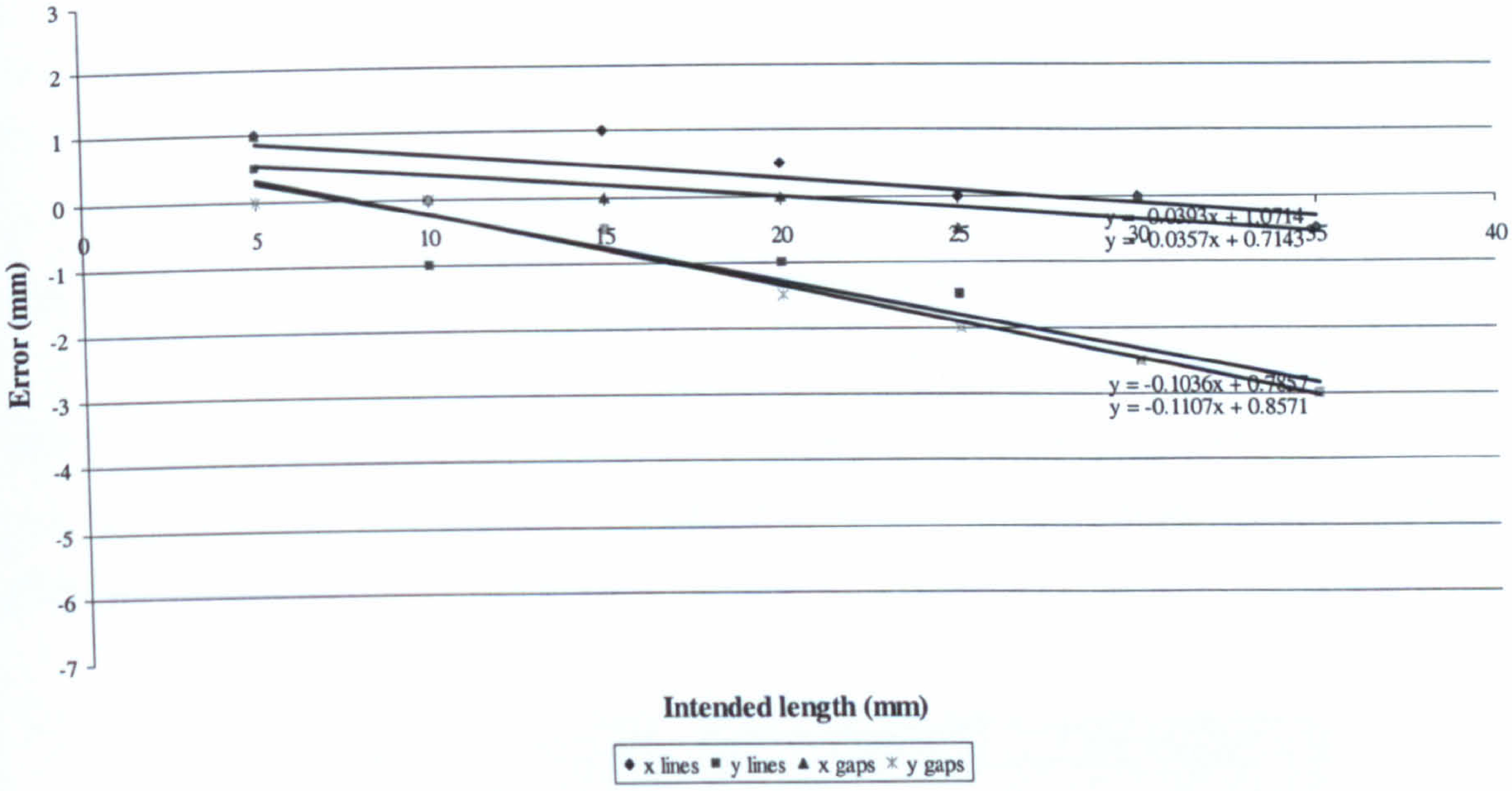

Figure 4.2.5 C: Absolute error versus intended length of single line scan.

The degree of error varied between +1 and -3mm. Values deviated up to 0.8mm from the trendlines fitted. It will obviously depend on the application as to whether this degree of inaccuracy is acceptable. This inaccuracy could be improved by applying scaling factors to the required geometry prior to processing. However it was not deemed necessary at this point, as the basic principle of using SLS to produce bioceramic implants was still being established. The error also varied by ±0.5mm, depending on the scan conditions used. It will therefore be necessary to determine a graph for each set of scan conditions used.

4.3 Production of multilayers

Multilayer components were attempted using the most successful parameters determined from the construction of the process maps. Instead of sintering the powder in a tray, the powder was placed on the build platform, which was lowered following the scanning of each layer. The overlap between the layers was varied between 0.25, 0.5, and 0.75 mm, with new layers of powder being spread by hand.

Multilayers were produced successfully with all three degrees of overlap. However some problems were occasionally experienced with ¾ mm overlap as spreading the fresh layer of powder would disturb the previously sintered layer due to the large interparticle friction of the powder dragging the layer underneath from its original position. When using a ¼ mm overlap, delamination of the layers occasionally occurred on handling of the samples due to insufficient bonding. The optimum overlap appeared to be ½mm overlap as it allowed better sintering between layers than the ¼mm overlap, whilst not exhibiting the problems in spreading fresh layers of powder, as experienced with ¾mm overlap. Multilayer components produced with a ½mm overlap can be seen in Figure 4.3A.

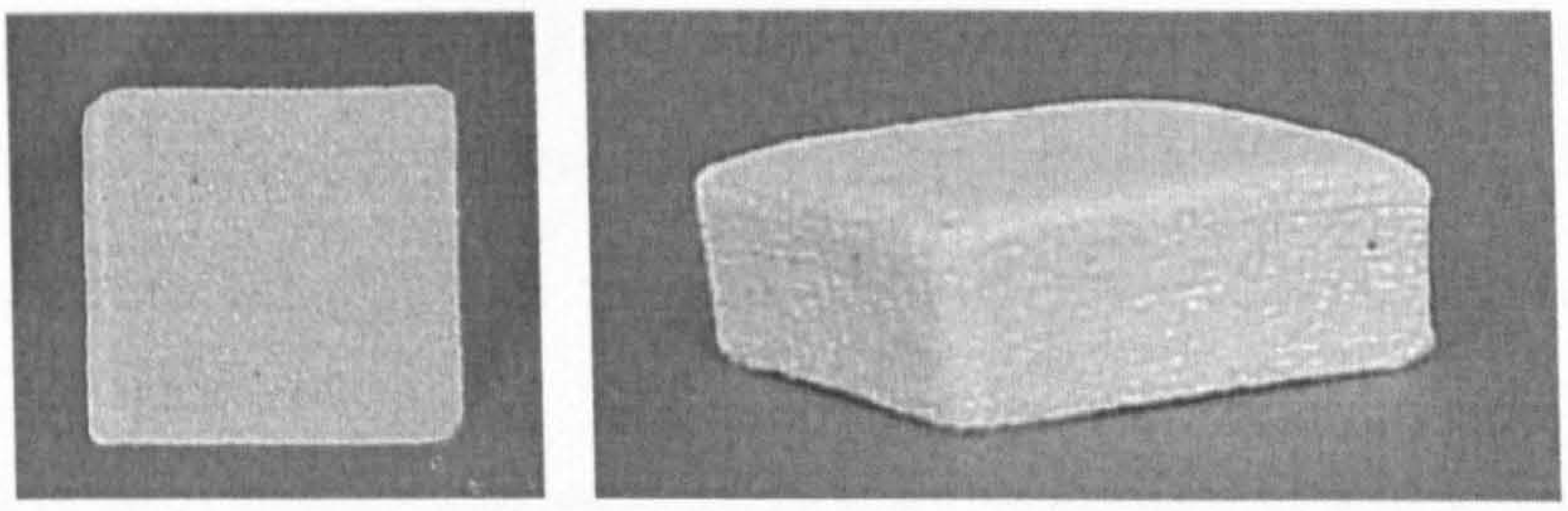

Figure 4.3 A: Multilayers 45-90µm produced using an indirect SLS procedure (30 layers)

4.4 Characterisation of parts produced by SLS

To understand the mechanisms that may be occurring during the laser sintering process, the multilayer parts produced by indirect laser sintering were examined by differential thermal analysis (DTA) and scanning electron microscopy (SEM). DTA was used to evaluate whether any crystal phases were being evolved during the process, and the temperatures at which this was occurring. SEM allowed the morphology of the sintered parts to be examined in order to gain an understanding of how the powder particles were being held together. The mechanical properties were not assessed at this point as although the produced parts had sufficient structural integrity for normal handling, they were not strong enough for any differences in strength to be noticed from altering any of the processing parameters or powder properties. Therefore this was carried out after the parts had been post-processed, and thus the results from this will be described in the following chapter.

4.4.1 Differential Thermal Analysis (DTA)

DTA was performed using a Stanton Redcroft DTA 674 with a standard heating rate of 10°C/min across the desired temperature range. The material to be tested was ground to a fine powder using a pestle and mortar. Two platimum-rhodium alloy crucibles were used, one containing 0.15 ± 0.001g of the test material and the other containing 0.15 ± 0.001g of powdered alumina as a reference. The samples were heated to 400°C at 15°C/min, then up to 1200°C at a reduced heating rate of 10°C/min, by which point it was assumed that all significant thermal events had occurred. Data was logged between 400 and 1200°C.

DTA traces of LDIG105 before and after laser sintering can be seen in Figure 4.4.1A. After the glass transition region, Tg, there are two sharp peaks, Tp1 and Tp2, as a result of exothermic events which, as explained in Chapter 2.5.1 correspond to crystallisation events and the evolution of two distinct crystal phases. The apatite phase is evolved at Tp1 and the mullite phase at Tp2. There is little difference between the two traces indicating that the material is not crystallising during the SLS process, as if crystallisation was occurring there would be a reduction in the height of these peaks.

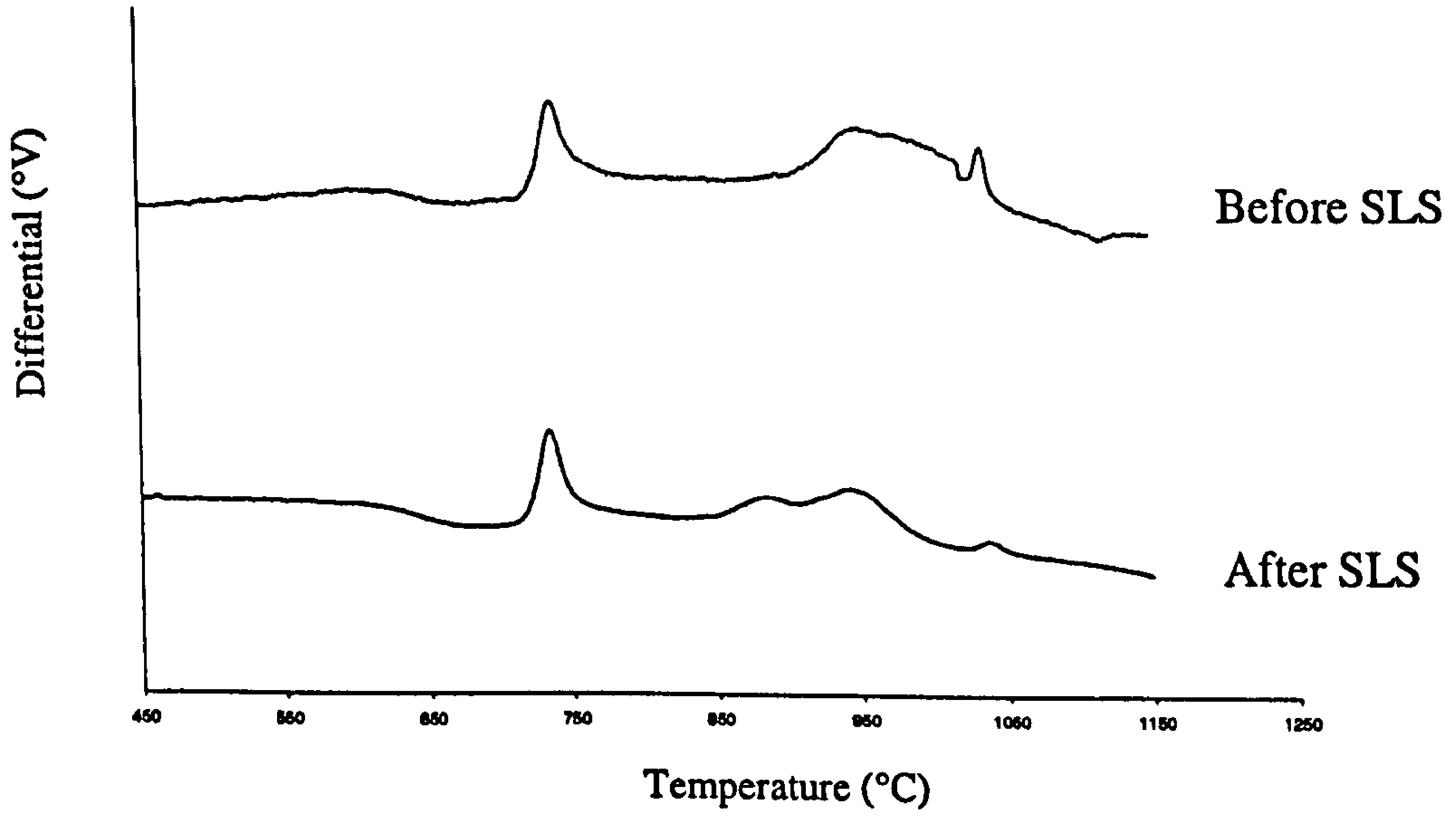

Figure 4.4.1 A: DTA traces of LDIG105 + 5% binder before and after laser sintering.

This is desirable as it means that the material is in effect a blank canvas, allowing greater control over the crystallisation of the desired phases during subsequent heat-treatment. Theoretically a time-temperature profile can be selected that would allow the maximum number of nuclei to be formed, producing a fine grained microstructure with maximum mechanical strength.

4.4.2 Scanning Electron Microscopy (SEM)

SEM was carried out on a Joel scanning electron microscope (JSM 35C) in the School of Process and Environmental Materials Engineering at the University of Leeds. The surface morphology of LDIG105 laser sintered samples produced from glass of particle size range 45-90µm with 5% acrylic binder, scanned using a laser power of 12W, 150mm/sec scan speed, beam overlap of ½ its diameter, and layer thickness of 0.25mm can be seen in Figure 4.4.2A.

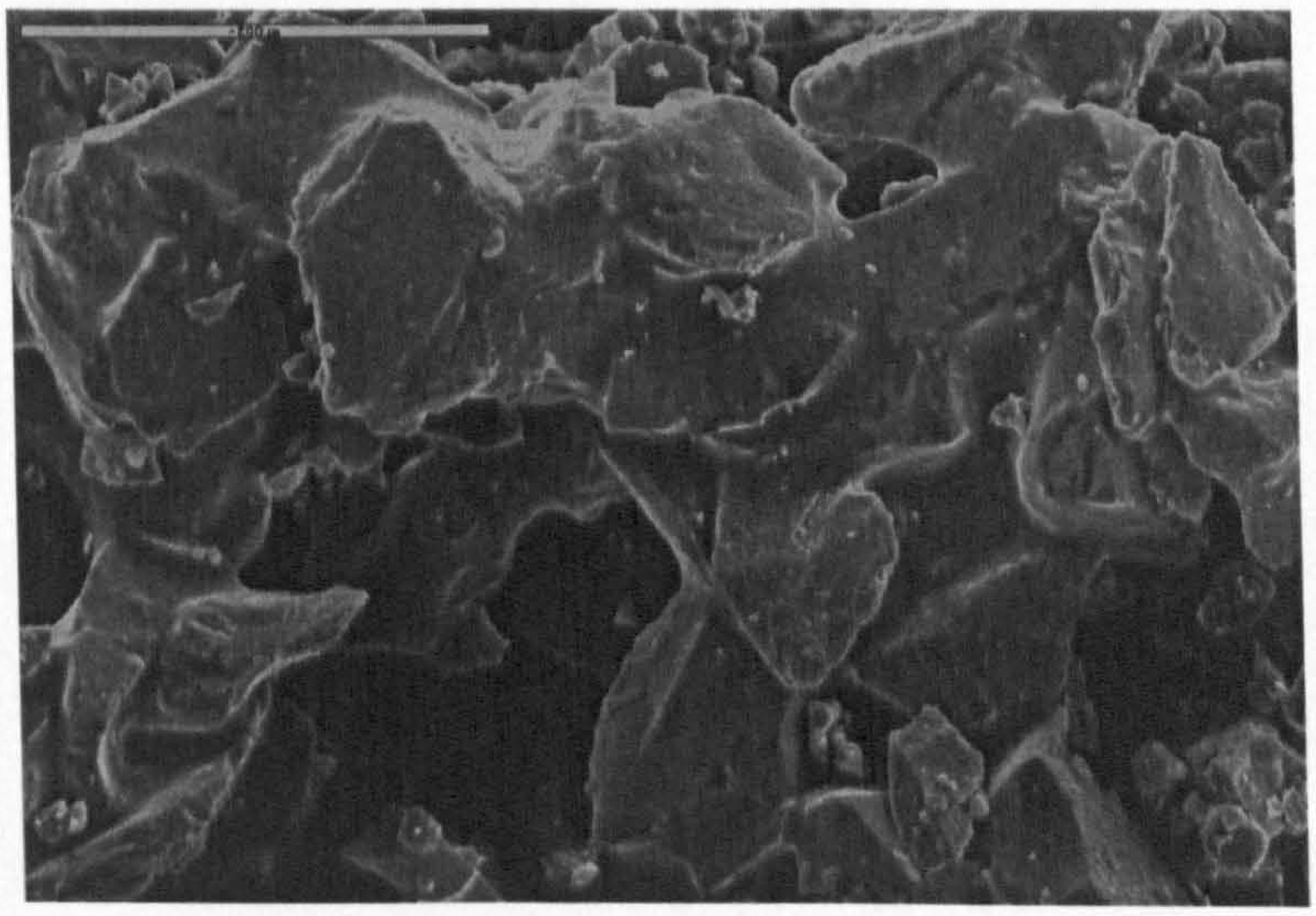

Figure 4.4.2 A: SEM micrograph of LDIG105 (glass particle size 45-90µm and binder content of 5wt%) following laser sintering. x500 (dimension bar = 200µm)

The particles are highly irregular in shape which is to be expected as the powder is produced by grinding the glass which is a very brittle material. It may also be seen that, despite sieving the powder to a 45-90µm particle size range, there are many particles less than 45µm in diameter. This may be due to particle agglomeration that was not entirely eliminated during the sieving process.

From this micrograph it can be seen that the individual glass particles are being held together by the polymer binder. It appears that during the laser sintering process, as a result of its high infrared absorption and low melting point, the polymer is melted and thereby connects the glass particles together without appreciably melting them, because of their high melting point. The material after selective laser sintering can therefore be confirmed as being in the 'green state', with the polymer looking to wet the particles well.

Chapter 5 Post-Processing

Following production of green parts by selective laser sintering, post-processing was carried out in order to remove the acrylic binder which may otherwise have rendered the parts unsuitable for biological use, and fully crystallise the material, evolving the apatite and mullite phases to improve both biological and mechanical properties. It is partly the presence of apatite crystals in a material that causes it to exhibit bioactive behaviour [Vogel, 1985], and the mullite phase not only improves the mechanical strength of the material [Clifford and Hill, 1996], but it also locks in the aluminium in the system which might otherwise induce cytotoxic behaviour [Hatton, 2000]. The evolution of these crystal phases was achieved using a number of different time-temperature profiles which are described in section 5.1. The post-processed samples were examined by DTA and XRD, the results of which are discussed in sections 5.2 and 5.3 respectively. Section 5.4 looks at the effect using a mixed glass particle size has on the density and flexural strength of the post-processed parts, and section 5.5 at the amount of shrinkage that occurs as a result of the binder removal and sintering of the glass-ceramic particles. Infiltration of the parts was then carried out in an attempt to further increase the part strength and is described in section 5.6. The choice of materials for infiltration was previously explained in section 3.3.

5.1 Heating regime - Time-temperature profiles.

Multilayer parts were produced by selective laser sintering LDIG105 glass powder with a particle size range of 45-90μm and 5wt% acrylic binder using a laser power of 12W, 150mm/sec scan speed, beam overlap of ½ its diameter, and layer thickness of 0.25mm, as described in Chapter 4.

In determining the post-processing conditions, the first concern was ensuring that the temperature used would be sufficient to burn off the acrylic binder. A DTA run of the laser sintered material was performed and is presented in Figure 5.1A. This showed the binder to burn off over the range of 240-300°C, indicated by a dip in the DTA curve caused by an endothermic event. As the intention was to heat the parts to 1200°C in order to evolve the crystalline phases, it was concluded that binder burnout would happen as part of the heat treatment cycle without needing any special consideration.

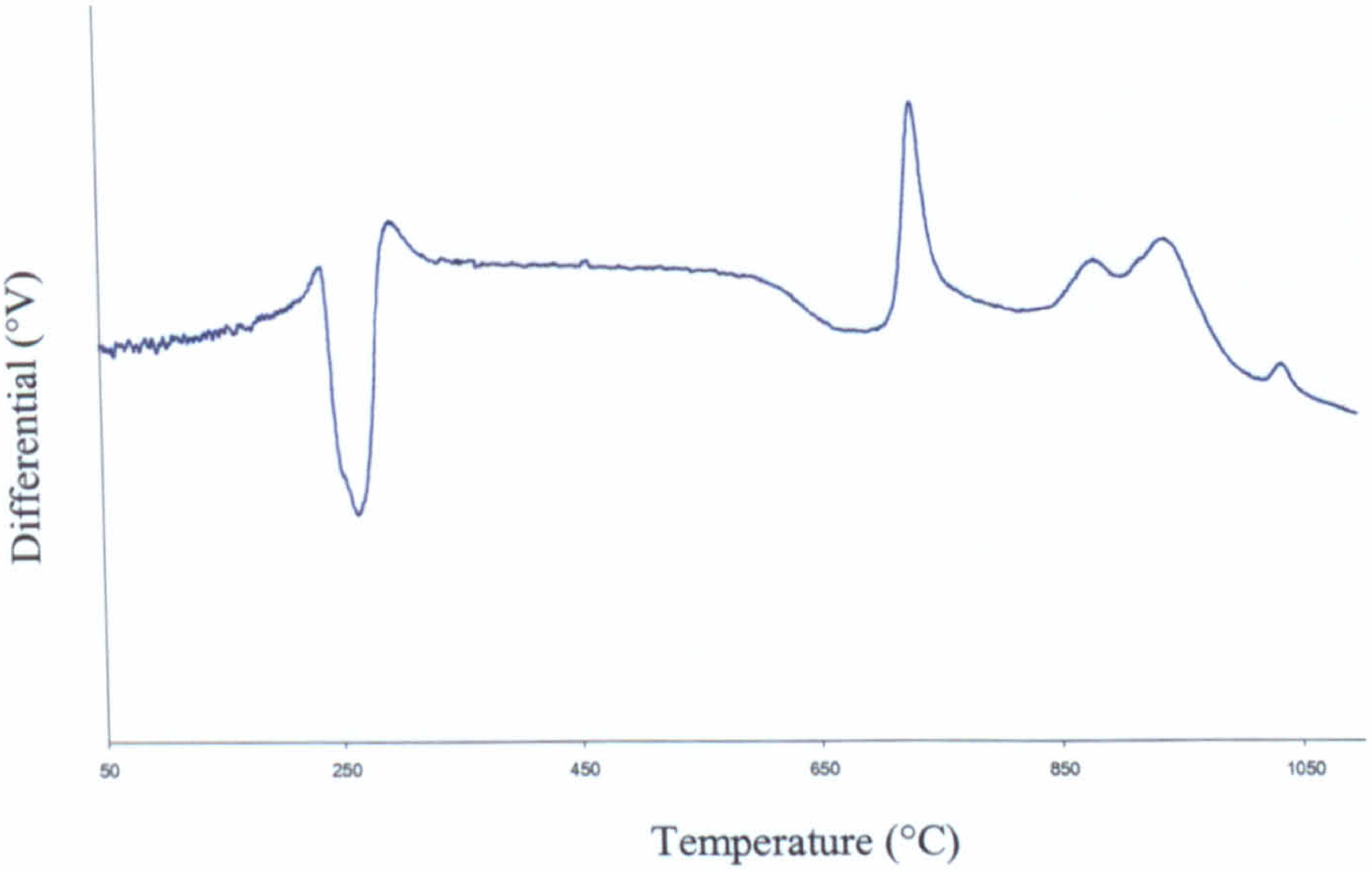

Figure 5.1A: DTA trace of LDIG105 and 5% binder

The parts produced by SLS were initially post-processed in a programmable furnace (UAF 15/5 furnace, Lenton Thermal Designs Ltd; Eurotherm 818 controller/programmer, Worthing, UK) using a conventional two tier heating regime, which involved heating the part to 730°C at 10°C/min, holding at this temperature for an hour, heating up to 1200°C at the same rate, holding for a further hour, then allowing the part to cool down to room temperature at the natural rate of the furnace. This post-processing route will be known forthwith as ppB. A dwelling temperature of 730°C was chosen for these samples as it was above the glass transition temperature, but below the onset of crystallisation, as determined from the DTA trace. This two tier heating regime is usually considered the idealised heat treatment schedule for glass-ceramics since the two holds correspond to nucleation and crystallisation stages, thus allowing more controlled crystallisation to occur by allowing the formation of a high density of nuclei before raising the temperature to allow crystal growth. Heating to

1200°C was considered sufficient to encourage the evolution of the crystal phases while also increasing the potential for liquid phase sintering.

The success of the heat treatment was assessed by measuring the flexural strength of the samples via a three-point bend test. For this, twenty rectangular specimens 20 x 3 x 3mm were fabricated via SLS and post-processed using the heat treatment described above. Twenty identical specimens that had only been laser sintered and had not been subject to any post-processing were also measured for comparative purposes. The tests were performed on a UKAS accredited Lloyd Instrument LR10K UTM equipped with a calibrated 500N (±5%) load cell fitted with a three-point flexural jig with roller supports and a span of 15mm – see Figure 5.1B. All specimens were tested at room temperature at a cross-head speed of 2mm/sec until fracture occurred. Fracture was typified by a sharp decrease in the force applied to the test specimen and the peak force was used for strength calculations. Strengths were determined from three-point flexural bend analysis using the normal expression,

$$\sigma = \frac{3}{2}\frac{Pl}{ab^2}$$

where P is the applied load, l the span of the two-point support, a the specimen width, and b the specimen thickness.

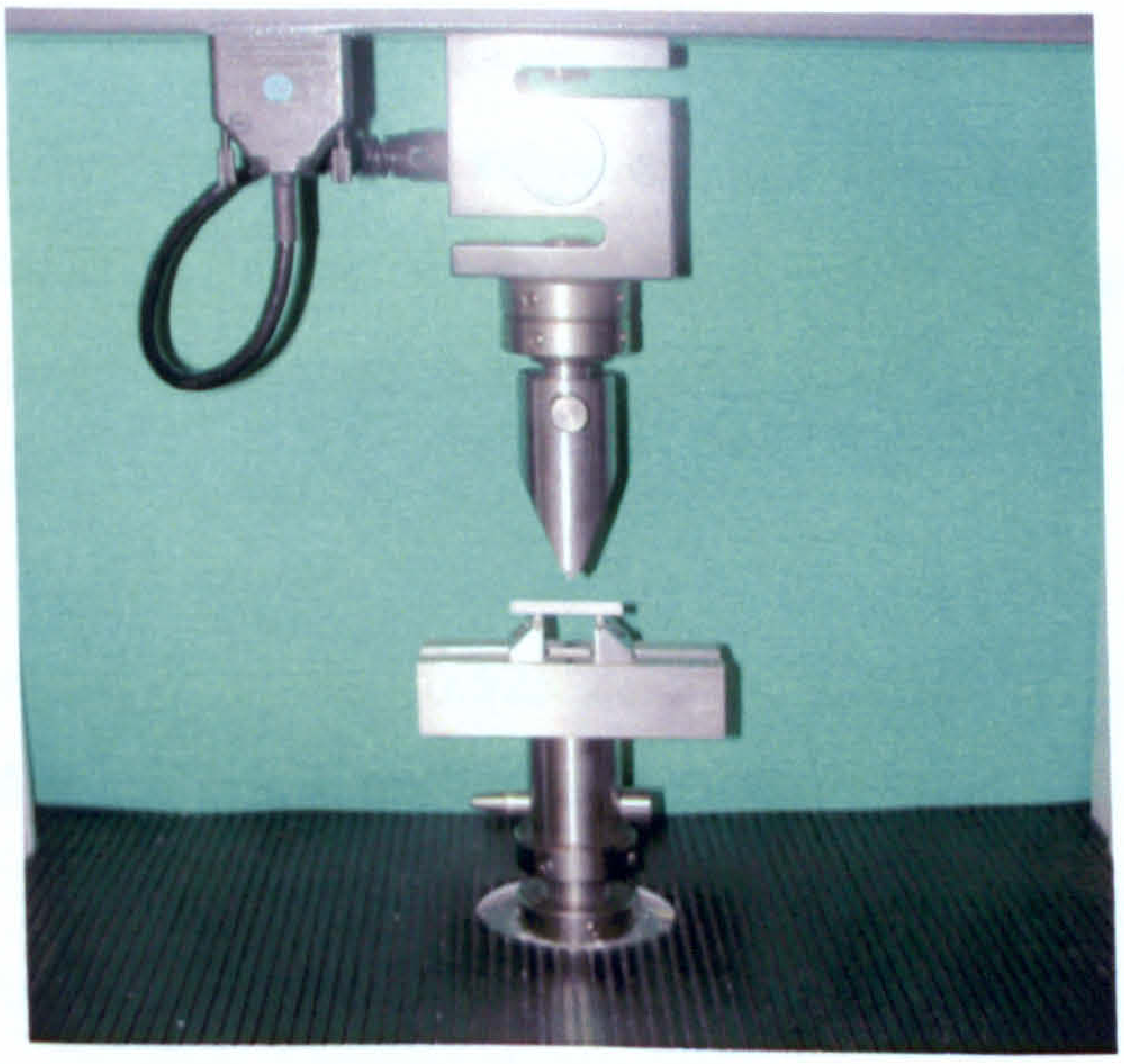

Figure 5.1 A: Photograph of the three-point bend test rig with LDIG105 beam

Prior to post-processing, the samples had a mean flexural strength of 2.43MPa (±0.12MPa). However following heat-treatment the strength of the parts reduced to a mean strength of only 1.02 MPa (±0.43MPa). This may be due to the large amount of crystal nuclei that are allowed to form as a result of the nucleation hold. It is thought that the amorphous glassy phase provides the material for liquid phase sintering as the temperature is raised. By holding at the nucleation temperature, there is more time for the development of crystal phases and a corresponding reduction in the quantity of the glassy phase needed for liquid phase sintering

It was thus concluded that a heating regime should be used that allowed more time for liquid phase sintering to occur before the crystal phases were formed. A second set of samples were therefore heated from room temperature to 1200°C at 10°C/min, without a nucleation hold in the middle, held at this temperature for an hour, then allowed to cool back down to room temperature at the natural rate of the furnace – known from this point as ppC. The flexural strength of these samples were also measured, and found to have a mean value of 1.51MPa (±0.36MPa), a slight improvement, but still below that measured directly after SLS.

Therefore in an attempt to further increase the likelihood of liquid phase sintering occurring before crystallisation another set of samples (ppD) were placed directly in a furnace pre-heated to 1200°C, held at this temperature for an hour, then allowed to cool at furnace rate. A final set (ppE) were subjected to a two cycle heat treatment where they were post-processed in the same way as the previous set, ppD, but after cooling back down to room temperature were heated again following ppC, in an attempt to fully crystallise the material.

Higher flexural strengths of around 6.52MPa (±0.38MPa) were achieved when the samples were placed in a furnace pre-heated to 1200°C (as in profile ppD), while no significant increase was achieved by taking the samples through both cycles, as in profile E – 6.85 MPa (±0.88MPa). When the material is placed directly into a very hot furnace there appears to be enough time for liquid phase sintering to occur before crystallisation, hence stronger parts can be produced. No significant increase in strength was achieved by taking the samples through both cycles, probably because by this point all the liquid phase sintering and crystallisation that was going to happen had already occurred.

The different time-temperature profiles used in this work are summarised in Figure 5.1C, and a graph comparing their variation in flexural bend strength can be found in Figure 5.1D .

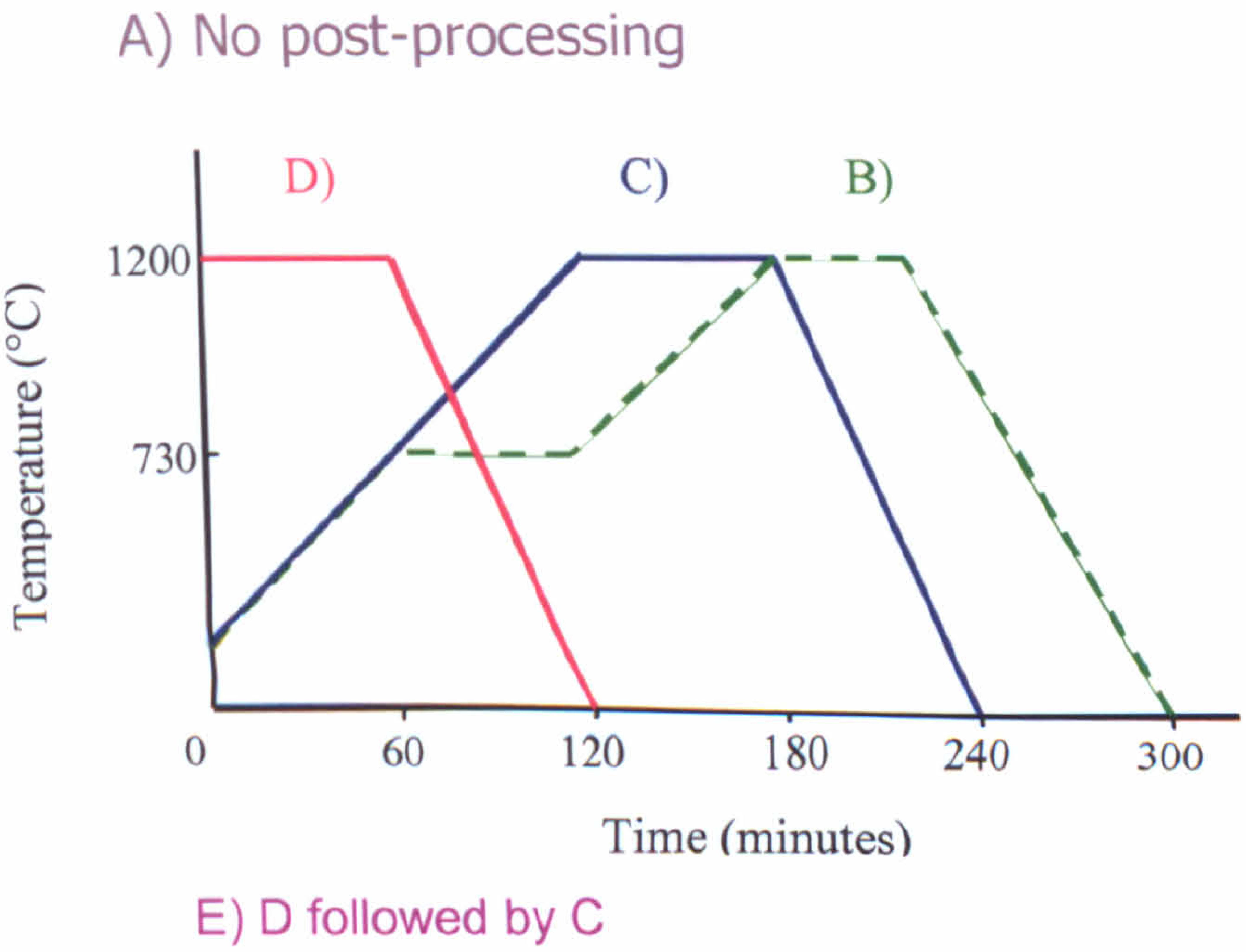

Figure 5.1 C: Graph illustrating the different time-temperature profiles used to post-process the laser sintered parts.

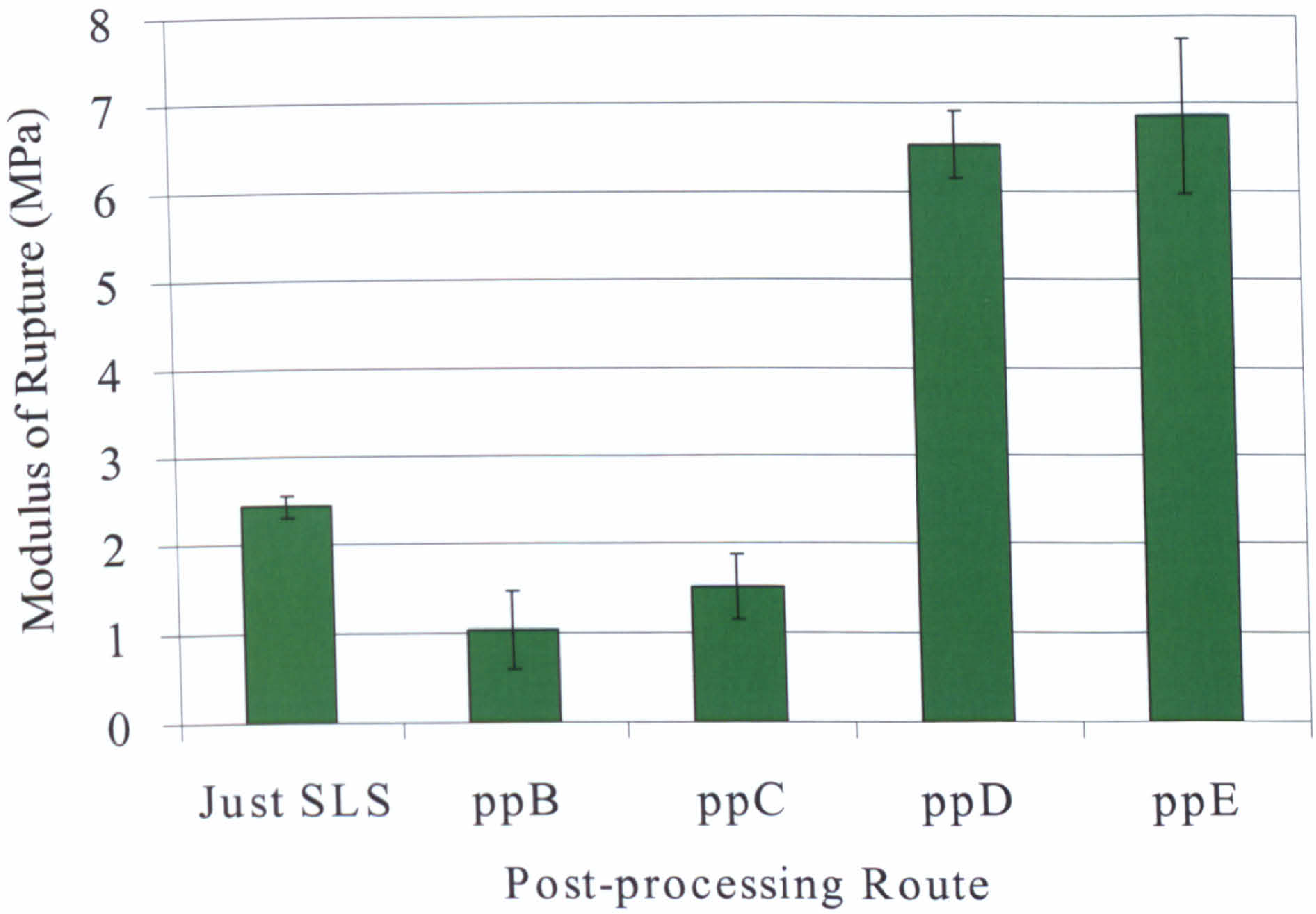

Figure 5.1 B: Graph demonstrating the effect of different heating regimes on the flexural strength of produced parts.

In an attempt to further understand this variation in strength, the microstructures of the parts subjected to different post-processing routes were examined by SEM, and the resulting micrographs are shown in Figure 5.1D. Before post-processing and after post-processing using ppC, the glass particles are angular in shape, but when the parts are placed in a furnace preheated to 1200°C, they become more spherical. This appears to confirm the theory that more liquid phase sintering is occurring in these samples, as by becoming more spherical they are reducing the total particle surface area, and thus the surface energy, which, as was seen in Chapter 2.4.1, is part of the driving force for the sintering process.

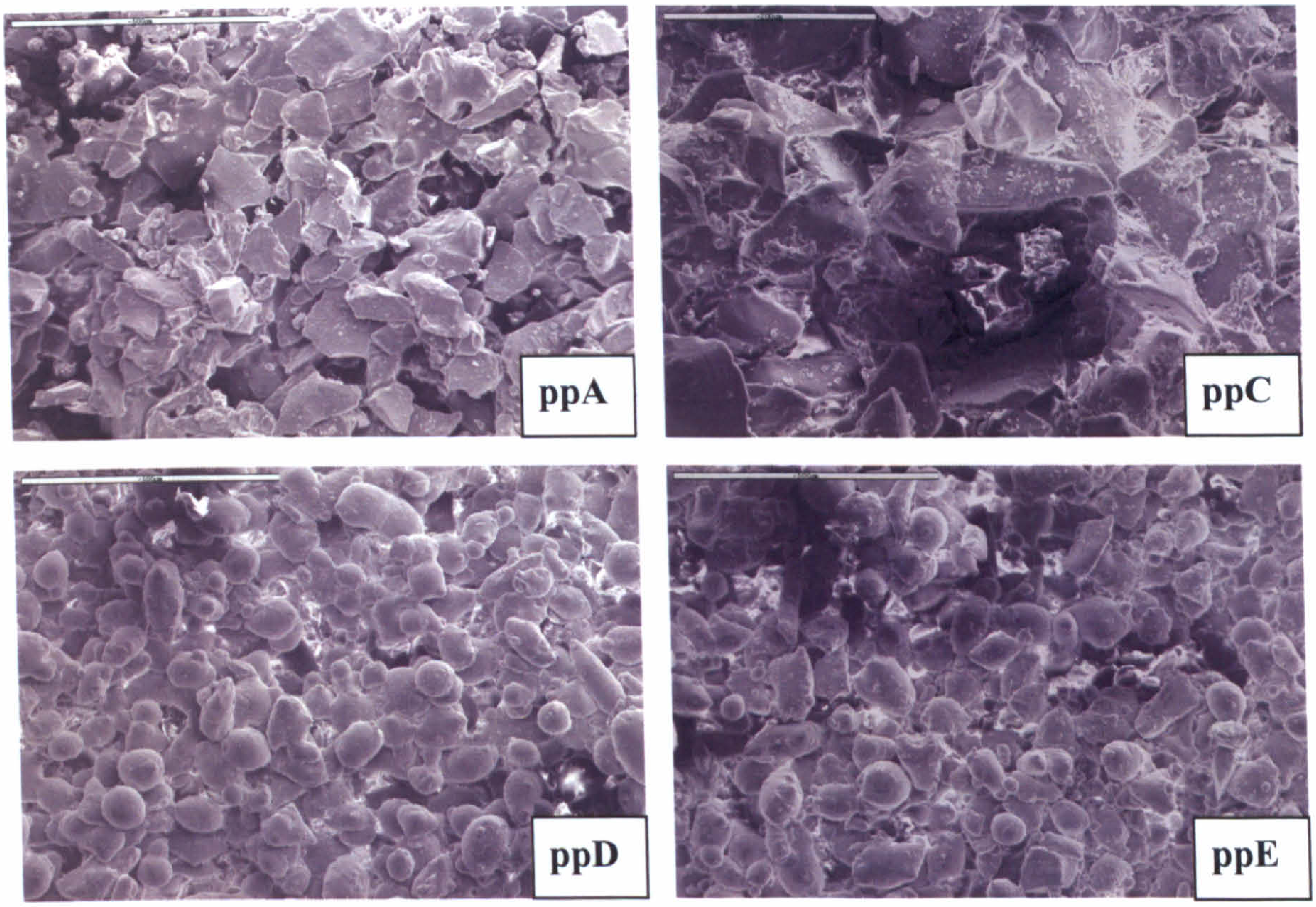

Figure 5.1 C: SEM micrographs of laser sintered LDIG105, post-processed using different time-temperature profiles. Scale bars on ppA, D and E are 500μm, and 200μm on ppC.

Higher magnification images of the necks forming between the particles can be seen in Figures 5.1E. The particles in samples produced using ppC are held together by very fine/weak necks, whereas those produced using ppD are much more substantial, explaining their superior strength.

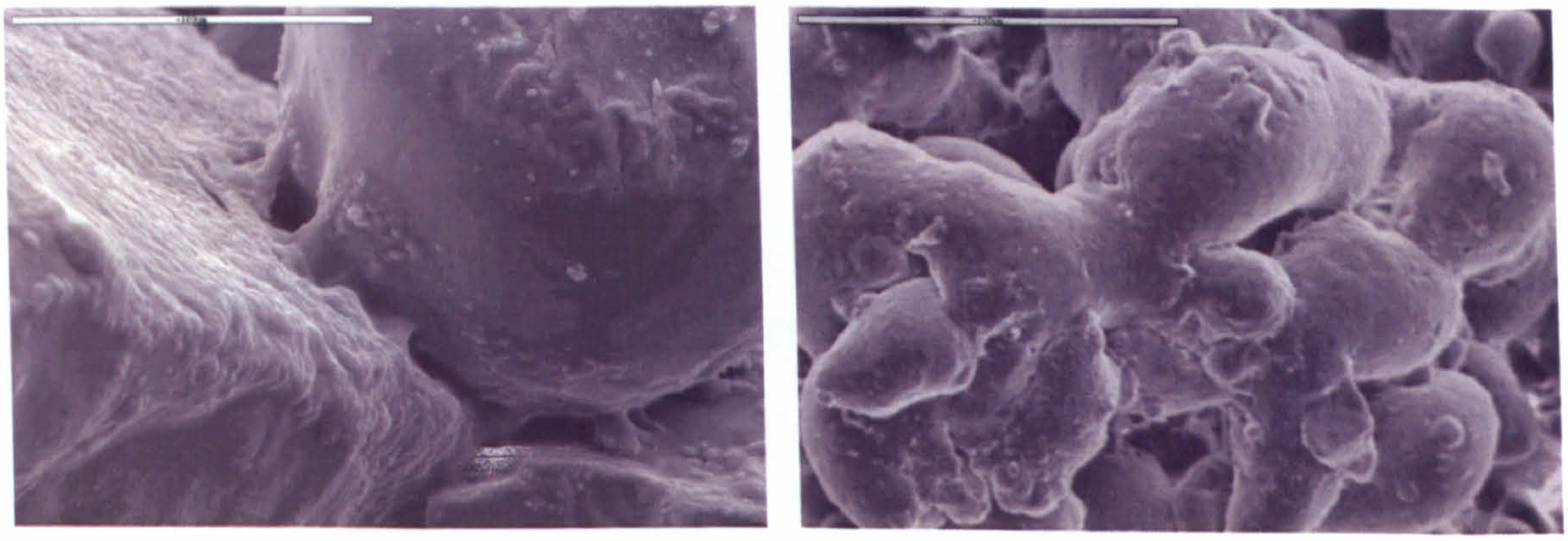

Figure 5.1 D: SEM micrographs of necks formed between particles post-processed using ppC (left) and ppD (right). Scale bar is 100μm on ppC and 200μm on ppD.

As there was little difference in the flexural strength of parts produced by ppD and ppE, it was decided for further experiments to post-process the laser sintered parts using ppD which only involves one heat treatment cycle, and thus reduces the furnace time.

5.2 Differential Thermal Analysis (DTA)

To understand the events occurring during the post-processing process, the material was analysed by DTA. A typical trace of the glass-ceramic after post-processing with ppD can be seen in Figure 5.2A. This can be compared to the trace obtained after laser sintering which was shown in Figure 4.4.1A. It can be seen that the peaks representing the crystal phases have been completely removed. This indicates that crystallisation of apatite, mullite, and anorthite must have occurred during the post-processing process.

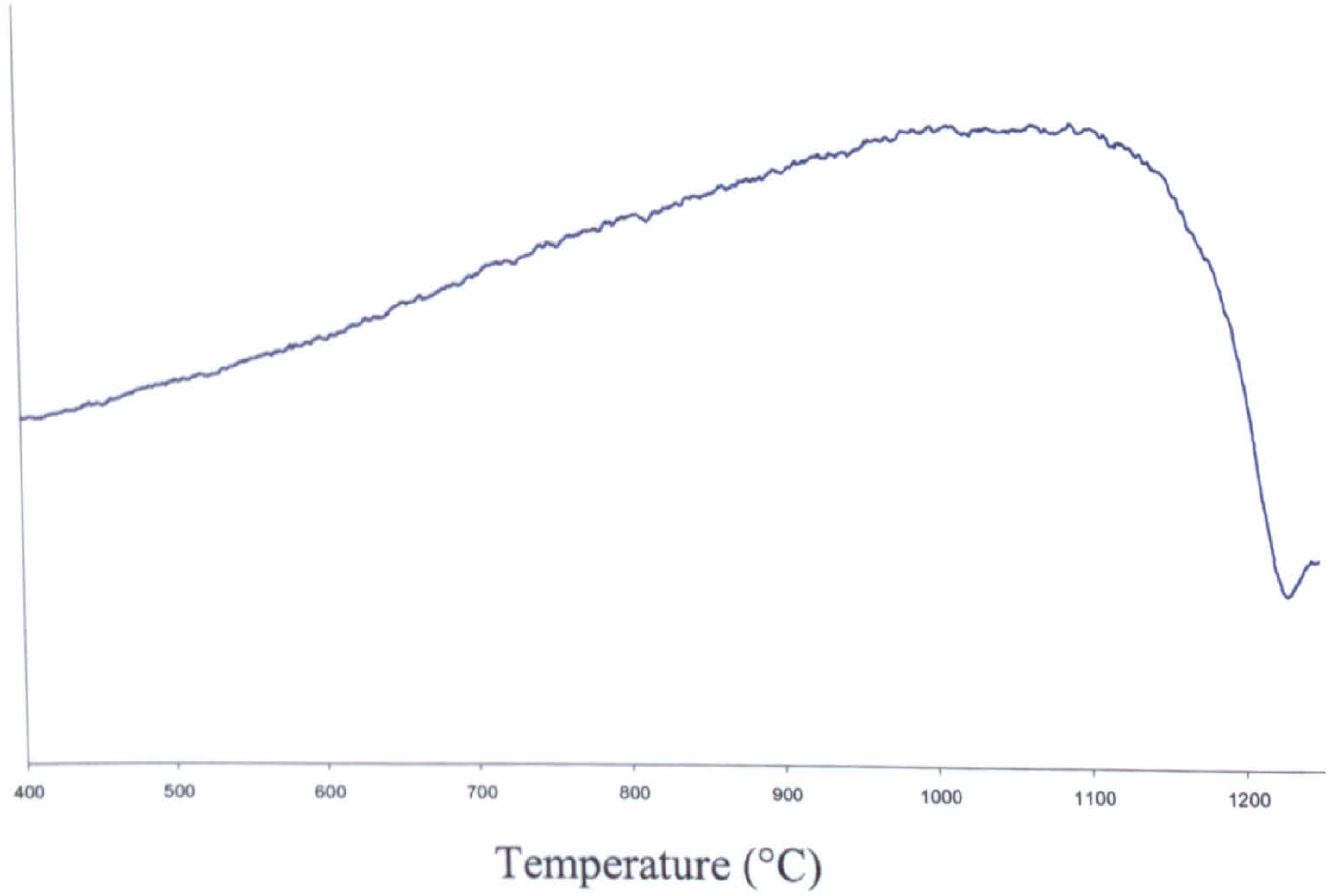

Figure 5.2 A: DTA trace of LDIG105 + 5% binder after post-processing using ppD.

5.3 X-Ray Diffraction (XRD)

The formation of the crystalline phases was evaluated by X-ray powder diffraction (XRD). XRD measurements were performed on crushed samples of laser-sintered LDIG105 (5wt% binder, 45-90µm particle size, 150mm/sec scan speed, 12W laser power, ½ beam overlap, 0.25mm layer thickness) using a Philips Analytical PW3050 with a copper anode, which gives an x-ray wavelength of 1.5406Å. The starting and the finishing angles were 10° and 50° respectively, the step size was 0.02° and the interval count time was between 6 and 12 seconds. Standards from the International Centre for Diffraction Data (ICDD) were used to characterise the resulting crystallographic spectra, with peaks of crystalline phases being identified using crystallographic Search-Match V2 software. The standards describe known crystal phases in terms of d-spacing or angle (2□) and relative intensity of the principle diffraction lines.

An XRD trace for LDIG105, post-processed using time-temperature profile D, can be seen in Figure 5.3A. Three phases have been identified – fluorapatite ($Ca_5(PO_4)_3(F)$ – ICDD#15-876), mullite ($Al_6Si_2 0_{13}$ – ICDD#15-776), and anorthite ($CaAl_2Si_2O_8$ - ICDD#12-301).

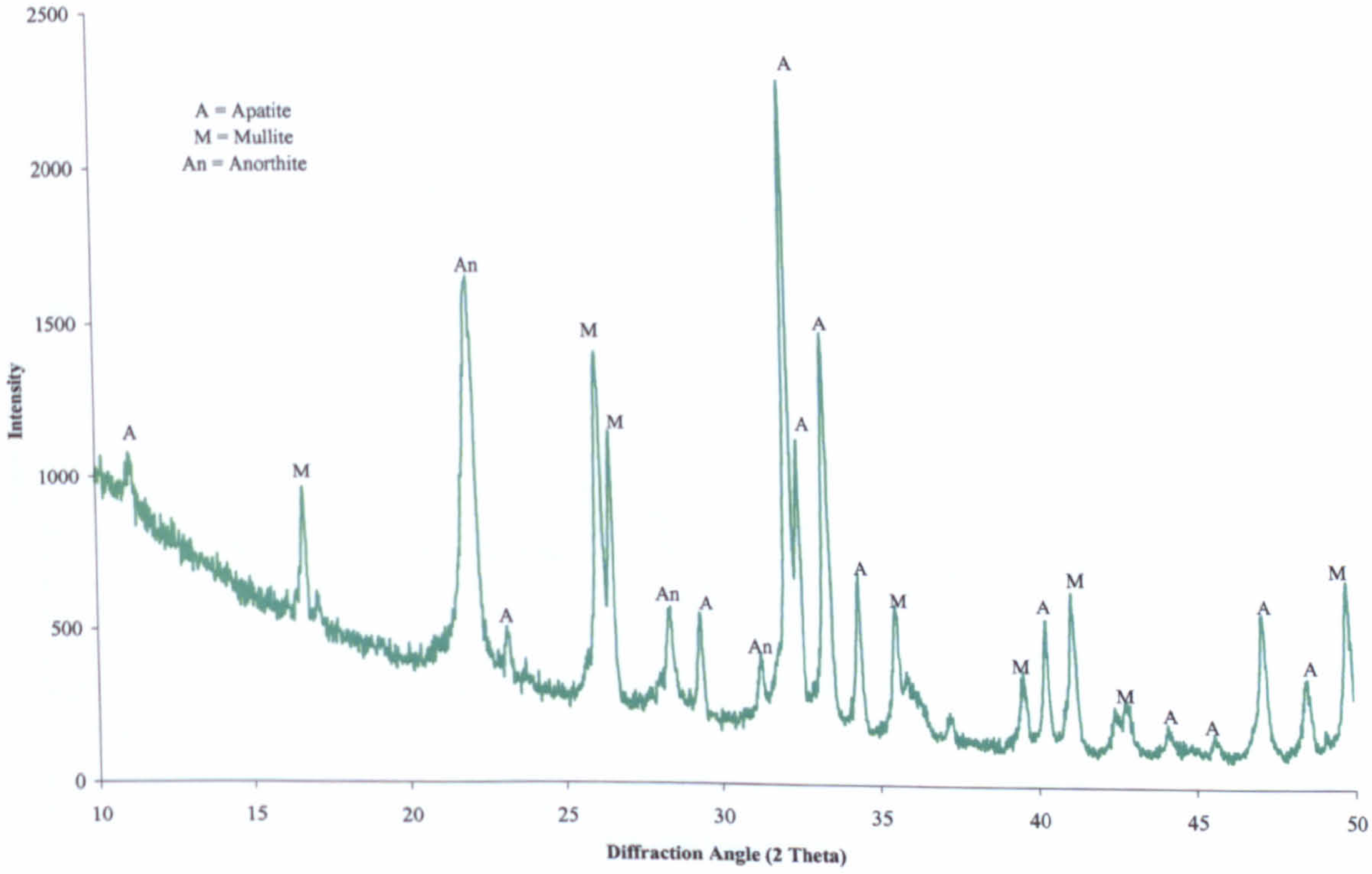

Figure 5.3A: XRD trace for LDIG105 post-processed using time-temperature profile D

Although LDIG105 is termed an apatite-mullite glass-ceramic, and apatite and mullite are the primary phases, it is polycrystalline in nature and thus there are also sometimes other minor phases present. In this case there appears to be anorthite, which has been found in other similar compositions. The powdered test material has a large surface area, and as this phase is known to occur via surface crystallisation [Clifford and Hill, 1996], its presence is not totally unexpected.

Figure 5.3B presents XRD traces for the different post-processing routes used, where it may be observed that all traces are very similar, having peak profiles that are almost identical. However, whilst the positions of the peaks in each trace correlate very well, the magnitudes of the peaks do not, with the material post-processed using ppD or ppE producing larger peaks than the materials post-processed using ppB or ppC. This does not necessarily indicate a variation in crystallinity, as it is the magnitude of the peaks within a given trace relative to one another, rather than between traces that is most significant. In all traces the relative heights of the peaks appear to be identical. However a decrease in the height of the emission spectra can sometimes correspond to a reduction in the amount of crystalline material, and given that ppB and ppC exhibited a significantly reduced strength compared to ppD and ppE, it is possible that this may also be the case.

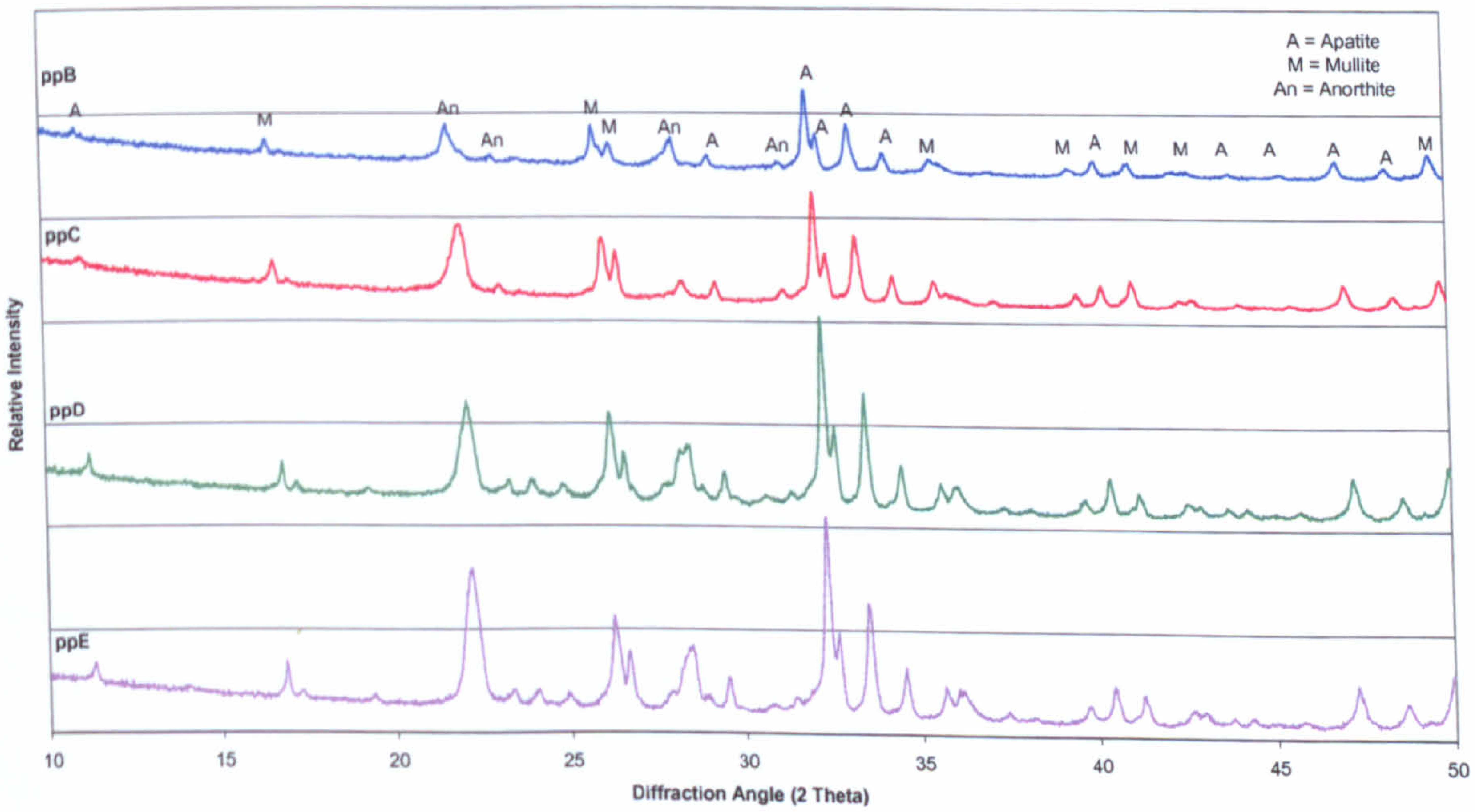

Figure 5.3B: Comparison of XRD traces for LDIG105 parts post-processed with varying heating regimes.

5.4 Mixed Particle Size

Parts made from a mixture of particle sizes as described in Chapter 4 were examined by SEM and tested for their flexural strength. Figure 5.4A presents a micrograph of a sample made from a mixture of 45-90μm and <45μm glass particles in a ratio of 75:25. The interconnections between the particles appear to be greater in number and considerably more substantial, and the number and size of the pores appear to have decreased.

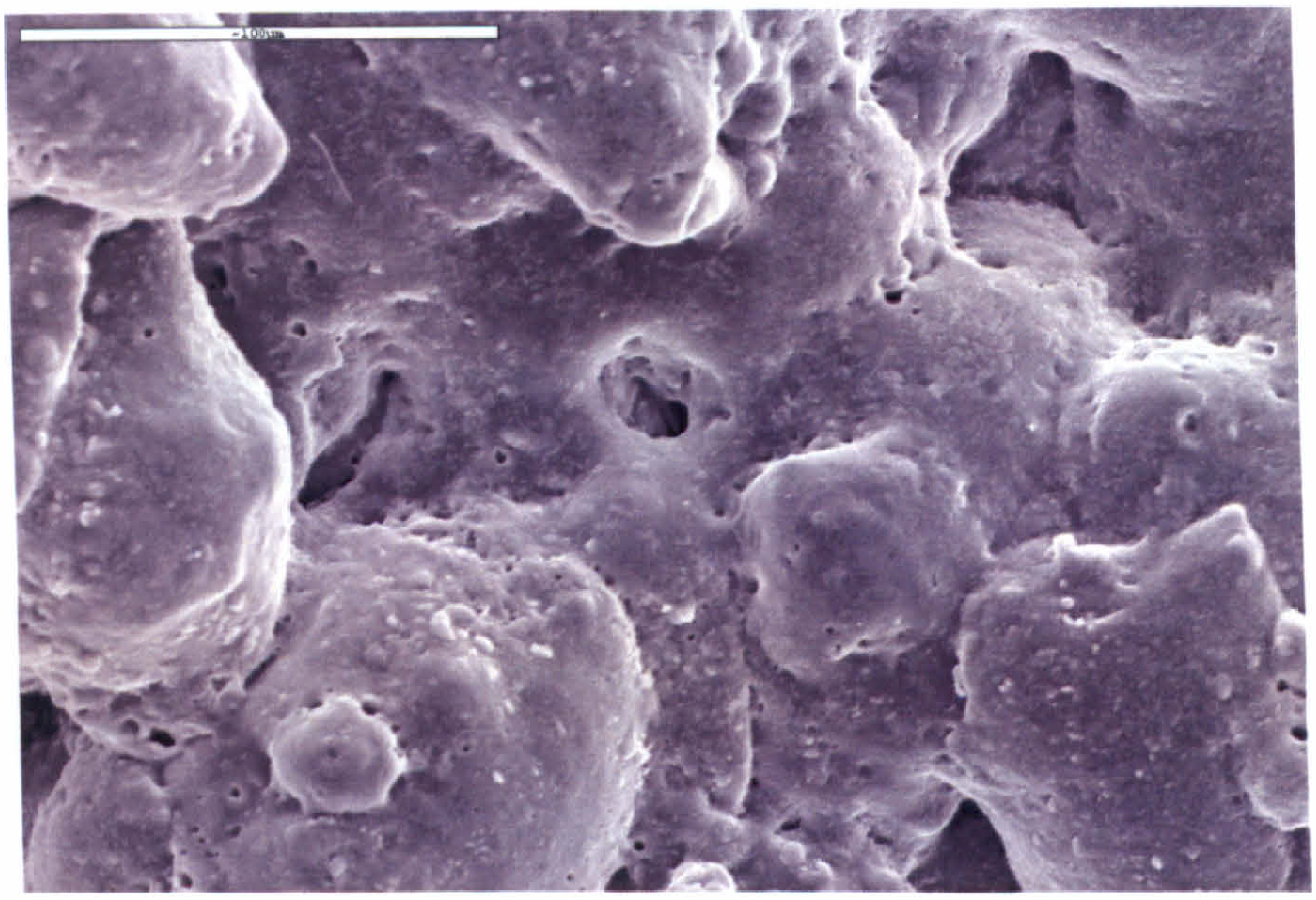

Figure 5.4A: SEM micrograph of LDIG105 produced from a 75:25 ratio of 45-90μm to <45μm glass particles

A comparison of the flexural strengths of the parts produced from blends of different glass particle sizes, post-processed using ppD, is shown in Figure 5.4B. The mean flexural strength of the 75% 45-90μm : 25% <45μm blend is 14.90MPa ±2.23MPa, whereas for 50% 45-90μm : 50% <45μm it is 16.22MPa ±3.42MPa. Both samples had a relative density of 1.03, compared to 1.009 using 100% 45-90μm particles. This suggests that improved particle packing of the powder bed is increasing the final density of the parts, resulting in greater strength. The density of these parts are still a considerable way off that of fully dense LDIG105, which has been shown to have a relative density of 2.9 [Lorrison, 2003], suggesting therefore that there is still the opportunity to improve this further. However with only a small difference between the flexural strength of the two mixed particle size samples, it is unlikely that improving packing further is going to result in any significantly large increase in strength. It is also important to retain a porous structure for the ingrowth of bone.

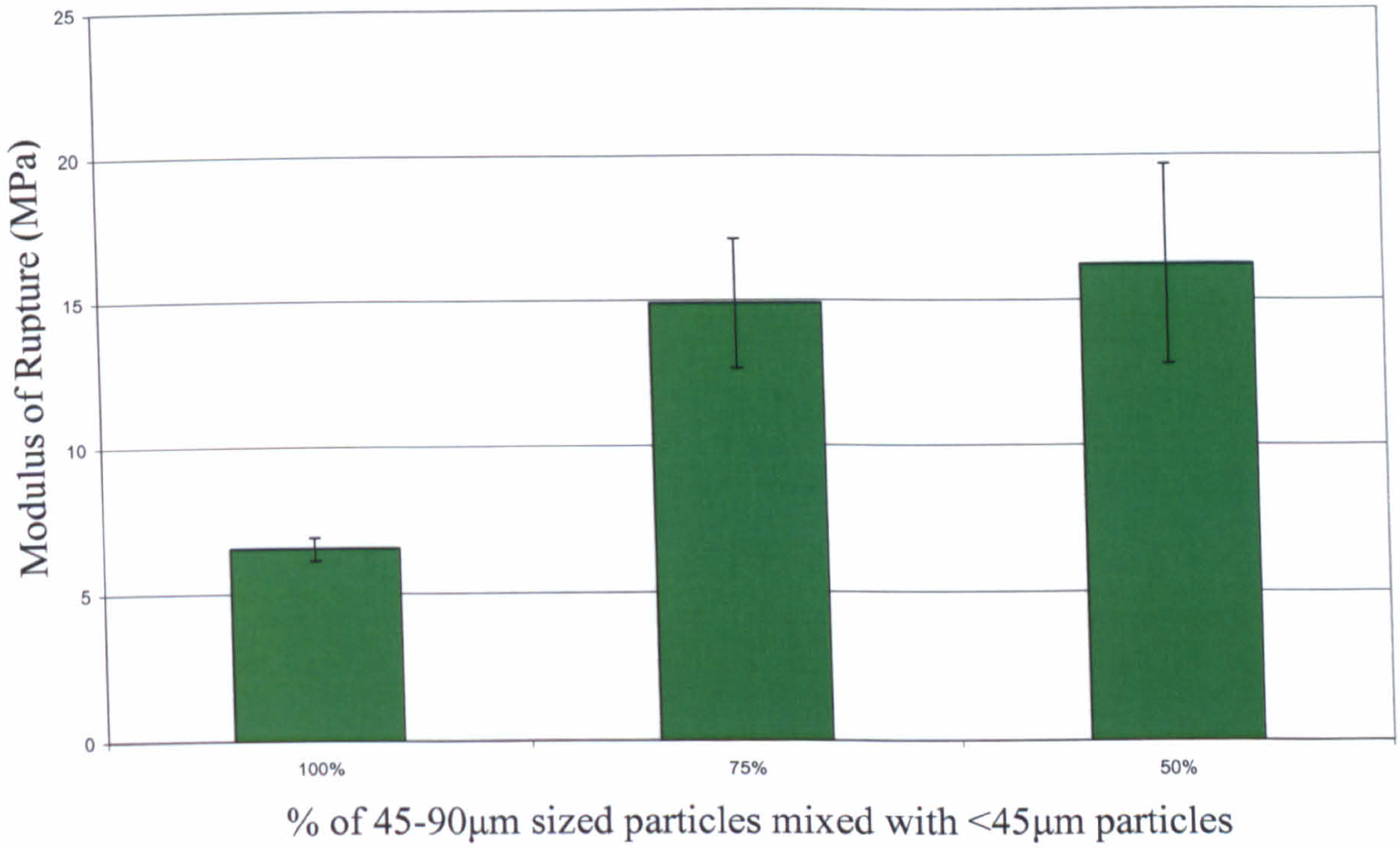

Figure 5.4B: Graph illustrating the effect of mixing different glass particle fractions on the flexural strength of post-processed parts.

5.5 Determination of shrinkage and distortion prior and post SLS

Sample dimensions were recorded after post-processing in order to evaluate shrinkage resulting from binder removal and sintering. The samples produced in Chapter 4.2.5 that were used to determine shrinkage during the laser sintering process, were post-processed using time-temperature profile D, after which their dimensions were measured. The results can be seen in Figures 5.5A and B. Figure 5.5A illustrates shrinkage from the actual dimensions of the sample prior to post-processing, whereas Figure 5.5B demonstrates this as an error from the dimensions originally desired. The data in Figure 5.5A was not consistent enough for a trendline to be fitted. However when plotted against the intended length before SLS, a more linear trend was observed.

It may therefore be possible to compensate for this when producing parts by scaling the original CAD model to take this data into account.

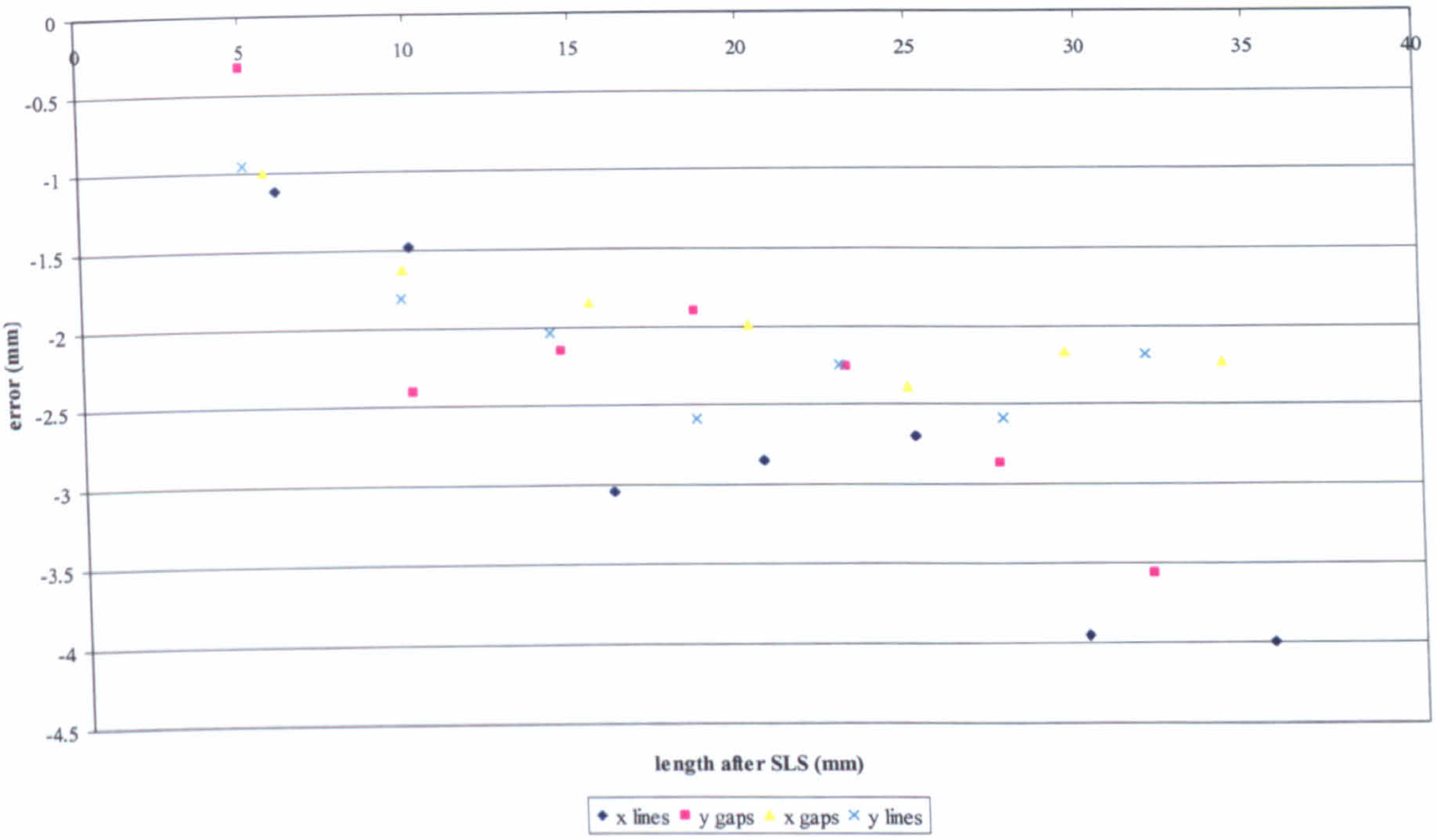

Figure 5.5: Shrinkage from actual values following post-processing

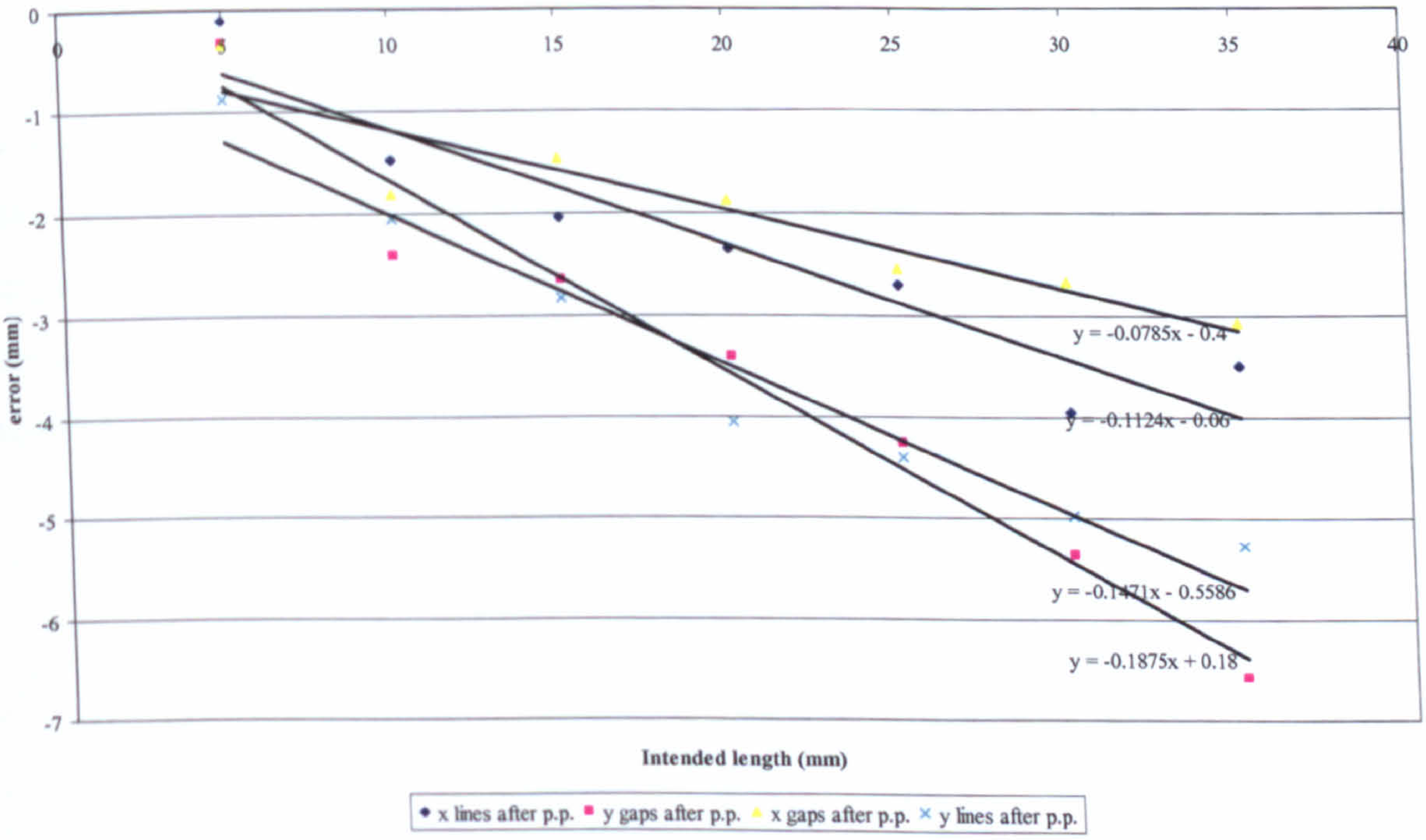

Figure5.5B: Shrinkage from desired dimensions following post-processing

5.6 Infiltration

It became clear that modifications in the time-temperature profile alone were not going to significantly increase the mechanical strength enough for the parts to be used in load bearing situations. It was therefore decided to try to improve strength by infiltrating the brown parts with a second material. Two materials were used – a resorbable phosphate glass and polymethylmethacrylate (PMMA). The reasons for selecting these materials and the methods used to produce them were described in Chapter 3.3. The parts used for this experiment were produced by selective laser sintering using a laser power of 100W, scan speed of 250mm/sec., scan line overlap of ½ the beam diameter, and layer overlap of 0.25mm. The samples were post-processed using post-processing route D (see section 5.2). Samples produced using only 45-90μm powder were used, as this represented a baseline for the processing technique. Initial experiments were performed on samples with dimensions of 20 x 20 x 5mm, with beams of 20 x 3 x 3mm then being infiltrated for measurements of flexural strength.

5.6.1 Infiltration with resorbable phosphate glass

A DTA trace for the phosphate glass, with formula $50P_2O_5$□$40CaO$□$10Na_2O$ (mol%), is shown in Figure 5.6.1A. The identity of the two crystal phases, Tp1 and Tp2, are unknown, but the endothermic event, represented by Tm, relates to the melting temperature of the glass. For successful infiltration to occur, the phosphate glass needed to be molten, and thus an infiltration temperature of greater than 750°C was required.

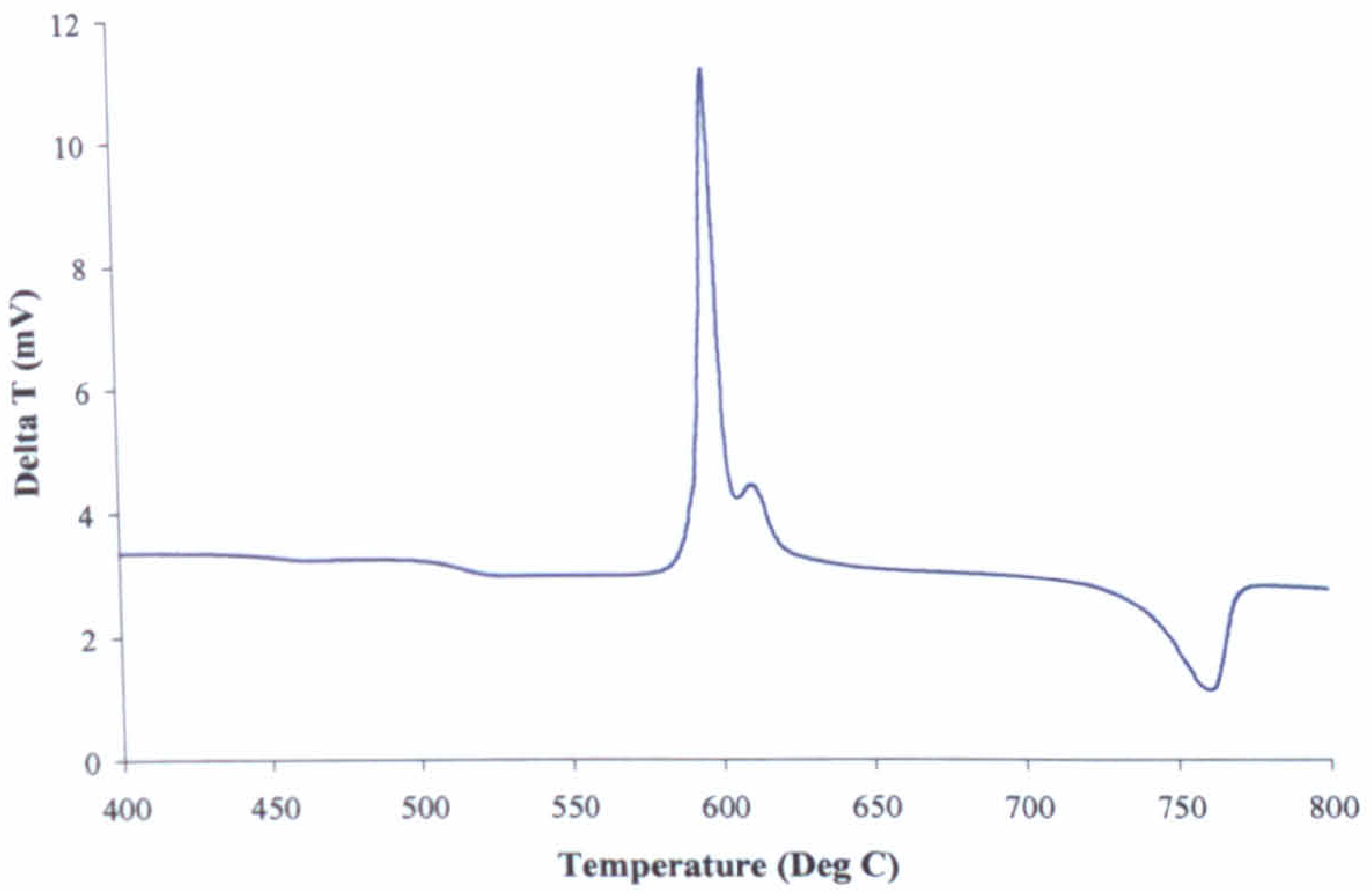

Figure 5.6.1A: DTA trace of the phosphate glass used for infiltration [Lorrison].

Initial attempts to infiltrate the brown parts with phosphate glass were made by simply placing an A-M preform in the furnace with a heap of glass powder on the top surface, heating to 900°C, holding at this temperature for an hour, then allowing the part to cool back down to room temperature at the natural rate of the furnace. Following this treatment, a small mound of melted glass could be seen on the top surface, but it was not possible to tell whether this was all the original glass, or whether some of it had successfully infiltrated and this was the surplus. Three point bend tests could not be used as an indication of whether the glass had infiltrated, as the results may have been affected by the excess glass remaining on the top surface of the beams. Therefore the samples were looked at with SEM, a typical micrograph from which can be seen in Figure 5.6.1B.

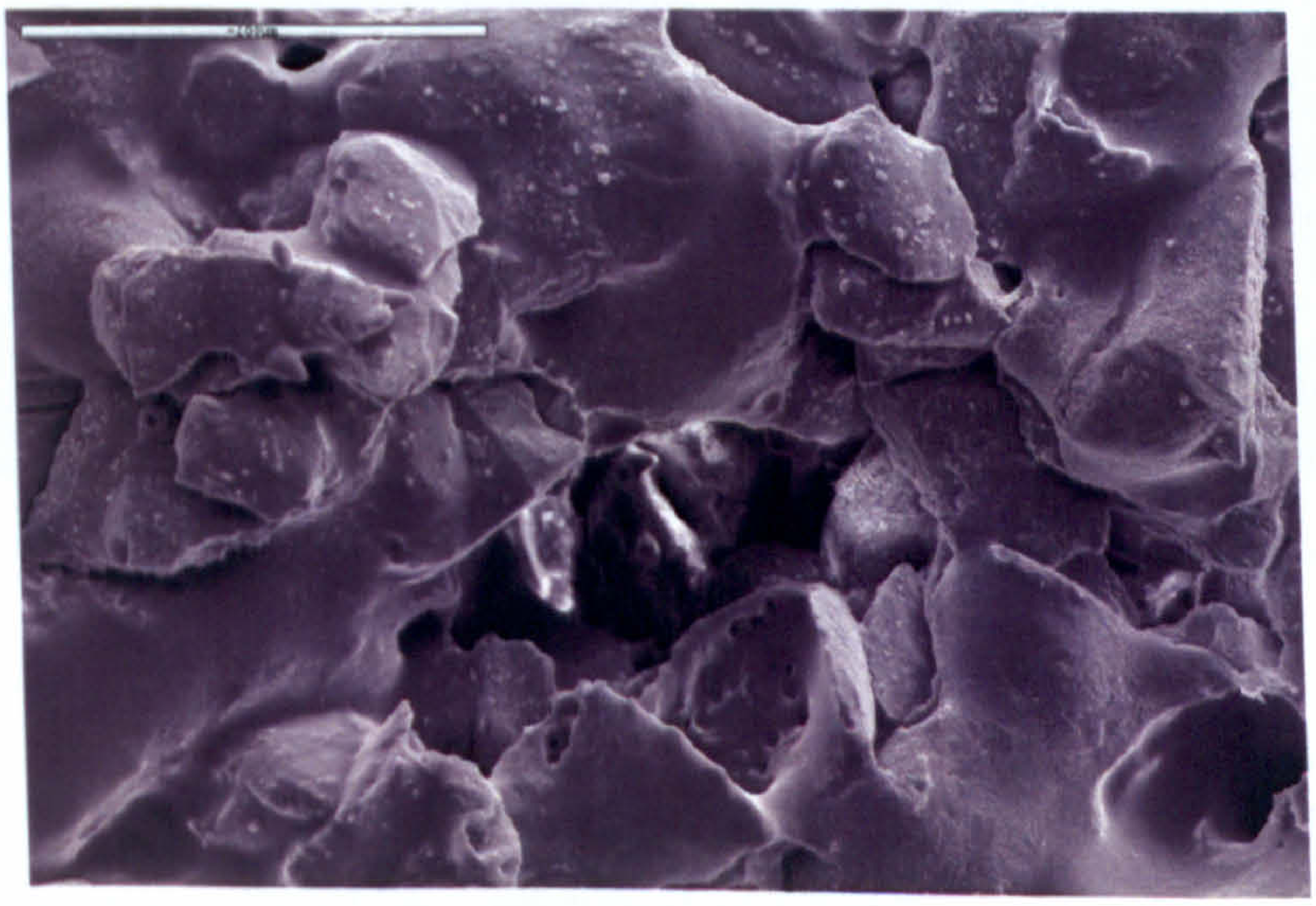

Figure 5.6.1B: SEM micrograph of specimen infiltrated with phosphate glass at 900°C

In this micrograph it can be seen that a reasonable amount of infiltration is occurring, with the phosphate glass appearing to surround and connect the LDIG105 glass-ceramic particles. However the material has not infiltrated completely into the structure as pores remain.

Micro CT analysis was also performed on the infiltrated parts using a μCT80 scanning system from ScancoMedical® (Bassersdorf, Switzerland). This system utilises a fan-beam, multi-slice mode with a 7μm spot size X-ray source from a tube with a current of 0.16mA and a mean energy of 40keV (60kVp). A sample holder with a diameter of 20mm was used, giving a resolution of 10 microns. A series of slices were obtained throughout the material, and compared to those taken from a material before infiltration. Typical images from the two samples can be seen in Figure 5.6.1C. Both samples provide evidence of a highly porous structure being produced. However, the morphology of the pores appears to have changed, going from the angular shape observed after heat treatment to a more spherical shape after infiltration. This seems to indicate well grown necks, as when the size of the necks between particles grow, the narrow openings near the necks disappear, and the pores become more spherical in shape.

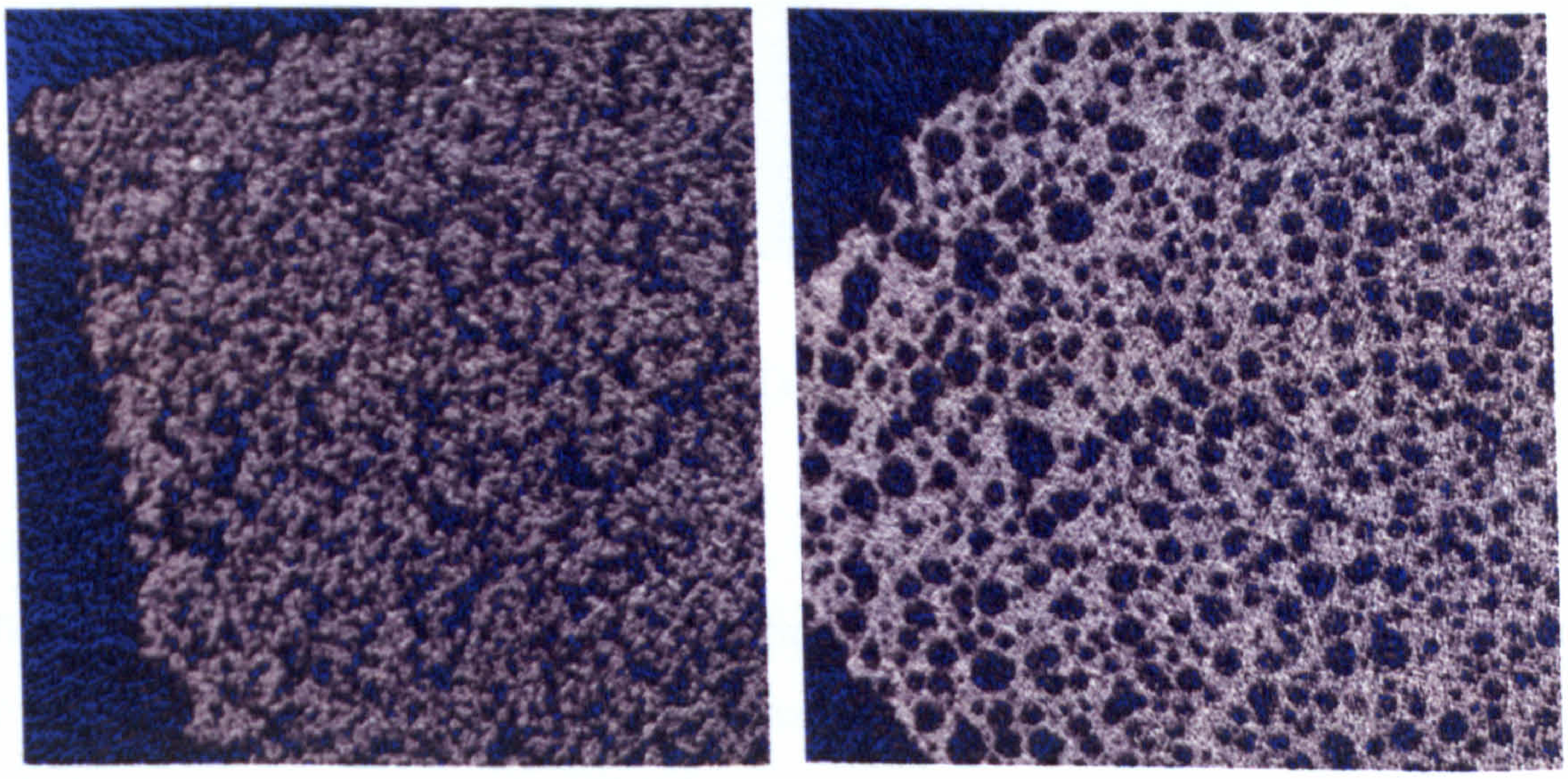

Figure 5.6.1C: Comparison of μCT scans of LDIG105 before and after infiltration with phosphate glass at 900°C.

It is not clear from these single slice images however if the porosity that can be observed is open or closed. As discussed in Chapter 2.4.3, open porosity is important since it allows the ingrowth of bone into the structure of the material, which ensures more secure anchorage of the implant into the bone defect. Therefore a 3D reconstruction of the slices was made, which can be seen in Figure 5.6.1D. From this image it appears that the material does have an open pore structure, which is reasonably uniform throughout the part.

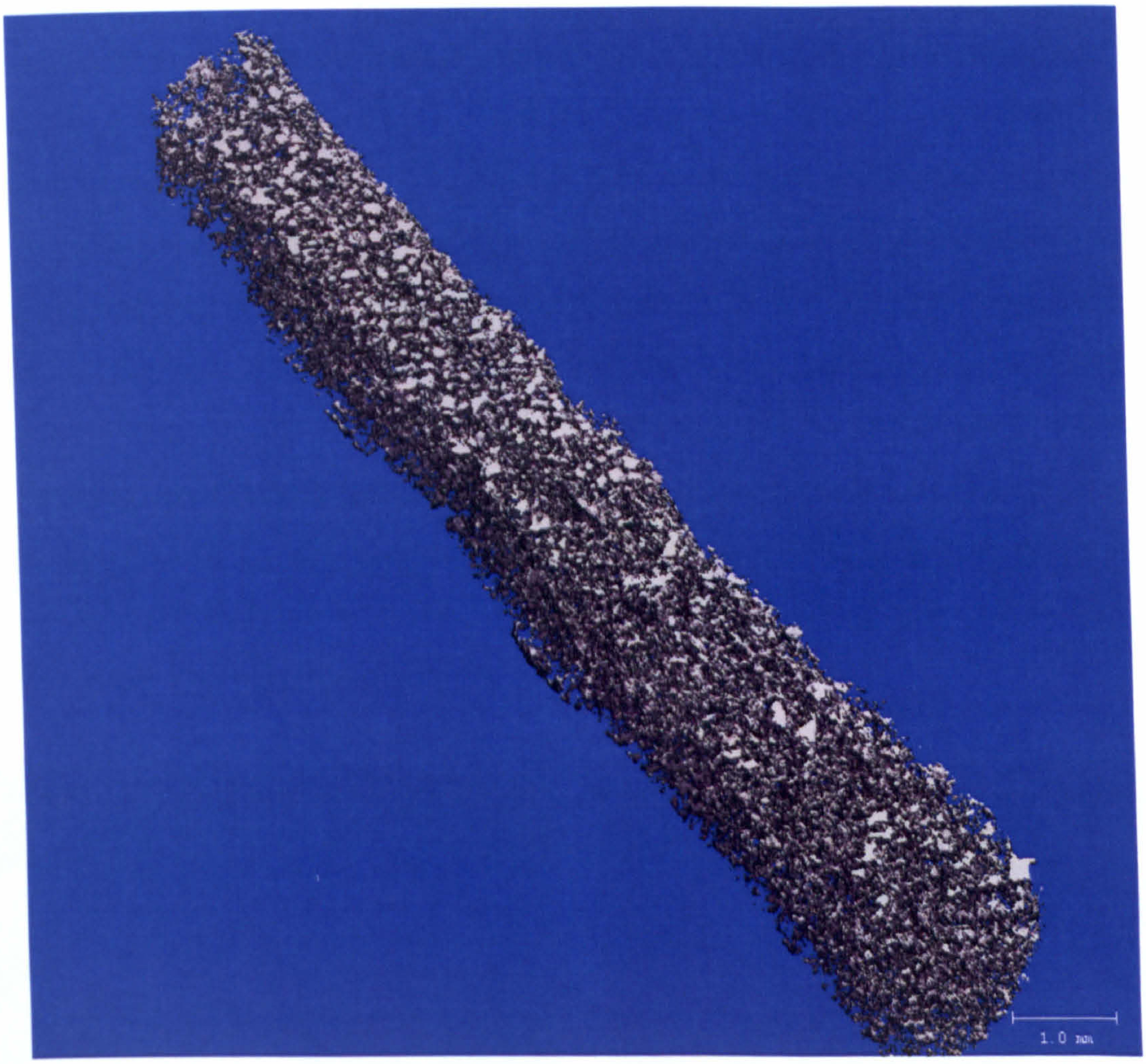

Figure 5.6.1D: 3D reconstruction of LDIG105 infiltrated with phosphate glass.

With both SEM and μCT indicating that the material was still highly porous after infiltration, there appeared to be the potential to infiltrate further and increase strength. Incomplete infiltration was unlikely to have resulted from not enough material being available, since there was a considerable amount of molten glass remaining on the top surface of the part after the initial attempt at infiltrating it. Therefore it appeared that a more effective method of infiltrating the parts was required.

Attempts were therefore made to improve the degree of infiltration, and to allow the amount of glass required to be more accurately determined, by infiltrating the parts under vacuum. The samples were placed in a vacuum furnace with 3g of phosphate glass placed on the top surface. The apparatus was evacuated to 50 Torr, while the vacuum chamber was heated from room temperature to 900°C at 10°C/min. After holding at this temperature for an hour, the vacuum was released to ambient pressure, and the specimen allowed to cool back down to room temperature at the natural rate of the furnace. Even using a vacuum, a large amount of phosphate glass remained balled up on the surface of the sample. Therefore the same method was used, but the temperature was raised to 1200°C. This proved more successful, with no phosphate glass remaining on the surface. The flexural strength of 20 of these infiltrated samples was measured and gave a mean flexural strength of 13.8±0.23MPa, more than twice that of the samples before infiltration. The parts were measured in all orientations incase the phosphate glass was unevenly infiltrating, but no difference in the results was observed. To compare the degree of infiltration occurring at 1200°C under vacuum to that seen at 900°C, and to ensure even infiltration of the parts was occurring, the parts were again analysed by SEM. Micrographs of the cross-sections of the infiltrated structure can be seen in Figure 5.6.1E.

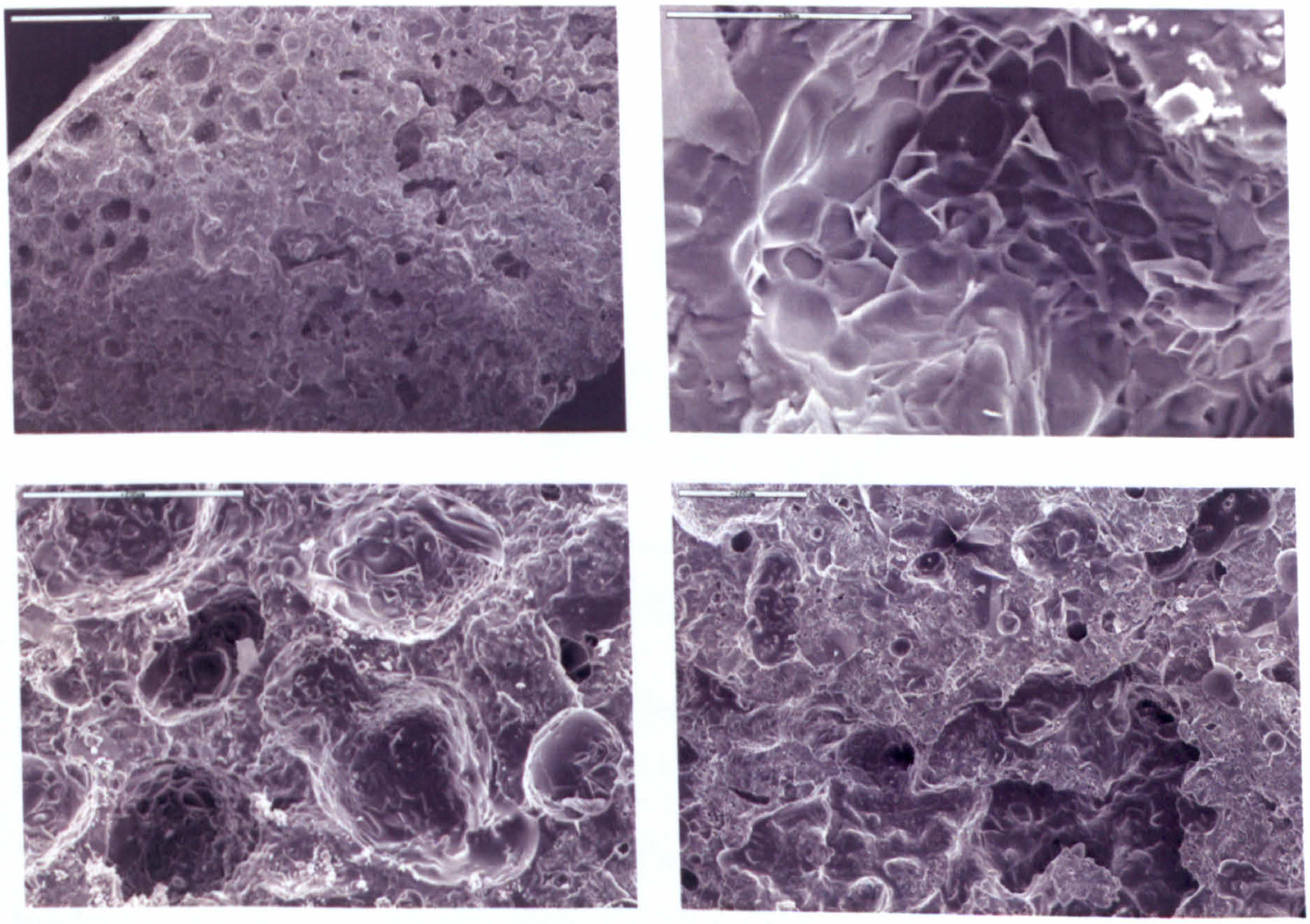

Figure 5.6.1E: SEM micrographs of parts infiltrated with phosphate glass at 1200°C

From these micrographs, not only does the porosity seem to have been almost completely eliminated, but there is a very different structure, suggesting that by heating to 1200°C the infiltrated phosphate glass has reacted with the LDIG105 material. From the SEM image in Figure 5.6.1E at the highest magnification, the structure appears to be made up of a number of hexagonal crystals, suggesting new crystal phases have been formed.

In order to identify these new phases, the infiltrated material was examined by XRD, the resulting XRD pattern is shown in Figure 5.6.1F. Comparing this pattern with that of LDIG105 before infiltration (Figure 5.3A) it is observed that the diffraction maxima of the fluoroapatite and mullite phases have disappeared, being replaced by a new phase, identified as Whitlockite ($Ca_3(PO_4)_2$ - JCPDS File No. 9-169). The diffraction maxima corresponding to anorthite have remained and increased in intensity.

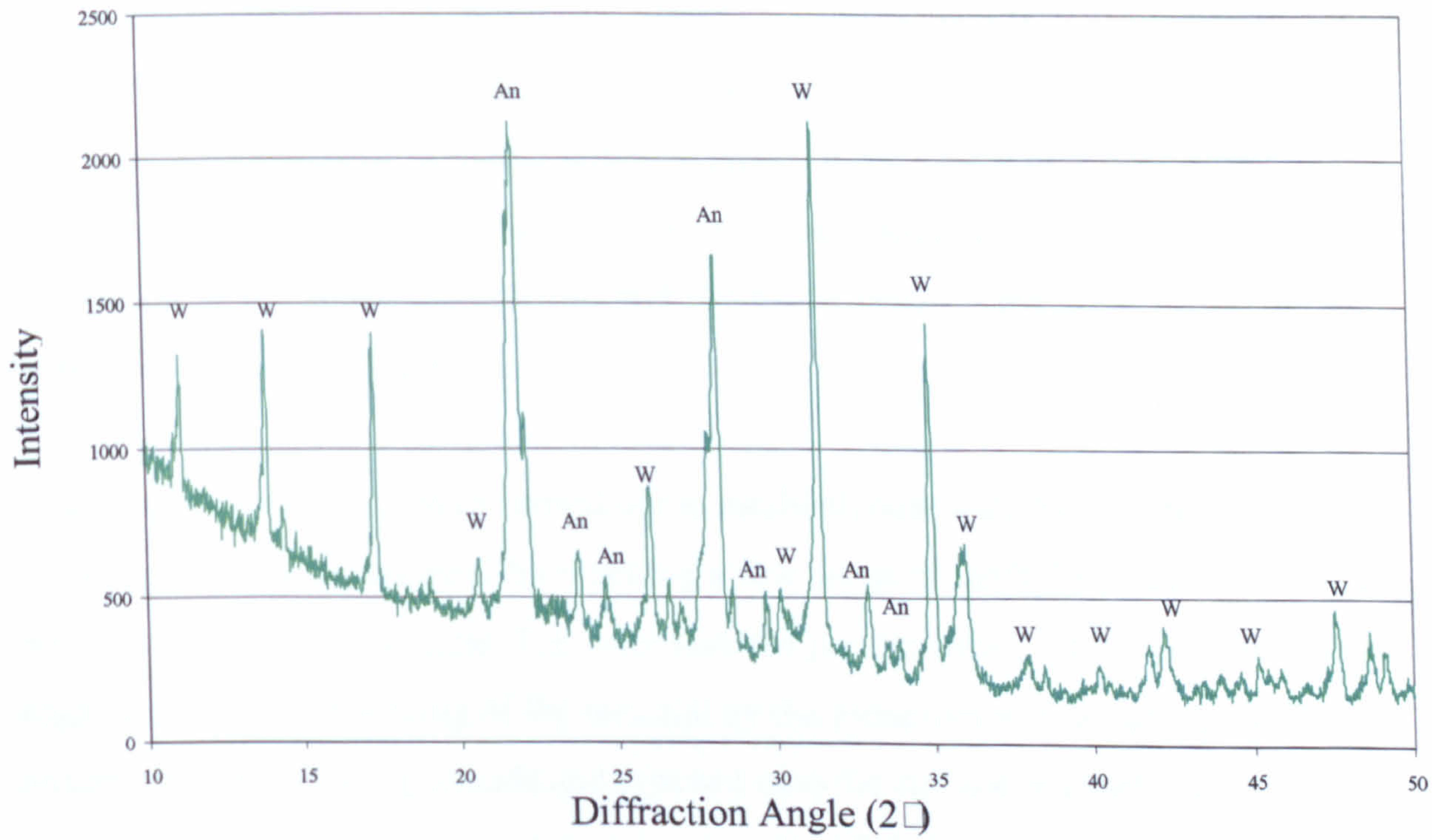

Figure 5.6.1F: XRD trace of LDIG105 infiltrated with phosphate glass at 1200°C.

This confirms the suggestion that the phosphate glass has reacted with LDIG105, to produce a new material. Fluorine appears to have been driven off the fluoroapatite form to produce apatite in the Whitlockite form, and the mullite has been dissolved with the silicon and aluminium possibly going into the residual glass. The anorthite remains unchanged, which suggests that it is this phase that is retaining the structure, as the dimensions and shape of the parts had not altered after infiltration. The calcium to phosphate ratio will also now be higher due to the addition of phosphate from the infiltrated glass.

5.6.2 Infiltration with PMMA.

Polymethylmethacrylate (PMMA) is commonly produced through addition polymerisation of methylmethacrylate with benzoyl peroxide. The peroxide linkage is split to form two identical radicals either by heating or by reaction with a chemical activator. When the radical reacts with a monomer molecule, the polymerisation reaction is initiated which in turn produces another active free radical species which is capable of further reaction. In this work, thermal activation was used to decompose the peroxide initiator and allow polymerisation to occur. The MMA used contained 0.01% hydroquinone which is included in the solution to ensure that it remains liquid during storage by reacting with radicals formed within the liquid to form stabilised radicals which are not capable of initiating polymerisation. It has previously been found that 2-5% benzoyl peroxide is sufficient to initiate polymerisation, as only a few free radicals are needed to propagate the process, and too much benzoyl peroxide results in some being left undissolved [Praestiin, 2001].

Preliminary experiments were carried out to establish how well the solution was able to wet the glass-ceramic material by pipetting a few drops of methylmethacrylate (MMA) onto the surface of the sample. The laser sintered part absorbed the liquid upon impact, suggesting sufficient wetting of the material by the monomer was occurring. MMA was mixed with 5% benzoyl peroxide and pipetted onto the surface of another glass-ceramic sample. It was placed in an oven preheated to 100°C for one hour. After cooling back down to room temperature, the surface of the sample was examined by SEM - a typical micrograph of the area can be seen in Figure 5.6.2A.

From this micrograph the PMMA can be seen to be closely covering the glass-ceramic particles, mostly taking their shape, providing a further indication of the polymers ability to sufficiently wet the laser sintered LDIG105 material.

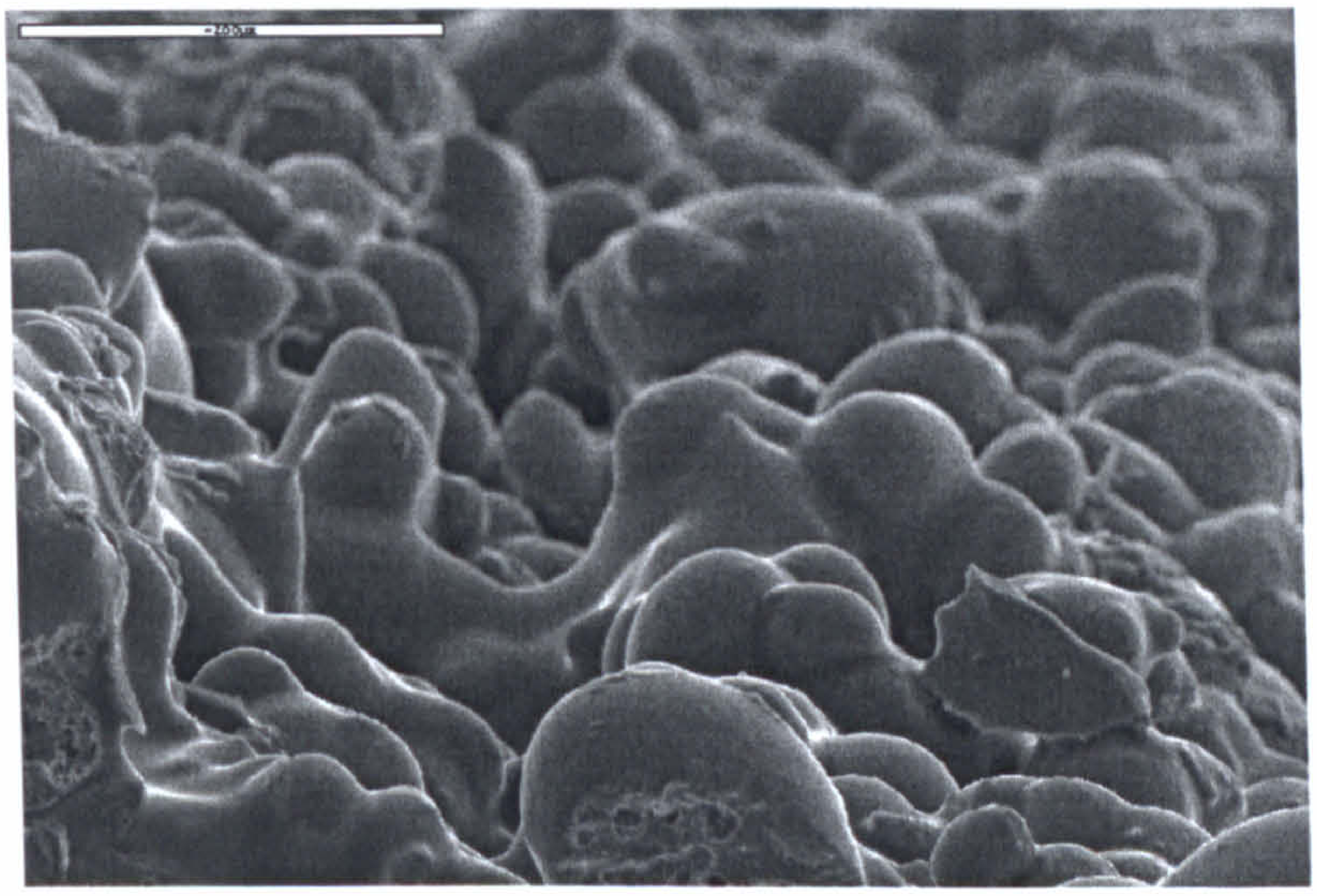

Figure 5.6.2 A: SEM micrograph of initial experiment to determine if PMMA wets the glass-ceramic. Scale bar is 200μm.

Once it had been confirmed that MMA satisfactorily wets the ceramic, infiltration was attempted by capillary action by immersing the samples in the solution of MMA and 5% benzoyl peroxide and heating over a water bath until the PMMA had fully set. There had been concerns that the hydroquinone inhibitor in the MMA would prevent the activation of the polymerisation reaction, and the hydroquinone would therefore need to be separated out from the MMA, but this did not prove the case, with activation occurring without separation. Once the PMMA had set, the sample was sectioned and examined by SEM. As the sample had been left to set in the PMMA, excess PMMA was present around the sample which can be seen on the left hand side of the micrograph taken from the outside edge.

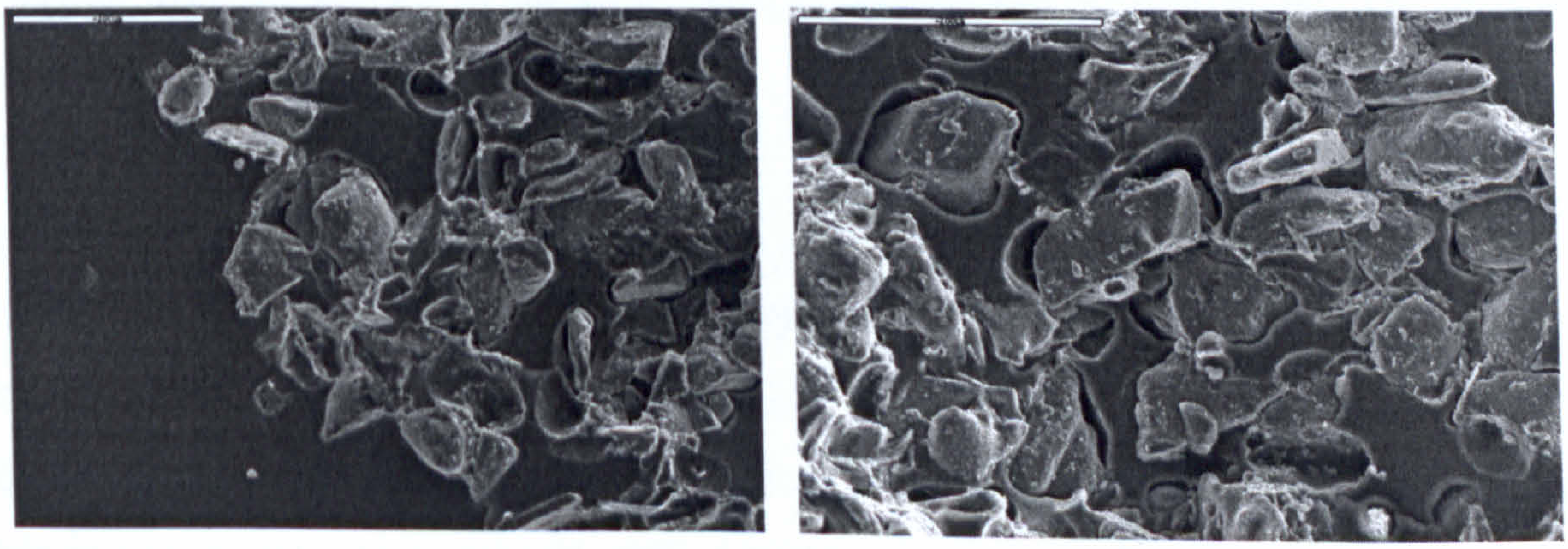

Figure 5.6.2 B: Post-processed samples infiltrated with PMMA by heat curing and allowed to set. The sample on the left is from the outside edge, and that on the right is from the centre of the infiltrated part. Scale bar is 200μm.

These micrographs demonstrate successful infiltration of the polymer throughout the part, with PMMA surrounding all the particles and completely filling in all the original pores. However reasonably large gaps around some of the particles can be seen, which is presumably due to the large volumetric shrinkage that occurs during polymerisation of MMA. Previous authors have reported shrinkage of around 21% when MMA is converted to PMMA [McCabe, 1990]. Shrinkage occurs because during polymerisation, the species that results from each addition reaction occupies less space than the two initial reacting species. Thus a small contraction results from each reaction, and as many hundreds of these reactions may occur during the polymerisation process, a large amount of shrinkage can occur. For this reason MMA is usually blended with beads of PMMA as this reduces the degree of shrinkage. However for infiltration purposes this approach it is not feasible as the addition of PMMA beads to MMA gives a mixture with a more dough-like consistency which is too thick to infiltrate into the pores.

Therefore two different approaches were attempted. The first involved samples being repeatedly dipped in freshly mixed MMA and 5% benzoyl peroxide, the idea being to slowly build up the PMMA in the pores and prevent excess on the surface. After each dip, the samples were placed in an oven preheated to 100°C for five minutes. After six dips the specimens were heated for a final ten minutes, before being allowed to cool back down to room temperature at the natural rate of the furnace. The second approach involved soaking the samples in the solution for two hours, before placing them in a preheated oven for ten minutes at 100°C. A period of two hours was sufficient for the solution to become of putty-like consistency without allowing it to fully set. Therefore upon removal of the samples from the solution, the excess polymer could be easily removed from the surface of the glass-ceramic, before allowing any infiltrated material to set fully upon subsequent heating.

Specimens infiltrated by both approaches were examined by SEM, and found to be identical in microstructure. The micrographs in Figure 5.6.2C are taken from the fracture surface of a dipped sample at various points of the cross-section. It can be seen that although the polymer does appear to be coating the glass-ceramic to some degree, this is not in any great volume, and significant porosity still remains. However the shrinkage away from the particles as was seen in the previously infiltrated samples does not appear to be occurring.

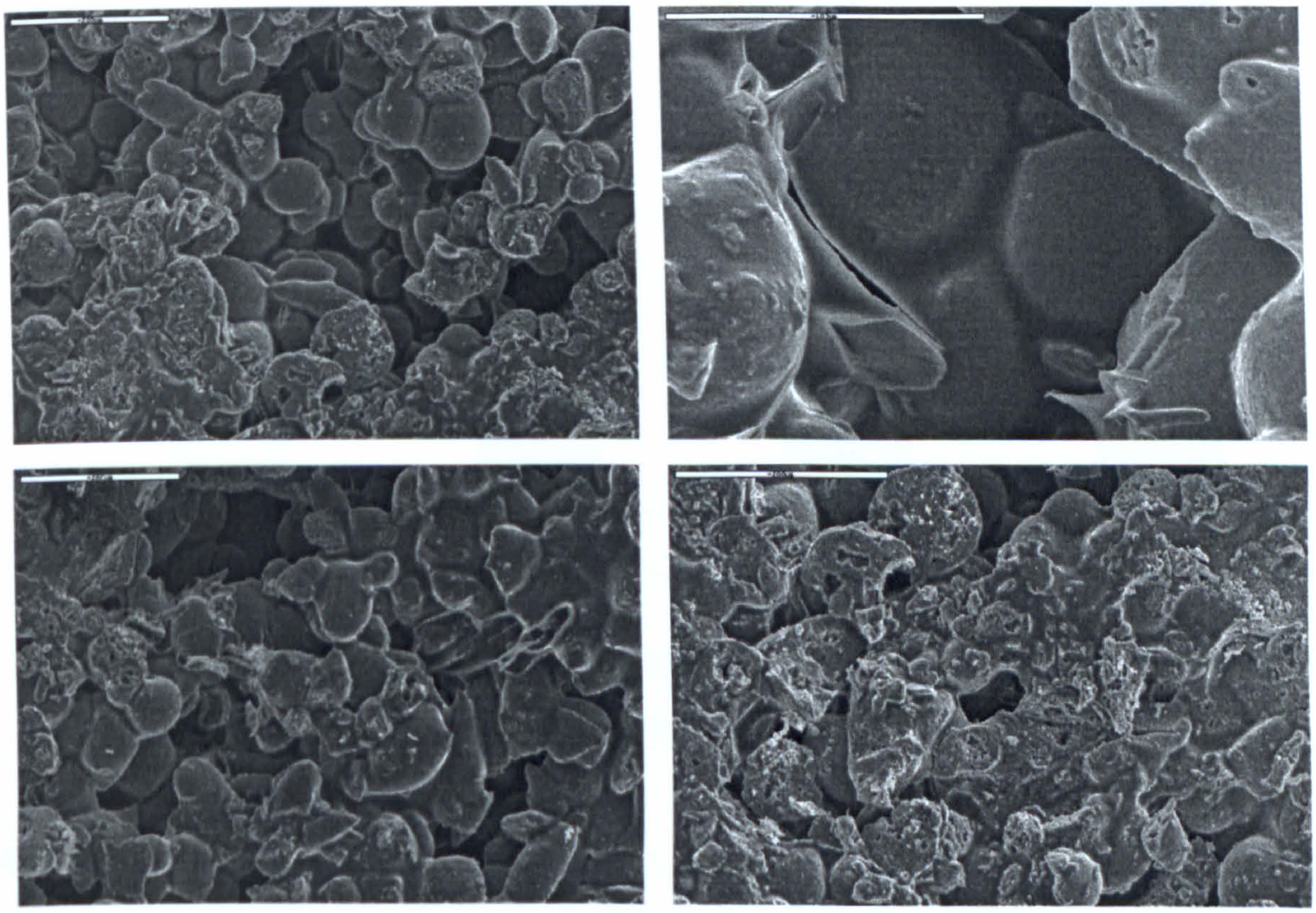

Figure 5.6.2 C: SEM micrographs of LDIG105 dipped in PMMA. Scale bars are 200μm, apart from the image at the top right which is 100μm.

It was not possible to measure the flexural strength of the samples that had been left to set in the MMA + 5% benzoyl peroxide since excess material remained around the specimens which would have affected the results. However 3-point bend tests were performed on twenty samples that had been dipped and twenty that had been soaked in the PMMA solution, giving mean flexural strengths of 7.55±1.1MPa and 8.81±0.5MPa respectively. The flexural strength of all the infiltrated materials are shown in Figure 5.6.2D where they may be compared to that of the material before infiltration. From this graph it can be seen that the flexural strength of the samples infiltrated with PMMA is greater than that before infiltration, but not by any particularly significant amount. This is hardly surprising since the coverage of the polymer on the glass-ceramic was relatively low, and much porosity still remained in the sample.

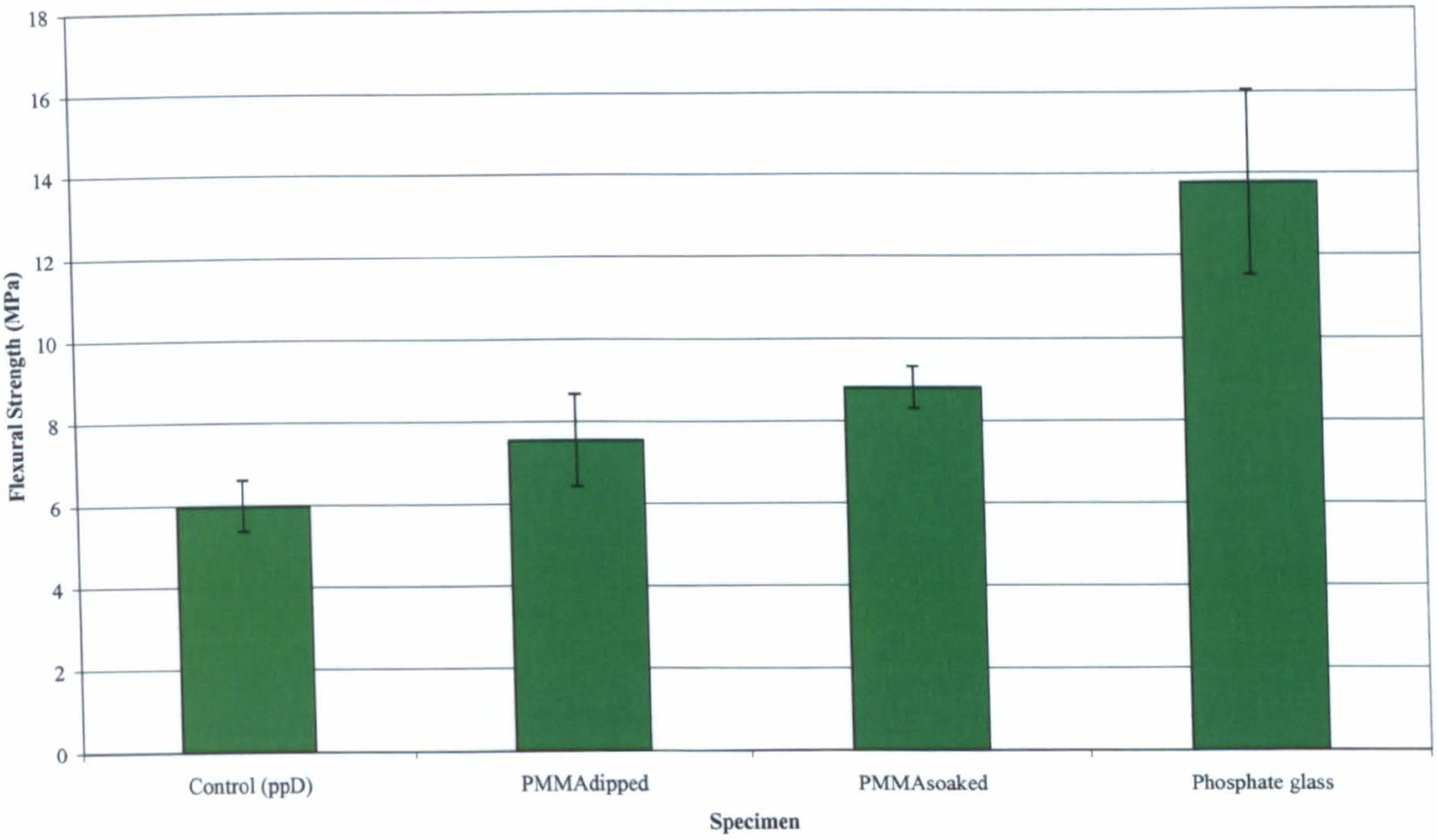

Figure 5.6.2D: Flexural strengths of LDIG105 infiltrated with PMMA and phosphate glass

However, infiltration with PMMA was only meant as an indication of whether it would be possible to infiltrate the glass-ceramic preforms with a polymer material. These preliminary experiments have proved that it is possible, but considerably more work needs to be carried out to optimise the infiltration process in order to increase the amount of material being infiltrated and reduce the time taken to infiltrate the samples.

Chapter 6 Assessment of biological properties

This section describes the experiments that were carried out to determine the biological properties of the glass-ceramic parts produced by indirect selective laser sintering. In order to assess baseline biocompatibility, both extract and contact cytotoxicity assays were performed. *In vitro* bioactivity was assessed by soaking the samples in a simulated body fluid for various time periods, and examining any apatite formation on the surface or a change in the pH or ion concentrations in the fluid after soaking. An *in vivo* study was also carried out, inserting the material into rabbit tibia.

The cytotoxicity studies were performed by Kearney, Lomas and Eagle at the UK National Blood Service. The bioactivity and *in vivo* experiments were carried out by the author at Nara Institute of Science and Technology (NAIST), Japan. Sectioning and SEM of *in vivo* samples was performed by A.Takeuchi, at NAIST, Japan.

6.1 Cytotoxicity

Circular samples 10mm in diameter, and 2mm in depth were produced by SLS using the method described in Chapter 4.2. A laser scan speed of 250mm/sec, laser power of 100W, scan line overlap of ½ the beam diameter, and layer overlap of 0.25mm was used to produce the green part. The samples were post-processed using post-processing route D (see section 5.2). Cast A-M samples, 10mm in diameter and produced as described in Chapter 3.4.1 acted as controls. Assessments of cytotoxicity were carried out according to ISO 10993-5 (biological evaluation of medical devices: tests for *in vitro* cytotoxicity) using both extract and direct contact methods.

6.1.1 Extract Method

The extract assay used normal human dermal fibroblasts (HDFs) and an immortalized human osteoblastic cell line, MG-63, as test cells. Following sterilisation by autoclaving at 121°C and 15bar for 20 minutes, the A-M samples were immersed in Dulbecco's modified Eagle's medium (DMEM) at a ratio of 10ml of medium to 1g of ceramic. Gentle agitation at 37°C for 24 hours was used to extract the samples, after which the extract solution was collected and stored frozen at -80°C. Fresh medium was added and the samples incubated under the same conditions for a further 144hours. Again, after the incubation the extract solution was collected and stored frozen. Negative controls were prepared by incubating extracting solution alone for the equivalent times. Two microculture assay plates were prepared by standard procedures – one containing human dermal fibroblasts (HDFs) and one containing MG-63 cells. The extract solutions were thawed and prepared into full culture medium by the addition of 10% (v/v) foetal calf serum, 2mM L-glutamine, 100ugml^{-1} penicillin, and 100ugml^{-1} streptomycin. A positive control of full medium containing 0.015% sodium dodecyl sulphate was also assessed. The extract solutions were added to the assay plates in quadruplicate samples and the plates incubated at 37°C for 24 hours. The solutions were then removed and a MTT viability assay run on the plates according to standard procedures [Lomas, 2003]. The MTT assay was used to quantify the ability of mitochondrial succinate dehydrogenases to metabolise the water soluble yellow dye, 3-[4,5-2-yl]-2,5-diphenyl-tetrazolium bromide (MTT) to a water-insoluble dark blue/purple formazan product [Plumb *et al.*, 1989]. The intensity of the colour produced by this product is directly proportional to the total number of living cells, which is quantified in a microplate reader at a wavelength of 570mm.

The results of the extract assays are presented in Figures 6.1A and B. The data has been analysed by one way ANOVA, and the minimum significant difference at p<0.05 calculated and displayed on the histograms.

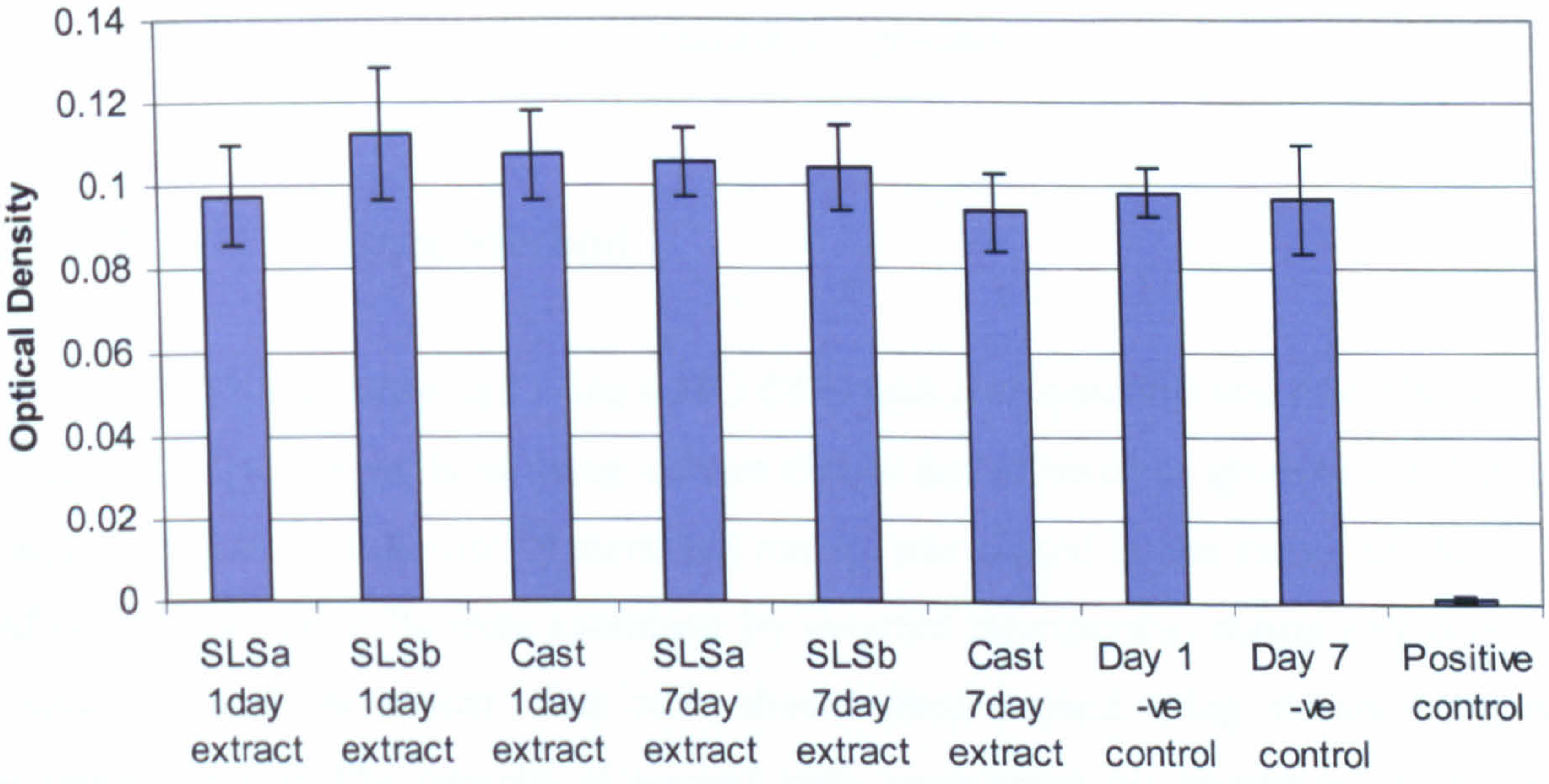

Figure 6.1 A: Cytotoxicity assessment of LDIG105 using human dermal fibroblasts.

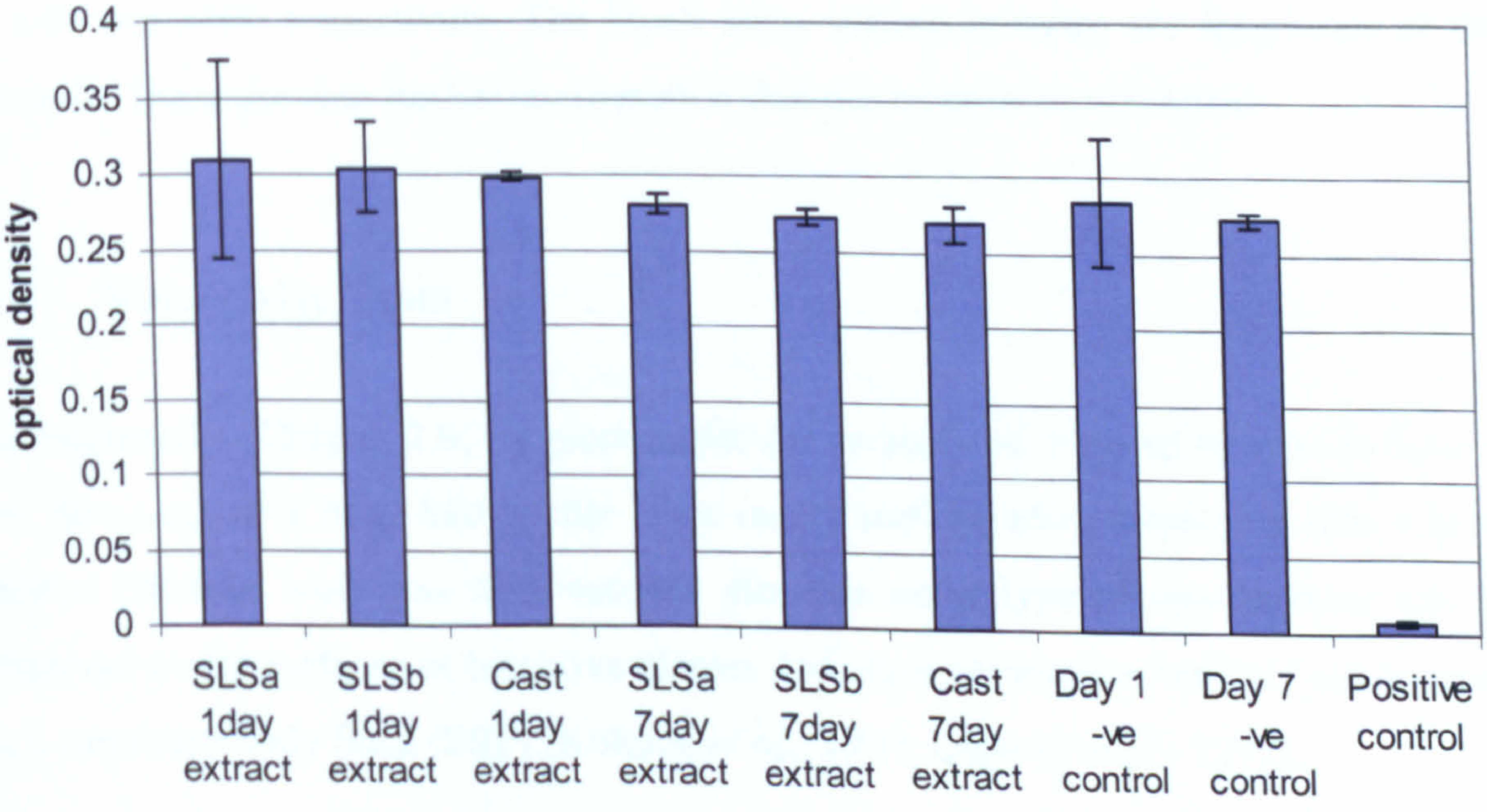

Figure 6.1 B: Cytotoxicity assessment of LDIG105 using MG-63 cells.

No significant difference was observed between any of the extracts and the negative control for either the HDFs or the MG-63 cells. The validity of the test was confirmed by the considerably lower value for the positive control, demonstrating that both cell types were susceptible to measurable degrees of cytotoxicity. It can therefore be concluded that as none of the test samples contained detectable levels of extractable cytotoxic chemicals, the material is non-toxic. It has also been shown that the process of laser sintering does not affect the cytotoxicity of the material as no significant difference was observed between the samples produced by this method and those produced by the conventional cast-crystallisation process.

6.1.2 Direct Contact Method

Direct assays were performed using a MG-63 human osteosarcoma cell line. Cells were seeded as a lawn in wells in tissue culture dishes and allowed to grow to confluence. Once confluent a small disc of sterilised matrix was placed in the centre of the well. After 18 hours the cells were examined by inverted microscopy, noting any zones of clearing around the matrix. The cells shown were stained using standard Giemsa staining protocol. Photographs of stained cells were taken for comparative purposes and can be seen in Figures 6.2A-E. Figures 6.2A and B are negative controls, with the former at x400 and the latter at x40 magnification. Figure 6.2C is the positive control at x40 in the presence of cyanoacrylate glue. Figures 6.2D and E are with the ceramic tile at x40 and x400 respectively. The black areas visible in these are fragments of the ceramic. These provide further confirmation that the material is non-toxic.

6.2 Bioactivity Tests

As discussed in Chapter 2.6, the prerequisite for an artificial material to bond to bone is the formation of a bone-like apatite layer on its surface when implanted into a bony defect. Previous work has demonstrated that this same type of apatite layer can be observed on the surfaces of bioactive glasses and glass-ceramics when they are exposed to a simulated body fluid (SBF) [Kokubo *et al.*, 1990; Ohtsuki *et al.*, 1991].

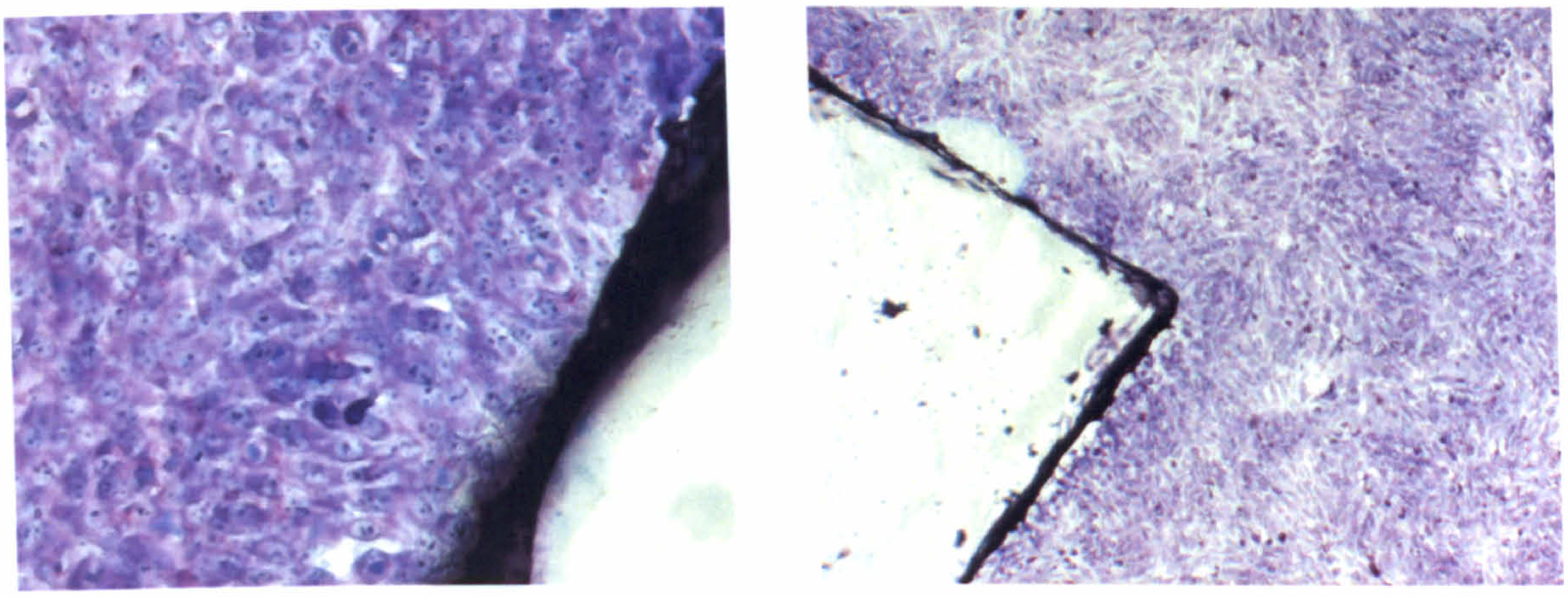

Figure 6.2 A (left) and Figure 6.2 B (right): Negative controls for direct contact assay to assess cytotoxicity, at x400 (left) and x40 (right).

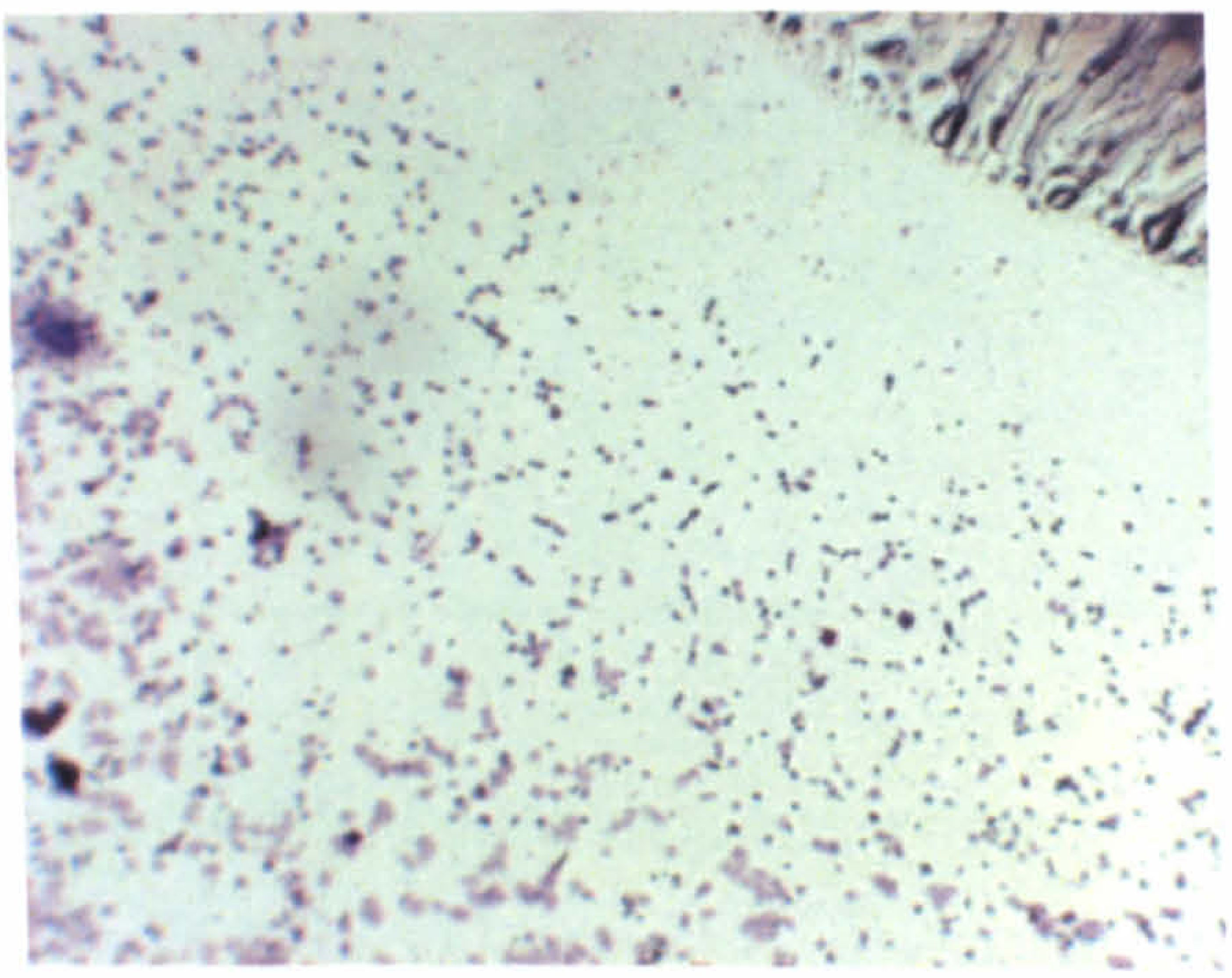

Figure 6.2 C: Positive control for direct contact assay (x40).

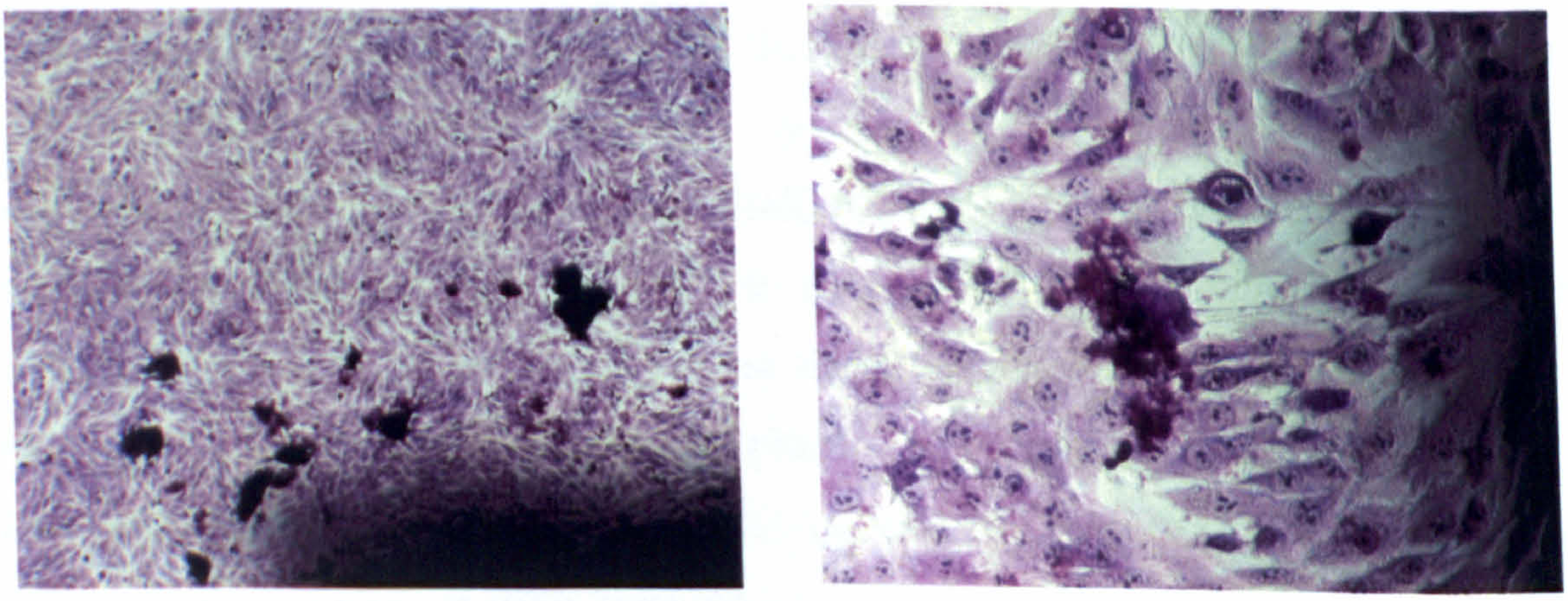

Figure 6.2 D and Figure 6.2 E: Direct contact assay of LDIG105 produced by SLS at x40 (left) and x400 (right) respectively.

This solution was proposed by Kokubo *et al* [1990] and has similar ion concentration to human blood plasma [Table 6.2A]. Therefore the rationale behind these experiments was that by soaking the laser sintered parts in SBF for a suitable time period, the ability to form an apatite layer on their surfaces could be determined, and thus the potential of the material to prove bioactive when implanted into the body could be predicted.

Ion concentration (mM)

	SBF	Human plasma
Na^+	142	142
K^+	5	5
Ca^{2+}	2.5	2.5
Mg^{2+}	1.5	1.5
Cl^-	147.8	103
HCO_3^-	4.2	27
HPO_4^{2-}	1.0	1
SO_4^{2-}	0.5	0.5

Table 6.2 A: Comparison of the ion concentrations in simulated body fluid (SBF) and human blood plasma.

LDIG105 samples fabricated both by selective laser sintering and by a conventional cast-crystallisation process were examined. Previous assessment of the bioactivity of glass-ceramics produced from glass in the system $SiO_2{\cdot}Al_2O_3{\cdot}P_2O_5{\cdot}CaO{\cdot}CaF_2$ have been performed on samples produced by conventional casting. Therefore it was considered necessary to test samples of LDIG105 that had been cast in addition to those produced by laser sintering, in order to determine whether laser sintering or the subsequent post-processing route altered the bioactivity of the parts. As the cast material was intended as a control, the process for producing it was taken from that developed by Lorrison [2003]. Bioglass®-type glass, a known bioactive material, and a non-bioactive commercial silica glass were used as controls.

6.2.1 Sample Preparation

The following materials were produced:

Apatite-Mullite glass-ceramic produced by SLS

Rectangular samples 30mm by 15mm, 3mm in thickness were produced using the method described in Section 4.2. A scan speed of 250mm/sec, laser power of 100W, scan line overlap of ½ the beam diameter and layer thickness of 0.25mm was used to produce the green part. The samples were post-processed using post-processing route D.

Apatite-Mullite glass-ceramic produced by SLS and infiltrated with phosphate glass

Rectangular samples 30mm by 15mm, 3mm in thickness were produced using the method described in Section 4.2. A scan speed of 250mm/sec, laser power of 100W, scan line overlap of ½ the beam diameter and layer thickness of 0.25mm was used to produce the green part. The samples were post-processed using post-processing route D and infiltrated with phosphate glass as described in section 5.3.1.

Apatite-Mullite glass-ceramic produced by conventional casting.

Samples were produced by conventional casting using the method described in section 3.4.1. They were cut into slices with a thickness of 2mm, and an approximate surface area of $15mm^2$.

Bioglass®-type glass produced by conventional casting

Bioglass®-type glass, with the composition $46.1SiO_2 \cdot 24.4Na_2O \cdot 26.9CaO \cdot 2.6P_2O_5$ (molar ratio) was prepared from reagent grade Na_2CO_3, $CaCO_3$, $Ca_2P_2O_7$, and SiO_2 as described in Chapter 3.4.2. Square samples with dimensions of approximately 10x10mm were produced.

Commercial Non-bioactive glass

A commercial glass (Matsunami Glass Ind. Ltd, Japan) was used with a composition in weight percent of 72.6 SiO_2, 1.8 Al_2O_3, 3.8 MgO, 7.9 CaO, 12.1 Na_2O, 0.1Fe.

6.2.2 Preparation of SBF

All glassware was thoroughly cleaned with neutral detergent, 1M HCl solution, and ion-exchanged distilled water. 600ml of ion-exchanged water in a 1000ml beaker was stirred at 36.5°C for 30 minutes. After this time the water was replaced by a further 600ml. The water was held at this temperature in a water bath, and continued to be stirred with a magnetic stirrer. Each chemical, listed in table 6.2B below, was added to the water, one by one in the order given in the table after the previous reagent was completely dissolved. The chemicals were weighed into weighing boats, with the remaining chemical on the weighing boat being washed into the beaker with ion-exchanged water. The pH of the solution was buffered at pH7.25 with 50mM trishydroxymethyl-aminomethane and 45mM HCl, and its temperature kept constant at 36.5°C.

Chemical	Amount/ $g.dm^{-3}$
NaCl	7.996
$NaHCO_3$	0.350
KCl	0.224
$K_2HPO_4.3H_2O$	0.228
$MgCl_2.6H_2O$	0.305
1mol/dm^3 HCl	40ml
$CaCl_2$	0.278
Na_2SO_4	0.071
$(CH_2OH)_3CNH_2$	6.057

Table 6.2 B: List of chemicals used to make up SBF (all supplied by Nacalai Tesque, Japan)

The solution was transferred to a glass volumetric flask and ion-exchanged water added to adjust the total volume to 1 litre. The flask was shaken, before transferring the solution to a polyethylene bottle for storage in a refrigerator at 5-10°C.

6.2.3 Soaking of samples

The surface area of all the samples was measured and the volume of SBF calculated according to the ratio of 0.1ml SBF to $1mm^2$. Sterile polystyrene bottles were rinsed with a little SBF solution, then filled with the required amount for each specimen. The bottles were placed in a water bath heated to 36.5°C and stirred with a magnetic stirrer. After 30 minutes, the samples were added to the solution, having first been washed in ultra pure water. Three samples of each material were used, each left for 1, 3, 7, or 14 days. The bottles were then transferred to an incubator at 36.5°C. Bottles containing only SBF were also incubated for each of the time periods, to be used as controls.

6.2.4 Removal of samples.

After the samples had been soaked for the specified time periods they were removed from the SBF solution with tweezers, washed for 1 minute in ultra pure water, allowed to dry, then transferred to polystyrene boxes within a dessicator for storage. The SBF solutions were shaken, then 12ml transferred into a centrifuge bottle and centrifuged for 5 minutes at 3000rpm. 2ml from the top of the centrifuge tube was then pipetted into a fresh polystyrene container containing 2ml of 0.1M HCl (to stabilize the solution). The solution was made up to 20ml by adding ultra pure water. The pH of the SBF solution (before centrifuging) was measured.

6.2.5 Analysis of samples

The surface of the samples were characterised by Scanning Electron Microscopy (SEM; S-3500N, Hitachi Co. Ltd., Japan) before and after soaking in SBF for each time period. The chemical composition and structure of any material deposited on the surface was studied by electron dispersive X-ray microanalysis (EDX; EMAX Energy EX-400, HORIBA, Ltd., Japan) and thin-film X-ray diffraction (TF-XRD; MXP3V, MAC Science Co. Ltd., Japan). The XRD measurement was performed by 2θ scanning with $CuK\alpha$ radiation. θ was fixed at 1 degree against the incident beam. For SEM analysis the samples were gold splutter coated and as the peak for gold overlaps that for phosphorus, SEM was performed after the other techniques. The evolution of element concentrations of Ca, P, Si, and Al in the solutions were determined by inductively coupled plasma atomic emission spectroscopic (ICP-AES; Optima 2000DV, Perkin Elmer Co. Ltd., Japan) analysis before and after soaking. For these measurements the sample solutions were diluted to bring the concentration of the elements of interest into the optimal measurement range of the instrument. The pH of the solutions was also measured using a pH meter and glass electrode.

6.2.5.1 TF-XRD

Figures 6.2.5.1A-E show the XRD pattern evolution with immersion time in SBF for the following materials:

6.2.5.1A – Bioactive Control – Bioglass®-type glass
6.2.5.1B – LDIG105 samples produced by casting
6.2.5.1C – LDIG105 samples produced by SLS
6.2.5.1D – LDIG105 samples produced by SLS and infiltrated with phosphate glass
6.2.5.1E – Non-bioactive Control – Commercial glass

For the known bioactive material, Bioglass®-type glass, two broad peaks were observed at 26 and 32° after soaking in SBF which were assigned to diffractions of an apatite phase using the International Centre for Diffraction Data (ICDD) standards data file number 09-0432. These results indicate that a low-crystalline apatite was deposited on the surface of the material after just one day of soaking in SBF solution. The intensity of these peaks increases with increasing soaking time until after three days of soaking when continued exposure to SBF does not result in any further increase, indicating that at this point the apatite layer is complete.

The presence of an apatite layer was not detected on the surface of the LDIG105 samples produced either by conventional casting or SLS as the diffractographs obtained were identical after all periods of soaking to those obtained before immersion in SBF. Peaks at 26 and 32° do already exist in these materials as a result of the crystalline

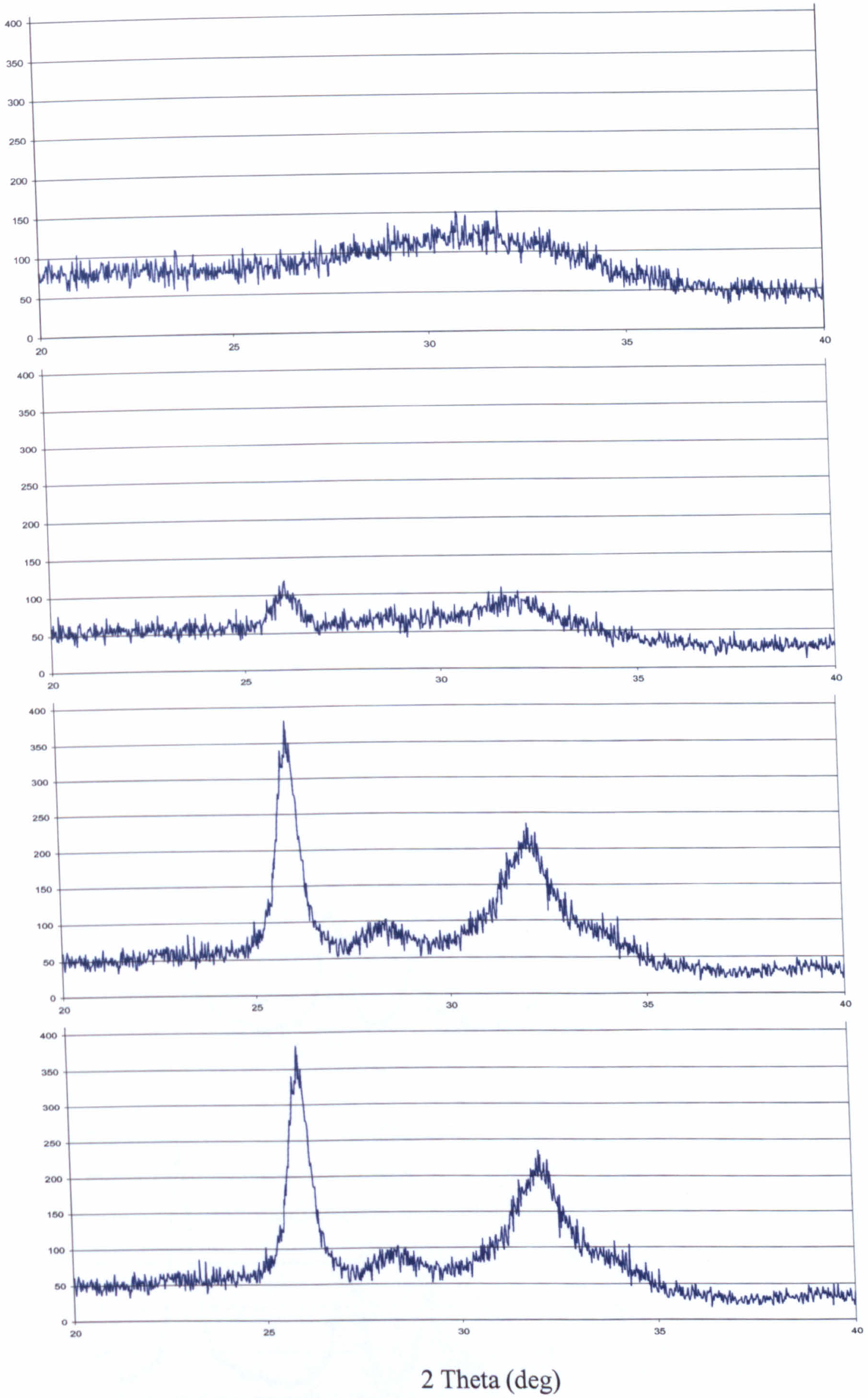

Figure 6.2.5.1 A: TF-XRD trace for bioglass®-type glass soaked in SBF for 0, 1, 3 and 7 days.

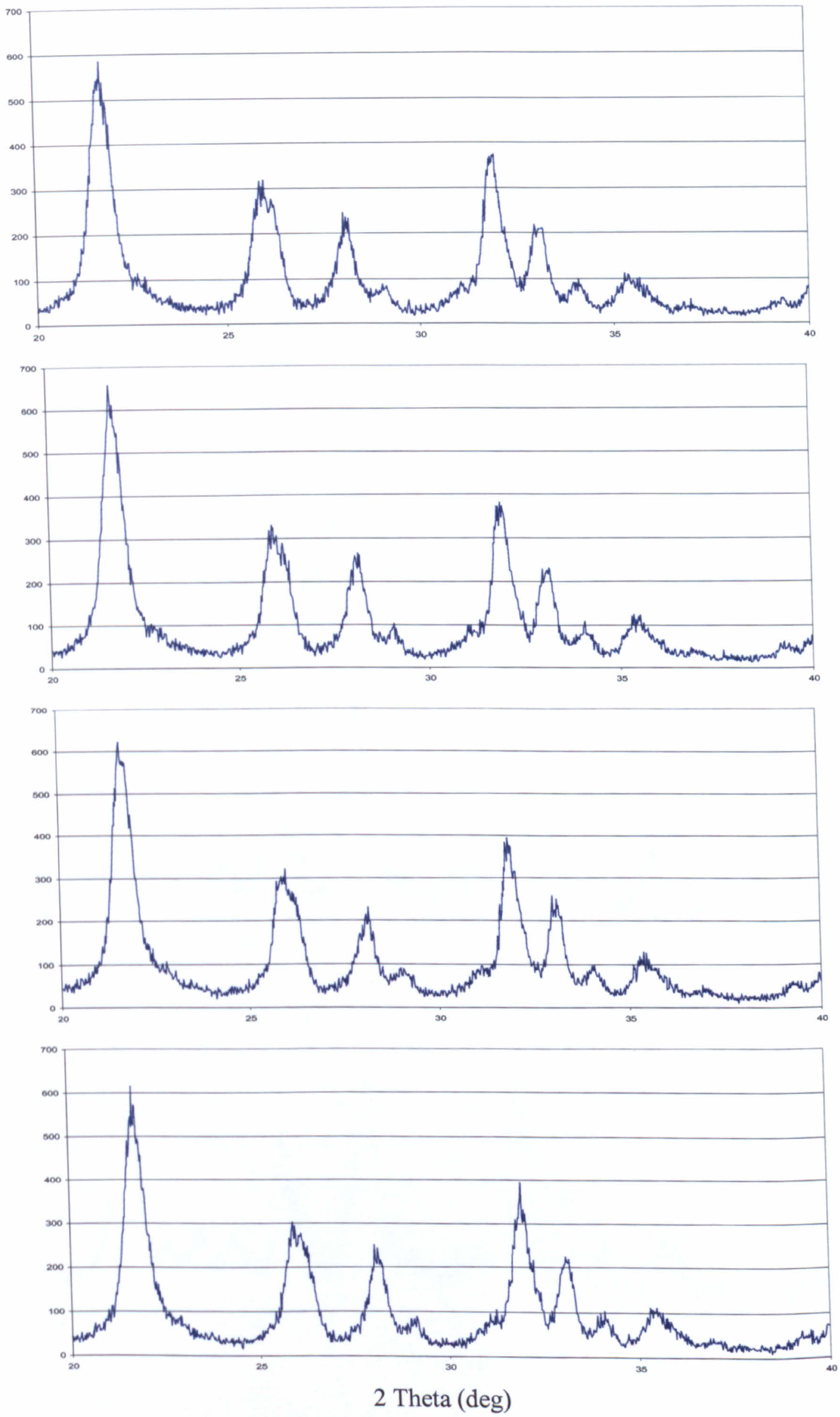

Figure 6.2.5.1 B: XRD for cast LDIG105 soaked in SBF for 0, 1, 3 and 7 days.

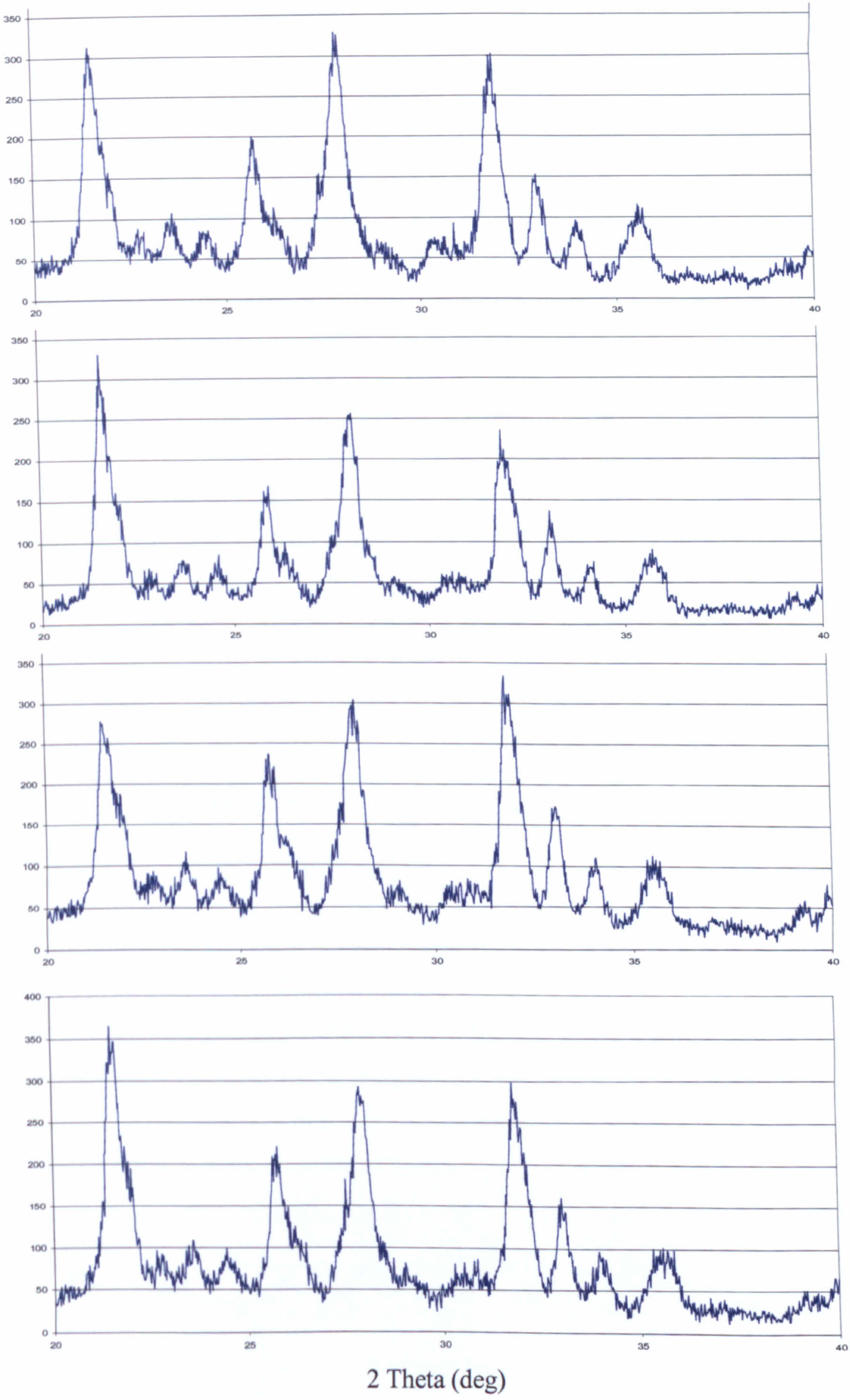

Figure 6.2.5.1 C: TF-XRD for SLS samples soaked in SBF for 0, 1, 3 and 7 days.

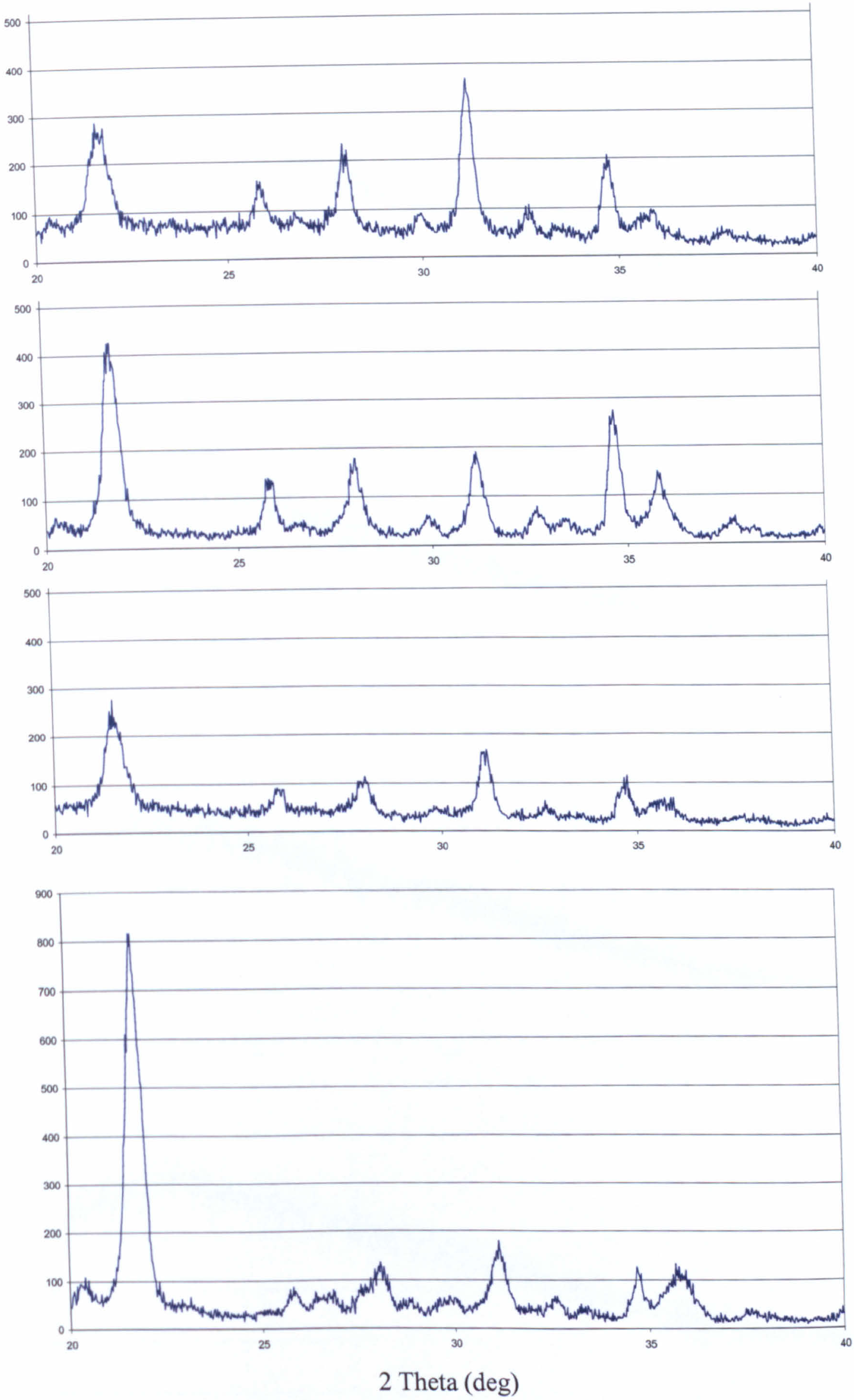

Figure 6.2.5.1 D: TF-XRD of SLS part infiltrated with phosphate glass for 0, 1, 3, and 7 days.

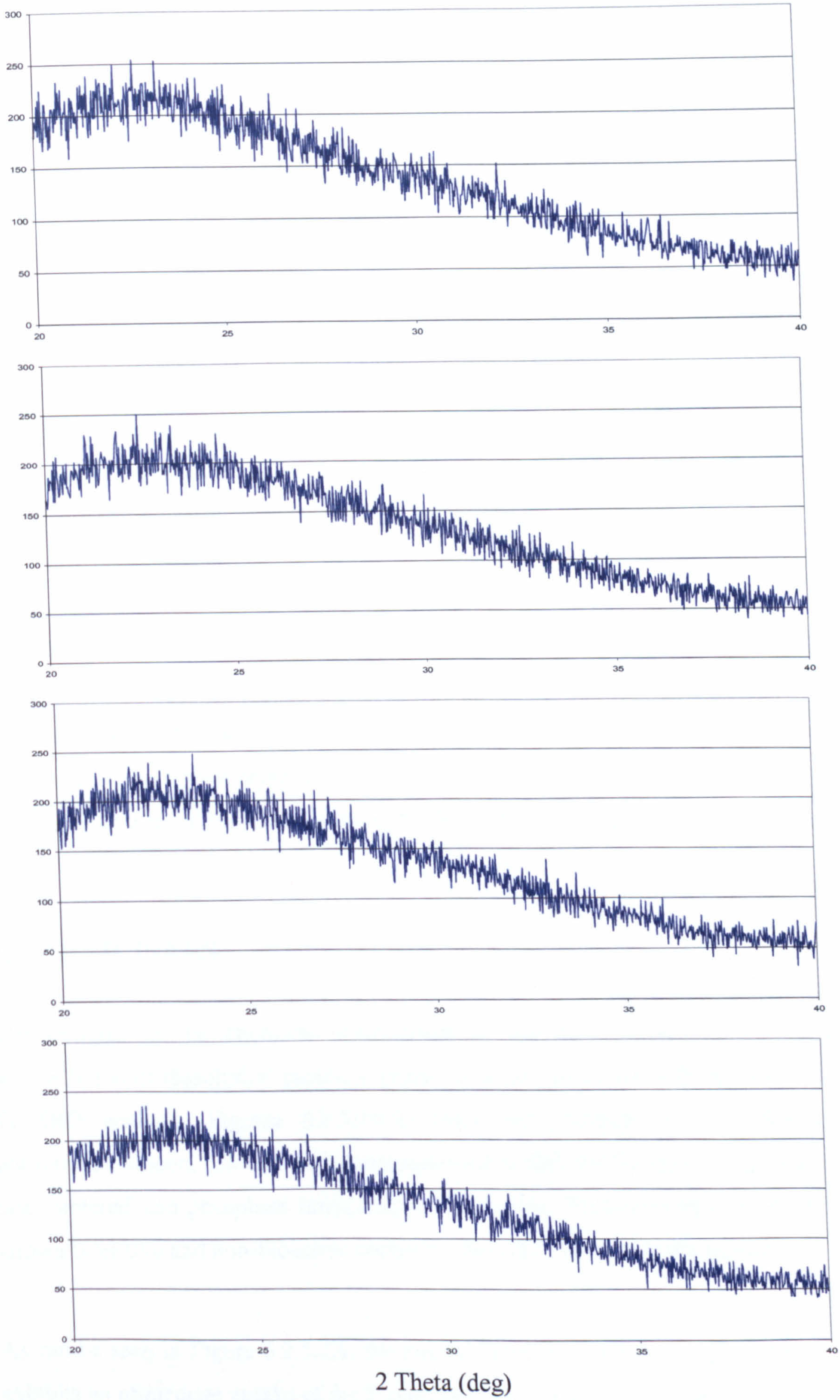

Figure 6.2.5.1 E: TF-XRD of commercial glass soaked in SBF for 0, 1, 3, and 7 days.

phases in the material, but there is no change in the width of these peaks after soaking in SBF which would be expected if an apatite layer was forming on the surface as it has a broader peak. One would also expect to see a reduction in the intensity of the other crystalline peaks in the material as the formation of any type of layer on the material surface would be masking their detection. This does not appear in the results for these samples, suggesting that LDIG105 produced either by conventional casting or by selective laser sintering is not bioactive.

A reduction in the intensity of the peaks for the SLS samples that were infiltrated with phosphate glass can be observed with increasing soaking time. This may be attributed to dissolution of phosphate phases in the glass-ceramic. However a large anorthite peak remains after 7 days of soaking in SBF. This suggests that selective dissolution has occurred, with anorthite showing little dissolution while the glass phase and apatite phase have dissolved easily.

The XRD pattern of the commercial glass did not show any diffraction maxima, which confirms its amorphous nature, and even after 14 days of soaking in SBF the XRD patterns correspond to an amorphous material. It is thus concluded that this material does not form an apatite layer on its surface upon soaking in SBF and therefore along with the bioactive control, the validity of the test can be confirmed.

6.2.5.2 ICP-AES

The changes in the chemical composition of the SBF solution as a result of accumulation of dissolution products appear to be in agreement with the results of the TF-XRD analysis. Figures 6.2.5.2A-D show the changes in concentrations of phosphorus, silicon, calcium and aluminium ions in SBF following soaking of the cast, laser sintered and phosphate infiltrated A-M samples. These can be compared to the known bioactive and non-bioactive controls which are included in the figures.

As can be seen in Figure 6.2.5.2A, the known bioactive material Bioglass®-type glass exhibits an immediate uptake of the P concentration, initially at a high rate, suggesting

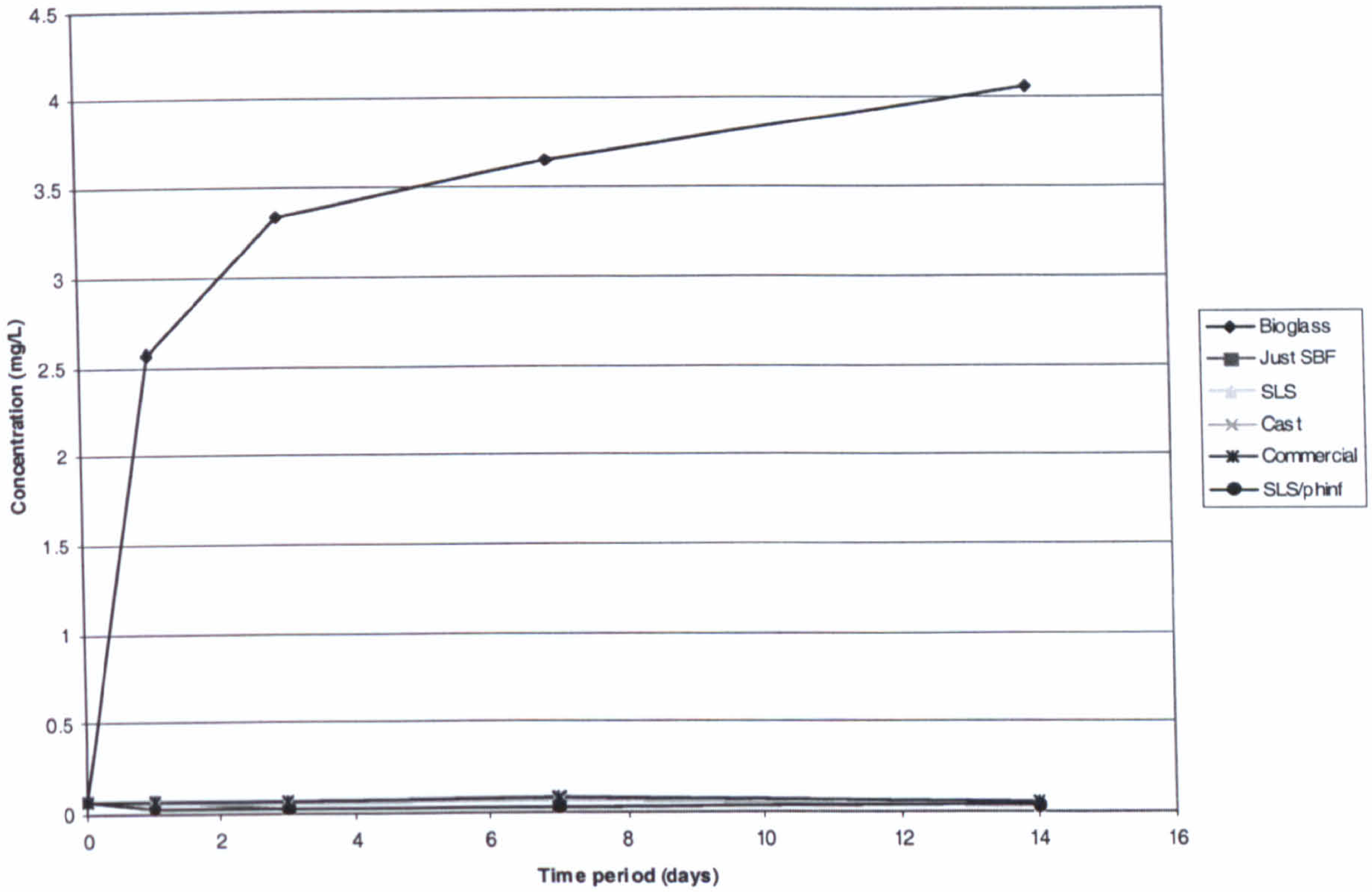

Figure 6.2.5.2 A: Change in concentration of Si ions in SBF following soaking of test materials for various time periods.

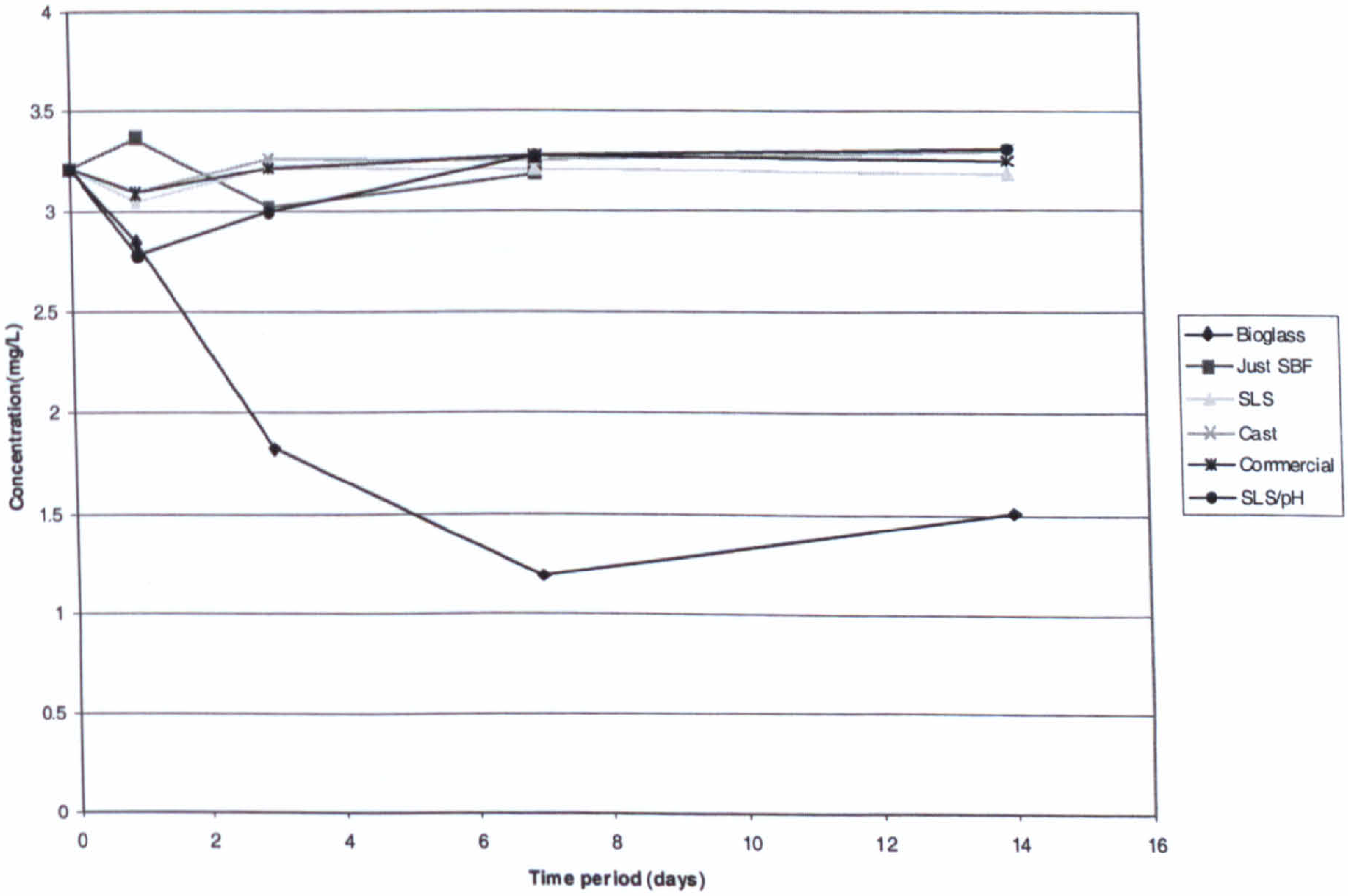

Figure 6.2.5.2 B: Change in concentration of P ions in SBF following soaking of test materials for various time periods.

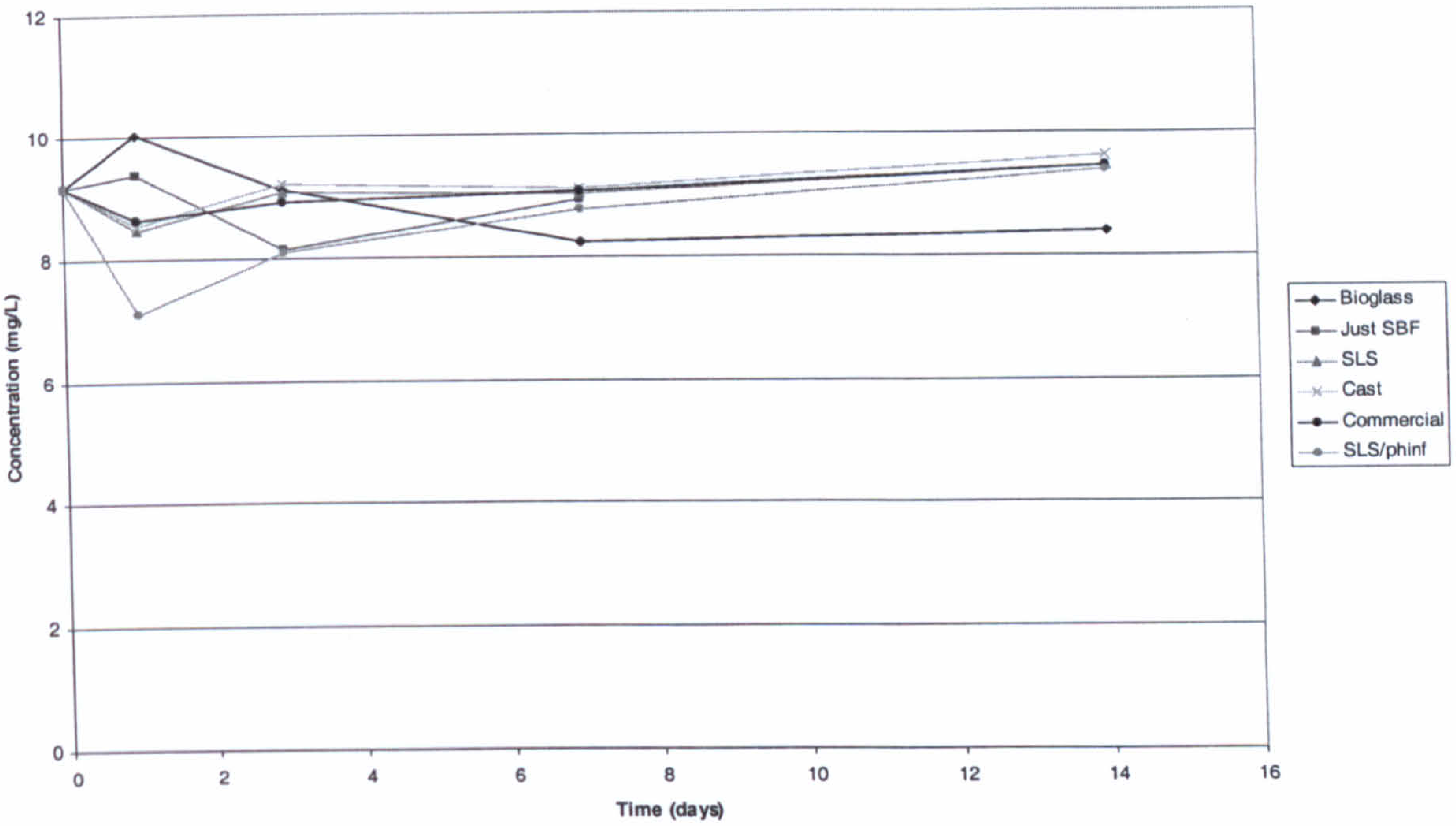

Figure 6.2.5.2 C: Change in concentration of Ca ions in SBF following soaking of test materials for various time periods.

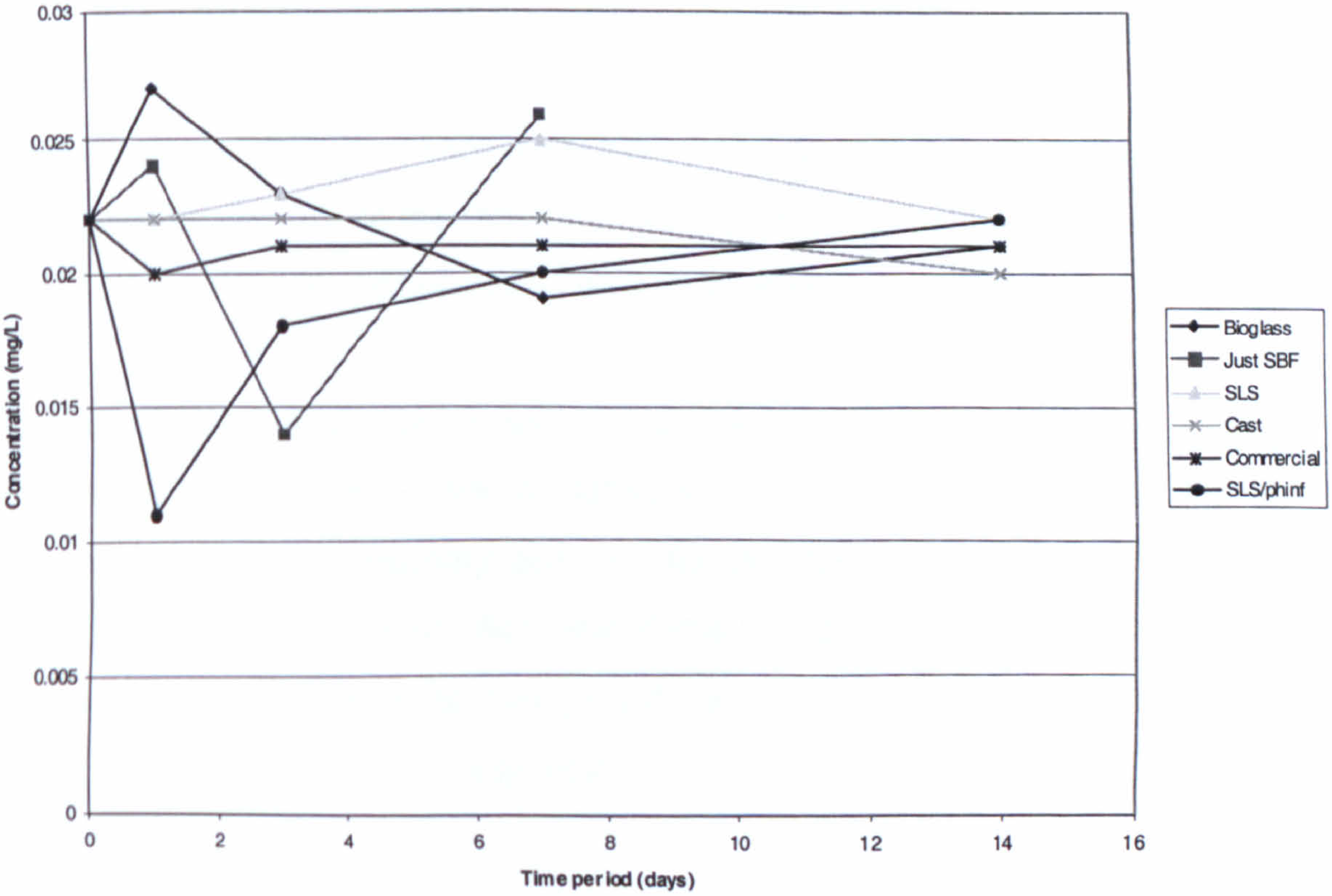

Figure 6.2.5.2 D: Change in concentration of Al ions in SBF following soaking of test materials for various time periods.

the formation of a new phase on the material surface. Taking into account the TF-XRD data, this layer is presumed to be calcium phosphate, but its composition will be confirmed later by EDX. The concentration of silicon ions in the solution shows a rapid increase upon soaking, attributed to the release of silicate ions dissolved from the glass. The concentration of calcium ions does not exhibit such an obvious increase or decrease. When a bioactive glass is soaked in SBF the variations that occur in the ionic concentrations in the solution are as a result of two opposite processes – the leaching of ions from the glass to the SBF, which increases the calcium and silicon concentrations, and the formation and growth of a calcium phosphate layer, which decreases the calcium and phosphorus concentrations in solution. Therefore a change in the concentration of calcium ions in the solution will not necessarily be detected as the two processes have opposite effects for this ion. These results are similar to those obtained previously for Bioglass®-type glass following soaking in SBF and thus the validity of the positive control can be confirmed.

Dissolution of silicate ions or a decrease in P concentration did not occur in any of the other materials. There was no change in the concentrations of any of the elements measured in SBF following soaking of the cast, laser sintered or phosphate infiltrated A-M samples, consistent with the SBF incubated with no material in it, and the SBF containing the non-bioactive commercial glass. The latter two solutions, along with the positive control, confirmed the validity of the experiment. These results provide further evidence that LDIG105 cannot exhibit bioactive behaviour *in vitro.*

The concentration of aluminium ions in solution was measured since the A-M glass includes Al_20_3, and as Al^3+ ions are toxic, it is of major importance in this study to ensure that they are not leaching into the solution. However as you can see in Figure 6.2.5.2D, the concentration of aluminium remained constant, and below 0.03mg/L for all materials and thus, over the time period measured, the leaching of Al^{3+} ions from LDIG105 does not appear to be a problem.

6.2.5.3 SEM and EDX

SEM micrographs and EDX profiles of the surface of Bioglass®-type glass before and after soaking in SBF for one, three and seven days are shown in Figures 6.2.5.3A-D.

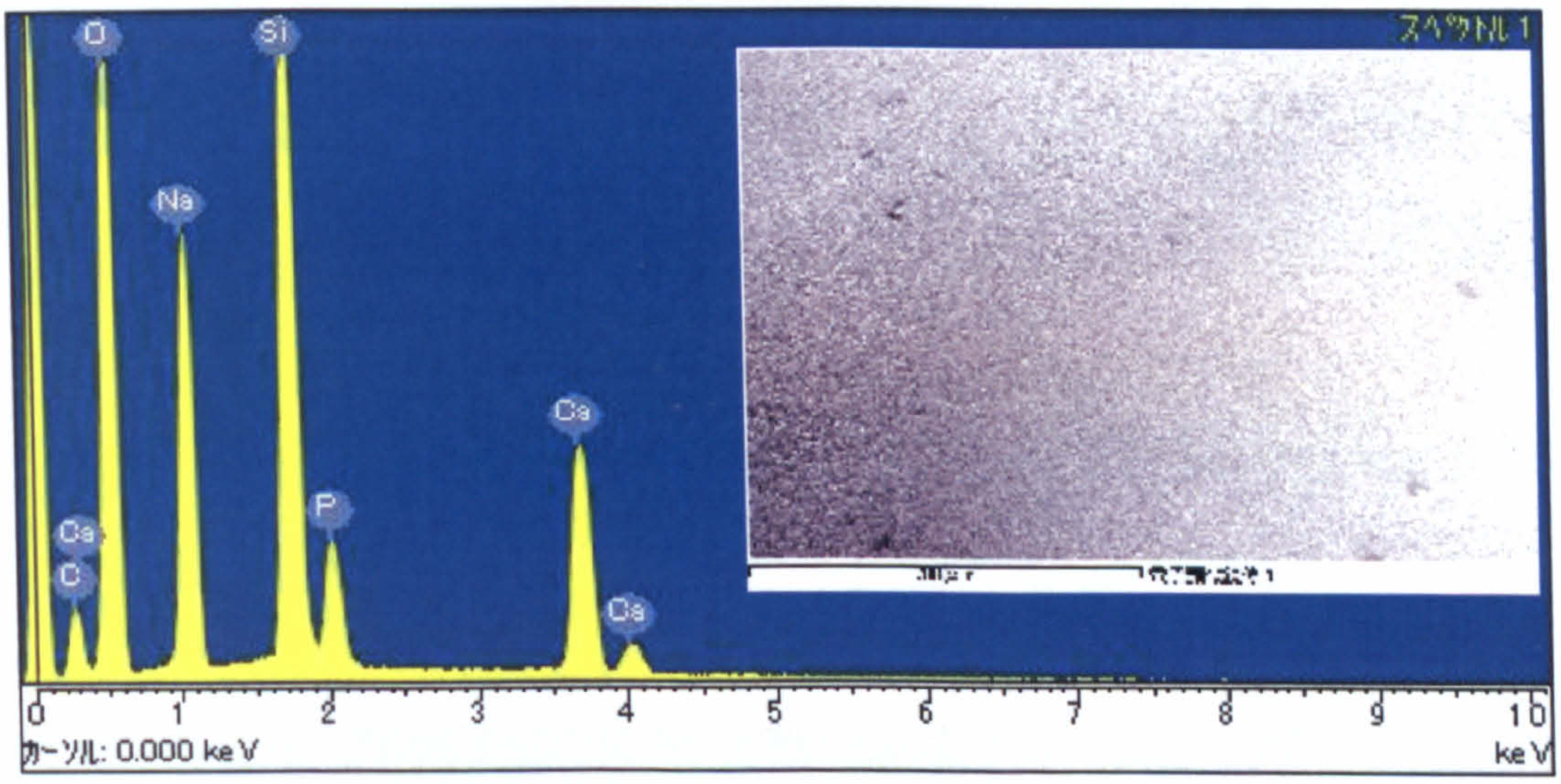

Figure 6.2.5.3 A: SEM micrograph and EDX profile for Bioglass®-type glass before soaking in SBF

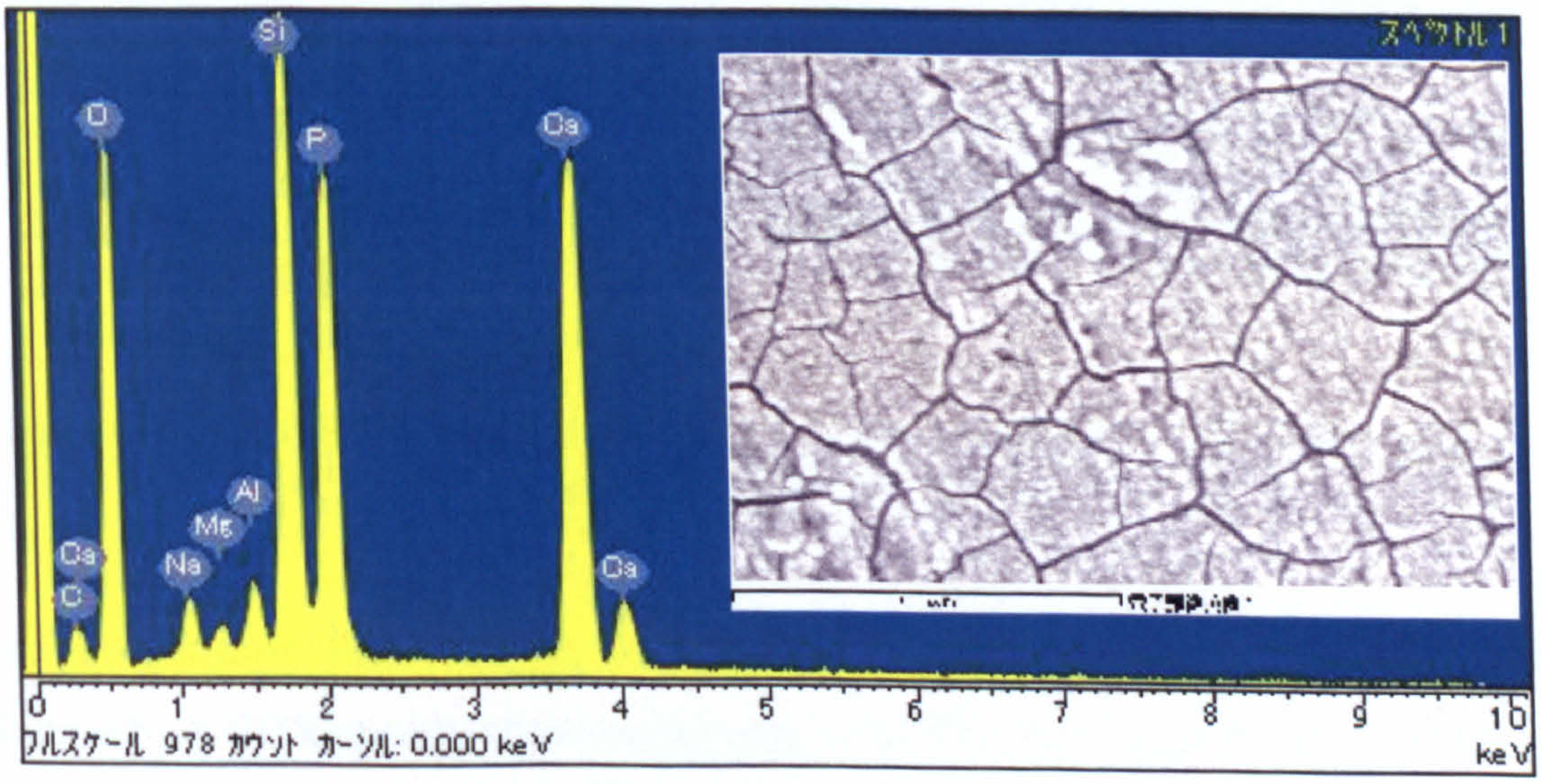

Figure 6.2.5.3 B: SEM micrograph and EDX profile for Bioglass®-type glass after soaking in SBF for 1 day

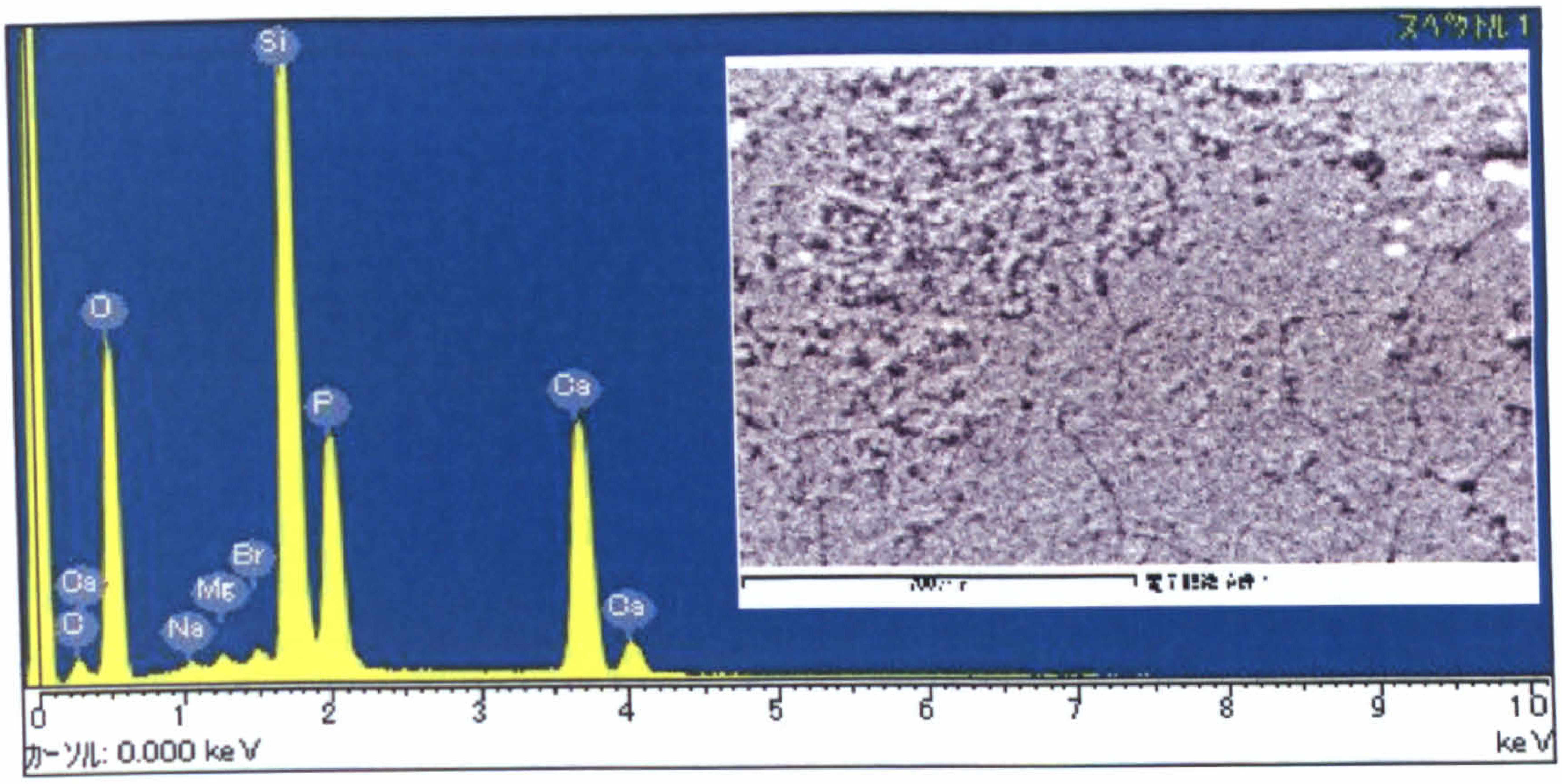

Figure 6.2.5.3 C: SEM micrograph and EDX profile for Bioglass®-type glass after soaking in SBF for 3 days

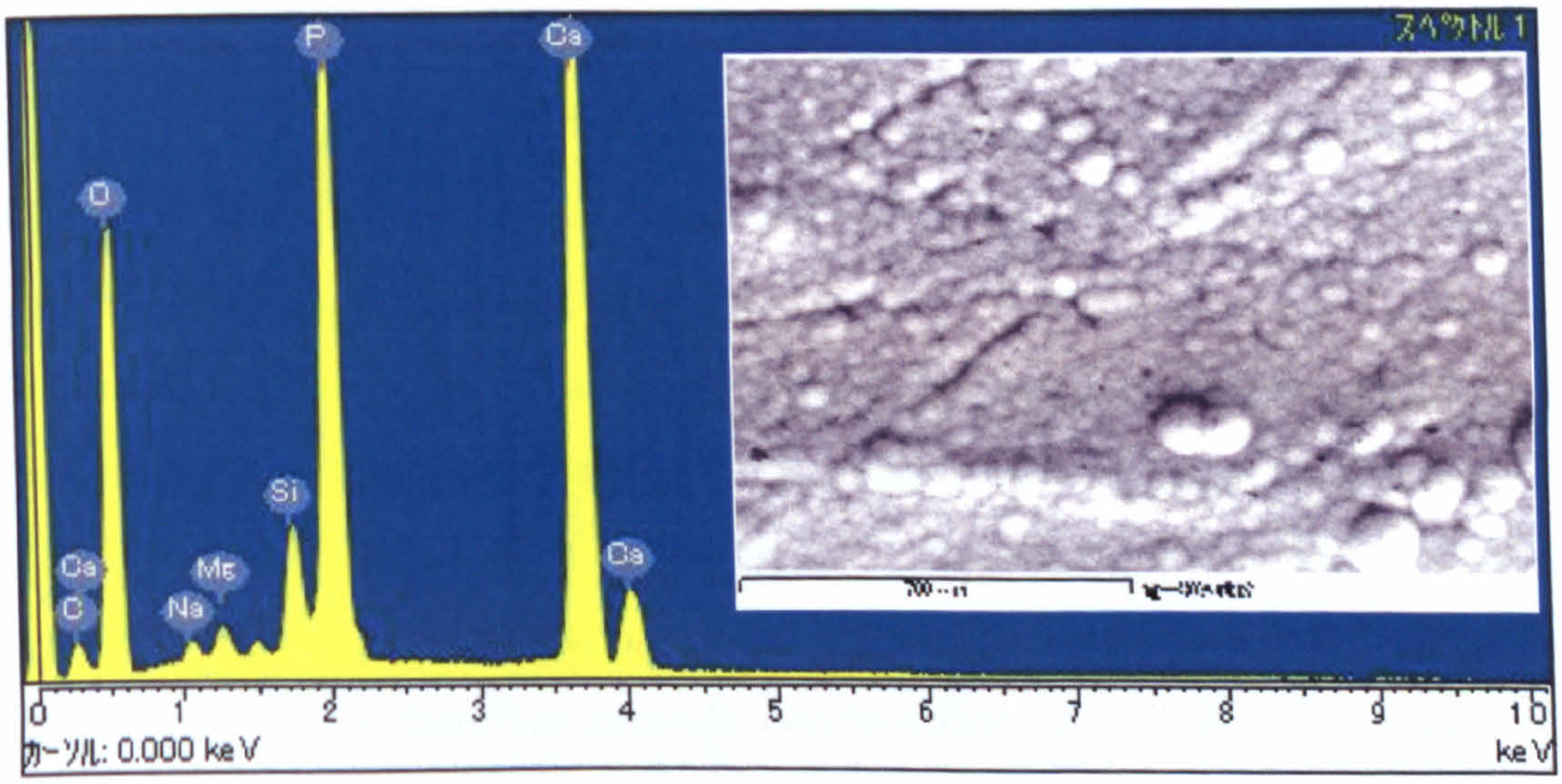

Figure 6.2.5.3 D: SEM micrograph and EDX profile for Bioglass®-type glass after soaking in SBF for 7 days

These images show the formation of a layer on the material surface after three days of soaking which EDX spectra shows to be rich in Si. This corresponds to the first stage in the formation of an apatite layer where a silica hydrogel layer is formed which induces the nucleation of apatite. This layer can be seen more clearly in Figure 6.2.5.3E, where it can be seen to be evenly covering the entire sample.

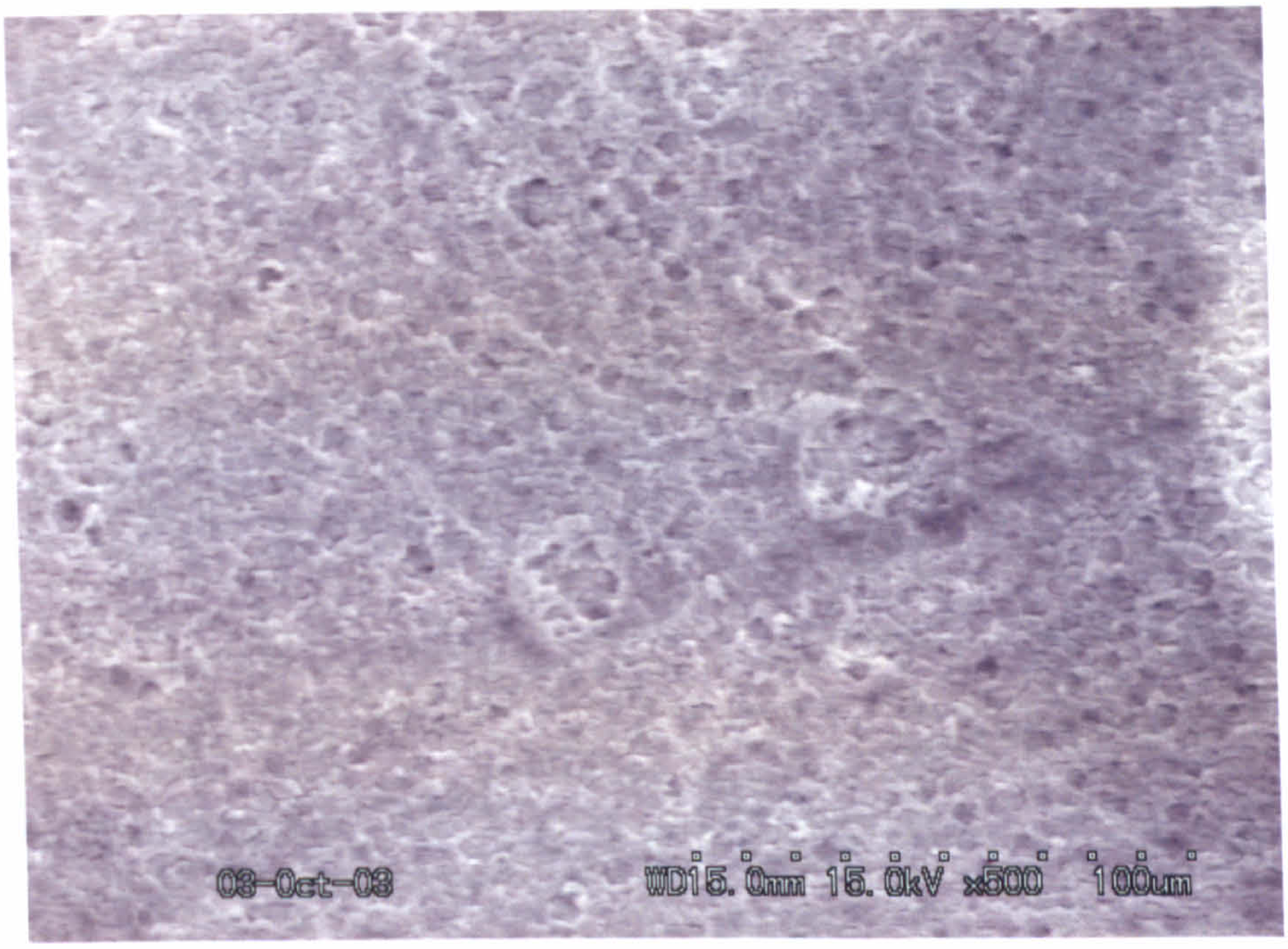

Figure 6.2.5.3 E: SEM micrograph of the surface of Bioglass®-type glass after 3 days of soaking in SBF

After 7 days of soaking, the EDX spectrum of the surface of Bioglass®-type glass shows a large increase in the concentrations of Ca and P, together with a significant decrease in Si – Figure 6.2.5.3D. SEM micrographs of this layer allow one to confirm the formation of a new type of layer constituted by spherical particles, which coat the entire surface of the material, as shown in Figure 6.2.5.3F. The morphology of the particles is very similar to that of apatite typically formed on the surface of Bioglass®-type glass, which is very similar in composition and structure to that of biological apatites. These results therefore provide confirmation of the bioactive nature of this material *in vitro.*

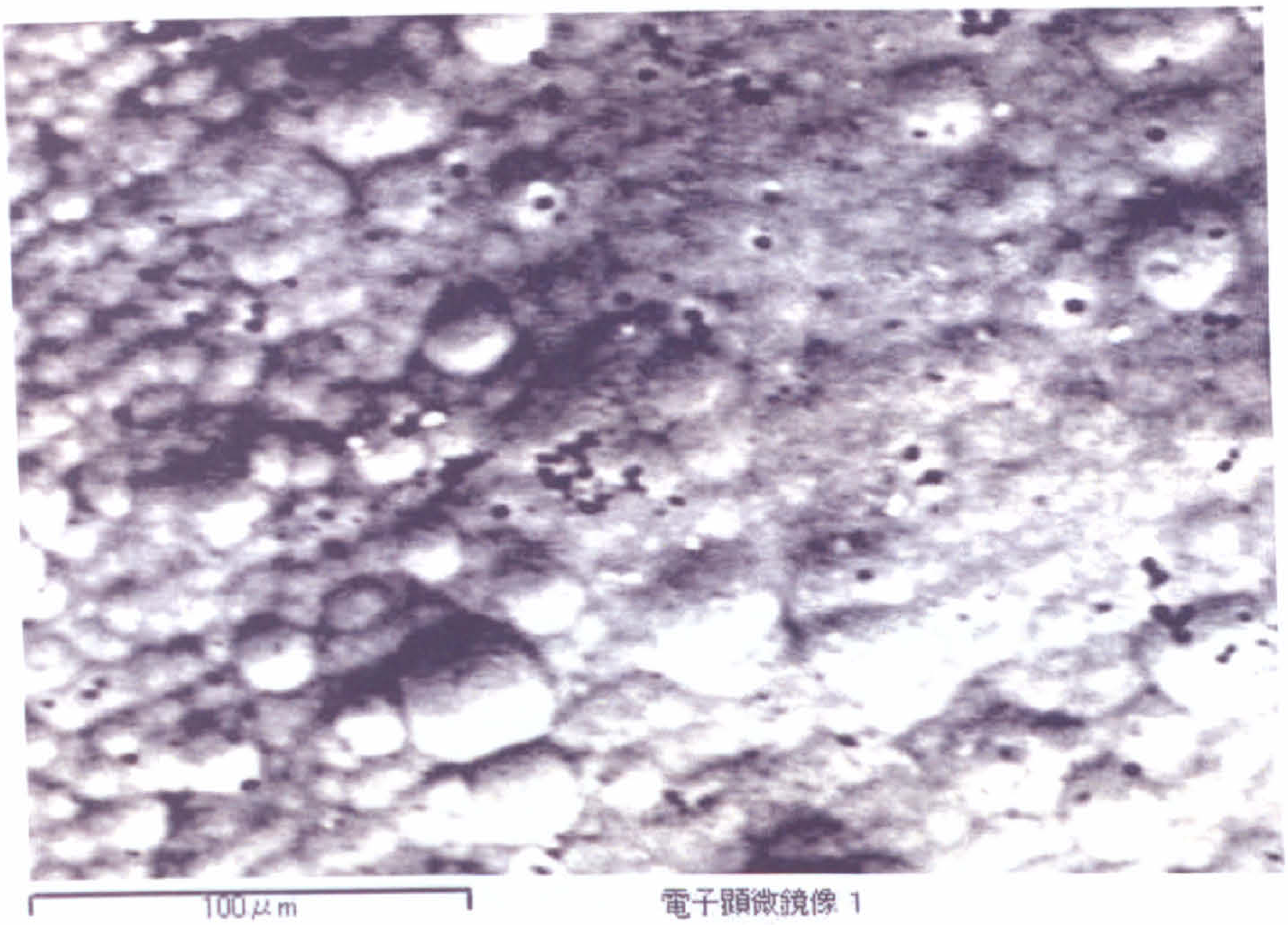

Figure 6.2.5.3 F: SEM micrograph of the surface of Bioglass®-type glass after 7 days of soaking in SBF

The SEM micrograph and EDX profiles for the commercial glass after 14 days of soaking in SBF are shown in Figure 6.2.5.3G. These were identical to those taken before soaking and at each of the other different time periods, it can be concluded that this material does not form an apatite layer *in vitro,* and thus combined with the positive control this result confirms the validity of the experiment.

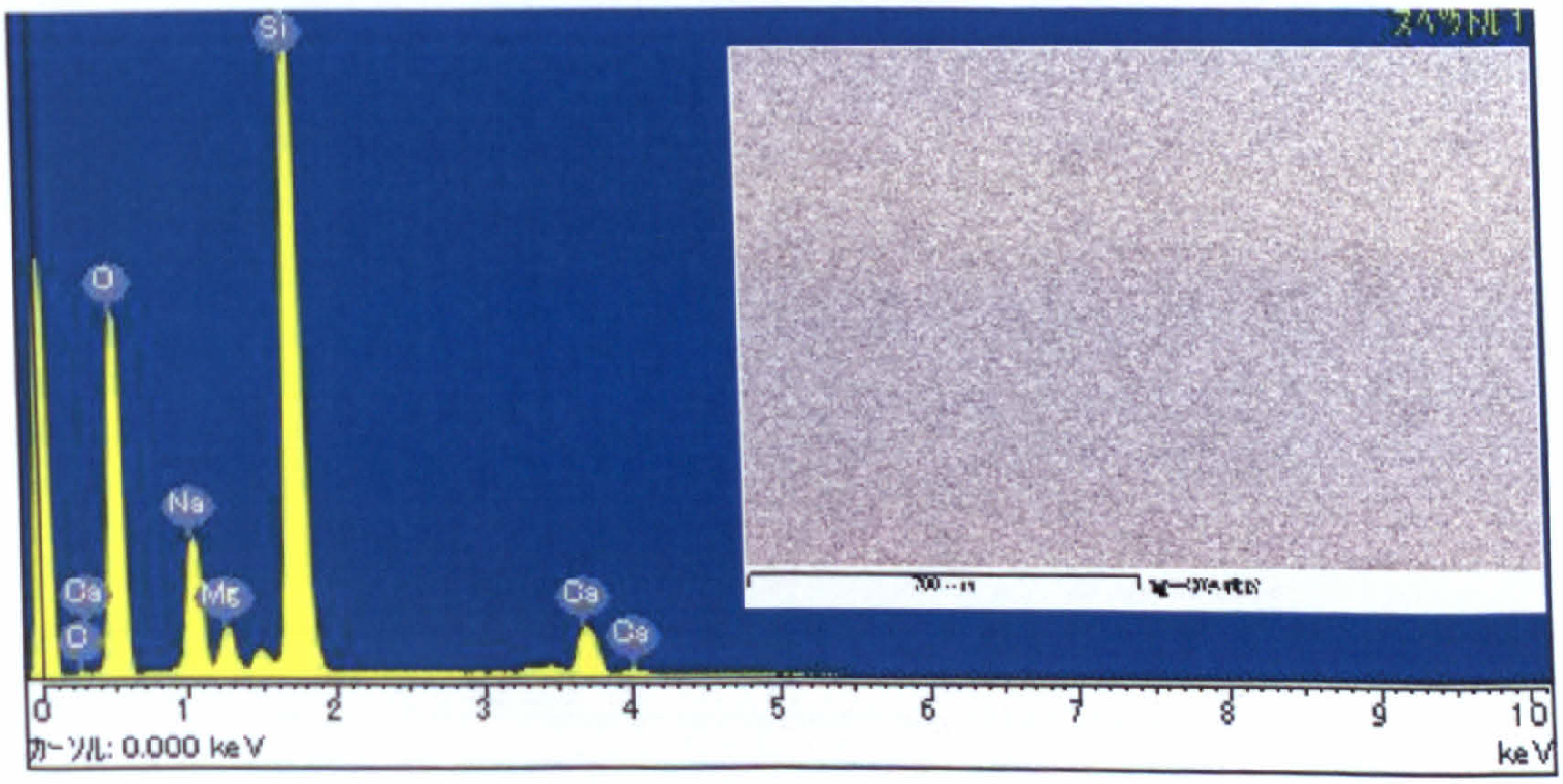

Figure 6.2.5.3 G: SEM micrograph and EDX profile for the commercial glass after soaking in SBF for 14 days

Similarly, there was no evidence of any layer forming on the A-M samples produced by either conventional casting or SLS. The SEM micrographs/EDX profiles for the two materials after 14 days are shown in Figures 6.2.5.3H and 6.2.5.3I respectively, and are identical to those taken before soaking and at each of the different time periods. This is particularly evident in the SEM micrograph of the cast A-M sample where scratches can still be seen on the surface of the material which would not be evident through any formed layer.

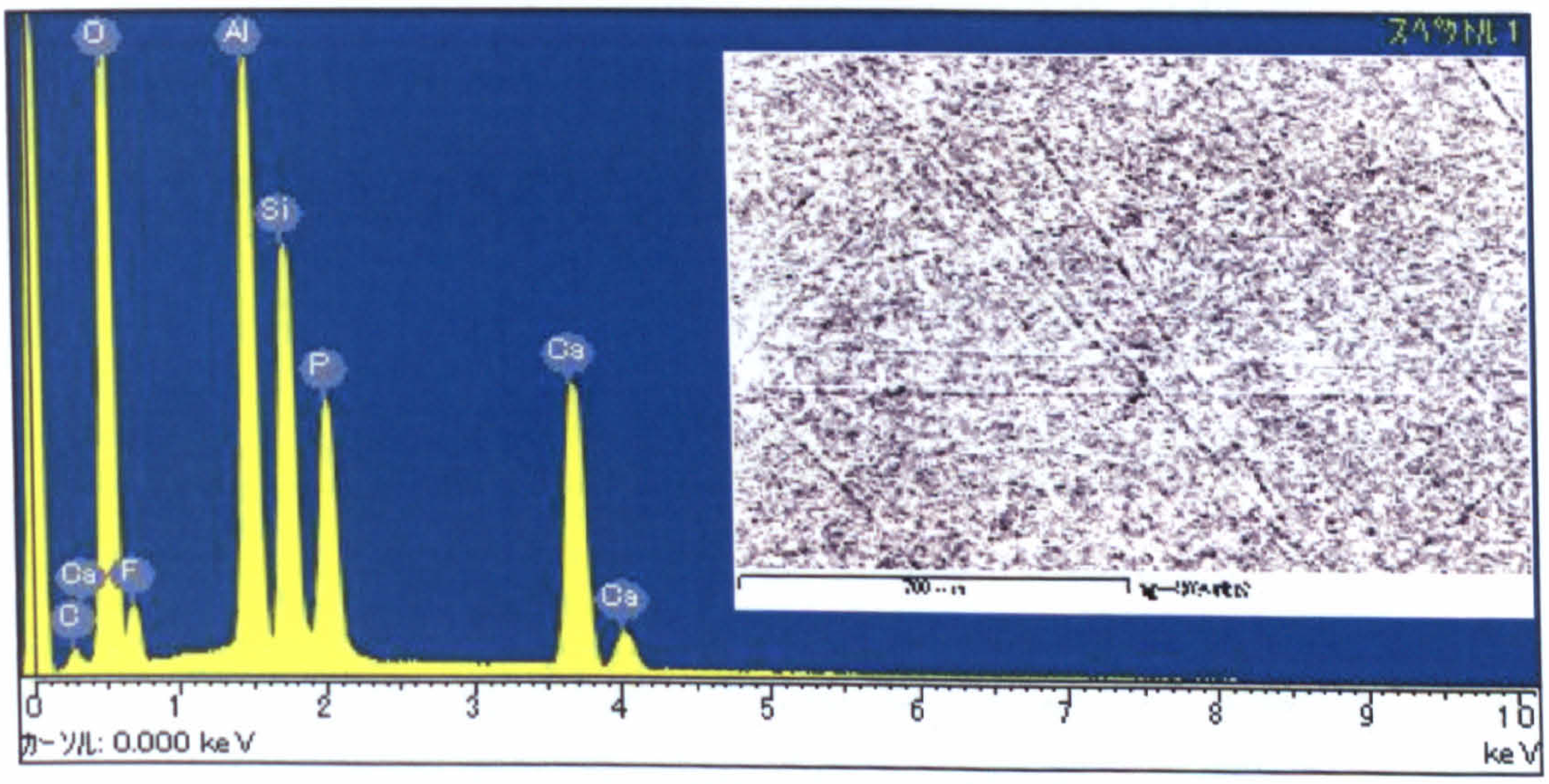

Figure 6.2.5.3 H: SEM micrograph and EDX profile for cast LDIG105 after soaking in SBF for 14 days

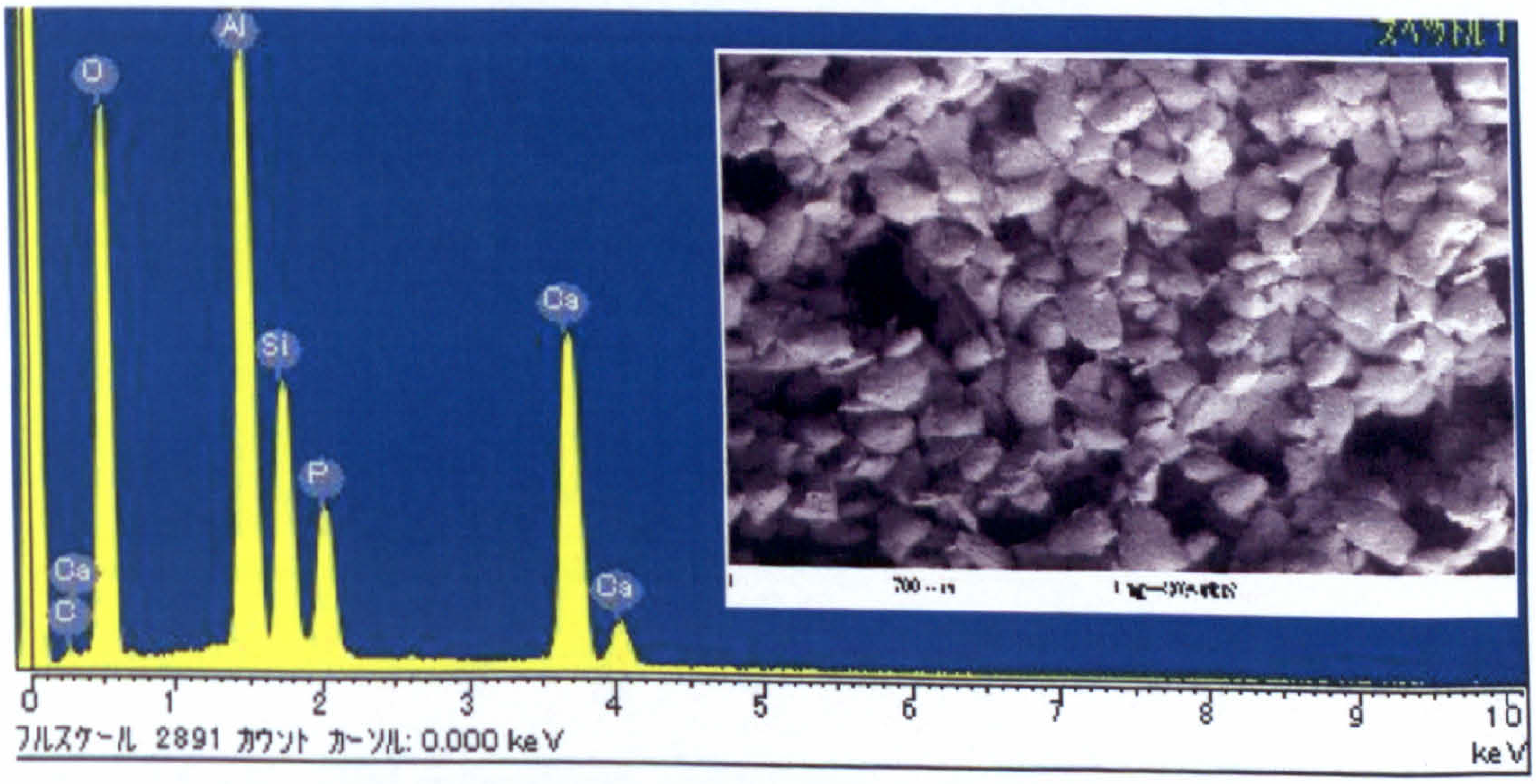

Figure 6.2.5.3 I: SEM micrograph and EDX profile for LDIG105 produced by SLS after soaking in SBF for 14 days

However changes were detected by SEM and EDX in the surface of LDIG105 produced by SLS and infiltrated with phosphate glass. Figure 6.2.5.3J shows the SEM micrograph and EDX profile for this material before soaking in SBF, which can be compared to those taken after soaking for 14 days, shown in Figure 6.2.5.3K.

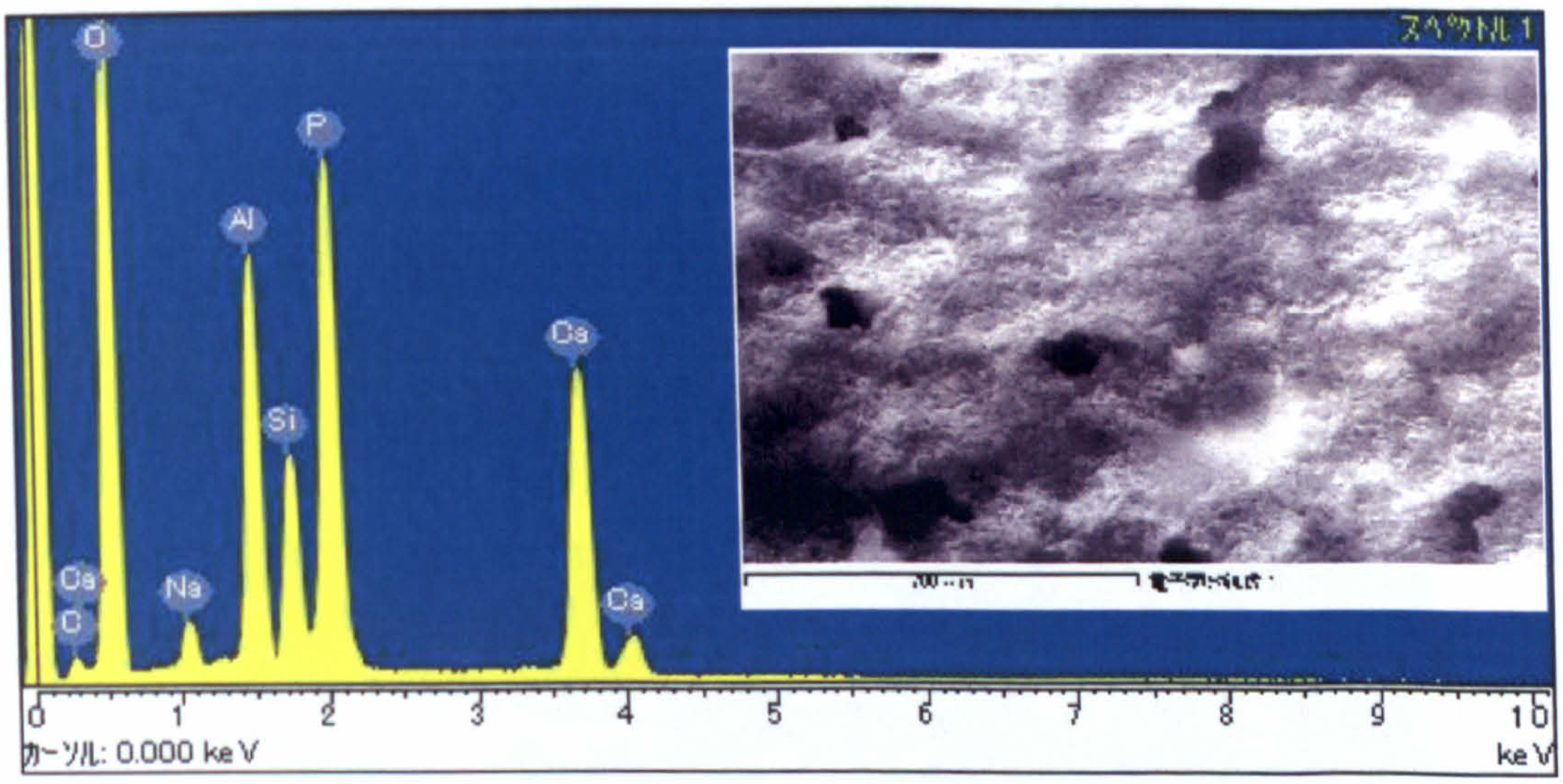

Figure 6.2.5.3 J: SEM micrograph and EDX profile for LDIG105 produced by SLS and infiltrated with phosphate glass before soaking in SBF

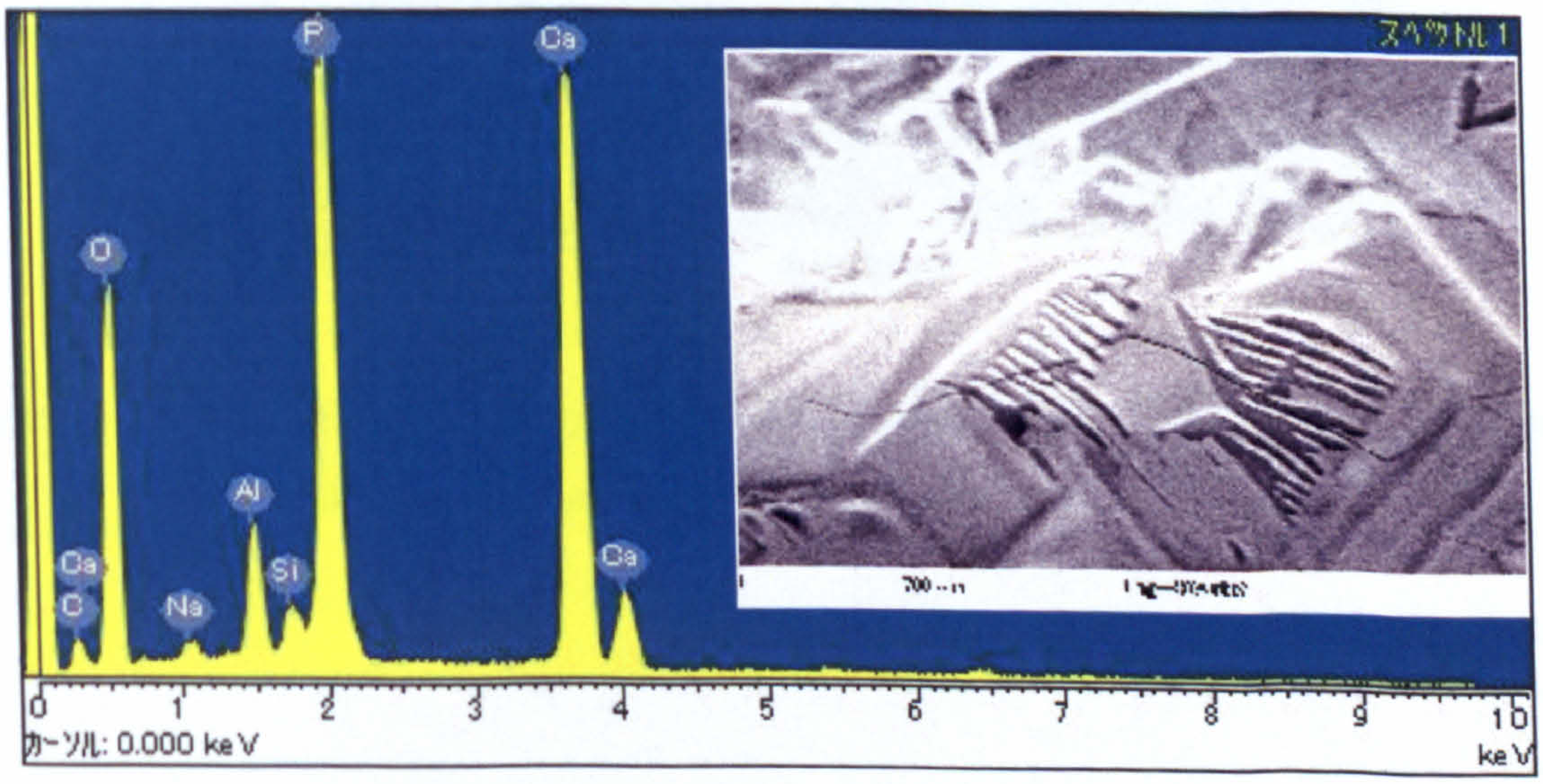

Figure 6.2.5.3 K: SEM micrograph and EDX profile for LDIG105 produced by SLS and infiltrated with phosphate glass after soaking in SBF for 14 days

These images show the formation of a layer on the material surface after soaking in SBF for 14 days which EDX shows to be rich in calcium and phosphate. Whilst this indicates the formation of a calcium phosphate layer, its morphology is quite different to that of the crystalline apatite usually seen after soaking bioactive materials in SBF. The CaP layer also did not cover the whole surface, but was present in small patches. The SEM micrograph in Figure 6.2.5.3L was taken after soaking the material for a longer period of 30 days. This image shows a very different microstructure to that observed before soaking in SBF. EDX analysis of the area reveals a significant decrease in Si compared to the pre-soaked material which appears to suggest corrosion of the glass phase of the material is occuring – see Figure 6.2.5.3M.

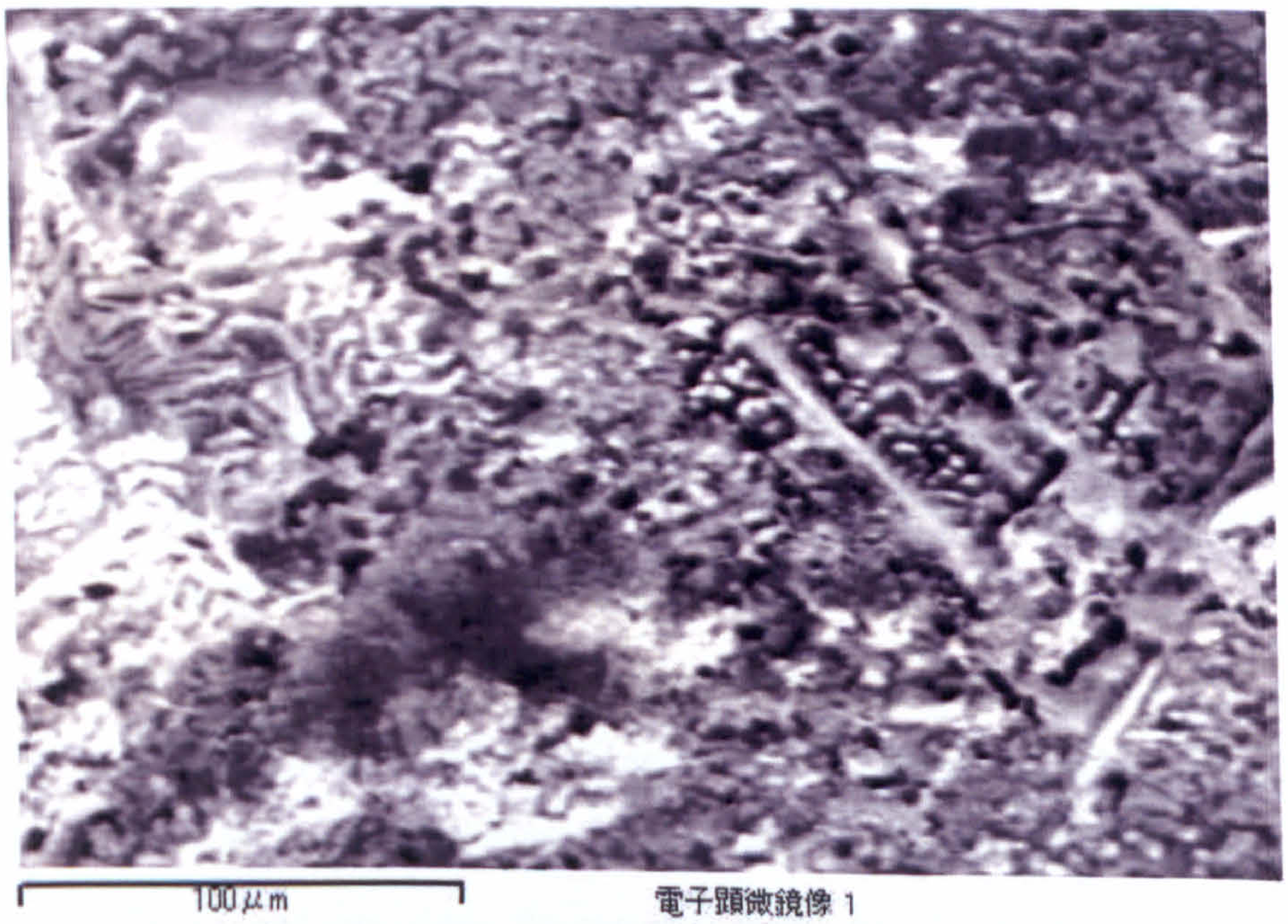

Figure 6.2.5.3 L: SEM micrograph of LDIG105 produced by SLS and infiltrated with phosphate glass after soaking in SBF for 30 days

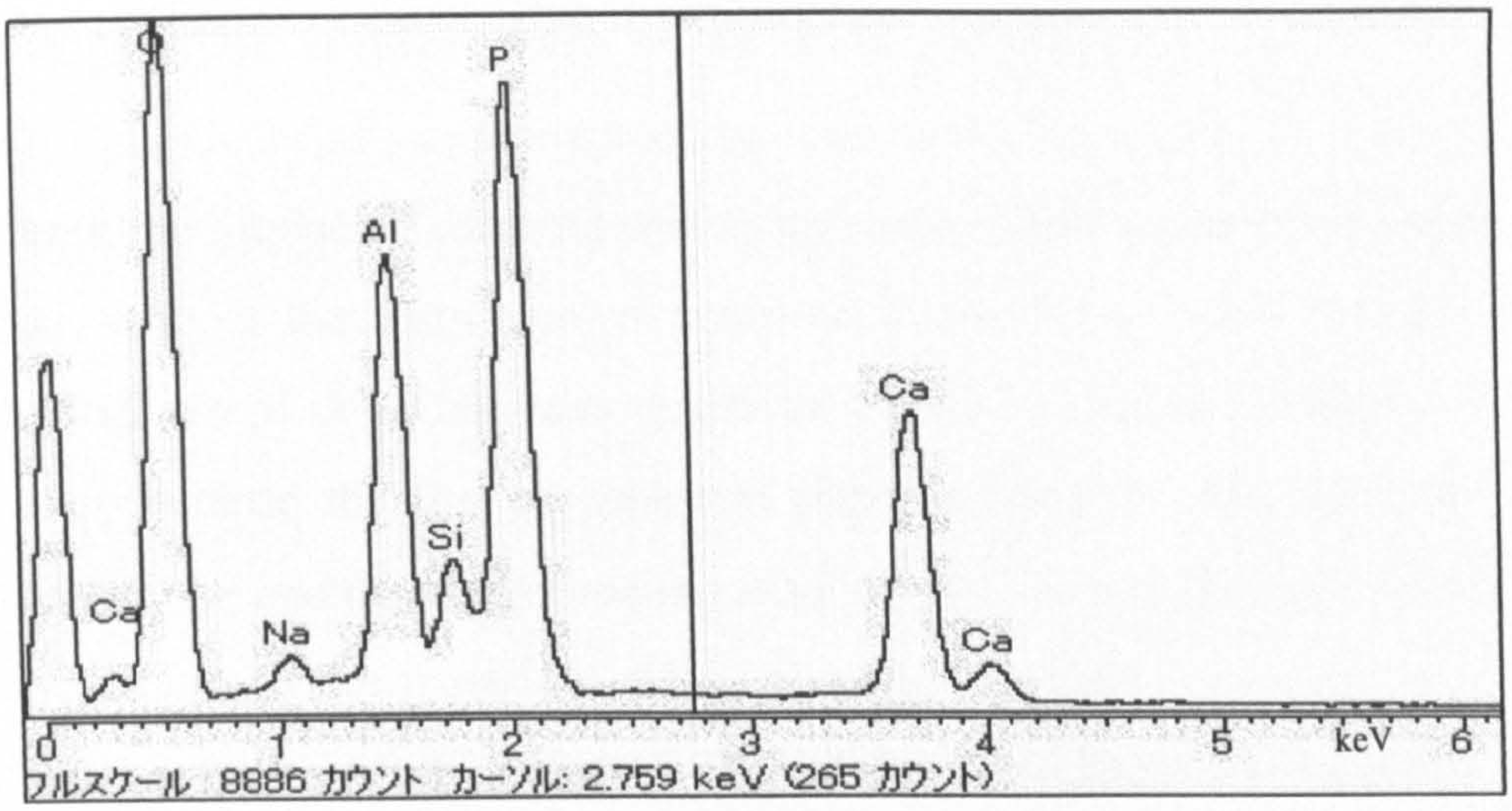

Figure 6.2.5.3 M: EDX profile for LDIG105 produced by SLS and infiltrated with phosphate glass after soaking in SBF for 14 days

The combination of all these results provided confirmation that an apatite layer had formed on the surface of Bioglass®-type glass which was similar in composition, crystallinity and structure to that typically present on this material after soaking in SBF. This layer is very similar to that of biological apatite, and thus has good potential to exhibit bioactive behaviour *in vivo*. Neither LDIG105 produced by casting or by SLS however showed any signs of forming this layer within the time period of the experiments suggesting that it is unlikely that this material would prove bioactive *in vivo*. Apatite formation on glasses and glass-ceramics is induced by dissolution of calcium ions and by formation of silica gel layers. The dissolution of calcium ions increases the degree of supersaturation of the surrounding body fluid with respect to hydroxyapatite. Silica gel provides favourable sites for heterogeneous nucleation on their surfaces. The results of the ICP analysis in this study demonstrated that dissolution of LDIG105 was considerably less than that of Bioglass®-type glass. Therefore, the reduced rate of apatite formation is attributed to the reduction in dissolution of LDIG105 in SBF. It is possible that this is due to the presence of Al_2O_3 in the starting composition, which is well known as a component which can increase the chemical durability of glasses [Paul, 1977]. It has previously been demonstrated that even a small addition of Al_2O_3 to glass compositions suppresses the bioactivity of glasses and glass-ceramics, by suppressing the dissolution of the Ca and Si ions from the material and thus the formation of an apatite layer on their surfaces in the body [Ohtsuki *et al.*, 1992].

However a previous *in vivo* study of an A-M glass-ceramic based on the same $SiO_2 \cdot Al_2O_3 \cdot P_2O_5 \cdot CaO \cdot CaF_2$ composition has shown the formation of a direct physical bond between the implanted material and surrounding bone tissue when implanted into a rat femur, without the formation of a fibrous tissue layer – see Chapter 2.2.6.2.2. Whilst the formula of this glass was modified slightly to make LDIG105, the change made was to increase the fluorine content, altering the Ca:P ratio to 1.56, which is closer to that of the apatite stoichiometric value of 1.67. It was thought that this change would have increased the materials ability to exhibit bioactive behaviour, rather than reduce it, as the *in vitro* study suggests. Therefore it was decided to perform an animal study to determine whether bioactive behaviour could be detected *in vivo*.

6.3 *In vivo* experiments

Five adult male Japanese white rabbits, each weighing around 20kg, were used for the study to assess the potential of LDIG105 to exhibit bioactive nature *in vivo*. They were reared at the Laboratory Animal Center, Nara Institute of Science and Technology (NAIST), Japan, where the experiments also took place. The guidelines for animal experimentation at NAIST [NAIST, 2003], were observed.

6.3.1 Sample Preparation

The materials used for the animal study were prepared as follows:

Apatite-Mullite glass-ceramic produced by SLS

Cylindrical samples 4mm in diameter and 10mm in length were produced using the method described in Section 4.3. A laser speed of 250mm/sec, laser power of 100W, scan line overlap of ½ the beam diameter and layer overlap of 0.25mm was used to produce the green part. The samples were post-processed using post-processing route D.

Apatite-Mullite glass-ceramic produced by conventional casting.

Cylindrical samples 4mm in diameter and approximately 10mm in length were produced by conventional casting used the method described in Chapter 3.4.1.

Commercially Produced Apatite-Wollastonite (Cerabone®)

An A-W glass-ceramic, commercially produced under the trade name Cerabone® and supplied by Nippon Electric Glass Co, Ltd, was formed into cylindrical samples of approximately 4mm in diameter and 10mm in length using grinding paper.

6.3.2 Surgical procedure

The samples were implanted using strict aseptic surgical techniques and ordinary sterile preparation (heating at 180°C for 3 hours). General anaesthesia was performed by intravenous injection of 50mg/ml sodium pentobarbital solution, and local anaesthesia administrated by subcutaneous injection of 1% lidocaine solution (Xylocaine®). Incision sites were shaved, cleaned, and disinfected. A longitudinal incision was made in the area of the rabbit's tibia on the anterior surface, extending from about 10mm below the knee joint for a distance of around 25mm. Superficial fascia and periosteal membrane were incised using a sharp dissection, to expose the bone surface – as shown in Figure 6.3.2A. A bone defect of around 4mm in diameter was made at the medial aspect of the proximal metaphysis of the rabbit tibiae using a motorised drill.

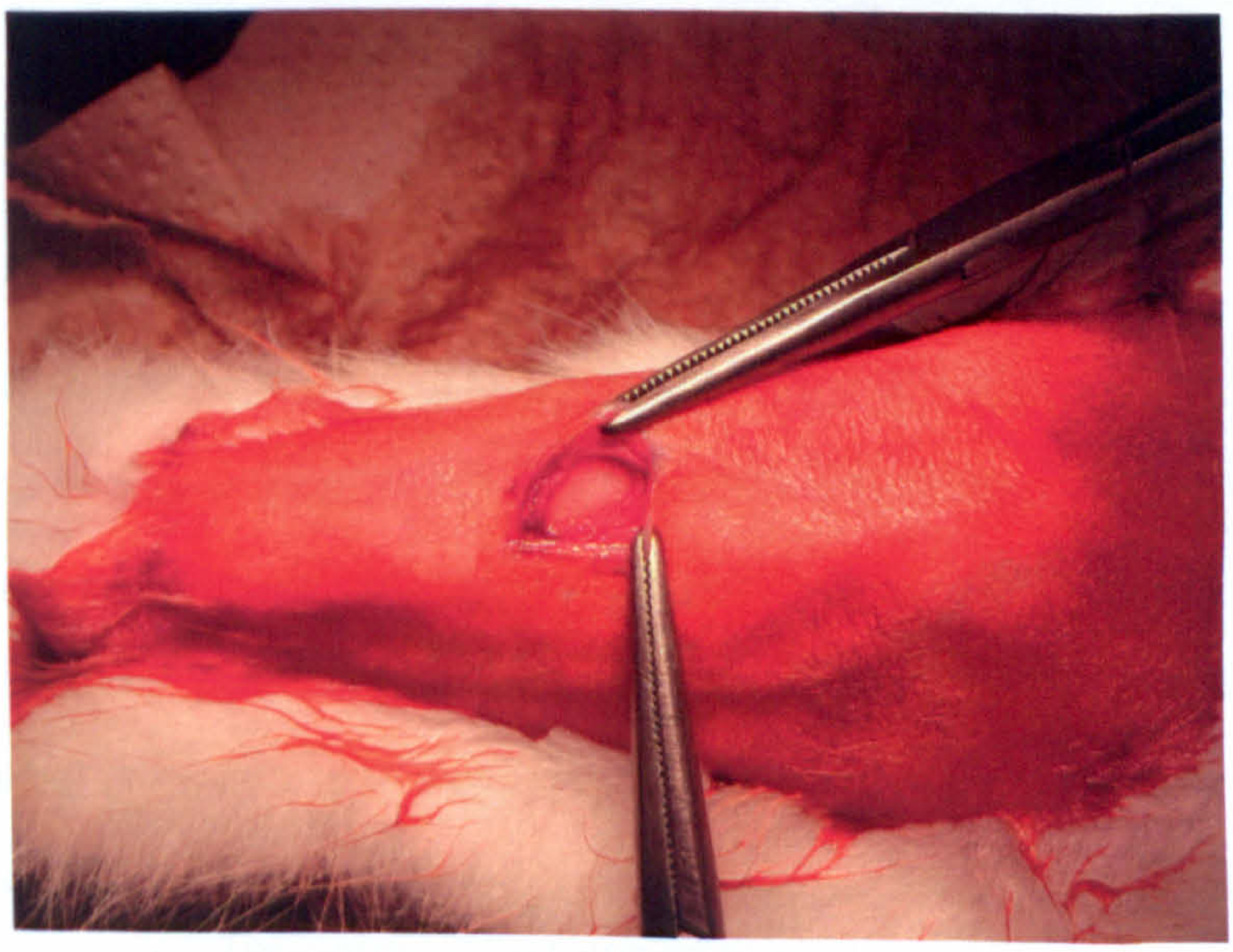

Figure 6.3.2 A: Exposure of bone surface for creation of bone defect.

The precise size of the defect was determined by the need to ensure that the gap between the implanted specimen and bone was less than 1mm. The specimens were inserted into the defects using finger pressure, before closing the skin with a nylon suture. One sample was placed in each of the rabbit's tibia, with two further samples being implanted under the skin in the rabbits back. The materials that were placed in each rabbit are listed in Table 6.3.2A. As controls, two of the defects were left to heal without any implant, denoted as "Blank". After the operation the animals were kept in standard individual cages, and were allowed to move unrestricted at all times.

Rabbit	Weight (g)	Sodium Pentbarbital solution (mL)	Leg		Back	
			Right	Left	Right	Left
No.1	1890	0.8	Blank	Cast	SLS	SLS
No.2	1789	0.8	A-W	SLS	Cast	Cast
No.3	1912	0.8	Cast	SLS	A-W	A-W
No.4	1891	0.6	Cast	SLS	SLS	SLS
No.5	1894	0.8+0.1	A-W	Blank	Cast	Cast

Table 6.3.2 A: Record of materials implanted into each rabbit

All wounds healed without complications, and none of the rabbits showed any signs of discomfort. The specimens were analysed weekly with X-ray computed tomography (X-CT; XCT Research SA+, STRATEC, Germany). After 4 weeks, the rabbits were sacrificed by excessively dosing with pentobarbital sodium solution. The implanted materials along with the surrounding bony tissues were extracted and all soft tissue was stripped from the bones - Figure 6.3.2B. No sign of inflammation or adverse tissue reaction was observed around any of the implants. The samples were fixed in 10% formaldehyde solution, then dehydrated by consecutive soaking for 1 day in each solution of a graded ethanol/water system (ethanol/water:70/30, 80/20, 90/10, 95/5, and 100/0 in mass ratio). The dried specimens were embedded in PMMA resin, cut through the centre with a micro-cutting machine (BS-300CPM, EXAKT), and the resulting surface ground with a micro-grinding machine (MG-400CSM, EXAKT). The obtained sections were observed by SEM.

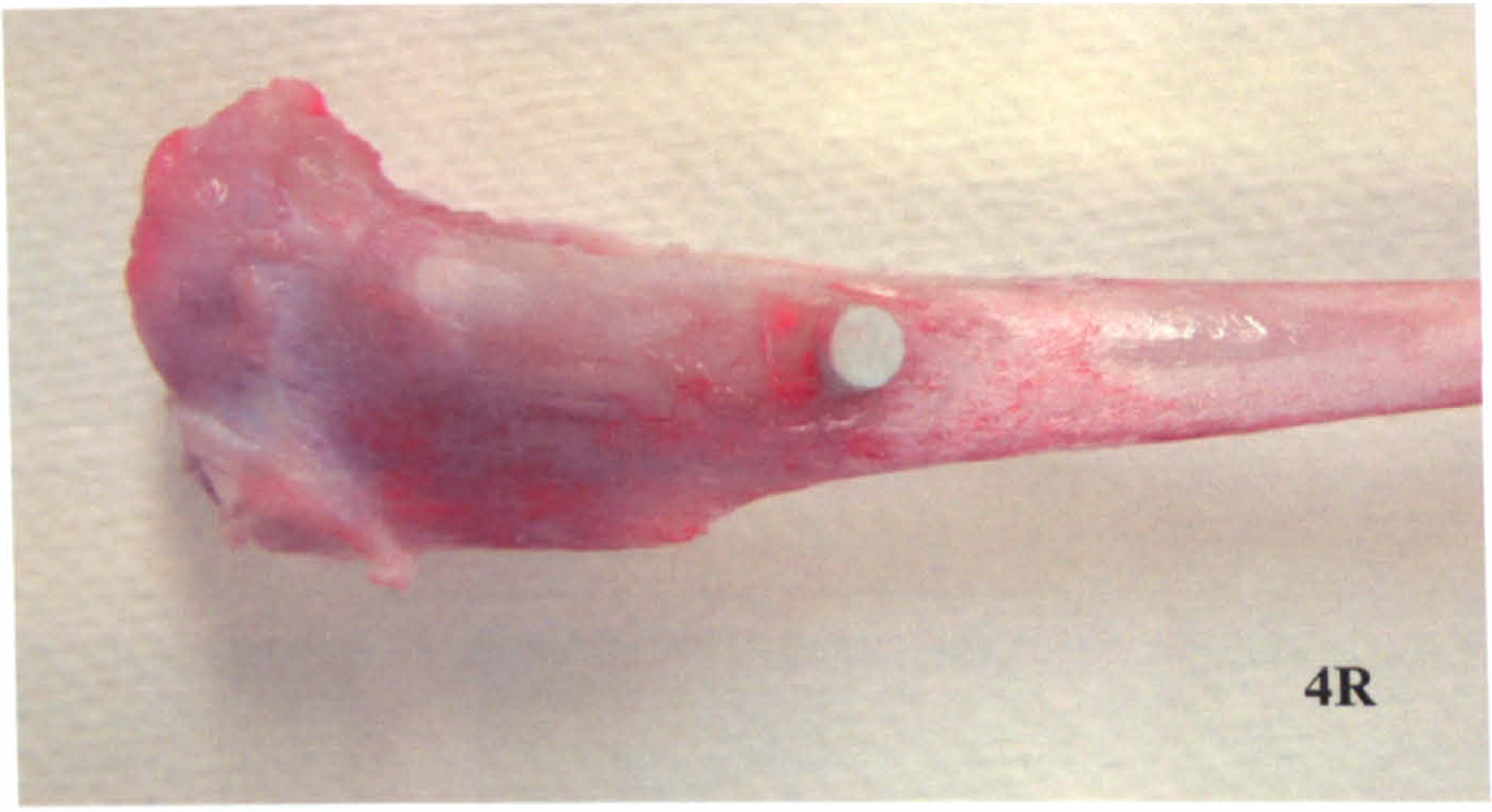

Figure 6.3.2 B: Photograph of extracted cast A-M specimen and surrounding bone

Images of the implanted materials obtained weekly by X-ray computed tomography whilst implanted in the rabbit are shown in Figures 6.3.2D-F. Progressive bone growth up to the surfaces of all three materials can be clearly seen over the four week period. These can be compared to the bone defects left unfilled as controls, which also show bone growth, but not in the same proportion as the defects that were filled with the test materials – See Figure 6.3.2C.

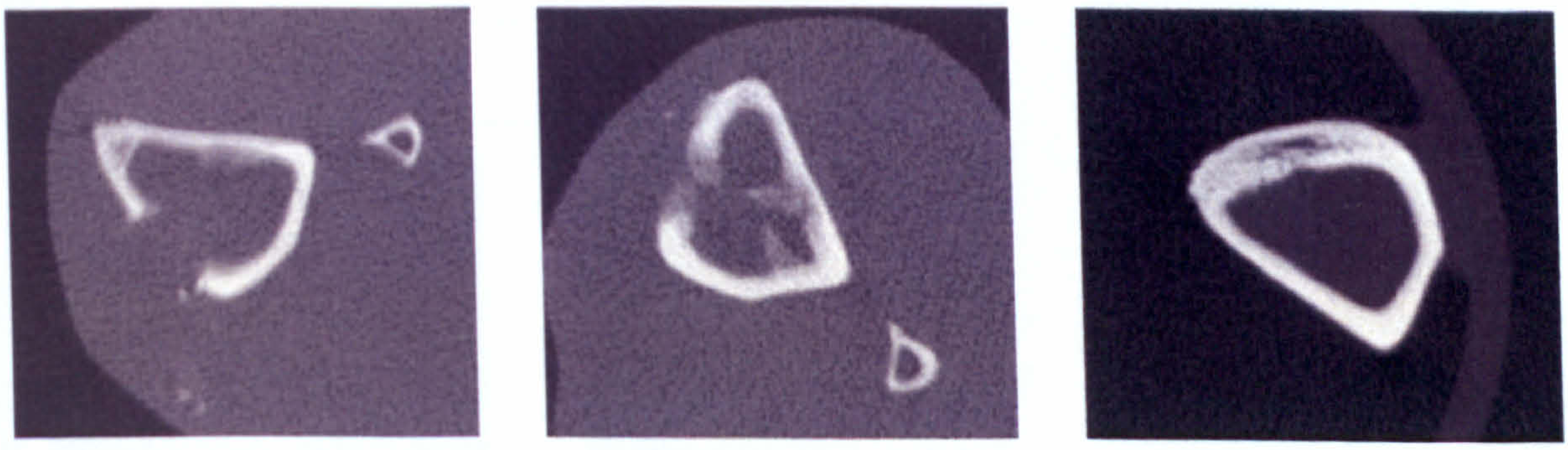

Figure 6.3.2 C: µCT images of "blank" defect 1, 2, and 4 weeks (from left to right) after implantation

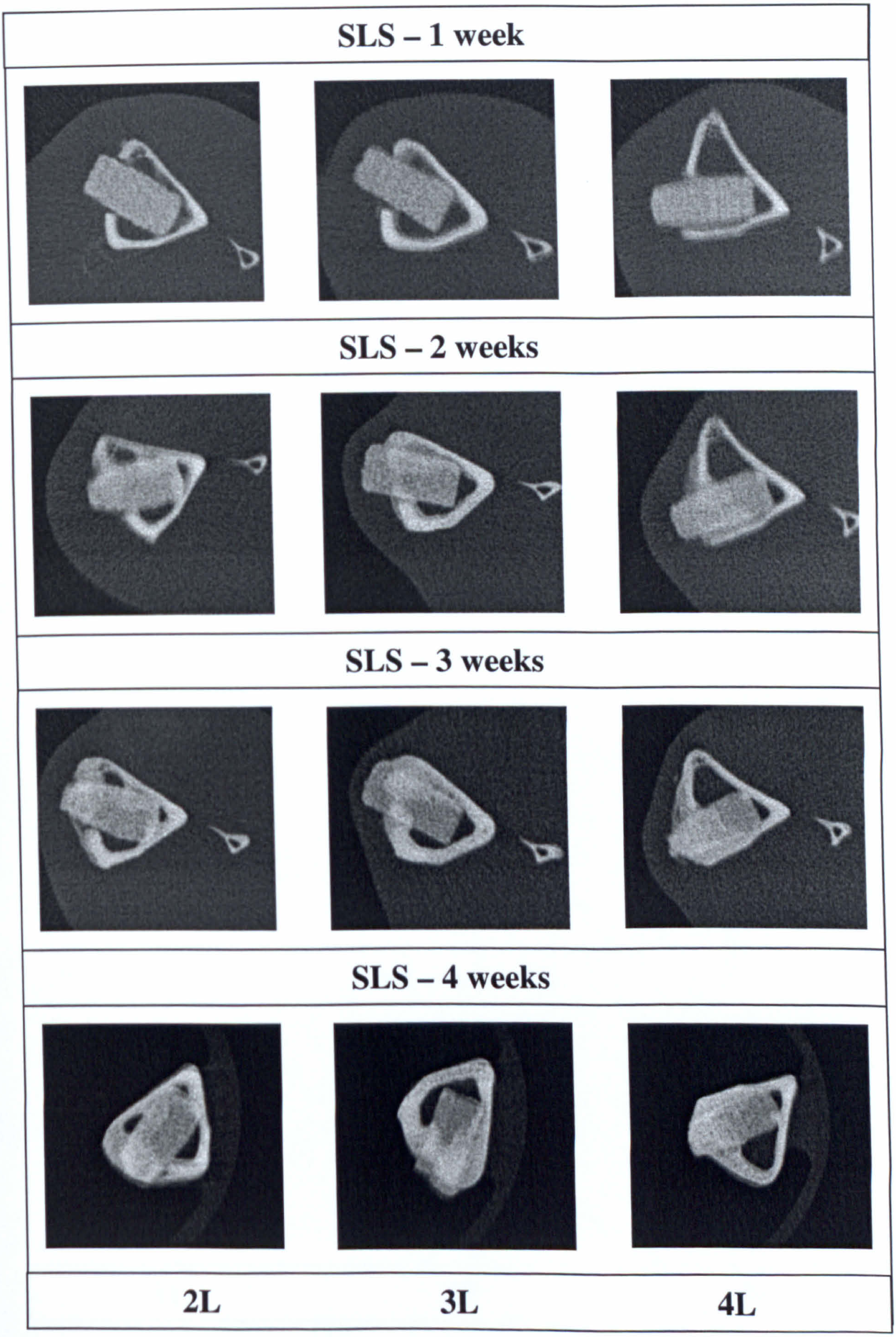

Figure 6.3.2 D: µCT images of LDIG105 produced by SLS implanted in rabbit tibia for varying time periods

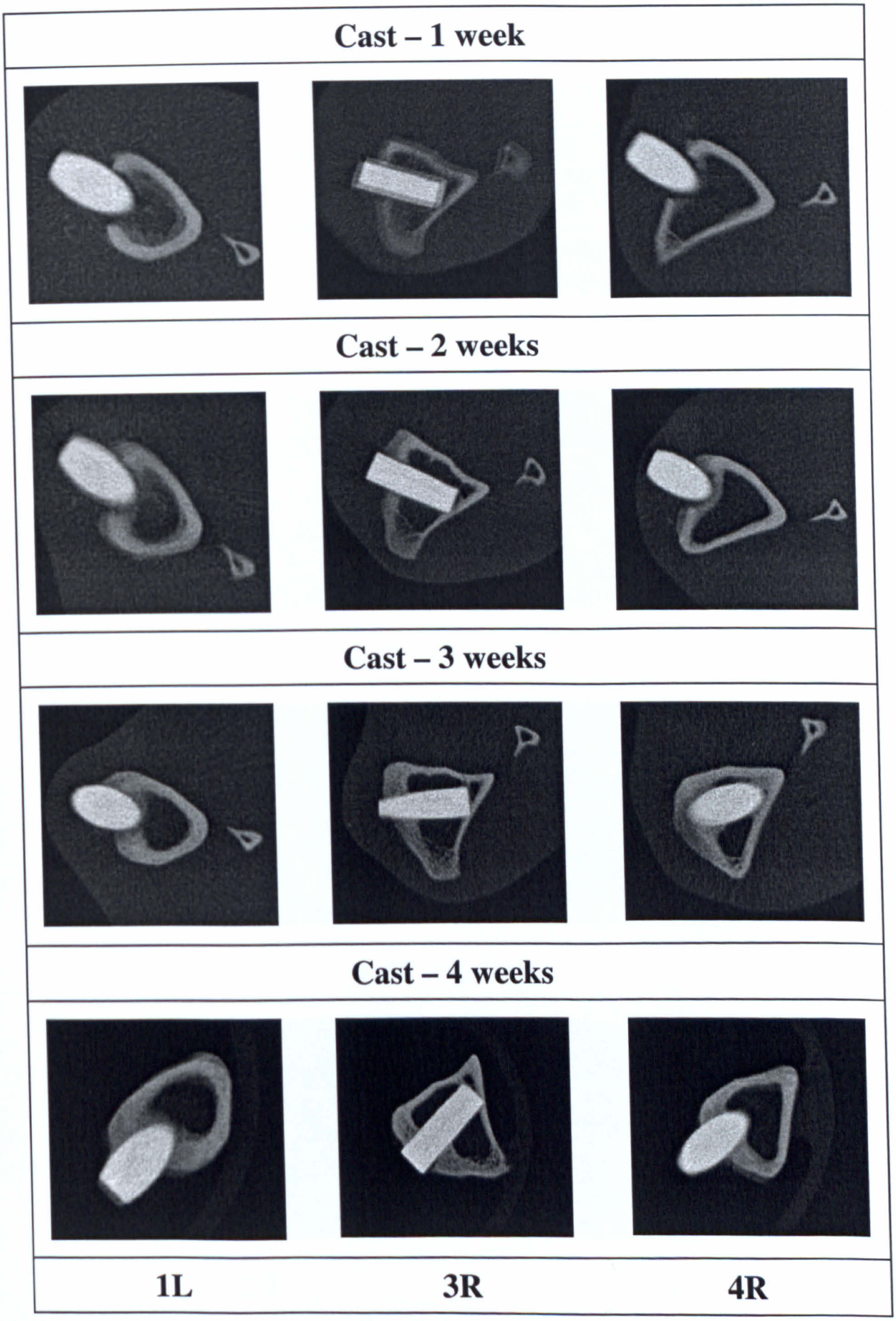

Figure 6.3.2 E: μCT images of cast LDIG105 implanted in rabbit tibia for varying time periods

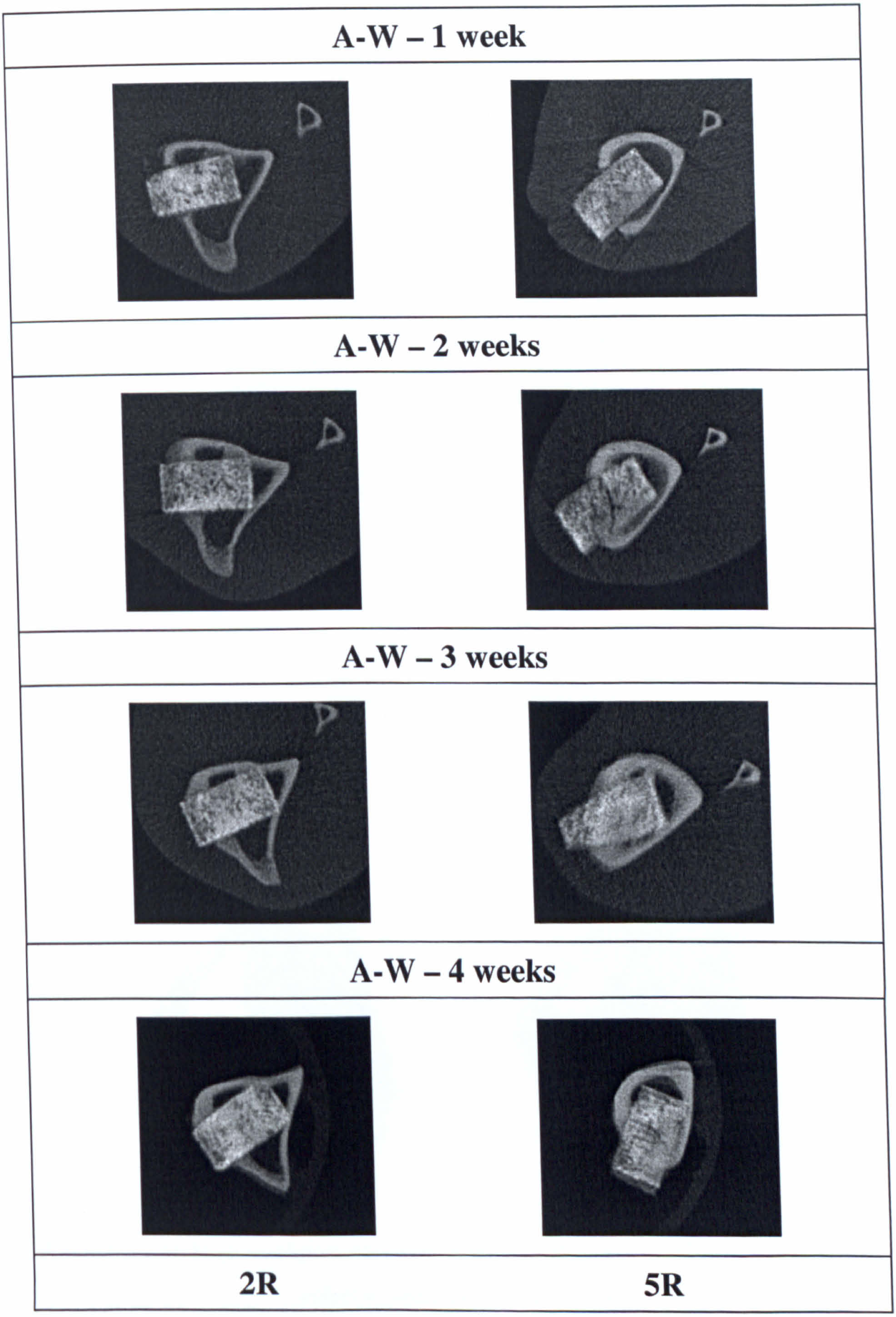

Figure 6.3.2 F: μCT images of A-W implanted in rabbit tibia for varying time periods

High resolution images of the defects obtained after the animals had been sacrificed are shown in Figures 6.3.2G-J, and confirm these observations. Two images are displayed for each material, taken from different parts of the μCT scan. It appears that bone ingrowth has occurred in the two porous materials, i.e. LDIG105 produced by SLS, and A-W.

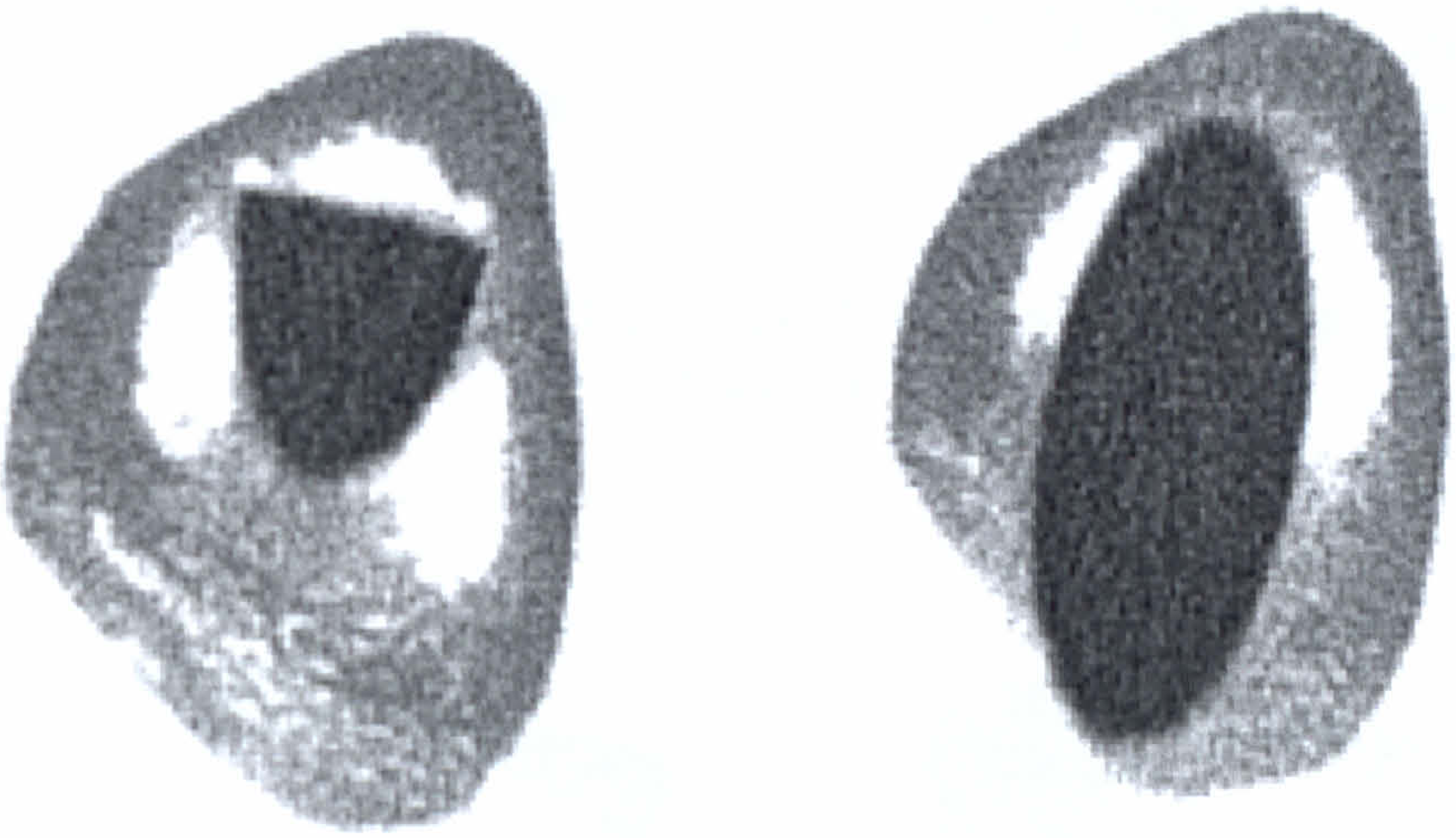

Figure 6.3.2 G: High resolution μCT images of cast LDIG105 in the bone defect 4 weeks after implantation

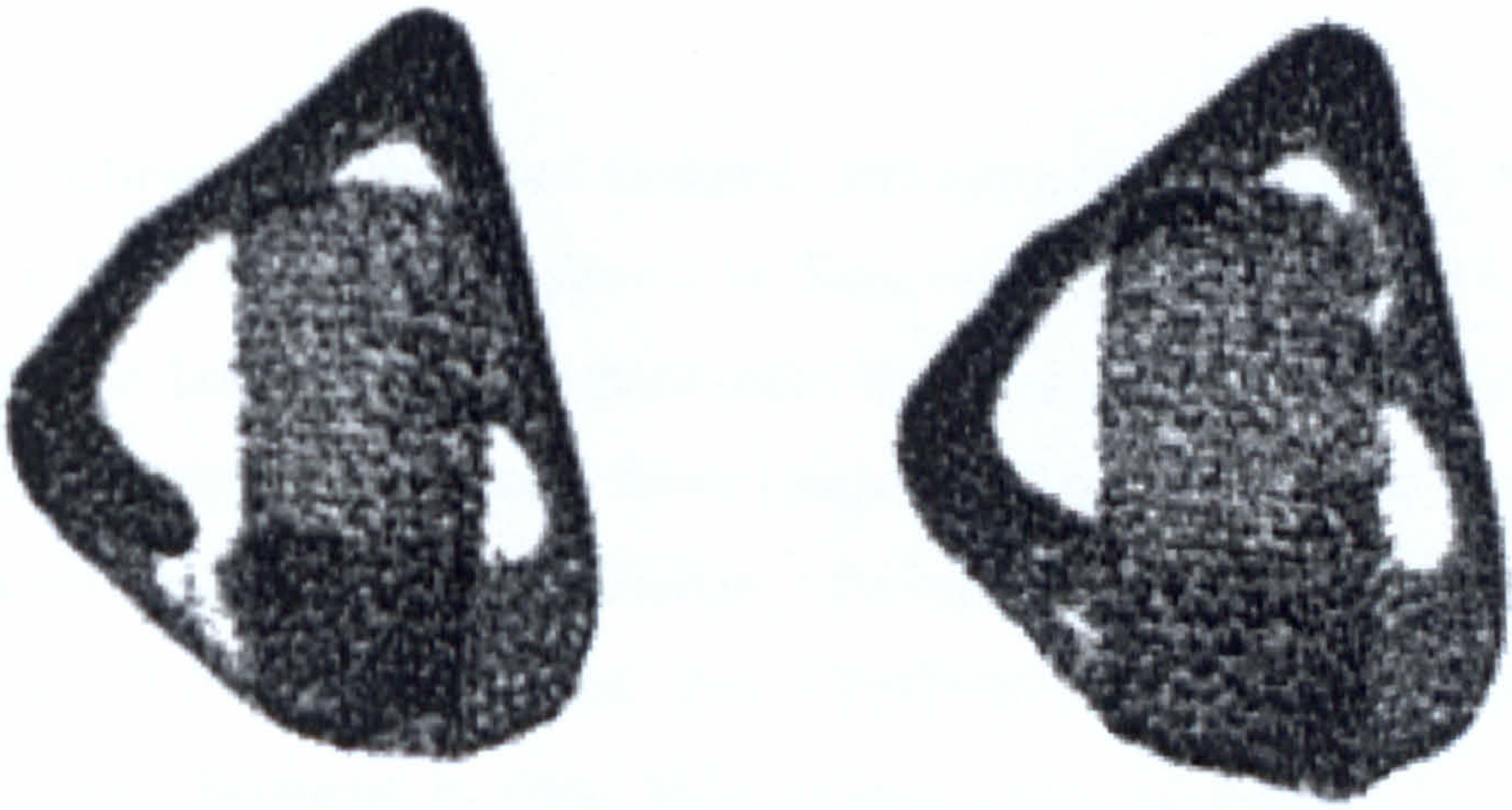

Figure 6.3.2 H: High resolution μCT images of LDIG105 produced by SLS in the bone defect 4 weeks after implantation

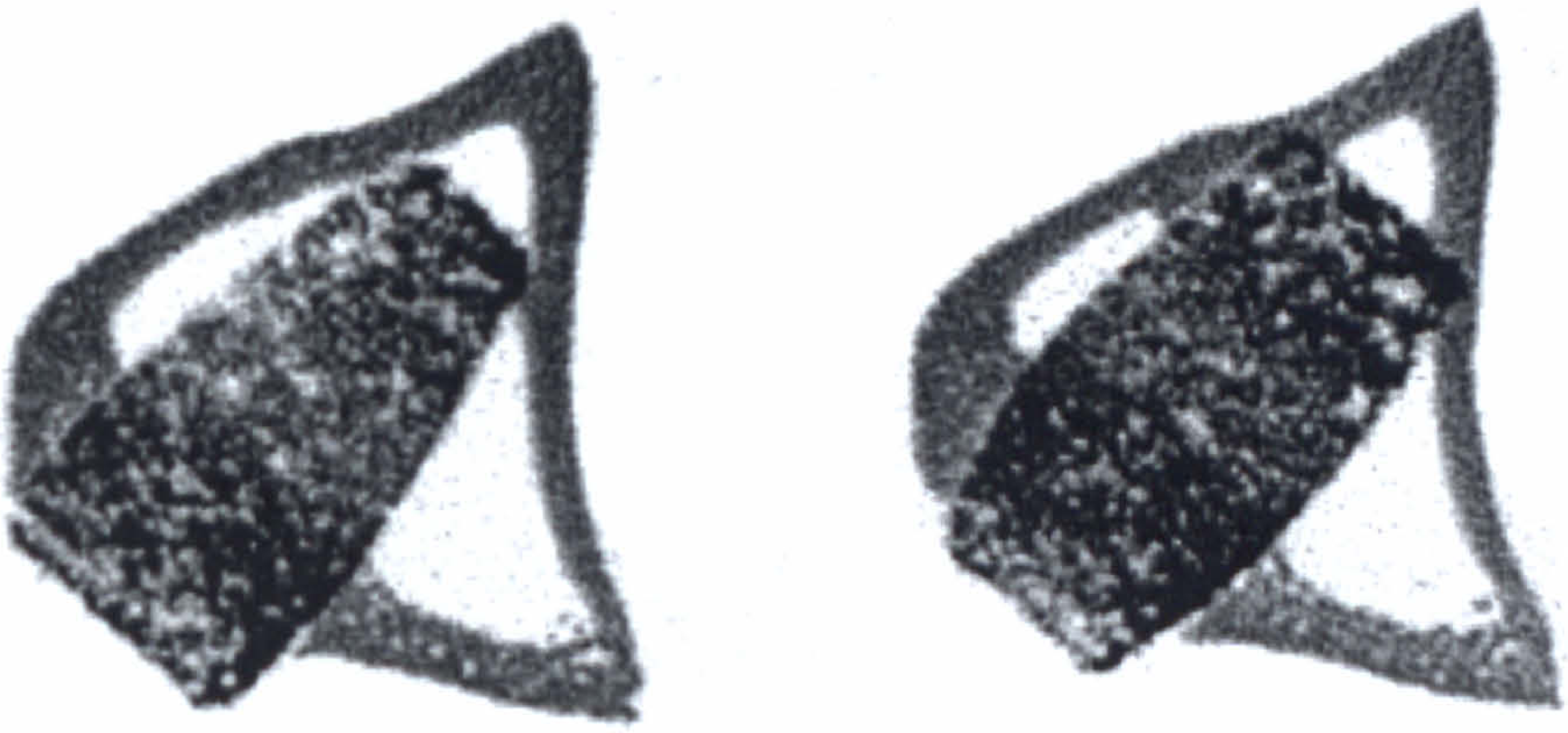

Figure 6.3.2 I: High resolution μCT images of A-W in the bone defect 4 weeks after implantation

Figure 6.3.2 J: High resolution μCT images of the "blank" bone defect 4 weeks after implantation

The interface between the implanted materials and surrounding bone can be seen more clearly in the SEM micrographs shown in Figures 6.3.2K-P. These provide further confirmation that bone is able to grow into the structure of the porous materials. However what is not so clear from these images is whether the material is actually forming a direct bond with bone, or whether a fibrous capsule is forming around it. The results of the SBF study indicated that LDIG105 was unlikely to demonstrate bioactivity *in vivo*. However in these SEM images, there are several areas where new bone does appear to be growing right up to the surface of the material, without the presence of a fibrous layer. Examples of these areas have been marked on the micrographs with green arrows. This is particularly evident in the images for LDIG105 produced by indirect SLS which compare well with the images of A-W in figures 6.3.2

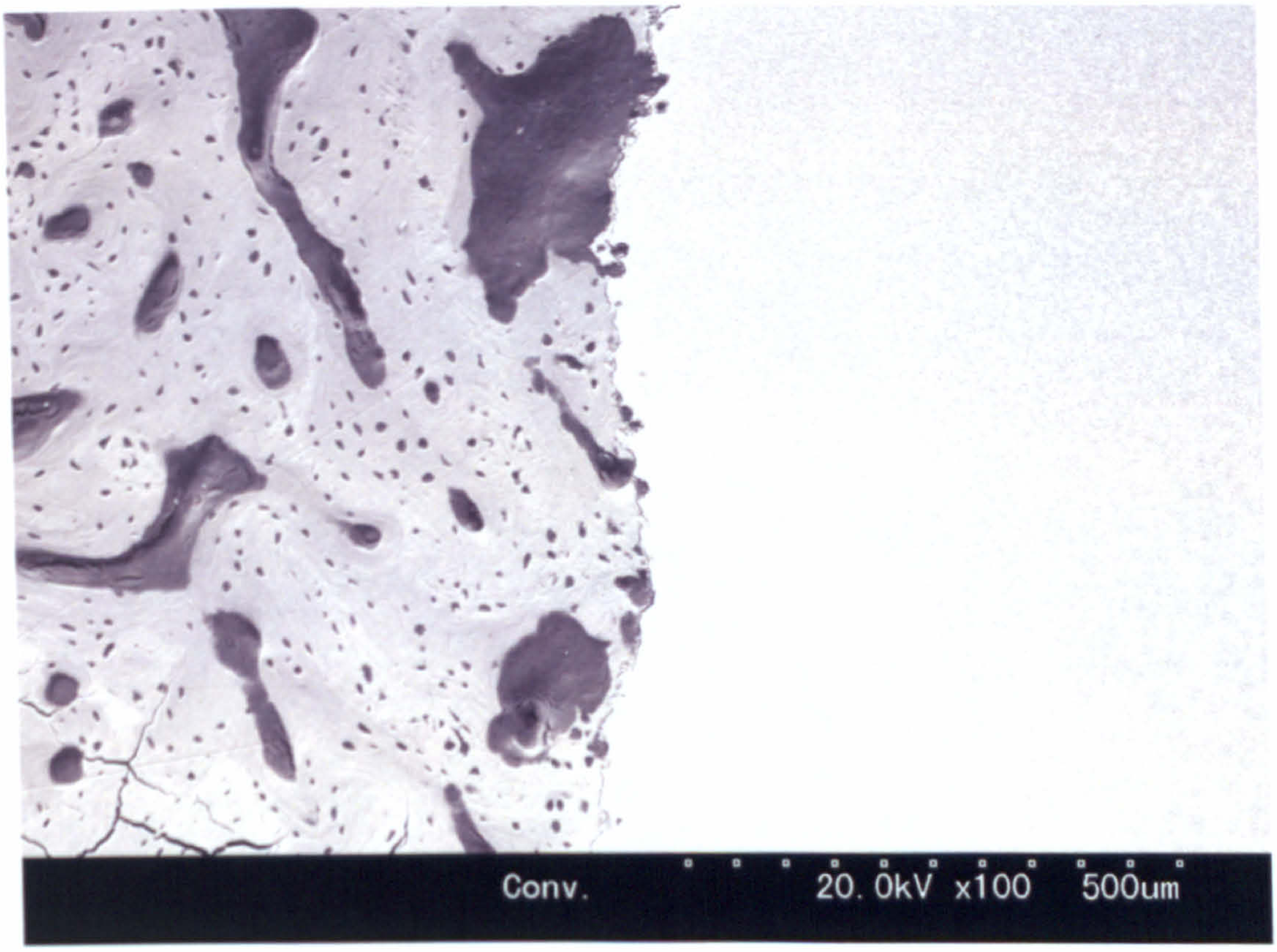

Figure 6.3.2 K: SEM micrograph of interface between LDIG105 produced by conventional casting and bone. x100.

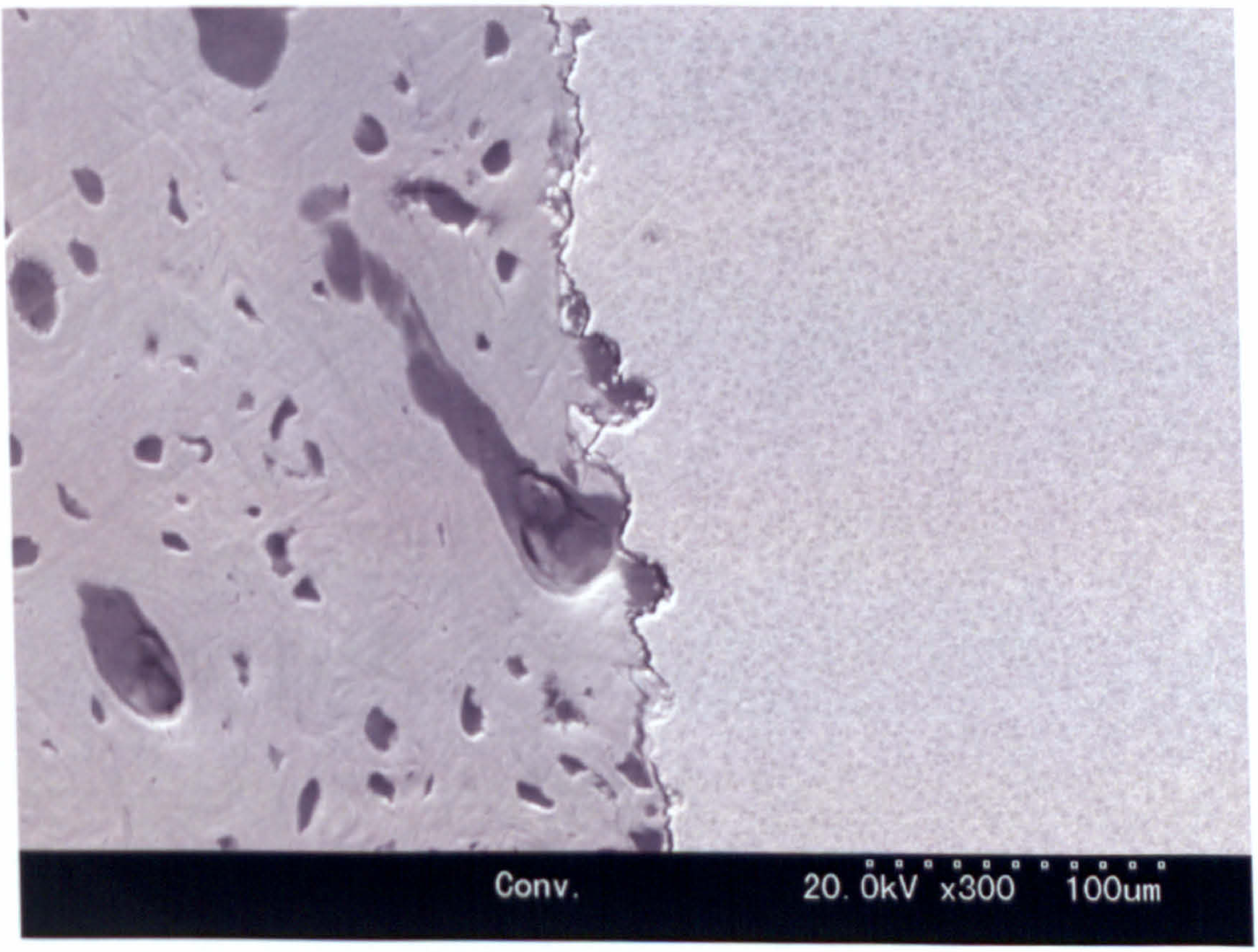

Figure 6.3.2 L: SEM micrograph of interface between LDIG105 produced by conventional casting and bone. x300.

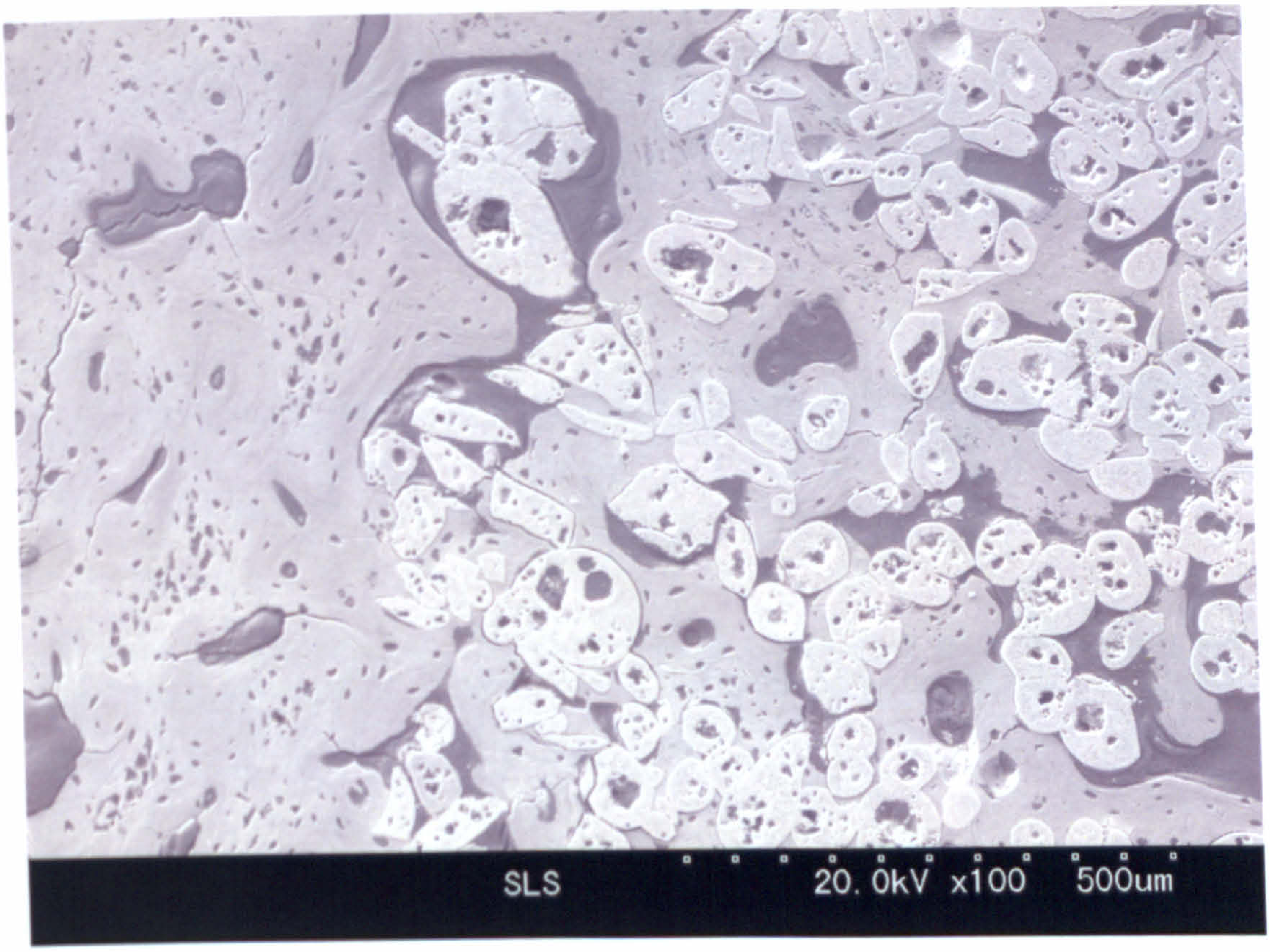

Figure 6.3.2 M: SEM micrograph of interface between LDIG105 produced by indirect SLS and bone. x100.

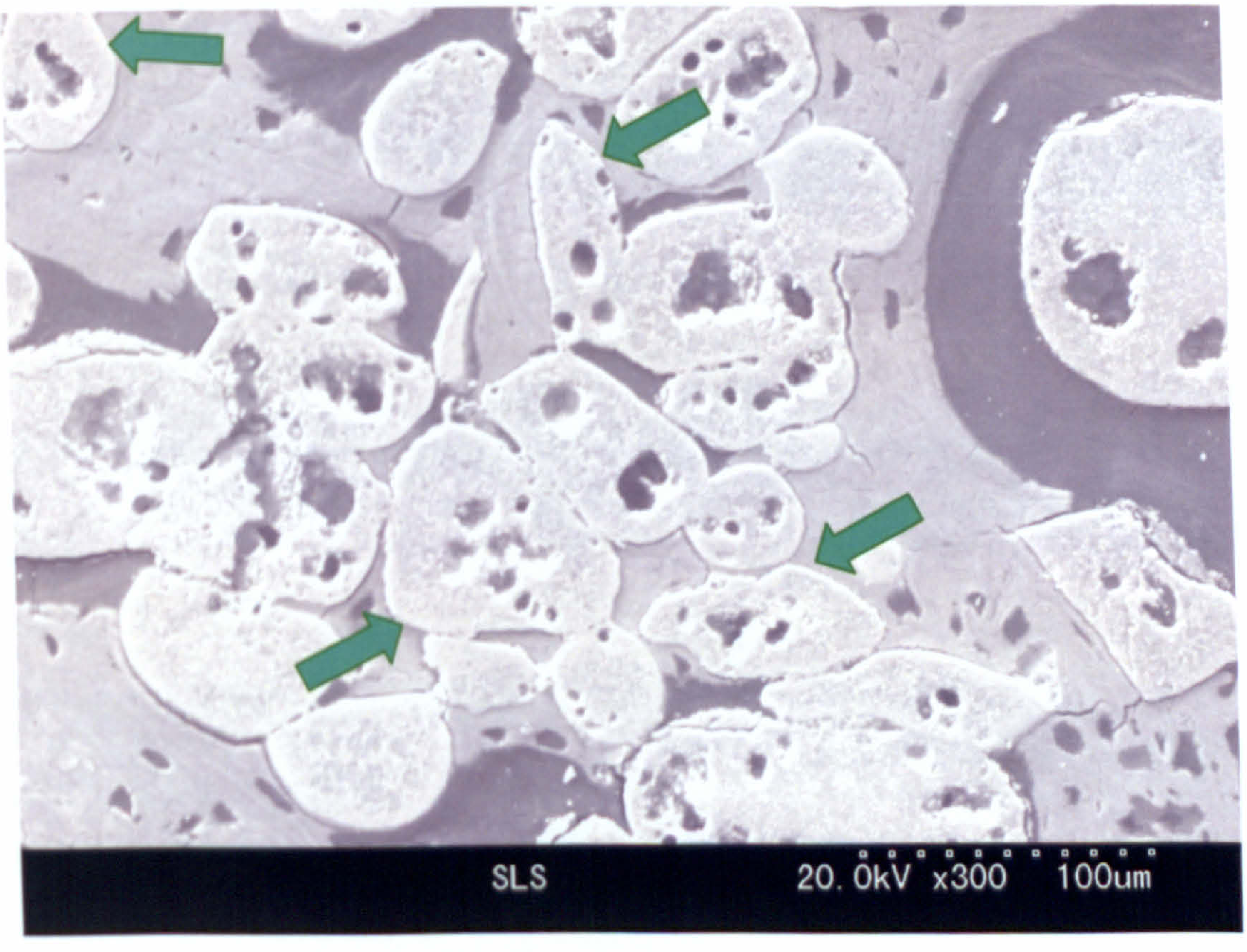

Figure 6.3.2 N: SEM micrograph of interface between LDIG105 produced by indirect SLS and bone. x300. Green arrows indicate areas of direct contact.

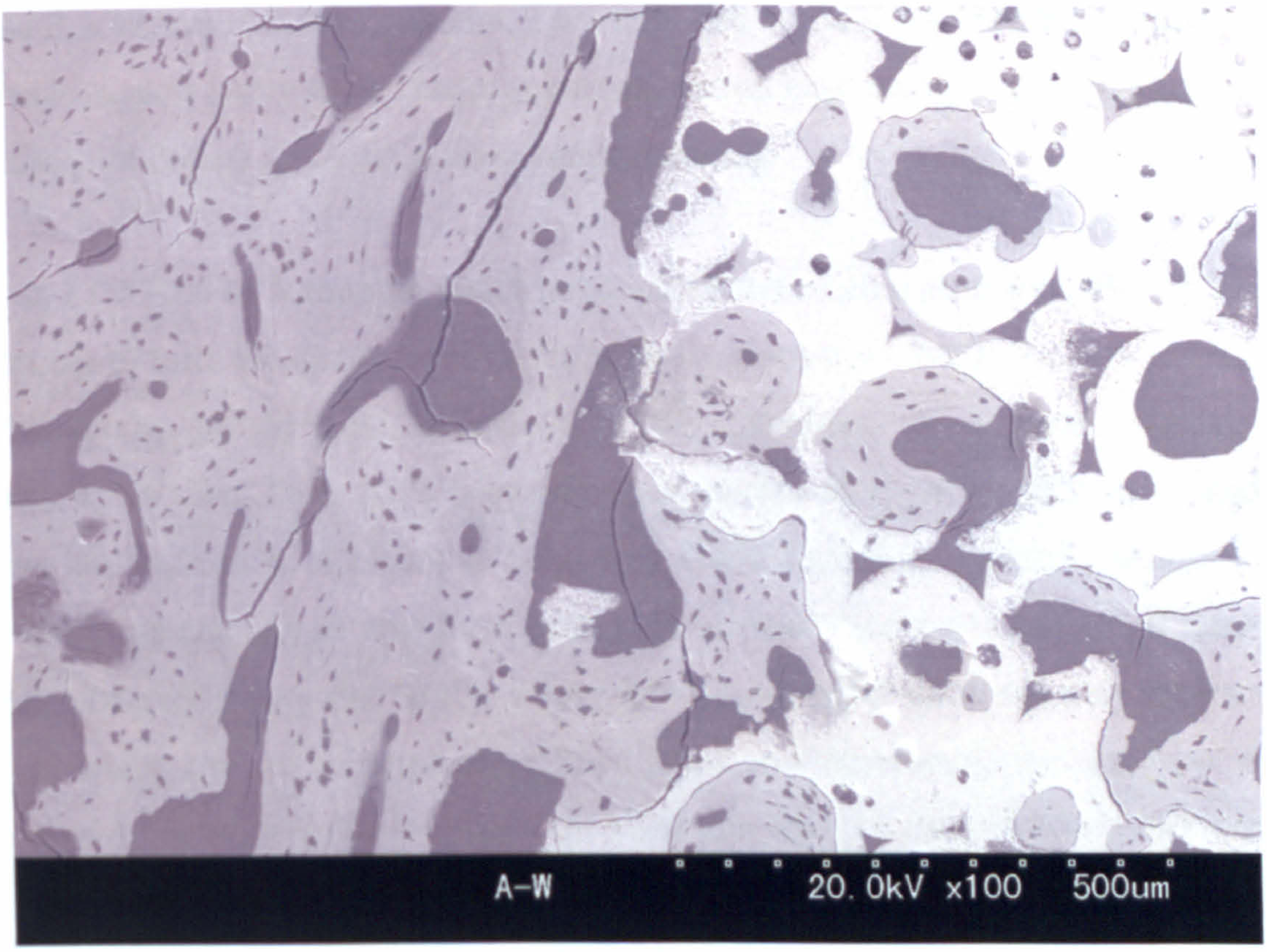

Figure 6.3.2 O: SEM micrograph of interface between A-W and bone. x100.

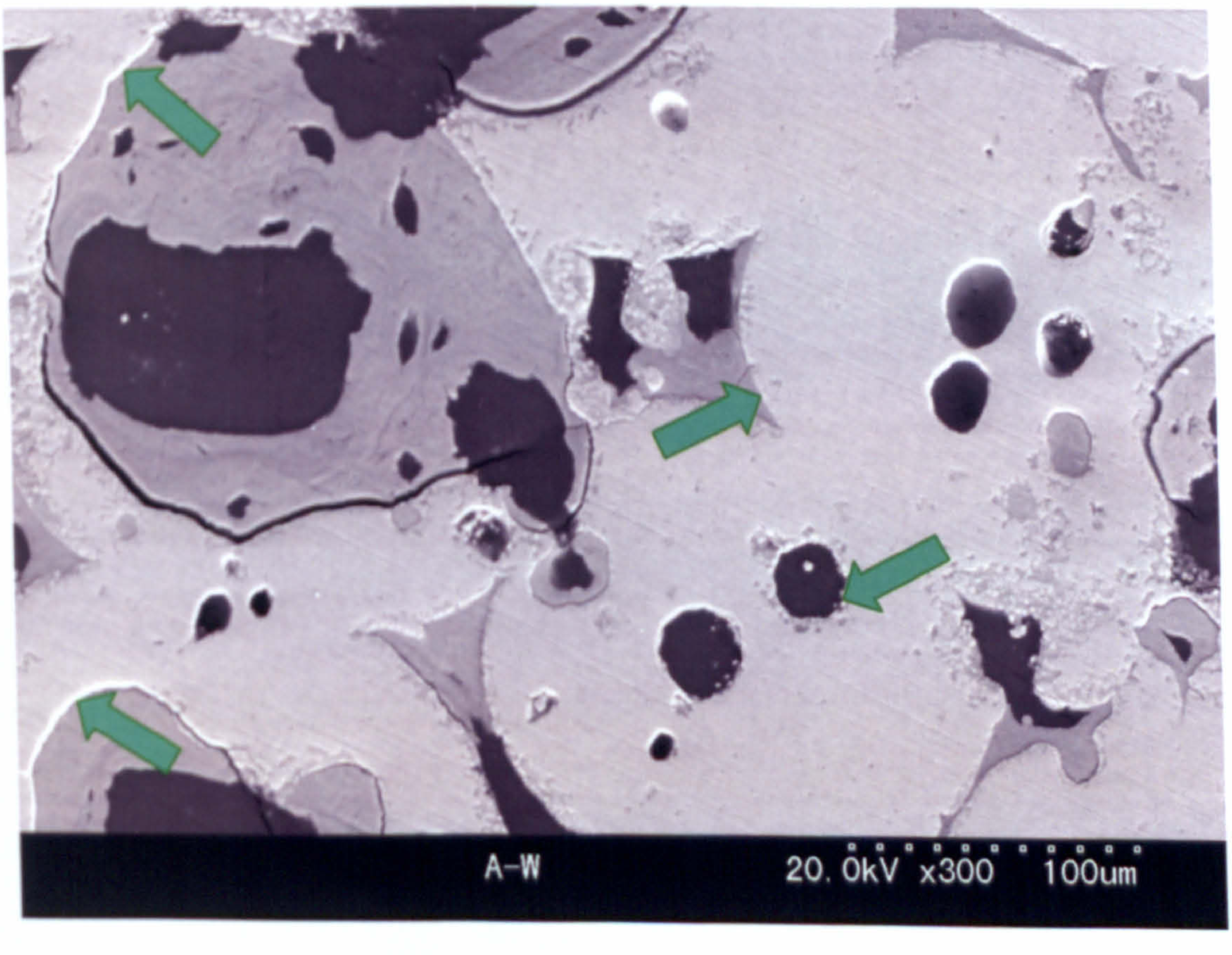

Figure 6.3.2 P: SEM micrograph of interface between A-W and bone. x300.

O and P, a known bioactive material. The slight gap between the cast glass-ceramic and the bone is most likely to be cracks generated during processing. It does not follow the interface but deviates into the glass-ceramic material.

So can LDIG105 be forming a direct bond with bone *in* vivo even though it appears to be unable to form an apatite layer under *in vitro* conditions? Whilst *in vitro* assessment of bioactivity provides an indication of the likelihood of a material exhibiting bioactivity *in vivo,* there have been previous reports of materials that have also not shown any indication of bioactive behaviour when soaked in a simulated body fluid, but upon implantation *in vivo* have been able to bond directly to bone [Gil-albarova, 2000]. However it may also be that a very thin fibrous layer has formed on the material surface which can not be detected by SEM alone and therefore further analysis would be required, for example by staining with Toluidine Blue, to determine whether or not a direct bond had been able to form between the two materials. Unfortunately this was not possible within the timeframe of this work.

Chapter 7 Discussion, Conclusions, & Future Work

7.1 General Discussion

The primary aim of this research was to investigate the feasibility of using an indirect selective laser sintering process to produce porous glass-ceramic implants for use in bone replacement applications. Through this work it has indeed been demonstrated that an apatite-mullite glass-ceramic with composition $4.5SiO_2{\cdot}3Al_2O_3{\cdot}1.6P_2O_5{\cdot}3CaO{\cdot}2CaF_2$ is able to be processed by indirect SLS, during which the acrylic binder, added to the glass powder prior to laser sintering, is melted to produce porous green parts with a strength of around 2.43 MPa and sufficient structural integrity for handling prior to post-processing. A wide range of SLS processing parameters can be used to produce these parts, the large processing window improving the chance of obtaining a combination of processing conditions that satisfies all requirements. The most significant of these is the fast laser scan speeds of up to and possibly exceeding 500mm/sec., which will allow parts to be produced rapidly and thus reduce costs. This can be compared to the same material produced by a direct laser sintering method, where a very small process window with scan speeds of only around 1 and 2mm/sec and laser powers of around 2-3W can be used to produce parts, and even then consolidation is poor – see Figure 7.1A [Lorrison, 2003].

So it is possible to process LDIG105 by indirect laser sintering, but are the parts produced suitable for use in bone replacement applications? The requirements of an implant to be used in bone replacement applications were discussed in Chapter 2. The first of these was that the material should be able to perform the function that necessitated its insertion, in the case of a bone replacement material, that it should regain the mechanical function of the bone by restoring skeletal continuity at the site of disease or injury. Confirmation that this can be achieved has been demonstrated by the μCT and SEM images of the material/bone defect following implantation of the produced materials in rabbit tibia. After four week the materials had not only spanned

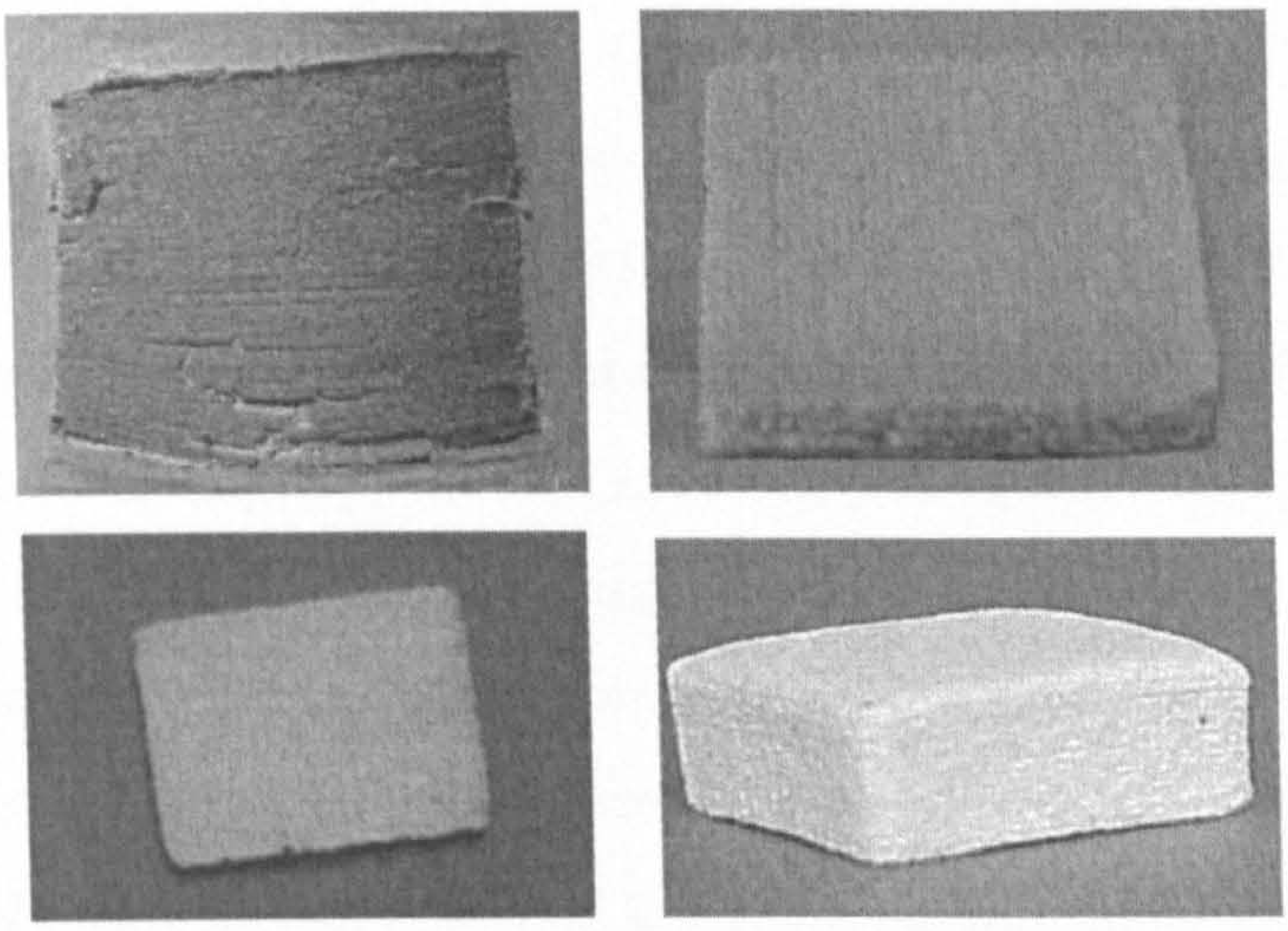

Figures 7.1A: Monolayer (left) and multilayer (right) components produced from LDIG105 by direct (top) [Lorrison, 2003] and indirect (bottom) SLS.

the defect, but allowed bone to grow up to the surface of the material, and when porous as a result of fabrication by SLS, had allowed bone to grow into the implant, proving good integration.

It was stated that a material should be selected that has adequate mechanical properties to cope with the forces applied to it, which will depend on the bone that it is intended to repair or replace. In this study, flexural strength was used as an indicator of the mechanical properties of the produced parts. Improvements were made to the strength through increasing the powder bed density and thus part density, optimisation of the time-temperature profile used for post-processing the parts, and infiltrating the laser sintered performs with a second material. The majority of these methods achieved greater strength by increasing the density of the parts and reducing the amount of porosity in the structure. As discussed previously, in bone replacement materials it is desirable to have some degree of porosity to allow the ingrowth of natural bone into the material, thus allowing a means of securing the implant into the bone defect. However with the exception of infiltrating with phosphate glass at 1200°C, all methods allowed a significant amount of porosity to remain. The phosphate glass is resorbable so although no pores will be present when initially implanted into the bone defect, the glass will gradually resorb over time, creating space in the pores for natural bone to grow into it. A graph showing how the flexural strengths of the materials produced in this study compare to that of natural bone can be seen in Figure 7.1B. It can be seen that specimens made from 50% 45-90μm and 50% <45μm mixed particle size, and specimens infiltrated with phosphate glass at 1200°C have flexural strength values similar to that of cancellous bone. Therefore in terms of strength, these materials could find uses in non-load bearing applications. However it can also be seen that none of the strengths achieved are close to that of cortical bone. Therefore if these materials are to be used in load-bearing situations, significant improvements to their strength need to be made. It is worth noting that being very porous, the samples made from a 50:50 mixed particle size are only 40% dense. Potential therefore remains to improve these strengths by increasing the density of the sintered parts further. Attempts have been made in this study to achieve this through infiltration with a second material, and although an increase in strength was achieved in particular by infiltrating with phosphate glass, it was not nearly significant enough to reach the strength required for load bearing applications. However infiltrating with phosphate glass resulted in a complete change in the crystal phases in the material, and thus the resulting base structure mechanical properties were not those of the original A-M material. It is possible therefore that by infiltrating with a material that does simply fill the pores of the A-M structure or that reacts with the glass-ceramic to form crystal phases with different mechanical properties, the strength of the parts could be more significantly increased.

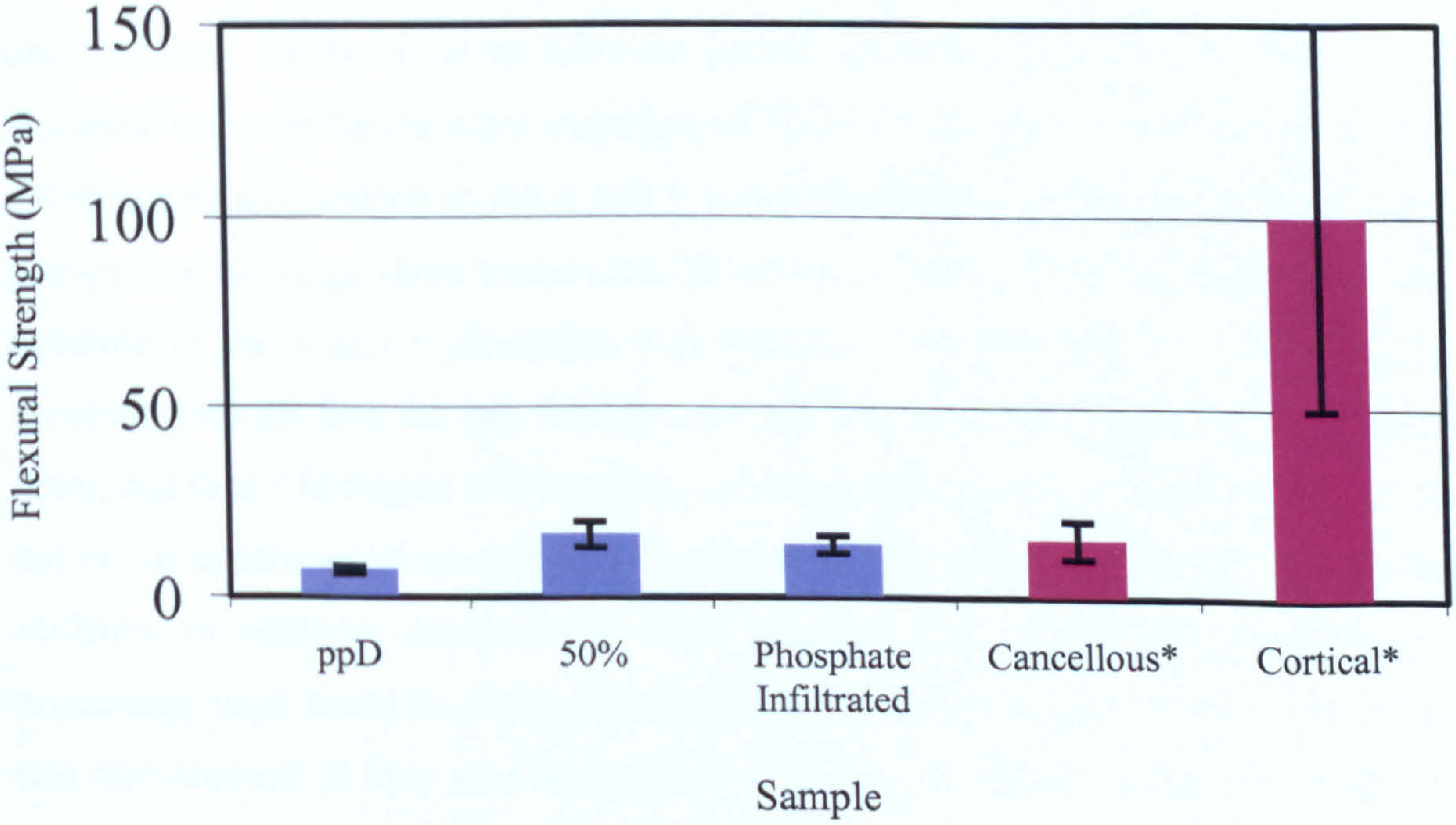

Figure 7.1B: Comparison of the flexural strength of laser sintered LDIG105 with natural bone.

Unlike engineering materials used in other applications, those intended for implantation must be able to maintain their mechanical properties in the extremely hostile environment of the human body. A ceramic material, which as a class of materials is known to have good resistance to the corrosive nature of body fluids and negligible foreign body reactions, was used for this reason. However its resistance was confirmed by soaking in the simulated body fluid, which didn't cause any degradation in any of the materials with the exception of the phosphate infiltrated samples, which are designed to degrade when in contact with body fluids.

Another important requirement of any material or combination of materials implanted into the body is that they should be biocompatible. The non-toxic nature of LDIG105 has been confirmed by both direct contact and extract cytotoxicity assays. The latter is particularly significant as it confirms that no aluminium ions are being leached out of the material. It also resided under the skin and in bone defects of rabbits without causing any obvious sign of discomfort or inflammation.

The need to be able to easily produce the material into complex shapes was also highlighted in Chapter 2, and the particular aspiration to produce custom-made implants has been the focus of this work. As discussed earlier, this work has shown that parts can be produced from an A-M glass-ceramic by indirect laser sintering, thus demonstrating the potential to fabricate patient specific implants from this material. However some problems were experienced with the accuracy of the produced parts, either due to a mismatch in the x and y scanning parameters, or shrinkage during the post-processing stage (heat treatment). The error resulting from discrepancies of laser sintering in the x and y directions was found to vary between +1 and -3mm. It is generally thought that the gap between the implant and bone should be no more than 1mm, and thus this degree of inaccuracy is undesirable. However this work was carried out on an experimental machine; for commercial SLS machines the reported value is ±0.2mm. In addition, dimensional errors resulting from shrinkage during the post-processing stage could be compensated for by scaling the original CAD model to take this into account. It may also be possible to reduce shrinkage during post-processing, for example by using a more controlled heat treatment.

Fixation of the material in the defect is also considered very important as loosening between the implant and surrounding bone is currently the main reason for skeletal implant failure. Ideally, in order to ensure the implanted material is tightly secured into the defect, a material that supports ingrowth of bone is required. It is generally accepted that to achieve this an interconnected porous matrix with pores in the approximate range of 100 to 600μm is required [Klawitter *et al*, 1971]. The combination of SEM and reconstructed μCT images of the post-processed laser sintered parts produced in this work demonstrated that this kind of structure was being achieved, and thus the potential for bone ingrowth *in vivo* was promising. When the porous parts were implanted in rabbit tibia, bone was seen to grow into the three-dimensional structure, demonstrating that the parts are able to act as osteoconductive scaffolds. The mechanical interlocking that results should help to prevent movement in the defect and provide an instant stable interface between the produced parts and bone. However as high porosity can adversely affect the mechanical strength of implants, it remains that a balance is required between providing a porous structure to support the ingrowth of bone, and maintaining adequate strength for the demands of a bone replacement material.

As discussed in Chapter 2, the chances of achieving secure fixation of the implant are increased by using a bioactive material. The ability of a material to bond to bone *in vivo* can normally be predicted by soaking the material in simulated body fluid, which results in the formation of a carbonate hydroxyapatite layer on the surface of bioactive materials. In this work however, no layer was seen to form on either the cast or laser sintered LDIG105 after 30 days of soaking in SBF, thus suggesting that the material is not bioactive. This may be due to the presence of Al_2O_3 in the starting glass which has previously been shown to suppress the bioactivity of glasses and glass-ceramics [Ohtsuki *et al.*, 1992]. However in a study of an A-M glass-ceramic based on the same SiO_2□Al_2O_3□P_2O_5□CaO□CaF_2 composition as LDIG105, bioactivity was demonstrated *in vivo.* It is thought that the Al^{3+} ions were incorporated within the crystal phase and therefore did not alter the surface reaction kinetics of the material. LDIG105 has a Ca:P ratio closer to that of the apatite stoichiometric value of 1.67, and thus it was expected that this difference would increase the material's ability to exhibit bioactive behaviour rather than decrease it. Although *in vitro* studies in SBF are useful in evaluating new materials, there are some materials, for example sintered hydroxyapatite, that have been found to exhibit bioactive behaviour *in vivo* even though they are unable (or the process is very slow) to form an apatite-layer under *in vitro* conditions [Gil-albarova, *2000*]. SEM images taken following retrieval of the laser sintered LDIG105 parts implanted in rabbit tibia for four weeks appear to show bone growing right up to the surface of the material, without the presence of a fibrous layer. Although this would need to be confirmed by histological analysis of the interface, it may therefore be possible that the formation kinetics of an apatite-layer on the surface of LDIG105 is very slow or even absent when soaked *in vitro* in a simulated body fluid, but nevertheless are able to show bioactivity *in vivo*. The longer the time required to form a direct bond between implant and bone, the less useful it is, as ideally the material should instantly form or at least begin to form a bond with bone, so that the structural and mechanical properties of the bone can be re-established. However, mechanical interlocking resulting from the porous nature of the material should provide initial strength, allowing the bond to form with time, producing a stronger interface.

So in summary, this work has shown that it is possible to process LDIG105 using an indirect selective laser sintering process, thereby demonstrating the feasibility of using this technology to process bioceramics into the complex shapes often required for bone replacement applications. Processing of the material involves three main stages:

- Green part manufacture (SLS processing): The polymer binder is melted and connects the glass particles together without appreciably melting them.
- Brown part manufacture: The laser sintered parts are heat-treated to remove the binder and evolve the crystal phases.
- Infiltration: Parts are infiltrated with a second material to improve strength.

Parts currently produced have a flexural strength similar to cancellous bone, which suggests they could find uses in non-load bearing applications. The biocompatibility of the material is good and there is evidence from *in vivo* studies that the porous structure is able to act as an osteoconductive scaffold.

7.2 Conclusions

Selective Laser Sintering

- It is possible to produce green parts of LDIG105 with good structural integrity using an indirect selective laser sintering process.
- During laser sintering the polymer binder is melted and connects the glass particles together without appreciably melting them.
- Increased consolidation of parts with the use of increasing laser power and decreasing scan speeds can be achieved, presumably due to the increased amount of energy supplied melting more of the binder and making it less viscous, and therefore better able to wet the ceramic.
- A significant reduction in the processing window was observed with decreasing particle size, although the surface finish and definition improved.
- The most promising compromise appears to be samples produced from glass with a particle size of 45-90μm.
- A considerably larger processing window is achieved with indirect SLS compared to direct fabrication of the same glass.
- The material after indirect laser sintering is still in an amorphous state.

Post-processing

- Heating the laser sintered parts to 1200°C results in the evolution of apatite, mullite, and anorthite crystal phases.
- A conventional nucleation-crystallisation post-processing route or gradual heating up to 1200°C results in parts with poor flexural strength due to the large amount of crystal nuclei that are allowed to form and the corresponding reduction in the quantity of the glassy phase needed for liquid phase sintering.
- Higher flexural strengths were achieved when the samples were placed directly into a furnace preheated to 1200°C as there appeared to be enough time for liquid phase sintering to occur before the crystal phases were formed.
- Parts produced from glass of a mixture of particle sizes have greater flexural strength than parts made from monosized particles, presumably due to improved particle packing of the powder bed which increases the final density of the part.

- Infiltration of the post-processed parts was possible with both polymer and ceramic materials, and was accompanied by an increase in part strength.
- Infiltrating with P_2O_5 at 1200°C led to a change in the crystal phases in the material.
- Currently produced parts have a flexural strength similar to that of cancellous bone.

Assessment of Biological Properties

- LDIG105 is non-toxic, demonstrated by both extract and direct contact assays.
- Neither LDIG105 produced by casting or by SLS showed any signs of forming an apatite layer following soaking in SBF for 30 days., suggesting that it is unlikely that this material would prove bioactive *in vivo.*
- However after 4 weeks *in vivo,* bone had grown into the porous structure of the laser sintered parts, and appeared to form a close bond with the material surface.

Overall Conclusions

- Indirect SLS can be used to produce porous 3-D parts of A-M glass-ceramics, with flexural strengths similar to that of cancellous bone.
- The biocompatibility of these parts is good, and bone is able to grow into their porous structure.
- Further work is needed to improve their mechanical strength if they are to be used in load bearing applications.

7.3 Suggestions for Further Work

This project aimed to bring together the two technologies of laser sintering and bioactive ceramics in order to examine the possibility of constructing bone replacement material of potentially complex geometry that would provide improved fits as a result of strong bonding to the surrounding bone, and close fits resulting from custom made implants. Whilst the potential of the laser sintering process has been demonstrated, the ability of the glass-ceramic LDIG105 to exhibit bioactive properties still requires confirmation. The *in vitro* study performed in this work suggested that LDIG105 was unlikely to prove bioactive *in vivo.* However when implanted in rabbit tibeae, bone appeared by SEM to be growing up to the surface of the material. Therefore staining and histological analysis of the bone-material interface is required to determine whether or not a direct bond is forming between the two materials or whether a thin fibrous layer is separating them. If this analysis highlights a lack of bioactivity, a more suitable material for use with this technology would need to be produced. Initially, the focus would be on modifying the current material. LDIG105 contains a large proportion of Al_20_3 which is well known as a component that increases the chemical durability of glasses, and hence reduces the ability of apatite to form in the body environment. Bioactivity of glasses may be enhanced by reducing the amount of Al_20_3 in the glass system or addition of components such as Na_2O or B_2O_3, which along with P_2O_5 often act to enhance apatite formation in simulated body fluid. However other materials could also be considered, for example apatite-wollastonite glass-ceramic or hydroxyapatite, as indirect SLS has the advantage that it can work with any post-processable material.

Following confirmation or development of a bioactive material, the strength of the bioactive bond would need to be evaluated. This is usually achieved by performing a push out test which measures the shearing force between the bone and material, after implantation *in vivo.*

The mechanical properties of the parts produced by SLS also need to be considered. Maximum flexural strengths of around 16MPa were achieved in this work, similar to that of cancellous bone. Therefore there are two options – to accept that this is the maximum strength that can be achieved by this material and explore the possibility of the material being used in non load-bearing applications or look to increase the strength of the parts so that they can be weight-bearing. Although a porous structure is required for the ingrowth of bone, the currently produced parts are only 40% dense and thus there is still potential to increase strength via infiltration of the porous structure with a second material. Attempts were made in this work to infiltrate the post-processed parts with PMMA and a resorbable phosphate glass, and an increase in flexural strength was seen as a result. However there is the potential to further increase strength by determining a more suitable material for infiltration. Infiltrating with phosphate glass resulted in a complete change in the crystal phases in the material, and thus the resulting base structure mechanical properties were not those of the original A-M material. It is possible therefore that by infiltrating with a material that does simply fill the pores of the A-M structure or that reacts with the glass-ceramic to form crystal phases with different mechanical properties, the strength of the parts could be more significantly increased. The ideal scenario would be to infiltrate the porous laser sintered parts with a resorbable material which would contribute to the strength of the implant immediately following implantation, but would then gradually resorb and be replaced by bone tissue which would grow into the re-forming pores and form a secure interlocking bond with the glass-ceramic material. Although attempts were made in this work to achieve this, the temperature required to infiltrate it into the porous structure caused it to react with the sintered LDIG105.

Once the desired strength has been achieved, other mechanical properties important to bone replacement materials, such as fatigue resistance and toughness need to be assessed.

References

Adell R, Lekholm U, Rockler B, -I Branemark P, Lindhe J, Eriksson B, Sborodone L. Marginal tissue reactions at osseointegrated titanium fixtures (1). A 3-yr longitundinal prospective study. *Int. J. Oral Maxillofacial Surgery 15(1), 39-52 (1986).*

Amprino R. Investigations of some physical properties of bone tissue. *Acta Anatomica 34, 161-186 (1958).*

Anderson JC, Leaver KD, Rawlings RD, Alexander JM. *Materials Science. 4th Edition 1990, Chapman & Hall, London. ISBN 0-442-31189-3.*

Anderson JM. Inflammatory Response to Implants. *Trans.Am.Soc., Intern.Organs 24, 101-107 (1988).*

Badylak SF. Xenogeneic extracellular matrix as a scaffold for tissue reconstruction. *Transplant Immunology (2004) In Press*

Barlow JW, Vail NK. A method of producing high temperature parts by way of low temperature sintering. *US Patent 5,284,695 8 Feb1994*

Bauer TW, Schils J. The pathology of total joint arthroplasty. II. Mechanisms of implant failure. *Skeletal Radiol 1999; 28:483-97*

Bhan S. Banking on the bone bank. Healthcare Management Express. Issue dated 1-15/10/03. www.expresshealthcaremgmt.com

Block B, Haken JK, Hastings GW. *Clinical Orthopaedics, 1970, 72, 239*

Bonfield W. Composites for Bone Replacement. *J Biomedical Engineering 1988; 10:522-6*

Boyd JD, Clark WELG, Hamilton WJ, Yoffey JM, Zuckerman S, Appleton AB. *Text book of Human Anatomy. Macmillan (1956).*

Bronzino JD. *The Biomedical Engineering Handbook. 532-609; 1995, Boca Raton, FL, CRC Press.*

Brown BH, Smallwood RH, Barber DC, Lawford PV, Hose DR. *Medical Physics and Biomedical Engineering. IOP Publishing Ltd 1999 ISBN 0-7503-0368-9*

Bundle CR, Evans CA, Wilson S. (Ed.) *Encyclopaedia of Materials Characterisation. 1992 by Butterworth-Heinemann. ISBN 0-7506-9168-9*

Burg KJL, Porter S, Kellam JF. Biomaterial developments for bone tissue engineering. *Biomaterials 21 (2000)2347-2359*

Burma P, Gardeniers JWM. Tissue Reaction around a hydroxyapatite coated hip prosthesis. Case report of a retieve specimen. *J Arthroplasty, 1995; 10:389-395*

Burnstein AH, Reilly DT, Martens M. Aging of bone tissue: Mechanical Properties. *J. Bone Joint Surg., 1976, 58A, 82-86*

Cao W, Hench LL. Bioactive Materials. *Ceramics International 22 (1996) 493-507*

Castle Island. *Castle Island's Worldwide Guide to Rapid Prototyping. http://home.att.net/~castleisland/home.htm Accessed on 10/01/04.*

Çehreli M, Şahin S, Akça K. Role of mechanical environment and implant design on bone tissue differentiation: current knowledge and future contexts. *Journal of Dentistry (2004) 32, 123-132*

Clifford A, Hill R. Apatite-Mullite Glass-Ceramics. *Journal of Non-crystalline Solids 196 (1996) 346-351*

DAMIEN CJ, PARSONS JR. Bone graft and bone graft substitutes: a review of current technology and applications. *J.Appl.Biomaterials, 1990, 2,187-208*

DARSELL J, BOSE S, HOSICK H, BANDYOPADHYAY A. From CT Scan to Ceramic Bone Graft. *J.Am.Ceram.Soc.,86 [7] 1076-80 (2003)*

DAVIDSON JA, SCHWARTZ G. Wear, creep and frictional heating of femoral implant articulating surfaces and the effect on long-term performance – Part 1, a review. *J Biomed Mater Res., Applied Biomaterials 21(3), 261-286 (1987)*

DICKENS PM. Rapid Prototyping - The Ultimate in Automation? *Assembly Automation. Vol.14 No2, 1994, pp.10-13.*

FRIEDMAN R, ET AL. Current Concepts in Orthopaedic Biomaterials and Implant Fixation. *The American Academy of Orthopaedic Surgeons 43 (1994) 1086-1109*

FUESTING T, BROWN L, DAS S, HARLAN N, LEE G, MORRIS J, BEAMAN J, BOURELL D, BARLOW JW, SARGENT K. Development of Direct SLS Processing for Production of Cermet Composite Turbine Sealing Components; Parts I and II. *Solid Freeform Fabrication Proceedings, Austin 1996, pp39-56*

GEESINK RGT, DE GROOT K, KLEIN CPAT. Bonding of Bone to Apatite-coated Implants. *J Bone Joint Surg [Br] 1988; 70-B:17-22*

GERMAN RM. *Powder Metallurgy Science. 2nd Edition. Metal Powder Industries Federation, New Jersey, 1994 ISBN 1-878954-42-3*

GIBSON I, SHI D. Material properties and fabrication parameters in selective laser sintering process. *Rapid Prototyping Journal Vol.3 No.4, 1997. pp.129-136*

GRIFFITH ML, CHU T, WAGNER W, HALLORAN JW. Ceramic Stereolithography for Investment Casting and Biomedical Applications. *Solid Freeform Fabrication Symposium Proceedings, 6, 31-38 (1996)*

GRIMM T, WOHLERS T. RP Applications: The possibilities are endless. *Time-Compression Technologies, Jan/Feb 2002.* www.timecompress.com

HARDY DC, FRAYSSINET P, GUIHEM A, LAFONTAINE MA, DELINCCE PE. Bonding of hydroxyapatite coated femoral prosthesis. *J Bone Joint Surg 1991; 73-B:732-740*

HATTON P. *Personal Communication, Centre for Biomaterials and Tissue Engineering, School of Clinical Dentistry, University of Sheffield, 2000*

HAUSER C. Selective Laser Sintering of a Stainless Steel Powder. *PhD Thesis, School of Mechanical Engineering, University of Leeds, UK. 2003.*

HENCH LL, PASCHALL HA. Direct Chemical Bonding Between Bioactive Glass-ceramic Materials and Bone. *J Biomed. Mater. Res. Symp., 4, 25-42 (1973)*

HENCH LL, SPLINTER RJ, ALLEN, WC, GREENLEE TK. Bonding mechanisms at the interface of ceramic prosthetic materials. *J.Biomed.Mater.Res., 2 (1972) 117-141*

HENCH LL. Bioactive Glasses: Mechanisms of Bioactive Bonding. *http://www.bg.ic.ac.uk/Lectures/Hench/BioGlass/cal3.htm Accessed on 28/01/02*

HENCH LL. Bioactive Glasses: theory and clinical applications. *In Bioceramics 7 (Eds OH Anderson and A Yli-Urpo), 1994, pp.3-14 (Butterworth-Heinemann, Oxford).*

HENCH LL. Biomaterials: a forecast for the future. *Biomaterials, 1998, 19, 1419-1423*

HENCH LL. Bioceramics: From concept to Clinic. *J.Am.Ceram.Soc.,1991, 74 [7], 1487-1510*

HENSON PM. The immunologic release of constituents from neutrophil leukocytes. II Mechanisms of release during phagocytosis, and adherence to non-phagocytosable surfaces. *J.Immunol. (1971) 107: 1547-1557*

Higashi S, Yamamuro T, Nakamura T, Ikada Y, Hyon SH, Jamshidi K. Polymer-hydroxyapatite composites for biodegradable bone fillers. *Biomaterials 1986; 7:183-7.*

Hill RG, Patel M, Wood DJ. Preliminary Studies on Castable Apatite-Mullite Glass Ceramics. *in Bioceramics 4, edited by W. Bonfield. GW. Hastings and KE. Tanner, (Butterworth-Heinemann, London, 1991) pp.79-86*

Höland W, Beall G. *Glass-ceramic Technology. 2002 by The American Ceramic Society, Ohio. ISBN: 1-57498-107-2*

Höland W. Biocompatible and bioactive glass-ceramics - state of the art and new directions. *Journal of Non-Crystalline Solids 219 (1997) 192-197*

Ishizaki K, Komarneni S, Nanko M. Porous Materials: Process technology and applications. *1998 by Kluwer Academic Publishers. ISBN 0-412-71110-9*

Jarcho M. Calcium phosphate ceramics as hard tissue prosthesis. *Clin. Orthop. Rel. Res., 1981, 157-259*

Johansson C, Lausmaa J, Ask M, Hansson HA, Albrektsson. Ultrastructural differences of the interface zone between bone and Ti6Al4V or commercially pure titanium. *J. Biomed. Eng., 1989, 11 (1): 3-8.*

Jones JR, Hench LL. Biomedical materials for new millennium: perspective on the future. *Materials Science and Technology. August 2001 Vol.17 891*

Kim SS, Utsunomiya H, Koski JA, Wu BM, Cima MJ, Sohn J, Mukai K, Griffith LG, Vacanti JP. Survival and function of hepatocytes on a novel three-dimensional synthetic biodegradable polymer scaffold with an intrinsic network of channels. *Ann Surg 1998; 228(1):8-13*

KLAWITTER JJ, HULBERT SF. Applications of Porous Ceramics for the Attachment of Load Bearing Orthopaedic Applications. *J. Biomed. Mater.Res.Symp., 2, 161 (1971)*

KLEIN CPAT, VAN DER LUBBE HBM, DE GROOT K. A plastic composite of alginate with calcium phosphate granules as implant material: an in vivo study. *Biomaterials 1987; 8:308-10*

KLOSTERMAN D, CHARTOFF R, OSBORNE N, GRAVES G, LIGHTMAN A, HAN G, BEZEREDI A, RODRIGUES S. Curved layer LOM of ceramics and composites. *Solid Freeform Fabrication Symposium Preceedings, University of Texas at Austin, Austin, TX, August, 1998, pp.671-680*

KOKUBO T, KUSHITANI H, SAKKE S, KITSUGI T, YAMAMURO T. Solutions able to reproduce in vivo surface-structure changes in bioactive glass-ceramic A-W. *J Biomed Mater Res., 1990, 24, 721*

KOKUBO T. A/W Glass-Ceramic:Processing and Properties. *pp.75-88 in An Introduction to Bioceramics. Edited by LL Hench and J Wilson. World Scientific, Singapore, 1993.*

KOKUBO T. Formation of biologically active bone-like apatite on metals and polymers by a biomimetic process. *Thermochimica Acta 280/281 (1996) 479-490*

KURTZ SM, MURATOGLU M, EVANS M, EDIDIN AA. Advances in the processing, sterilisation and crosslinking of ultra-high molecular weight PE for total joint arthroplasty. *Biomaterials, 1999, 20, 1659-1688*

LEE G, BARLOW JW. Selective laser sintering of bioceramic materials for implants. *SFF symposium proceedings, Vol.4, 1993, pp.376-80. Marcus HL et al.(Eds),*

LEE WE, RAINFORTH WM. *Ceramic Microstructures: Property Control by Processing. Chapman and Hall, 1994. ISBN 0412431408*

LEES S, DAVIDSON CL. The Role of collagen in the elastic properties of calcified tissues. *Journal of Biomechanics, 1977, 10, 473-475*

LEONG KF, PHUA KKS, CHUA CK, DU ZH, TEO KOM. Fabrication of porous polymeric matrix drug delivery devices using the selective laser sintering technique. *Proc Instn Mech Engrs Vol.215 Part H ImechE2001*

LIN F-H ET AL. Preparation of a biphasic porous bioceramic by heating bovine cancellous bone with $Na_4P_2O_7.10H_2O$ addition. *Biomaterials 20: 475-484 1989*

LOMAS R. *Personal Communication, Yorkshire Tissue Bank, Sheffield, 2000*

LORRISON JC. Selective Laser Sintering of Bioceramics. *PhD Thesis, School of Mechanical Engineering, University of Leeds, UK. 2003.*

MARTIN RB, BURR DB. *The Structure, Function, and Adaptation of Compact Bone. 1989, New York, Raven Press.*

MARTIN RB. Bone as a Ceramic Composite Material. *Materials Science Forum Volume 293 (1999) pp.5-16. Trans Tech Publications, Switzerland*

MARTINI FH. *Fundamentals of Anatomy and Physiology. 3rd Edition, 1995 by Prentice Hall, Inc. ISBN 0-13-357683-3*

MCCABE JF. *Applied Dental Materials. 7th Edition. 1990 by Blackwell Science Ltd. ISBN 0-632-02826-2*

MCCALDEN RW, MCGEOUGH JA, BAKER MB, COURT-BROWN CM. Age related changes in the tensile properties of cortical bone. *J. Bone Jt. Surg., 1993, 75A(8), 1193-1205*

MCELHANEY JH. Dynamic response of bone and muscle tissue. *Journal of Applied Physiology, 1966, 21, 1231-1236*

McMillan PW. *Glass-ceramics. 2nd Edition. 1979 Academic Press Inc. (London) Ltd. ISBN 0-12-485660-8*

Merkx MAW et al. Incorporation of three types of bone block implants in the face. *Biomaterials 20: 639-645. 1999*

Millennium Research Group. *European Markets for Orthopaedic Biomaterials. 2001 May; EUB00102*

Nee AYC, Fuh JYH, Miyazawa T. One the improvement of the stereolithography (SL) process. *Journal of Materials Processing Technology 113 (2001) 262-268*

Nelson JC, Xue S, Barlow JW, Beaman JJ, Marcus HL, Bourell DL. Model of the SLS of bisphenol-A polycarbonate. *Industrial and Engineering Chemistry Research, Vol 32, 1993, p2, 305-17*

Ohtsuki C, Iida H, Hayakawa S, Osaka A. Bioactivity of titanium treated with hydrogen peroxide solutions containing metal chlorides. *J Biomed Mater Res 1997; 35:39-47*

Ohtsuki C, Kokubo T, Yamamuro T. Compositional dependence of bioactivity of glasses in the system $CaO\text{-}SiO_2\text{-}Al_2O_3$: its *in vitro* evaluation. *Journal of Materials Science: Materials in Medicine 3 (1992) 119-125*

Ohtsuki C, Kushitani H, Kokubo T, Kotani S, Yamamuro T. Apatite formation on the surface of Ceravital-type glass-ceramics in the body. *J Biomed. Mater. Res., 25, 1363-1370 (1991)*

Paul A. Chemical durability of glasses; a thermodynamic approach. *J Mater Sci 12 (1977) 2246-2268*

Pham DT, Dimov S, Lacan F. Selective Laser Sintering: Applications and Technological Capabilities. *Proc Instn Mech Engrs Vol 213 Part B 1999*

PIEKARSKI K. *Journal of Applied Physics, 1970, 41, 215-223*

PLUMB JA, MILROY R, KAYE SB. Effects of the pH dependence of 3-(4,5-dimethyldiazol-2-yl)-2,5-diphenyltetrazolium bromide-formazan absorption on chemosensitivity determined by a novel tetrazolium-based assay. *Cancer Research 1989; 15:4435-4440*

PRAESTHN PB. Rapid Prototyping of Surgical Instruments. *MSc Thesis, School of Mechanical Engineering, University of Leeds, UK. 2001.*

RAMAKRISHNA S, MAYER J, WINTERMANTEL, LEONG KW. Biomedical applications of polymer-composite materials: a review. *Composites Science and Technology 61 (2001) 1189-1224*

RATNER BD, HOFFMAN AS, SCHOEN FJ, LEMONS JE (EDS.). Biomaterials Science: An Introduction to Materials in Medicine. *1996, Elsevier Science (USA). ISBN 0-12-582461-0*

REILLY DT, BURSTEIN AH, FRANKEL VH. The elastic modulus for bone. *Journal of Biomechanics, 1974, 7, 271-275*

REVELL PA, AL SAFFAR N, KOBAYASHI A. Biological reaction to debris in relation to joint prostheses. *Proc Inst Mech Eng 1997; 211:187-97*

RHO J-Y, KUHN-SPEARING L, ZIOUPOS. Mechanical Properties and the hierarchical structure of bone. *Medical Engineering and Physics 20 (1998) 92-102*

RICHERSON D.W. *Modern Ceramic Engineering, Second edition, Marcel Dekker, Inc, (1992).*

ROGERS B, STEPHENS S, GITTER A, BOSKER G, CRAWFORD R. Double-Wall, Transtibial Prosthetic socket fabricated using selective laser sintering: A Case Study. *American Academy of Orthotists and Prosthetists. 2000 Vol 12, Num 3, pp97-100*

SAHA S, PAL S. Mechanical characterisation of commercially made carbon-fiber reinforced PMMA. *Journal Biomed. Mater. Res., 1986, 20:817-26*

STEVENS A, LOWE J. *Histology. Mosby Year Book Europe Limited, London, 1993. ISBN 0-397-44633-0*

STEWART DR. Concepts of glass-ceramics. *In Pye, Stevens, La Course, editors. Introduction to glass science. New York: Plenum Press:237-271*

STRNAD Z. Role of the glass phase in bioactive glass-ceramics. *Biomaterials Vol.13, No.5 (1992)*

TAYLOR C. *Personal Communication, School of Mechanical Engineering, University of Leeds, Leeds, 2001*

VALLET-REGÍ M. Ceramics for medical applications. *J.Chem.Soc., Dalton Trans., 2001, 97-108*

VOGEL W. *Chemistry of Glass, The American Ceramic Society, 1985*

WAGNER HD, COHN D. Use of high-performance polyethylene fibers as a reinforcing phase in poly(methylmethacrylate) bone cement. *Biomaterials 1989; 10:139-41*

WEINER S, TRAUB W, WAGNER HD. Lamellar Bone: Structure-Function Relations. *Journal of Structural Biology 126, 241-255 (1999)*

WEINER S, TRAUB W. Organisation of hydroxyapatite crystals within collagen fibrils. *FEBS Lett. 206, 262-266 (1986)*

WILLIAMS DF. *The Williams' Dictionary of Biomaterials. Liverpool University Press, UK. 1999*

WILSON J, CLARK AE, DOUEK E, KRIEGGER J, SMITH WK, ZAMET JS. Clinical applications of bioglass implants. *Bioceramics, Vol.7, ed. Ö.H.Andersson and A.Yli-Urpo. Butterworth-Heinemann, Oxford, 1994, pp.415-422.*

YAN WQ, NAKAMURA T, KOBAYASHI M, KIM HM, MIYAJI F, KOKUBO T. Bonding of chemically treated titanium implant to bone. *J Biomed Mater Res 1997; 37:265-275*

YAN X, GU P. A review of rapid prototyping technologies and systems. *Computer-Aided Design. Vol.28 No.4, pp.307-318, 1996*

YASZEMSKI MJ, PAYNE RG, HAYES WC, LANGER R, MIKOS AG. Evolution of bone transplantation: molecular, cellular and tissue strategies to engineer human bone. *Biomaterials 17 (1996) 175-185*

YAY Y, ARVIER JF, BARKER TM. Technical Note: Maxillofacial biomodelling - Preliminary Result. *Br.J.Radiol.1995; 68:519-523*

ZEIN I, HUTMACHER DW, TAN KC, TEOH SH. Fused deposition modelling of novel scaffold architectures for tissue engineering applications. *Biomaterials 2002; 23(4):1169-85*